New Approaches to the Design of Liquid Crystal-based Biosensors

A Thesis Submitted for the Degree of
DOCTOR OF PHILOSOPHY

by

Sumyra Sidiq

Department of Chemical Sciences
Indian Institute of Science Education and Research (IISER) Mohali
Sector 81, Knowledge City, S. A. S. Nagar, Mohali, 140306.
Punjab, India.

February 2016

DEDICATED TO

My Beloved Parents, Siblings

&

My Fiancé

DECLARATION

The work presented in this thesis entitled "***New Approaches to the design of Liquid Crystal-based Biosensors***" has been carried out by me under the supervision of **Dr. Santanu Kumar Pal** in the Department of Chemical Sciences, Indian Institute of Science Education and Research (IISER) Mohali, Mohali.

This work has not been submitted in part or full for a degree, diploma or a fellowship to any other university or institute.

Whenever contributions of others are involved, every effort is made to indicate this clearly with due acknowledgements of collaborative work and discussions. This thesis is a bona fide record of original work done by me and all sources listed within have been detailed in the bibliography.

Sumyra Sidiq

Date:

Place:

In my capacity as the supervisor of the candidate's thesis work, I certify that the above statements by the candidate are true to the best of my knowledge.

Dr. Santanu Kumar Pal

Associate Professor

Department of Chemical Sciences

Indian Institute of Science Education and Research Mohali

Date:

Place:

ACKNOWLEDGEMENTS

It would not have been possible to write this doctoral thesis without the help and support of the numerous people around me including my teachers, family, friends and colleagues. At the end of my doctoral research, it is a pleasant task to express my gratitude to all those who contributed in many ways to make this thesis possible and made it memorable for me.

It is difficult to overstate my gratitude to my project supervisor ***Dr. Santanu Kumar Pal*** *for giving me this wonderful opportunity to explore the exciting field of Liquid Crystals as Sensors and for his suggestions and meticulous scrutiny of the thesis work. His words of encouragement and constant surveillance on the progress of the study motivated and helped me throughout my work. I am highly thankful to my supervisor for the time he spent in explaining me the various aspects of our field. Without his guidance; this work would never have been possible. I am highly indebted for his amicable understanding attitude.*

I also thank ***Dr. Angshuman Roy Choudhury*** *and* ***Prof. Ramesh Kapoor****, members of my doctoral committee for fruitful discussions during the yearly assessment of my work.*

I acknowledge IISER Mohali for NMR and Raman facilities. I would like to thank Department of Chemical Sciences and Biological Sciences for various departmental facilities like UV-vis, FTIR spectrophotometers, Circular Dichroism, Spectrofluorometer etc. I also acknowledge ***Mr. Inderjeet Singh*** *lab technician of physical teaching lab for helping in performing thermal evaporator instrument. I would also like to acknowledge* ***Mr. Prateek****, technician of cell sorter for helping in performing flow cytometry.*

I would like to acknowledge our director, ***Prof. N. Sathyamurthy****, for providing the space and all the research and infrastructural facilities. I am also thankful to HOD, Department of Chemical Sciences* ***Prof. K. S. Viswanathan*** *for permitting the use of various departmental facilities and also for various useful discussions regarding PM-IRRAS experiments. I am grateful to all the faculties of IISER for their teaching and constant encouragement.*

I would like to thank ***Dr. Arunika Mukhopadhaya*** *and* ***Mr. G. V. R. Krishna Prasad*** *for helping with Cell-based and Flow Cytometry experiments.*

I would like to thank ***Shruti***, ***Satyam***, ***Chinmoy***, ***Maheswararao***, ***Junaid*** *and* ***Muzafar*** *for helping in various aspects of my thesis work.*

My sincere thanks to ***Ms. Shilpa Setia****, my lab-mate cum friend, for her support and encouragement at various stages of my work at IISER Mohali. It was a very pleasant experience to work with her and learn. I am also thankful to my current and former lab-mates* ***Dibyendu***, ***Joydip***, ***Indu Verma***, ***Indu Bala***, ***Golam***, ***Harpreet***, ***Monika***, ***Vidhika***, ***Supreet***, ***Manmohan***, ***Aneeshma***, ***Akash***, ***Srijit*** *and* ***Sudhakar*** *for their help and cooperation and for making the working atmosphere in the lab extremely enjoyable and cheerful. My special thanks to* ***Joydip*** *being my favorite junior in the lab.*

I wish to thank my friends ***Shilpa***, ***Shruti***, ***Satyam***, ***Chinmoy***, ***Maheswararao***, ***Junaid*** *and* ***Gurpreet*** for their cheerful companionship and for their timely encouragement. *A special vote of thanks to my dear friends* ***Uzma***, ***Saqib***, ***Nighat*** *and* ***Nazima*** *for their companionship and concern.*

I also thank all the lab assistants (chemistry and biological teaching labs), staff members of stores, purchase office, administrative office, account section, library and computing facility of IISER Mohali for their help and co-operation during the course of time.

I am highly thankful to ***Dr. Aijaz Ahmad Dar and Dr. Mohsin Ahmad Bhat****, my M.Sc. project supervisors for giving me the flavor of research.*

I deeply express my gratitude to my parents, ***M. Sidiq*** *and* ***Shamima***; *my siblings,* ***Zahida*** *and* ***Suhail*** *and my fiancé,* ***Muzafar*** *for their never-ending support and inspirations throughout my life. Their constant motivation and believe in me, made me travel this longer. I sincerely acknowledge* ***Arshid Bhaiya***; ***Zahoor Bhaiya***; *my jiju,* ***Mir Shakeel***; ***Uzma***; ***Sabra***; *my little cuties* ***(Salif & Huda)*** *and* ***all my family members*** *for their love, support, encouragement and care throughout my life for my welfare.*

I acknowledge ***DST***, ***India*** *for providing international travel support to participate in International Liquid Crystal Conference held in Dublin, Ireland in 2014. I am thankful to* ***UGC***, ***India*** *for research fellowship for five years and* ***IISER Mohali*** *for financial support to carry out the experimental work, giving me the fellowship on time and also for providing all the research facilities that enabled me to complete my Ph.D.*

Contents

Chapter 1

Introduction: Liquid Crystals and Sensors

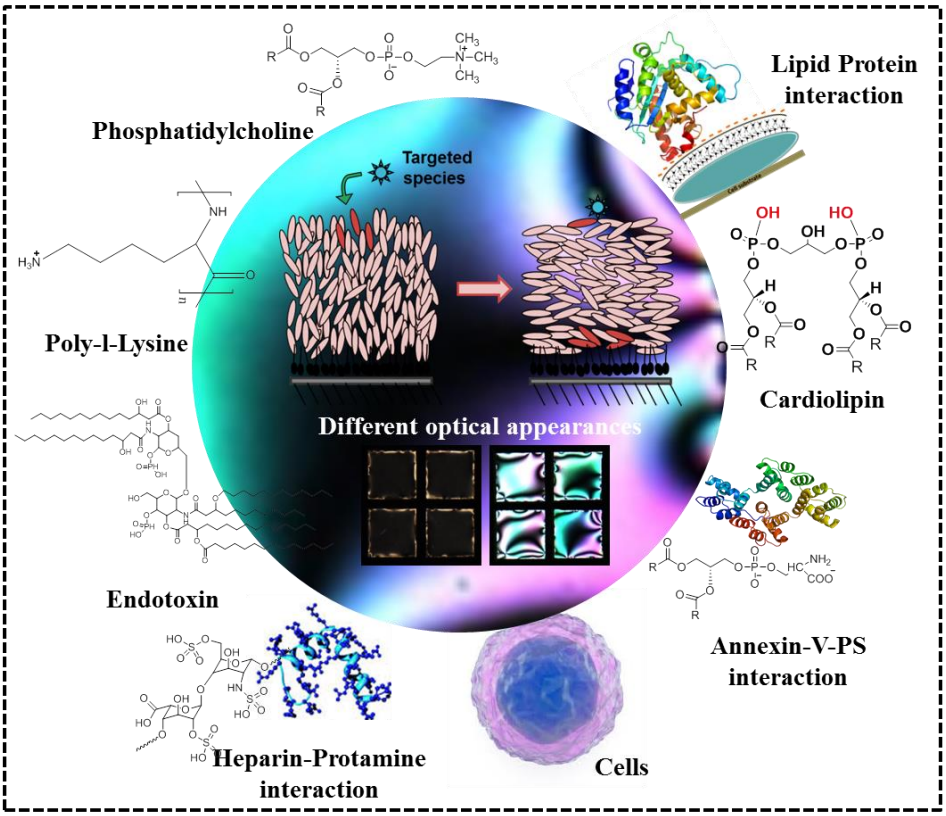

Besides the maturation of liquid crystal (LC) display market, LC materials are pushing the boundaries in the burgeoning field of optical and bio-sensing systems. Biosensors fabricated with LC materials can allow label-free observations of biological phenomenon. LCs thus offers the opportunity to design materials that can both mimic the biological systems and as well directing the behaviors of the biological systems.

1.1 Overview

Life is, in a molecular nous, the interactions between biomolecules like cells, proteins, lipids, nucleic acids and other biomolecules. Every life process is governed by interactions occurring in our bodies or at their interfaces. For instance, each biomolecule has its own specific function but, its function is realized only when it reacts or interacts with other molecules in the living cells. Such interaction is stable in some cases but unstable and momentary in other cases. The pre-requisite to understand biomolecular function in the context of life and metabolism is to analyze the interaction of biomolecule with each other. Among these interactions, protein-protein and protein-lipid interactions are of pronounced interest and importance. However, the interaction of proteins with other molecules including nucleotides, sugars and other small molecules are equally important. Molecular recognition of biomolecular interactions governs the affinity and specificity of complex formation and determines their biological functions. Any disturbance or malfunction in the normal mode of action of an interaction may cause disease and illness. Thus, to provide a rational guide to therapeutic design a better qualitative and quantitative understanding of the physical forces underlying biomolecular interactions is required. Therefore, understanding molecular recognition in biomolecular interactions is of enormous scientific and practical importance.

Biosensors are one of the approaches to study these interactions.[1,2] A biosensor is an analytical device which uses a biological or a biologically derived recognition system associated with a physico-chemical transducer to estimate the presence and/or concentration of the target substance by translating biological reactions into a quantifiable and a processible physical signal. The two most important characteristics of biosensor are its sensitivity and selectivity towards a target molecule (analyte). Selectivity depends only on properties of receptor element of the biosensor since that is where the analyte interacts with biosensor. Sensitivity is determined by both the biological compound and the transducer. A wide range of materials have been explored for the design of interfaces that mediate desired interactions with biological systems.[3-10] Most of them either require a label to be attached to the incoming analyte or involve complex optical and surface patterning methods for readout. This has motivated the search for label free platform for the development of cheap and ultrasensitive bio-sensor with the possibility of multiplex detection.

Liquid crystalline phases are encountered in a variety of biological systems (e.g., concentrated DNA)[11-15] but, only recently the use of synthetic liquid crystals (LCs) as material interfaces to biological systems has been explored.[16-44] LC-based sensors have exploited some unique properties possessed by LCs. Firstly, orientations of LCs are very sensitive to interfacial interactions and the orientational responses can be amplified to the LC bulk phase up to hundred micrometers away from an interface. This property allow label-free observations with LCs to detect and amplify the molecular-level information on surfaces into micrometer spatial readouts as the LC molecules act to enhance the optical appearance of signals of any interfacial phenomena. Secondly, the elastic force within LC phase and the liquid-like mobility of LC molecules can amplify LC responses within tens of milliseconds. This allows the use of LCs for fast and real-time detection. Thus, the mobile nature of the LC makes them promising for biological applications. Thirdly, LC molecules are birefringent and the orientational changes of LCs can be readily visualized under crossed polarizers. This allows the use of LCs for simple optical detection without any use of complex and expensive instrumentation. The sensitivity of the ordering transition of LCs to the nanoscale topography and chemical functionality of surfaces enable the amplification and transduction of biologically relevant binding events into optical outputs visible to naked eye.[16-44] The study of LC materials for bio-sensing relies on the interaction between the sensing LC medium and the bio-molecule of interest. The dynamic and responsive properties of synthetic LCs appear potentially useful in a range of fundamental and applied biological contexts. However, realization of this potential requires advancement in the area of research involving the interfacial design of LC-based biosensors which is the aim of this thesis.

In this thesis, we focus on the interfacial engineering of thermotropic LCs such as those which form nematic phases that are largely immiscible with water. This class of LCs can be used to define interfaces with aqueous phases at which biological interactions can be reported. This thesis aimed towards new approaches for developing LC-based stimuli responsive materials that are anticipated towards improving the fundamental understanding of biomolecular interactions and provides a gateway for the further advancement in LC-based sensor designing.

1.2 Liquid crystal

Liquid crystals (LCs) are defined as the state of matter characterized by the level of order and mobility that is intermediate between that of crystalline solids and isotropic liquids (Figure 1.1).[45-49] It possesses some typical properties of a liquid (e.g., fluidity, inability to support shear, formation and coalescence of droplets) as well as some crystalline properties (anisotropy in optical, electrical and magnetic properties, periodic arrangement of molecules in one spatial direction etc.). The direction of the averaged orientational order of LC molecules is called the director of the LC.

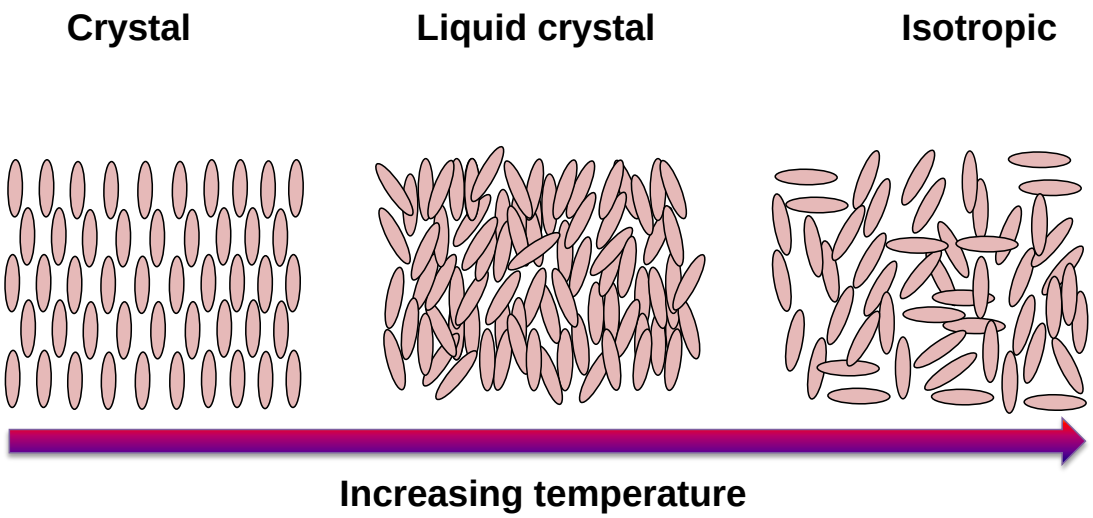

Figure 1.1 Schematic illustration of the LC phase exist between the crystalline and isotropic phases.

In general molecules that exhibit LC phases are anisometric in their shape (e.g., rod-like or disc-like).[45,46] These molecules are termed mesogens. In contrast, the self-assembly of isometric molecules into anisotropic assemblies can also lead to liquid crystallinity.[45-46] LCs shows general properties like birefringence, response to magnetic and electric fields, optical activity in twisted nematic phases and sensitivity to temperature resulting in color changes. These remarkable properties of LCs made them ubiquitous in diverse applications. To date, besides the familiar displays being the most common applications of LC technology, numerous studies on LCs have also been performed to provide unparalleled opportunities to

facilitate the basic understanding of the science and to develop new non-display applications. LCs which are widely used in flat panel displays, have found more and more applications in biological assays and chemical sensors over the past decade.[16-44,50-53]

1.3 Historical perspective

The birth of the LC field lies within the study of biological materials. Until the late 1800s, scientists described physical matter as existing in three states (solid, liquid and gas).[48] In 1888, however, Austrian botanist Friedrich Reinitzer isolated a form of cholesterol (cholesterol benzoate) and observed the existence of two melting points.[54] The first melting point of cholesteryl benzoate (Figure 1.2) was observed at 145.5 ºC and a second melting point at 178.5 ºC and between the two was a milky liquid phase. Above 178.5 ºC the phase was clear.

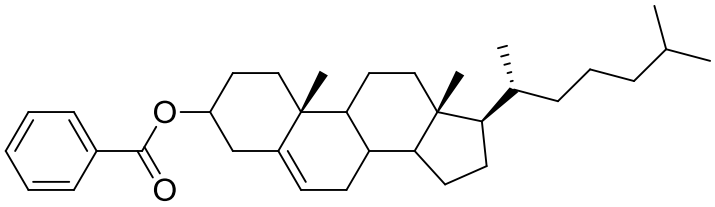

Cholesteryl Benzoate

Figure 1.2 Chemical structure of cholesteryl benzoate.

He then contacted physicist Otto Lehman in Germany who was investigating the crystallization of materials using polarized light microscopy.[55] Lehman investigated these samples under polarized light microscopy and deduced that the opaque fluid observed by Reinitzer was a distinct phase of matter. It exhibited properties of both liquids and solids; he coined the phrase "liquid crystal". Subsequently, Lehmann confined this unusual material to droplets,[55] which became the basis for a modern-day technology known as polymer-dispersed liquid crystals (PDLCs).[56,57] Soon afterward, a classification scheme was introduced in 1922 by Georges Freidel, who identified the phases of LCs as being nematic, smectic or cholesteric (chiral nematic).[58] The term "mesogen" was also adopted to describe a molecule that forms a LC (a "mesophase"). The advances in the LC science grew rapidly in the 1960s

and 1970s to yield new LC phases and enable many of the useful properties of LCs during which its promise for display technologies largely drove the basic and applied research.[59] In terms of the ties between biology and LC materials, it was found that LCs are ubiquitous in nature as phospholipid cell membranes as well as myelin, a lipid material protecting the nerves, are liquid crystalline. The same holds for some concentrated DNA and protein solutions, for instance the secretion of a spider that is used to generate silk. The connection between liquid crystallinity and biology advanced further with "the aspect of molecular patterns" most underestimated in the consideration of biology phenomena is that found in LCs.[60,61] This early work has sparked more recent developments as LC research starts to move into and combine with many of the fundamental aspects of the biosciences to generate new areas of application. Indeed, potential uses of LCs recently cited in the scientific literature that include artificial muscles,[62,63] acoustic polarizers,[64,65] tunable lasers[66] and optical data storage.[67] As a step forward, Abbott and his coworkers in 2003 use LC as responsive material interfaces for biological membranes.[17] Then a large subset of the LC community is making use of new understanding of these materials to develop innovative sensor devices for applications. This area of research involving new LC devices will no doubt drive forward new research in these fundamental and applied sciences.

1.4 The nematic mesophase

The most widely investigated LC phase is the nematic phase of the thermotropic calamatic LCs. The thermotropic LCs exhibit changes in phase as a function of temperature. These are catalogued as either rod-like (calamitic) or disk-like (discotic). The nematic phase is characterized by long-range orientational order i.e., the long axes of the molecules tend to align along a preferred direction. The locally preferred direction may vary throughout the medium which is defined by a vector n(r) giving its local orientation. This vector is called a director. Since its magnitude has no significance, it is taken to be unity. There is no long-range positional order of the molecules of a nematic phase. The molecules appear to be able to rotate about their long axes and also there seems to be no preferential arrangement of the two ends of the molecules if they differ. Hence, the sign of the director is of no physical significance, $n = -n$. Optically, a nematic behaves as a uniaxial material with a center of symmetry. A schematic illustration of the relative arrangement of the molecules in the

nematic phase is shown in Figure 1.3a. The thread like structures were observed under polarized optical microscope with crossed polars from which nematics take their name (Greek word means "thread") (Figure 1.3b).[47]

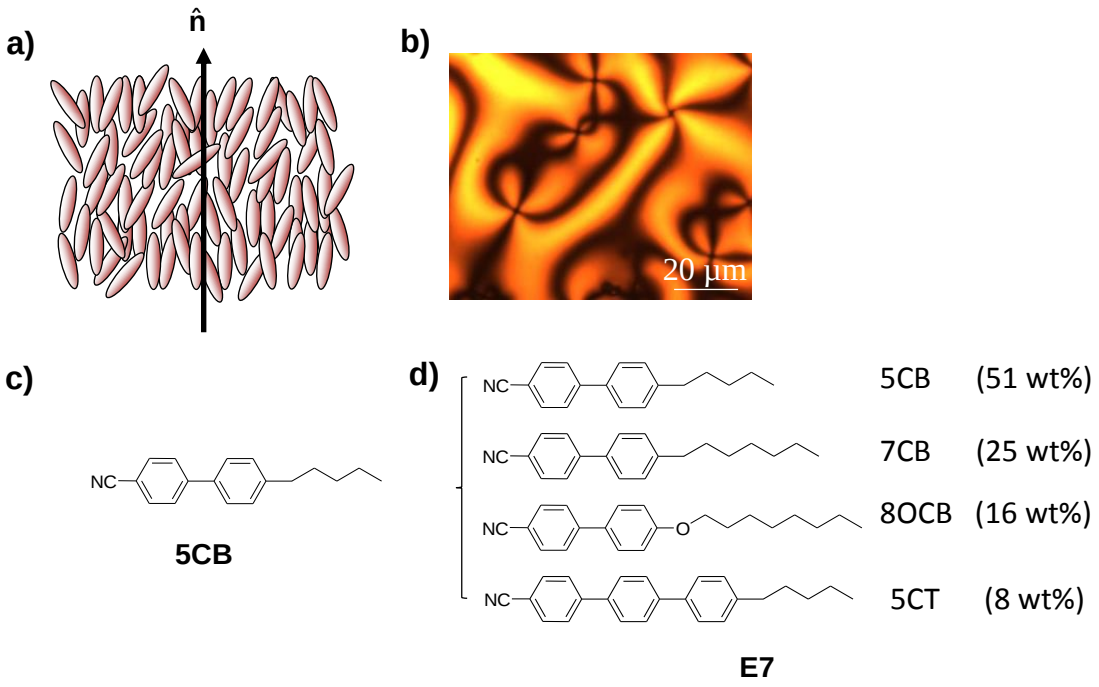

Figure 1.3 a) Schematic of the nematic mesophase. The nematic phase has uniaxial symmetry, as indicated by the arrow. b) Nematic texture under polarized optical microscopy. Chemical structures of nematic LC c) 5CB and d) E7.

These threads have been termed disclinations by Frank. The most commonly known compounds exhibit nematic mesophase under room temperature are 5CB and E7 (Figure 1.3c,d). The 5CB (4-cyano-4'-n-pentylbiphenyl) is crystalline below 18 ºC, but displays the nematic mesophase from 18 ºC up to 35 ºC, above which 5CB behaves like a conventional fluid. E7 is a mixture of four alkoxycyanobiphenyls (*n*CBs) with different aliphatic chain length: 51 wt.% 5CB, 25 wt.% 4-cyano-4'-*n*-heptyl-biphenyl (7CB), 16 wt.% 4-cyano-4'-*n*-oxyoctyl-biphenyl (8OCB) and 8 wt.% 4-cyano-4'-*n*-pentyl-p-terphenyl (5CT). The E7 exhibit nematic phase between -10 ºC to 60 ºC. The transition temperature from the nematic to the isotropic phase is known as the T_{NI}. In this study, we are primarily interested with these thermotropic nematic LCs for studying interfacial interactions.

The degree of order in a nematic LC is typically quantified by the orientational order parameter, S, which is defined as the average of the second Legendre polynomial (Equation 1.1).[47] The angle between the director and the local molecular orientation is defined by θ. For completely disordered (isotropic) sample, $S = 0$, while for a perfectly orientationally ordered sample, $S=1$. Typically values of S for LCs are 0.3 to 0.8. This order parameter is a way to quantify the degree of order in a LC and it affects the anisotropy of material properties such as birefringence or dielectric anisotropy.

$$\boldsymbol{S = \langle P_2(cos\theta)\rangle = \langle \frac{3cos^2\theta - 1}{2} \rangle} \quad (1.1)$$

1.5. Liquid crystal and their behavior at interfaces

The properties of nematic mesophase of calamatic LCs that make them promising class of materials for studying their interfacial interactions with biological systems are mentioned below.

1.5.1 Surface anchoring of liquid crystals

The orientational ordering of LCs is remarkably sensitive to the interfacial interactions exhibiting between the mesogens and the confining medium. This phenomenon is called surface induced anchoring of LCs. The lowest free-energy orientation of the director of a LC relative to the surface is commonly called the "easy axis" of the LC.[68-69] Application of external field on a LC in contact with a surface can cause a director to deviate from the easy axis, the amount of energy it takes to do so is determined by the anchoring energy, thus leading to the orientation-dependent free energy of the interface. The orientation dependence of the interfacial free energy is often described as [48,70]

$$\boldsymbol{S = S_0 + \frac{1}{2} W_a sin^2(\theta_s - \theta_e)} \quad 1.2$$

Where S is the interfacial free energy, S_0 is the interfacial free energy part that is independent of orientation, W_a is the anchoring energy, θ_s is the orientational of surface director and θ_e is the orientational of easy axis.

Past studies have established that the orientational ordering of LCs is typically controlled by orientation-dependent part of the surface energy on the scale of 10^{-3} to 1 mJ/m^2.[48,70,71] A subtle change in the topography and chemical functionality of a LC interface that perturb the interfacial energetics on this scale can, therefore, potentially lead to orientational transitions in LCs.

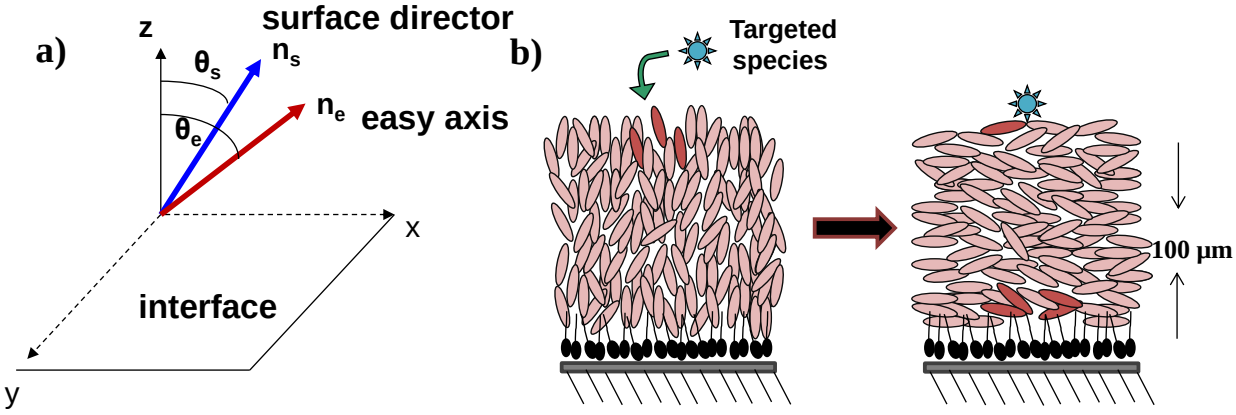

Figure 1.4 a) Orientation of the director and easy axis of the LC. b) Surface responsiveness of orientational ordering of nematic LCs to interfacial interactions.

Unlike isotropic liquids, this surface induced orientational preference is communicated over a distance of 100 µm from an interface (much greater than the size of nematic mesogen) as shown in Figure 1.4. This long-range orientational ordering of molecules lead to anisotropic optical properties that is easily transduced by using optical methods.[47,48]

1.5.2 Elasticity of liquid crystals

Elasticity of LCs is exhibited due to the long range orientational ordering of molecules in a LC phase. The lowest free energy state for a nematic is one in which all the mesogens are uniformly aligned with the director. Furthermore, uniform alignment may be incompatible with boundary conditions or external fields. The orientation of LC fixed at the confined boundary by surfaces (i.e., an infinite anchoring energy) typically leads to distortions of the director. Nematic LCs can undergo three basic deformations: splay, twist and bend as shown in Figure 1.5.

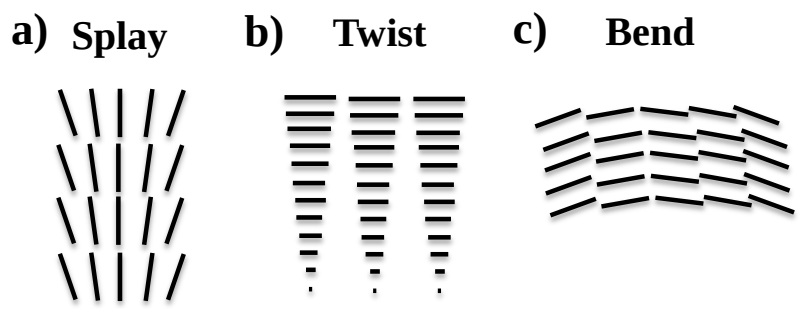

Figure 1.5 Schematic illustrations of three modes of strain of LCs: a) splay, b) twist and c) bend.

Understanding the energy of these deviations from uniform alignment is important to determine the equilibrium profile of the director of the nematic LCs. The situation is greatly simplified if we use a continuum approximation which is justified by the much larger length scale (~1 μm) over which the director deviates relative to the molecular size (~ 20 Å). The Frank and Oseen equation showed that in a confined LC system, an arbitrary curvature of a director can be described in terms of three basic types of deformation: splay, twist and bend with associated elastic constants K_{11}, K_{22} and K_{33}, respectively.[47] Each of these deformations has an associated elastic constant, which is in general temperature dependent. The LC elastic free energy density (F_d) associated with the strain of a nematic LC, namely,[48,70-72]

$$\boldsymbol{F_d} = \frac{1}{2}\boldsymbol{K_{11}}(\boldsymbol{\nabla} \cdot \underline{\boldsymbol{n}})^2 + \frac{1}{2}\boldsymbol{K_{22}}(\underline{\boldsymbol{n}} \cdot \boldsymbol{\nabla} \times \underline{\boldsymbol{n}})^2 + \frac{1}{2}\boldsymbol{K_{33}}\left(\underline{\boldsymbol{n}} \times (\boldsymbol{\nabla} \times \underline{\boldsymbol{n}})\right)^2 \qquad 1.3$$

Where *n* is the director of the nematic LC.

For a low molecular weight LC, the elastic constants are typically on the order of 10^{-11} N.[71] The relative importance of elastic energy stored within the LC film and orientation-dependent surface energetics contribution to the total free energy of LC depends on the geometry of the LC system and underlies many of the interesting interfacial phenomena.

1.5.3 Birefringence

LCs are birefringent due to their anisotropic nature. Birefringence is the property of all anisotropic materials,whether uniaxial or biaxial. Nematic LC fall within the uniaxial

category in which the index of refraction for light polarized is one direction is different from the other two.[48] The index of refraction for light polarized parallel and perpendicular to this direction is called the extraordinary index (n_e) and ordinary index (n_o), respectively. In a LC, n_e corresponds to $n_\parallel$ and n_o corresponds to $n_\perp$. The optical anisotropy of a material is defined as the difference between $\Delta n = (n_\parallel - n_\perp)$. The material is said to be positive uniaxial if the optical anisotropy is positive (n_e is greater than n_o in a uniaxial system). If the opposite is true, the material is said to be negative uniaxial. The two indices of refraction in a nematic LC equal the square root of the corresponding relative permittivities. Therefore, it is not the optical anisotropy or birefringence that is most directly related to the order parameter but the difference in the squares of the two indices $n_\parallel^2 - n_\perp^2$. For this reason, the quantity is frequently used to get an estimate of the order parameter. Therefore, when a light enters a LC phase (as LCs are birefringent) the light polarized parallel to the LC director will travel at a different velocity from the one polarized perpendicular to the LC director. This phenomenon forms a basis for examining the optical image of LCs using a simple polarized microscopy.

1.5.4 Anchoring angles of liquid crystals

The anchoring angle of LCs can be described by a polar angle, θ (out of plane) and an azimuthal angle, ϕ (in plane) as shown in Figure 1.6.[48]

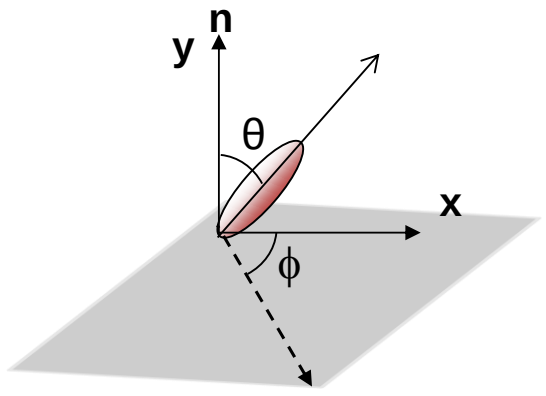

Figure 1.6 Schematic illustrations of a polar angle, θ (out of plane) and an azimuthal angle, ϕ (in plane).

Polar angle is the angle between the director (n̂) and the normal to the surface y. Polar anchoring can be of three types (1) planar anchoring ($\theta = 90°$), (2) homeotropic anchoring ($\theta = 0°$) and (3) tilted anchoring ($0° < \theta < 90°$). Azimuthal angle represents the in-plane orientation of the LC director with respect to a reference azimuthal axis x. Azimuthal anchoring can be of two types; (1) uniform anchoring where an averaged azimuthal orientation exists and (2) degenerate anchoring where all azimuthal orientations are equally probable.

1.6 Application of liquid crystals as sensor at liquid crystal-aqueous interfaces

Besides the use of LCs in displays, LCs have become promising tools in biological sensing area. The unique properties possessed by LCs include surface anchoring; elasticity and birefringence allow the potential of LC as biosensors for visual detection of biological molecules. Changes in the surface chemistries and topography of an analyte can change the surface anchoring of the LC. This change in the alignment of the molecules propagates from surface to bulk LC sample due to its elasticity. This alignment change of LC can be detected optically as LC molecules are birefringence. These properties permit LCs for label-free detection of targeted analytes with high sensitivity and without any use of complex and expensive instrumentations. In this thesis, we focused on interfaces between aqueous phases and thermotropic LCs because the mobility of molecules is high at aqueous interfaces and the interface is deformable. The advantage of the presence of the aqueous phase provides an environment that can preserve the activity of biological species.

Motivated by the potential utility of LC material as a tool in chemical and biological sensing, a variety of approaches have been used to create LC-aqueous interfaces for investigating interfacial phenomenon including planar interfaces created by stabilizing films of LCs in micro-fabricated structures.[16,17,20,28,73] These micro-fabricated structures include TEM grids, micro-wells and micro-pillars. This approach uses a metallic grid (copper/gold) supported on a chemically functionalized solid surfaces to form a stable LC film with a thickness that is approximately that of the metallic grid (Figure 1.7a). The underlying solid surface is treated to define the orientation of the LC on the bottom surface. For example, surfaces treated with octadecyltrichlorosilane (OTS) or N,N-dimethyl-N-octadecyl-3 aminopropyltrimethoxysilyl

chloride (DMOAP) give rise to homeotropic anchoring (Figure 1.7b)[17] whereas self-assembled monolayers (SAMs) formed from hexadecanethiol ($C_{16}H_{33}SH$) and many other alkanethiols on gold films will give rise to a planar orientation of the easy axis of the LC.[74] The pores of the grid provide a mechanically stable support for the LC and prevent dewetting of the thin film of LC. After capillary forces are used to fill the pores of the grid with LC, the supported LC film is immersed in an aqueous solution to create an approximately flat LC-aqueous interface. The director of the LC is shown inside one square of the grid. At the bottom of the LC film, the director of the LC is perpendicular to the surface (homeotropic alignment on OTS/DMOAP) and on the top surface the LC is shown with an orientation parallel to the interface.[17]

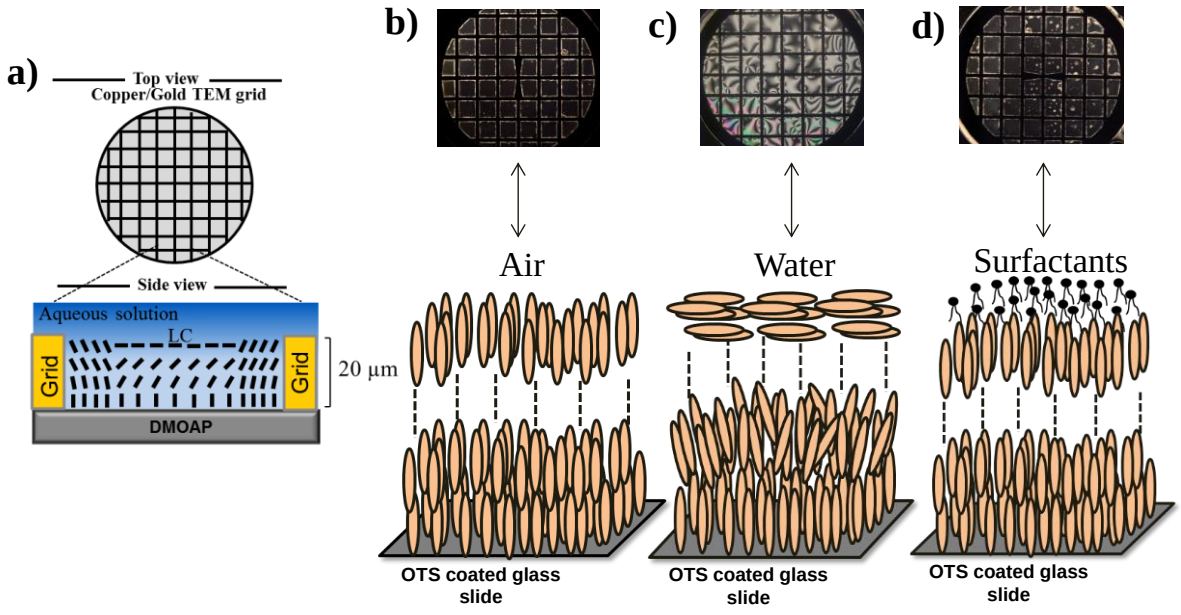

Figure 1.7 a) Schematic illustrations of an experimental system that can be used to create stable LC-aqueous interfaces. Optical image and cartoon representation of the anchoring of 5CB in contact with b) air, c) water and d) surfactants.

As a result hybrid anchoring conditions induce bright optical appearance (Figure 1.7c). Then, the influence of adsorbed biomolecules induces dark optical appearance which is consistent with the homeotropic (perpendicular) orientation of LC (Figure 1.7d). The influence of the molecular-level structure of biomolecules (mostly amphiphiles) adsorbed at the LC-aqueous

interface on the ordering of LCs has investigated to provide insight into the mechanisms of interaction that give rise to the homeotropic ordering.[17] This study also support for the hypothesis that the interaction of the LC with the amphiphiles is mediated primarily *via* the tail of the lipid.[20,75,76] In addition, the mobilities of molecules are far greater at LC-aqueous interfaces than at solid surfaces and then, studies of LC-aqueous interfaces can be used to unmask the influence of LCs on the interfacial organization of adsorbates.[77] It has been also revealed that the nematic elasticity of LCs can lead to changes in the phase behavior of lipid monolayers formed at these interfaces. This observation suggests that the manipulation of the elastic energy stored in a LC might enable active control of the organization and phase behavior of molecules at those interfaces. These aqueous interfaces of synthetic LCs can be used to explore the translation of these biological design principles to engineered systems. In addition, it provides an opportunity of reporting of biomolecular interactions through the triggering of ordering transitions in LCs at aqueous interfaces. Early studies in this area have shown that the LCs offer potentially important opportunities for the creation of biological sensors because LCs probe the structure of molecules present at interfaces.[17,23] For example, the ordering transitions triggered by the lipids assembled at LC-aqueous interfaces are easily differentiated from the ordering transitions triggered by proteins.[78] Furthermore, it is now clear that various aggregated states of proteins at the LC-aqueous interface can be clearly differentiated by the ordering of the LC.[17,78] In contrast, many existing principles for bio-sensing rely on the detection of the optical mass of molecules captured at an interface and are thus insensitive to the structure of analytes.

Another platform for LC biosensors in aqueous environment is LC droplets. The equilibrium director configuration within a LC droplet is governed by a delicate energetics balance that involves surface (orientation-dependent interfacial energy) and volumetric (bulk elastic energy) contributions (Figure 1.8). The orientation-dependent interfacial energy scales with the square of the droplet radius (WR^2; W is the anchoring strength coefficient and R is the droplet radius) whereas the bulk elastic energy of the LC droplet scales linearly with droplet radius (KR; K is the elastic constant of the LC).[71,79,80] These thermodynamic considerations lead to the prediction that LC droplets with $R < K/W$ will avoid spatial variation of the orientation of the LC within the droplet. Droplets with $R > K/W$ are large and contain defects

in equilibrium. Defects are localized regions of LC that partially melt in response to a high local elastic free energy density of the LC. Specifically, the cores of defects which are typically about 10 nm in size, possess levels of orientational order that are lower than that of the bulk LC.[81,82] In general, defects are easily identified in bright field micrographs of LC droplets because the defect cores, although nanoscopic in size, possess refractive indices that differ substantially from that of the surrounding LC and strongly scatter light. Therefore, defects are frequently used to aid in characterization of the director configuration of LC droplets. The contribution of defects to the total free energy of a droplet is typically two orders of magnitude lower than the surface anchoring and elastic energies and therefore, often neglected.

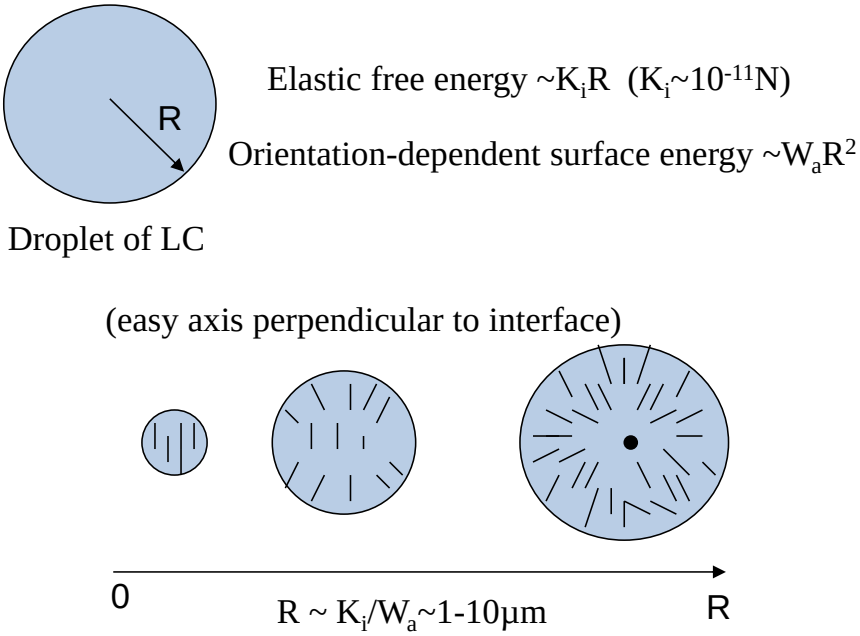

Figure 1.8 The interplay between the bulk effects and surface effects in LC phases can be illustrated with the simple example of a LC droplet.

Despite their small core energies, however, defects appear to play an important role in mediating the interactions of LC droplets with some biological amphiphiles.[83] Recent studies have shown that size-dependent ordering of LCs within micrometer-sized droplets that possess precisely defined sizes and interfacial chemistry.[84,85] The large surface areas, rich phases, well-defined director configurations and unique tunable optical properties of LC

droplets have been widely appreciated as an emerging design of functional LC materials that respond to remarkably low concentrations of specific biomolecular species.[83] These studies also reveal the importance of interactions of molecular species at defects in determining the configurations of LC droplets. These LC droplets have also been used as template for spherical and non-spherical polymeric and chemical patches.[86] This area is an exciting frontier of materials chemistry involving LCs that deserves additional studies.

1.7 Importance of Biomolecules addressed in this thesis

1.7.1 Endotoxin

Endotoxins are part of the outer membrane of the cell wall of Gram-negative bacteria.[87] The outer membrane acts as a protective permeability barrier and is impermeable to large molecules and hydrophobic compounds. Lipopolysaccharide (LPS) is essential to the function of the outer membrane. It establishes a permeability barrier and also prevents penetration of the bacteria by bile salts and other toxic molecules. It also acts as barrier to lysozyme and many anti-microbial agents. In an animal host, it may impede destruction of the bacterial cells by serum components and phagocytic cells. The biological activity of endotoxin is associated with the LPS. LPS is composed of two major parts, the hydrophobic lipid A portion and the hydrophilic polysaccharide portion (commonly called the "O" region). The structure of the lipid A portion is fairly well conserved and has been shown to be responsible for numerous *in vivo* and *in vitro* effects of endotoxin. But the nature (length and chemical composition) of the polysaccharide side chain varies between genera, species, and even strains of gram-negative bacteria and corresponds to its immunogenicity.[87,88] LPS elicits a variety of inflammatory responses so it may be a part of the pathology of gram-negative bacterial infections. *In vivo*, gram-negative bacteria probably release minute amounts of endotoxin when the bacteria die or grow. This may be important in the stimulation of natural immunity.

Endotoxin is playing a very important role in developing sepsis. When it enters the bloodstream it will be phagocytosed by macrophages. The macrophages will produce mediators like tumor necrosis factor, interleukin, platelet activating factor, thromboxane A2

and reactive oxygen species.[88] These mediators induce the septic syndrome with fever, hypothermia, tachycardia, tachypnoea, oliguria, acidosis and hypotension. This severe illness could lead to septic shock and multiple organ failure (MOF).[88] Low activities of endotoxin stimulate the immune response, higher activities can lead to septic shock.[88] Endotoxin is suspected in some environmental investigations as a possible cause for the sick building syndrome. A reliable and precise method is needed to introduce endotoxin activity limits.

1.7.2 Phosphatidylcholine

Phosphatidylcholine (PC) is a ubiquitous, naturally occurring phospholipid molecule and are the primary building blocks of cellular membranes.[89] PC is important for normal cellular membrane composition and repair. PC's role in the maintenance of cell-membrane integrity is vital to all of the basic biological processes. PC is also the major delivery form of the choline. Choline is an essential nutrient and a precursor in the synthesis of the neurotransmitter acetylcholine that allows nerve cells to communicate with muscles and each other and is essential for proper heart and brain function.[90] PC is also necessary for the production of surfactants which are critical for lung function and gastrointestinal health.[91] PC is involved in the hepatic export of very-low-density lipoproteins. PC is also required for many vital functions in the cardiovascular, reproductive, immune and nervous systems. PC is also used for treating hepatitis, eczema, gallbladder disease, circulation problems, high cholesterol and premenstrual syndrome; for improving the effectiveness of kidney dialysis; for boosting the immune system and for preventing aging. Research indicates PC's most beneficial role is in the prevention and treatment of various forms of liver disease and toxicity. PC is the primary active ingredient in cosmetic injection products used to "dissolve" fat which include Lipodissolve, Lipolight, Lipolyse, Lipotherapy and others. PC may be indicated to protect liver cells from viral damage, reduces fibrosis and prevents cell death from drugs, alcohol and other chemical toxins.[92-94] It may also be indicated for the treatment of some manic conditions. There is some evidence that PC may be useful in the management of Alzheimer's disease and some other cognitive disorders.[95] Alzheimer's disease has a diminished ability to synthesize or utilize the neurotransmitter acetylcholine, particularly in those areas of the brain related to memory. A possible future role in cancer therapy is also suggested by recent research.

1.7.3 Cardiolipin

Cardiolipin (diphosphatidylglycerol) is commonly referred to as the signature phospholipid of mitochondria.[96,97] Mitochondria are organelles that synthesize ATP *via* oxidative phosphorylation.[98] The mitochondrion has a complex double membraned structure called as inner membrane and outer membrane. The outer membrane forms a smooth permeable lipid surface of mitochondria. In contrast, inner membrane is virtually impermeable and therefore highly selective. Alterations in mitochondrial structure directly affect mitochondrial functions. Cardiolipin (CL) is exclusively exposed to the cytoplasmic side. The enrichment of CL in the inner membrane, specifically in the matrix side, is of great significance for the organization and operation of the electron transport chain and oxidative phosphorylation. In this phospholipid, a glycerol molecule acts as a bridge between the phosphate groups of two phosphatidic acid molecules.

The mitochondrial electron transport chain coupled to ATP synthesis is responsible for conversion of the chemical energy of sugars, amino acids and fatty acids into ATP.[99-101] The decline in this mitochondrial function is thought to be the basis for aging and many complex diseases. An interesting observation is that mitochondrial CL is known to be required for normal mitochondrial bioenergetics and its peroxidation and depletion are thought to contribute to age-related decline in mitochondrial function. The key functions of CL are to support spatial organization of mitochondrial cristae to create the proton trap necessary for sustaining the proton gradient and ATP synthesis and to facilitate optimal electron transfer among the redox partners by acting as a platform for assembly of respiratory complexes and super-complexes. Many of the respiratory complexes require CL for optimal function. Indeed, an even increasing number of evidences show that CL is very susceptible to oxidative damage with several consequences to mitochondrial and cellular functions. CL facilitates electron transfer from Complex III to Complex IV as it plays an important role in anchoring cytochrome *c* (cyt *c*) to the inner mitochondrial membrane. Cyt *c* is the only non-integral soluble protein of the electron transport chain on the inner mitochondrial membrane which transfers electrons from complex III to complex IV. While coenzyme Q within the inner mitochondrial membrane facilitates electron transfer from complex I to complex III. CL provides an anionic platform for electrostatic interaction with the highly cationic cyt *c* so

that it is loosely attached to the electron transport chain. Under normal physiological conditions, the electrostatic interaction of cyt *c* with CL is supported by high levels of ATP. However, in pathological conditions such as ischaemia ATP concentration decreases, cyt *c* becomes tightly associated with CL *via* hydrophobic interactions.[101] This cyt *c*/CL complex results in unfolding of cyt *c* and restoring π-π* interaction within cyt *c* to facilitate electron transfer and converts cyt *c* from an electron carrier into a peroxidase/oxygenase which cannot participate in electron transfer. As a peroxidase, cyt *c* serves to catalyze the oxidation of CL. Oxidized CL causes alterations in the mitochondrial inner membrane structure which promotes detachment of cytochrome *c*. Targeting and optimizing CL and the cyt *c*/CL complex represents a novel and innovative approach for the treatment of mitochondrial related dysfunction and bioenergetic failure. Thus, the study of CL is potentially important for therapeutical and clinical point of view.

1.7.4 Cells

Cells are the structural and functional units of all living things from microorganisms to humans and they are considered the smallest form of life. Cells found in animals, plants, fungi and some single-celled organisms are called as eukaryotic cells. These cells possess a number of internal structures called organelles. The most prominent organelle is the nucleus which contains the cell's genetic material, DNA. Nucleus controls all cell activities. Another type of cell is known as prokaryotic cells found in bacteria and Archaea which are both groups of single-celled microorganisms. These cells lack nucleus and other organelles and tend to be smaller than eukaryotic cells. In addition to the nucleus, the human cell (eukaryotic type) contains other important organelles like cell membrane, cytoplasm, mitochondria, ribosomes, endoplasmic reticulum, vesicles, Golgi bodies etc. These cellular organelles work together to carry out life functions. Each organelle and cell part has a specific role within a cell. This role is important to the proper functioning of both the cell and the organism. For example, cell membrane separates the inside of the cell from the external environment, controls the flow of materials into and out of the cell. Cytoplasm includes the organelles and other life-supporting materials such as sugar and water, all contained by the cell membrane. Mitochondria's function is to convert energy from food to the body's main energy source, adenosine triphosphate (ATP). Ribosomes are molecular factories that make

proteins, which make up much of a cell's structure and are required for activities necessary for the cell's survival. Endoplasmic reticulum a network of membrane-covered channels that transport materials made in the cell is connected to the nucleus. Vesicles membrane-covered sacs that transport and/or store materials inside the cell and sometimes help these materials cross the cell membrane to enter or exit the cell. Golgi body sorts and packages proteins from endoplasmic reticulum and send them to their final destination inside the cell (within the cell or outside the cell). Cells represent the biological machinery that makes the proteins, chemicals and signals responsible for everything happening inside our bodies. Thus, to study cells helps us to understand how organisms including humans function. It helps us to protect cells to prevent infection and other harmful effects, observe cells to diagnose disease, treat cells to heal illnesses and stop harming cells through our choices and actions. For example, diseases such as the meningitis, malaria, diabetes, a type of cancer, cystic fibrosis, or Alzheimer's and their disorders are caused by problems at a cell or molecular level. Physical damage such as a burn or broken bone also causes damage at cell level. Monitoring cell functions and cell-to-cell communication in the cellular environment has enormous implications for cell biology and regenerative medicine.[102,103] By understanding how cells work in healthy and diseased states, cell biologists working in animal, plant and medical science will be able to develop new vaccines, more effective medicines, plants with improved qualities and through increased knowledge a better understanding of biological processes that keep us healthy and shed light on new ways to treat disease. Cellular research has already led to cancer therapies, antibiotics, cholesterol-lowering medicine and improved drug delivery systems. However, monitoring cellular function in real time and much more remains to be discovered.

1.8 Characterization Techniques

1.8.1 Polarizing Optical Microscopy (POM)

POM is a simple and useful technique to characterize and quantify the orientations of LCs. The interpretation of the optical appearance of LCs is determined in terms of orientational preference. In this technique, a LC sample is placed in between two polarizers where the bottom polarizer linearly polarizes a light from a light source while the top polarizer

(analyzer) is arranged to orient perpendicular against the bottom one. LCs are birefringent, i.e., possess two direction-dependent indices of refraction and depending on the orientation of the LC relative to the plane of polarization of light, may rotate the plane of polarization of the transmitted light.[46,47]

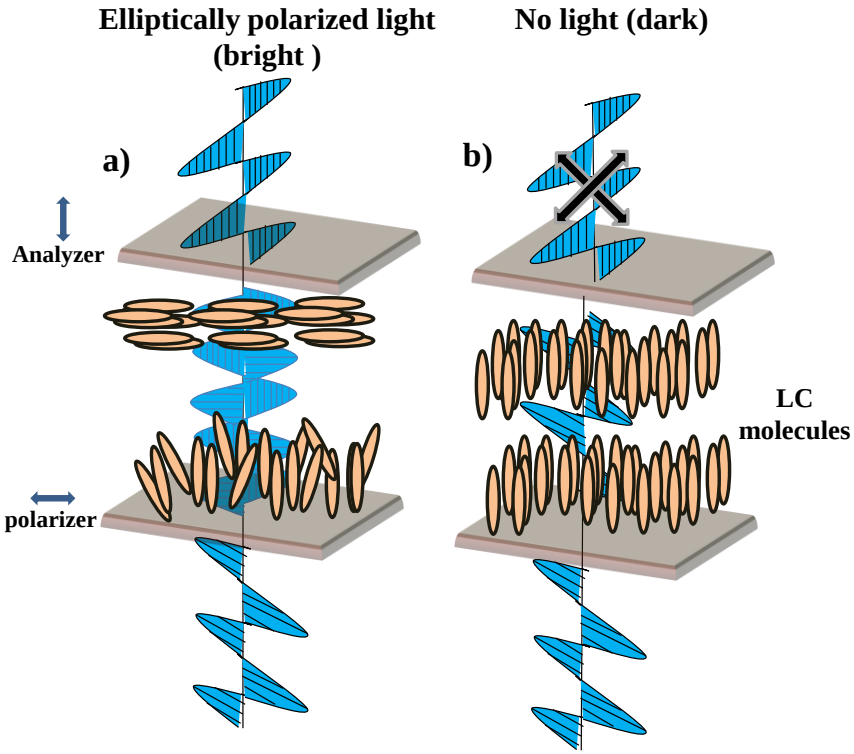

Figure 1.9 The working principle of polarized optical microscope under crossed-polarizers. The optical output of the anchoring conditions of LCs a) tilted anchoring and b) homeotropic anchoring between polarizer and analyzer.

A variety of anchoring conditions of LCs is often described as homeotropic (normal to the interface), planar (parallel to the interface) or tilted (at some acute angle to the interface). Homeotropic anchoring is where the LC molecules are oriented such that their long axes are normal to the supporting substrate. When the LC molecules are so oriented polarized light will be fully blocked by the analyzer and the corresponding LC optical texture appears uniformly dark even upon a 360° rotation of the samples (Figure 1.9a). Tilted anchoring is where the LC molecules exhibit tilt as the orientation of the LC molecules is perpendicular to the surface (homeotropic alignment on OTS/DMOAP) and on the top surface, the LC

molecules oriented parallel to the interface. When the LC molecules are so oriented, a thin film of the LC exhibits birefringence and colored texture results when viewed under crossed polarizers (Figure 1.9b).

1.8.2 Polarization modulation infrared reflection absorption spectroscopy (PM-IRRAS)

PM-IRRAS is a spectroscopic measurement technique for characterizing the chemical structure and molecular orientation of thin films and monolayers on reflecting surfaces (mostly metal substrates).[104] This technique is based on the modulation of a linearly polarized infrared beam which is divided into a s-polarized beam (with its electric field parallel to the sample surface) and a p-polarized beam (with its electric field perpendicular to the sample surface). The absorption of IR light by a molecule adsorbed on a metal surface is also influence by the dielectric behavior of the metal. On the metallic surface the electric field of the incident light and the dipole moment of the adsorbed molecule interact with the metal electrons, thus imposing a strict dipole selection rule, also known as metal surface selection rule. According to this selection rule, only the vibrations with a dynamic dipole moment component perpendicular to the surface will be excited whereas dynamic dipole moment component parallel is screened by metal electrons which can generate an image dipole oriented opposite to those of the molecule. The advantage of the fact is that the adsorbate or the thin layer on the reflecting metallic substrate interacts mainly with p-polarized light species on the metal whereas s-polarized light vanishes due to destructive interference. Moreover, at grazing angle of incidence, the absorption of p-polarized infrared radiation by a thin film on a metal surface is enhanced so that even sub monolayer quantities of chemisorbed species can be observed in the p-polarized infrared reflectance spectrum. In contrast, at a high angle of incidence, the absorption of s-polarized radiation by the same film is virtually zero. This polarization disparity has been used to deduce the average molecular orientation and conformation of monolayers of molecules adsorbed onto metals. In addition, it is able to discriminate surface contributions from the isotropic gas phase as the molecules in an isotropic gas environment can absorb both p-polarized and s-polarized IR light as shown in Figure 1.10. Besides orientation measurements, the greatly increased absorption of p-polarized over s-polarized radiation by thin films at the metal surface can be utilized to obtain the differential reflectance spectrum of the adsorbed surface species by polarization

modulation (PM) of the incident light. The PM-IRRAS measurements at grazing incidence yield a sensitive and surface-selective method for obtaining infrared reflection-absorption spectra of very thin films on metal substrates.

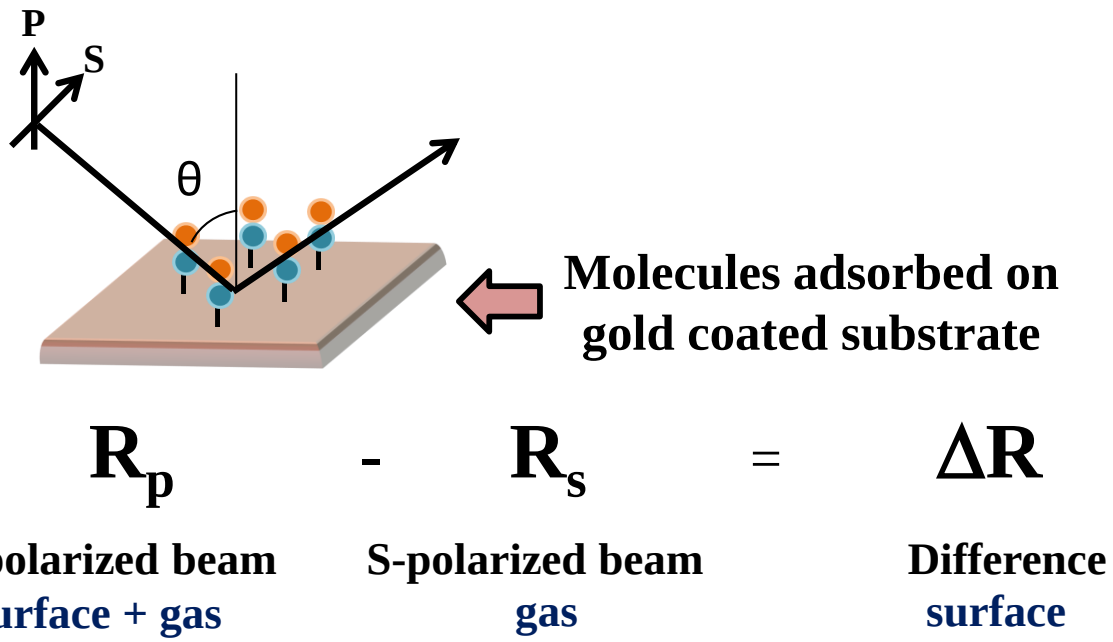

Figure 1.10 Working principle of PM-IRRAS.

In this thesis, we have performed PM-IRRAS measurements on micro-pillar assembly to provide the additional evidence of intermolecular and conformational insight of the built interface. Micro-pillars are arrays of micro-fabricated structures having large surface area and spatially distinct surface topography (Figure 1.11). However, because of their small dimensions and large aspect ratio these structures cause high surface area to volume ratio. Therefore, they are susceptible to surface forces such as liquid capillary forces when immersed and dried from the liquid.[105-107] The approaches to form LC thin films for sensing include manually pipetting LC into the square openings of a transmission electronic microscopy (TEM) grid or using arrays of micro-fabricated pillars to stabilize thin LC film.[108] Therefore, we have found that micro-pillar assembly as a better choice than grid assembly for PM-IRRAS measurements.

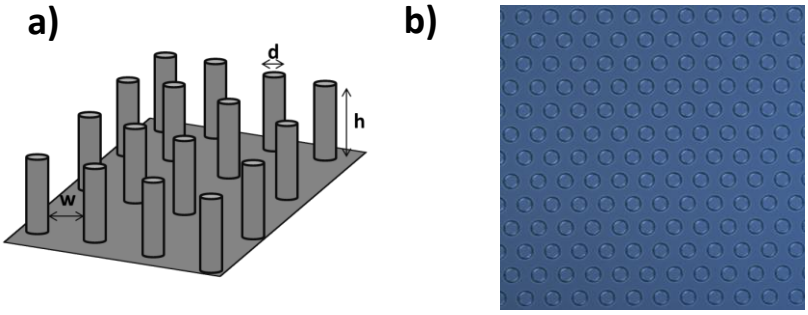

Figure 1.11 Schematic (side view) and b) optical micrograph of micro-pillar assembly.

1.9 Outline of Thesis

The result described in this thesis explores the use of thermotropic LCs for probing and imaging molecular-scale interactions occur at LC-aqueous interface. LC-based system is a promising platform for chemical and biological sensing due to the unique properties of LCs. In this thesis, enthused by the budding utility of LC materials in biological applications (particularly, reporting biological interactions), we address progress that has been made toward the design of interfaces of LC materials such that desired interactions are realized between the LC materials and biological systems. Here, we focused on the design and modulation of LC-based interfaces that are anticipated with the better approaches for developing LC-based stimuli responsive materials.

Second chapter advances the design of stimuli-responsive materials based on colloidal particles dispersed in LCs. We demonstrate that the thin films of CLC gel are stable under water and can be driven through anchoring transitions by adsorbates at LC-aqueous interfaces. In particular, we have shown that films of CLC gels undergo easily visualized ordering transition in presence of a bacterial phospholipid such as LPS (endotoxin). These composite LC materials are robust, can be easily molded and thus offer a general and facile approach to the preparation of free LC interfaces suitable for the design of responsive materials.

We also found that response of the domains of the LCs within the CLC gels vary significantly, suggesting that manipulation of domain and shape may provide the basis of

general and facile method to tune the response of these LC composite materials to interfacial phenomena. Specifically, we observed that LC domain size depends on two factors. First, the wt. % of colloidal particles (here PS microspheres) in CLC gels and second, the nature (hydrophilic/hydrophobic) of the chemically functionalized glass substrates on which gels are formed. It was found that larger domains (more free interfaces to interact with external stimuli) produce faster responses over smaller domains, as expected. In contrast, very small size LC domains do not span the thickness of the CLC gels and thus the orientation of the LC is not under control of the external surfaces of these domains.

Third chapter reports a new pathway for the easy formation of spontaneous uniform LC droplets. While the techniques reported in the past have resulted in the preparation of LC droplets with a life span of a few hours, our approach has provided LC droplets with a stability of days to months. We observed the spontaneous formation of well-developed LC droplets with radial defects in the presence of phosphatidylcholine (PC) within the confined boundary created by a grid system. The study also shows that the response of these droplets due to the interactions between an enzyme and the topological defects in the LC may be exploited in applications such as sensing.

Fourth chapter provides an investigation of interfacial phenomena occurring at LC-aqueous interfaces that triggers an orientational ordering transition of the LC in the presence of cardiolipin (CL) by varying pH, salt concentration and valence. In particular, the effects of three different conformational isomeric forms of the CL are observed to cause the response of the LC ordering to vary significantly from one to another at those interfaces. Fluorescence microscopy measurements further suggest that pH-dependent conformational forms of the CL have different ability to self-assemble at LC-aqueous interfaces leading to dissimilar orientational behavior of the LC. Langmuir−Blodgett (LB) and polarization modulation infrared reflection absorption spectroscopy (PM-IRRAS) measurements provide further insight in modulation of the lipid packing efficiency and alkyl chain conformation of the CL at different pH and ionic conditions. Overall, these results offer a promising approach to differentiate different conformations (label free detection) of the CL through ordering transition of the LC at LC-aqueous interfaces.

In fifth chapter we report a simple methodology to produce biocompatible LC droplets through Poly-*l*-Lysine (PLL)-LC interactions *in situ* for reporting presence of cells and to monitor the interaction of cells with their environments in real time. Polarization modulated infrared reflection absorption spectroscopy (PM-IRRAS) revealed that LCs containing nitrogen atoms form hydrogen bonds with PLL that provide dynamic LC response in aqueous media mediated by topological defects in those droplets. We fabricated biocompatible PLL-coated LC droplets in micrometer range that affords the detection of cells and cell-environment interactions. The biocompatibility of these PLL-coated LC droplets has been determined using flow cytometry which exhibit their potential to move in cellular environment. In addition, the responsive PLL-coated droplets have been used as a template for reporting Annexin-V PS interaction (a tool to measure apoptosis) as a proof of example. The findings presented in this chapter suggest that PLL-LC interaction in aqueous media could provide a simple and versatile route towards building cell-based therapeutics.

Sixth chapter demonstrates that PLL-modified LC emulsion droplets can be used as exquisitely sensitive reporters for the selective detection of heparin and protamine. The heparin selectively binds over the PLL-coated LC droplets that results an ordering transition from radial to bipolar as characterized from polarizing optical microscopy. Addition of protamine onto heparin adsorbed PLL-coated droplets causes a reordering of the LCs due to the stronger affinity of heparin to protamine. Fluorescence microscopy and zeta potential measurements were performed to characterize the adsorption of these proteins on PLL-laden LC droplets. In summary, we found that PLL-modified LC emulsion droplets can act as a potential tool for sensitive and selective detection of heparin and protamine for laboratory and bedside diagnosis.

References

(1) Fan, X.; White, I. M.; Shopova, S. I.; Zhu, H.; Suter, J. D.; Sun Y. *Anal. Chim. Acta* **2008**, *620*, 8–26.

(2) Velasco-Garcia, M. N. *Sem. Cell Dev. Biol.* **2009**, *20*, 27–33.

(3) Bozzini, S.; Petrini, P.; Tanzi, M. C.; Zürcher, S.; Tosatti, S. *Langmuir* **2009**, *26*, 6529−6534.

(4) Prime, K. L.; Whitesides, G. M. *Science* **1991**, *252*, 1164−1167.

(5) Li, L. Y.; Chen, S. F.; Zheng, J.; Ratner, B. D.; Jiang, S. Y. *J. Phys. Chem. B* **2005**, *109*, 2934−2941.

(6) Kühnau, U.; Petrov, A. G.; Klose, G.; Schmiedel, H. *Phys. Rev. E* **1999**, *59*, 578−585.

(7) Stuart, M. A. C.; Huck, W. T. S.; Genzer, J.; Muller, M.; Ober, C.; Stamm, M.; Sukhorukov, G. B.; Szleifer, I.; Tsukruk, V. V.; Urban, M.; Winnik, F.; Zauscher, S.; Luzinov, I.; Minko, S. *Nat. Mater.* **2010**, *9*, 101−113.

(8) Bhat, R. R.; Chaney, B. N.; Rowley, J.; Liebmann-Vinson, A.; Genzer, J. *Adv. Mater.* **2005**, *17*, 2802−2807.

(9) Halstenberg, S.; Panitch, A.; Rizzi, S.; Hall, H.; Hubbell, J. A. *Biomacromolecules* **2002**, *3*, 710−723.

(10) Curtis, A.; Wilkinson, C. *Biomaterials* **1997**, *18*, 1573−1583.

(11) Vollrath, F.; Knight, D. P. *Nature* **2001**, *410*, 541−548.

(12) Chapman, D. Ann. N.Y. *Acad. Sci.* **1966**, *137*, 745−754.

(13) Dogic, Z.; Fraden, S. *Langmuir* **2000**, *16*, 7820−7824.

(14) Nakata, M.; Zanchetta, G.; Chapman, B. D.; Jones, C. D.; Cross, J. O.; Pindak, R.; Bellini, T.; Clark, N. A. *Science* **2007**, *318*, 1276−1279.

(15) Zanchetta, G.; Nakata, M.; Buscaglia, M.; Bellini, T.; Clark, N. A. *Proc. Natl. Acad. Sci. U.S.A.* **2008**, *105*, 1111−1117.

(16) Brake, J. M.; Abbott, N. L. *Langmuir* **2002**, *18*, 6101−6109.

(17) Brake, J. M.; Daschner, M. K.; Luk, Y. Y.; Abbott, N. L. *Science* **2003**, *302*, 2094−2097.

(18) Brake, J. M.; Daschner, M. K.; Abbott, N. L. *Langmuir* **2005**, *21*, 2218−2228.

(19) Kim, E. B.; Lockwook, N.; Chopra, M.; Guzman, O.; Abbott, N. L.; de Pablo, J. J. *Biophys. J.* **2005**, *89*, 3141-3158.

(20) Lockwood, N. A.; de Pablo, J. J.; Abbott, N. L. *Langmuir* **2005**, *21*, 6805-6814.

(21) Lockwood, N. A.; Mohr, J. C.; Ji, L.; Murphy, C. J.; Palecek, S. P.; de Pablo, J. J.; Abbott, N. L. *Adv. Funct. Mater.* **2006**, *16*, 618-824.

(22) Park, J. S.; Teren, S.; Tepp, W. H.; Beebe, D. J.; Johnson, E. A.; Abbott, N. L. *Chem. Mater.* **2006**, *18*, 6147−6151.

(23) Brake, J. M.; Abbott, N. L. *Langmuir* **2007**, *23*, 8497−8507.

(24) Kinsinger, M. I.; Sun, B.; Abbott, N. L.; Lynn, D. M. *Adv. Mater.* **2007**, *19*, 4208-4212.

(25) Park, J. S.; Abbott, N. L. *Adv. Mater.* **2008**, *20*, 1185−1190.

(26) Price, A. D.; Schwartz, D. K. *J. Am. Chem. Soc.* **2008**, *130*, 8188−8194.

(27) Birchall, L. S.; Ulijn, R. V.; Webb, S. J. *Chem. Commun.* **2008**, 2861−2863.

(28) Sivakumar, S.; Wark, K. L.; Gupta, J. K.; Abbott, N. L.; Caruso, F. *Adv. Funct. Mater.* **2009**, *19*, 2260−2265.

(29) Lin, I. H.; Meli, M. V.; Abbott, N. L. *J. Colloid Interfaces Sci.* **2009**, *336*, 90-99.

(30) Gupta, J. K.; Zimmerman, J. S.; de Pablo, J. J.; Caruso, F.; Abbott, N. L. *Langmuir* **2009**, *25*, 9016-9024.

(31) Bi, X.; Hartono, D.; Yang, K. L. *Adv. Funct. Mater*. **2009**, *19*, 3760-3765.

(32) Hartono, D.; Qin, W. J.; Yang, K. L.; Yung, L. Y. L. *Biomaterials* **2009**, *30*, 843−849.

(33) Hartono, D.; Lai, S. L.; Yang, K. L.; Yung, L. Y. L. *Biosens. Bioelectron.* **2009**, *24*, 2289-2293.

(34) Hartono, D.; Xue, C. Y.; Yang, K. L.; Yung, L. Y. L. *Adv. Funct. Mater*. **2009**, *19*, 3574-3579.

(35) Kinsinger, M. I.; Buck, M. E.; Abbott, N. L.; Lynn, D. M. *Langmuir* **2010**, *26*, 10234-10242.

(36) Bi, X.; Yang, K. L. *Biosens. Bioelectron.* **2010**, *26*, 107-111.

(37) Tan, L. N.; Bertics, P. J.; Abbott, N. L. *Langmuir* **2010**, *27*, 1419-1429.

(38) Tan, H.; Yang, S.; Shen, G.; Yu, R.; Wu, Z. *Angew. Chem. Int. Ed.* **2010**, *49*, 8608-8611.

(39) Omer, M.; Khan, M.; Kima,Y. K.; Lee, J. H.; Kang, I. K.; Park, S.-Y. *Colloids Surf. B: Biointerfaces* **2014**, *121*, 400–408.

(40) Khan, M.; Park, S. Y. *Anal. Chem.* **2014**, *86*, 1493−1501.

(41) Omer, M.; Park, S.-Y. *Anal. Bioanal. Chem.* **2014**, *406*, 5369–5378.

(42) Khan, M.; Park, S.-Y. *Biosens. Bioelectron.* **2015**, *68*, 404–412.

(43) Munir, S.; Park, S.-Y. *Anal. Chim. Acta.* **2015**, *893*, 101-107.

(44) Munir, S.; Khan, M.; Park, S.-Y. *Sens. Actuators B.* **2015**, *220*, 508–515.

(45) Chandrasekhar, S. *Liquid Crystals*, Cambridge University Press, **1992**.

(46) Collings, P. J. *Liquid crystals: nature's delicate phase of matter*, Princeton University Press, **2002**.

(47) de Gennes, P. G.; Prost, J. *The physics of liquid crystals*, Oxford University Press, **1994**.

(48) Collings, P. J.; Hird, M. *Introduction to Liquid Crystals Chemistry and Physics*, Taylor & Francis: London, **1997**.

(49) Woltman, S. J.; Crawford, G. P.; Jay, G. D. *Liquid crystals: frontiers in biomedical applications*, World Scientific Publishing Company, **2007**.

(50) Gupta, V. K.; Skaife, J. J.; Dubrovsky, T. B.; Abbott, N. L. *Science* **1998**, *279*, 2077-2080.

(51) Shah, R. R.; Abbott, N. L. *Science* **2001**, *293*, 1296-1299.

(52) Yang, K. L.; Cadwell, K.; Abbott, N. L. *Sens. Actuator B-Chem.* **2005**, *104*, 50-56.

(53) Xu, H.; Bi, X. Y.; Ngo, X. M.; Yang, K. L. *Analyst* **2009**, *134*, 911-915.

(54) Reinitzer, F. *Monatsh. Chem.* **1888**, *9*, 421–441.

(55) Lehmann, O. *Flussige Kristalle*, Engelmann, Leipzig, **1904**.

(56) Ren, H. W.; Fan, Y. H.; Gauza, S.; Wu, S. T. *Opt. Commun.* **2004**, *230*, 267–271.

(57) Liu, Y. J.; Sun, X. W.; Shum, P.; Yin, X. J. *Opt. Express* **2006**, *14*, 5634–5640.

(58) Friedel, G. *Ann. Phys.* **1922**, *18*, 273-474.

(59) Kawamoto, H. *Proc. IEEE* **2002**, *90*, 460-500.

(60) Stewart, G. T. *Liq. Cryst.* **2003**, *30,* 541–557.

(61) Stewart, G. T. *Liq. Cryst.* **2004**, *31*, 443–471.

(62) Li, M.-H.; Keller, P.; Yang, J.; Albuoy, P.-A. *Adv. Mater*. **2004**, *16*, 1922-1925.

(63) Urayama, K.; Kondo, H.; Arai, Y. O.; Takigawa, T. *Phys. Rev. E* **2005**, *71*, 051713/1-051713/8.

(64) Terentjev, E. M.; Warner, M. *Eur. Phys. J. E* **2001**, *4*, 343-353.

(65) Stenull, O.; Lubensky, T. C. *Phys. Rev. E* **2004**, *69*, 051801/1-051801/13.

(66) Finkelmann, H.; Kim, S. T.; Munoz, A.; Palffy-Muhoray, P.; Taheri, B. *Adv. Mater.* **2001**, *13*, 1069-1072.

(67) Ikeda, T.; Tsutsumi, O. *Science* **1995**, *268*, 1873-1875.

(68) Jerome, B. *Rep. Prog. Phys.* **1991**, *54*, 391–451.

(69) Gupta, V. K.; Abbott, N. L. *Phys. Rev. E* **1996**, *54*, 4540–4543.

(70) Lockwood, N. A.; Gupta, J. K.; Abbott, N. L. *Surf. Sci. Rep.* **2008**, *63*, 255–293.

(71) Lavrentovich, O. D. *Liq. Cryst.* **1998**, *24*, 117-125.

(72) Poulin, P.; Weitz, D. A. *Phys. Rev. E* **1998**, *57*, 626-637.

(73) Cheng, D.; Sridharamurthy, S. S.; Hunter, J. T.; Park, J.-S.; Abbott, N. L.; Jiang, H. *J. Microelectromech. Syst.* **2009**, *18*, 973–981.

(74) Mullin, C. S.; Guyot-Sionnest, P.; Shen, Y. R. *Phys. Rev. A* **1989**, *39*, 3745-3747.

(75) Fletcher, P. D. I.; Kang, N. G.; Paunov, V. N. *ChemPhysChem* **2009**, *10*, 3046–3053.

(76) Brake, J. M.; Mezera, A. D.; Abbott, N. L. *Langmuir* **2003**, *19*, 6436–6442.

(77) Brake, J. M.; Daschner, M. K.; Abbott, N. L. *Langmuir* **2005**, *21*, 2218−2228.

(78) De Tercero, M. D.; Abbott, N. L. *Chem. Eng. Commun.* **2009**, *196*, 234–251.

(79) Huang, W.; Tuthill, G. F. *Phys. Rev. E* **1994**, *49*, 570−574.

(80) Drzaic, P. S. *Liquid Crystal Dispersions*; World Scientific Publishing Company: Singapore, **1995**.

(81) Ruhwandl, R. W.; Terentjev, E. M. *Phys. Rev. E* **1997**, *56*, 5561−5565.

(82) Zhang, Z. X.; van Duijneveldt, J. S. *Soft Matter* **2007**, *3*, 596−604.

(83) Lin, I. H.; Miller, D. S.; Bertics, P. J.; Murphy, C. J.; de Pablo, J. J.; Abbott, N. L. *Science* **2011**, *332*, 1297−1300.

(84) Gupta, J. K.; Sivakumar, S.; Caruso, F.; Abbott, N. L. *Angew. Chem. Int. Ed.* **2009**, *48*, 1652−1655.

(85) Sivakumar, S.; Gupta, J. K.; Abbott, N. L.; Caruso, F. *Chem. Mater.* **2008**, *20*, 2063−2065.

(86) Mondiot, F.; Wang, X.; de Pablo, J. J.; Abbott, N. L. *J. Am. Chem. Soc.* **2013**, *135*, 9972−9975.

(87) Raetz, C. R.; Whitfield, C. *Annu. Rev. Biochem.* **2002**, *71*, 635-700.

(88) Cohen, J. *Nature* **2002**, *420*, 885-891.

(89) Dowhan, W. *Annu. Rev. Biochem.* **1997**, *66*, 199–232.

(90) Canty, D. J.; Zeisel, S. H. *Nutr. Rev.* **1994**, *52*, 327-339.

(91) Kanno, K.; Wu1, M. K.; Scapa, E. F.; Roderick, S. L.; Cohen, D. E. *Biochim. Biophys. Acta.* **2007**, *1771*, 654–662.

(92) Hanin, I.; Ansell, G. B. eds. *Lecithin. Technological, Biological and Therapeutic Aspects.* New York and London: Plenum Press; **1987**.

(93) Jenkins, P. J.; Portmann, B. P.; Eddleston, A. L.; Williams, R. *Liver* **1982**, *2*, 7-81.

(94) Lieber, C. S.; De Carl, L. M.; Mak, K. M.; Kim, C.-I.; Leo, M. A. *Hepatol.* **1990**, *12*, 1390-1398.

(95) Little, A.; Levy, R.; Chuaqui-Kidd, P. H.; Hand, D. *J. Neur. Neurosurg. Psych.* **1985**, *48*, 736-742.

(96) Daum, G. *Biochim. Biophys. Acta* **1985**, *822*, 1–42.

(97) Hoch, F. L. *Biochim. Biophys. Acta* **1992**, *1113*, 71–133.

(98) Houtkooper, R. H.; Vaz, F. M. *Cell. Mol. Life Sci.* **2008**, *65*, 2493–2506.

(99) Paradies, G.; Paradies, V.; Benedictis, V. D.; Ruggiero, F. M.; Petrosillo, G. *Biochim. Biophys. Acta* **2014**, *1837*, 408–417.

(100) Ren, M.; Phoon, C. K. L.; Schlame, M. *Prog. Lipid Res* **2014**, *55*, 1–16.

(101) Birk1, A. V.; Chao1, W. M.; Bracken, C.; Warren, J. D.; Szeto1, H. H. *Br. J. Pharmacol.* **2014**, *171*, 2017–2028.

(102) Halin, C.; Mora, J.; Sumen, C.; von Andrian, U. *Annu. Rev. Cell. Dev. Biol.* **2005**, *21*, 581–603.

(103) Cook, B. N.; Bertozzi, C. R. *Bioorg. Med. Chem.* **2002**, *10*, 829–840.

(104) Frey, B. L.; Corn, R. M.; Weibel, S. C. *Polarization−Modulation Approaches to Reflection−Absorbtion Spectroscopy.* In Handbook of Vibrational Spectroscopy;

Chalmers, J., Griffins, P. R., Eds.; John Wiley & Sons: Chichester, U.K., **2001**; Vol. 2, p 1042.

(105) Cesa, C. M.; Kirchgessner, N.; Mayer, D.; Schwarz, U. S.; Hoffmann, B.; Merkel, R. *Rev. Sci. Instrum*. **2007**, *78*, 034301/1-034301/10.

(106) du Roure, O.; Saez, A.; Buguin, A.; Austin, R. H.; Chavrier, P.; Siberzan, P.; Ladoux, B. *Proc. Natl. Acad. Sci. U.S.A.* **2005**, *102*, 2390-2395.

(107) Chandra, D.; Yang, S. *Acc. Chem. Res.* **2010**, *43*, 1080-1091.

(108) Sridharamurthy, S. S.; Cadwell, K. D.; Abbott, N. L.; Jiang, H. *Smart Mater. Struct*. **2008**, *17*, 012001/1-012001/4.

Chapter 2

Thin Films of Colloid-in-Liquid Crystal Gels for Optical Amplification of Biomolecular Interactions

A novel self-supporting liquid crystal-aqueous interface formed from the thin films of micro-structured colloid-in-liquid-crystal (CLC) gels were prepared that contain micrometer sized dynamic domains of nematic LC are stable under water and undergo surface-driven ordering transitions in presence of bacterial endotoxin. The structural manipulation of domain size and shape of thin films of CLC gels provide the basis of a general and facile method to tune the sensitivity of response of these LC composite materials to interfacial phenomena. These CLC gels are mechanically robust and can be easily molded; we believe this class of composite LC material may be broadly useful for the design of chemically-responsive devices.

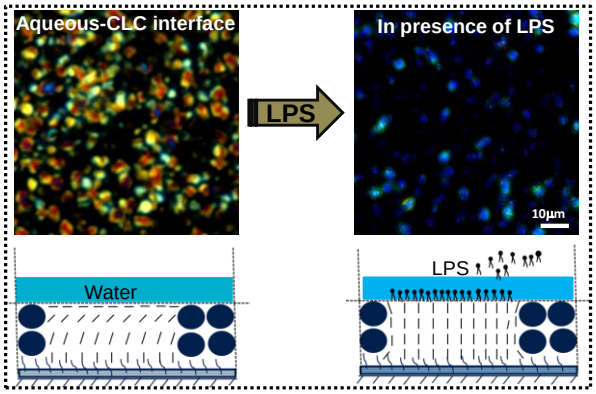

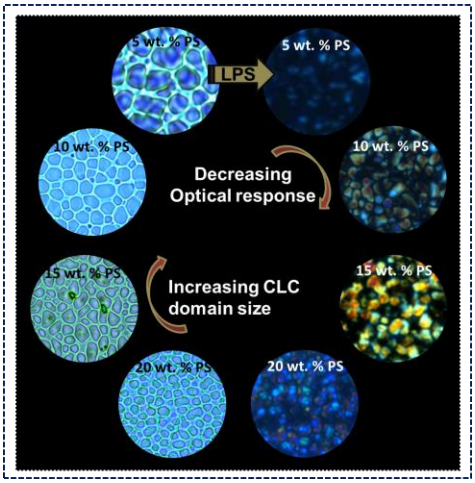

Thin Films of Colloid-in-Liquid Crystal Gels for Optical Amplification of Biomolecular Interactions

2.1 Introduction

Liquid crystal (LC) phases used as solvent for colloidal particles provide new ways of control over the spatial organization of colloidal systems. The difference from ordinary colloid arises from long-range nature of the orientational order in LCs which is responsible for many fascinating optical, electrical and mechanical properties of these materials[1] and the resulting structure in the colloid. The interaction between the colloidal particles in a structured fluid such as LC has recently attracted many researchers from both fundamental and applied point of view. When the colloidal particles are dispersed in a nematic LC, they disrupt the nematic order and minimization of the elastic energy leads to the formation of anisotropic colloidal structures.[2] When the particles are sufficiently large depending on the strength and direction of the nematic anchoring on the particle surface, various types of topological defects (such as a hyperbolic *hedgehog*, a Saturn ring, and boojums) have been formed.[3-8] The behavior of colloid is determined by the dimensionless parameter WR/K, where W is the nematic anchoring energy on the particle surface, K the Frank elastic constant and R the particle radius.[9] A spherical colloid particle in a nematic LC creates a topological defect in the director field, if WR/K >> 1. When this parameter is small (which in our case, with PS particles of R ~ 1 μm), the particle introduces only a small perturbation into the nematic matrix. The nematic-induced inter-particle interaction brings a new range of effects to the system: super molecular structures,[2,10-12] cellular structures[9,13] and even a soft solid[13] can be observed.

The soft solid formed by mixing a well characterized model colloid with a well characterized thermotropic LC is a novel interesting type of soft matter which has wide variety of potential applications. It has been shown that colloid-in-liquid-crystal (CLC) composites formed by mixing polymethylmethacrylate (PMMA) particles with 5CB results in a soft solid with an unexpectedly high storage modulus and also acts as a switchable electro-optical material.[11] Previous reports have shown that these CLC gel formation is not limited to functionalized PMMA particles and 4-cyano-4'-*n*-pentyl-biphenyl (5CB) but can be formed using sulphate

coated polystyrene (PS) microspheres and LC mixtures which make it possible to rigidify LCs using colloidal networks so as to tune mechanical properties that enable the adhesion, spreading and proliferation of fibroblasts.[14] CLC gels have been shown to undergo ordering transitions when supported on chemically functionalized surfaces and exposed to organophosphonates.[15]

In this study, we report a novel self-supporting LC-aqueous interface formed from the thin films of micro-structured CLC gels that contain micrometer sized dynamic domains of nematic LC which undergo surface-driven ordering transitions in presence of a bacterial glycophospholipid. These films of CLC gels containing dynamic LC domains are mechanically stable, robust and easily processed. The micro-structured CLC gels described in this study are based on the suspensions of PS microspheres of 1 μm in diameter in low molecular weight E7 nematic LC. E7 is a mixture of four alkoxycyanobiphenyls (*n*CBs) with different aliphatic chain length: 51 wt. % 5CB, 25 wt. % 4-cyano-4'-*n*-heptyl-biphenyl (7CB), 16 wt. % 4-cyano-4'-*n*-oxyoctyl-biphenyl (8OCB) and 8 wt. % 4-cyano-4'-*n*-pentyl-p-terphenyl (5CT). Past reports demonstrated that when colloidal suspensions of microspheres are prepared in the isotropic phase of LCs followed by cooling below their isotropic-nematic transition temperature (T_{NI}), they form birefringent waxy semi-solid (gel) with significant storage modulus (G'~10^3-10^5 KPa).[14] This gelation has been suggested to result from the formation of a particle network resulted from expulsion of colloids from the nematic LC as it cools down from isotropic to nematic phase. It is driven by orientational elasticity of the nematic phase and the anchoring energy and surface tension at LC-particle interface; however the mechanism is not fully understood. The study described in this work builds from previous reports which have demonstrated that self-assembly of amphiphilic molecules at LC-aqueous interfaces can trigger ordering transitions in LCs.[16] Although, many of these studies are observed using nematic LC such as 5CB, 5CB droplets, the influence of colloidal network within the LC gel in the surface-driven ordering transition has not been previously demonstrated.[17-21] Lipopolysaccharides (LPS) are the amphiphillic molecules and consist of three components: Lipid A, a R polysaccharide and an O polysaccharide. Lipid A is hydrophobic and membrane anchoring region of LPS and is mainly responsible for toxicity (Figure 2.1). In humans, it leads to the "endotoxic shock

(sepsis)".[22,23] Past reports demonstrated the detection of endotoxin using micrometer-sized droplets of nematic LC,[17] fluorescence labelling,[24] capacitive biosensor,[25] mass spectrometry,[26] self-assembled monolayers based quartz crystal biosensors,[27] etc.

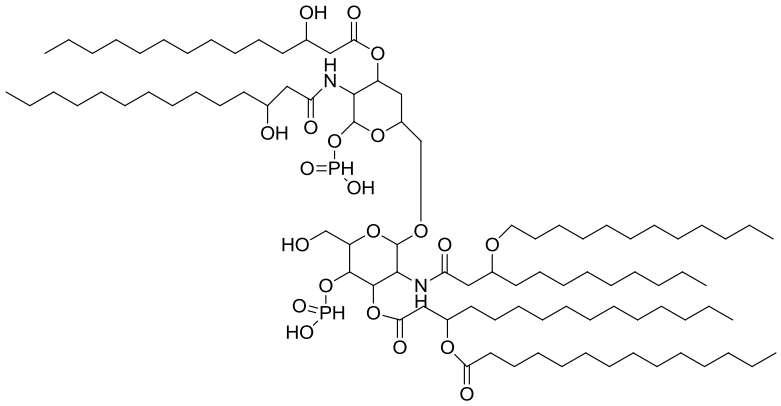

Figure 2.1 The chemical structures of lipid A part of LPS.

Most of these techniques involve complex instrumentation, laborious technique, laboratory based instrumental apparatus which limits their widespread use. The study reported here is a promising development in order to realize a portable, stable and robust sensing system for endotoxin detection.

2.2 Objective

In this study, we sought to determine if it was possible to use organized networks of micrometer sized particles to form LC containing composite materials that would hold its structure at LC-aqueous gel interface and also retain their responsiveness to changes in chemical environment at those interfaces. As the size of the LC rich domains can be as large as 6-10 μm (Figure 2.2), we hypothesized that it may be possible to trigger surface-driven ordering transitions within these domains by forming the gels in thin films in presence of specific biomolecules.

In this work, we demonstrate that the ordering of LC in the confined nematic domains can be coupled to the molecular interactions of LC with a bacterial glycophospholipid (LPS from *Escherichia Coli*) at the LC-aqueous interface. In particular, we have found that the sensitivity can be improved by forming a gel which is highly stable and retained its structure on one of the confining surfaces or when the supporting surface was immersed into water.

Unlike LC, these CLC gels are self-supporting, mechanically strong and can be easily handled.

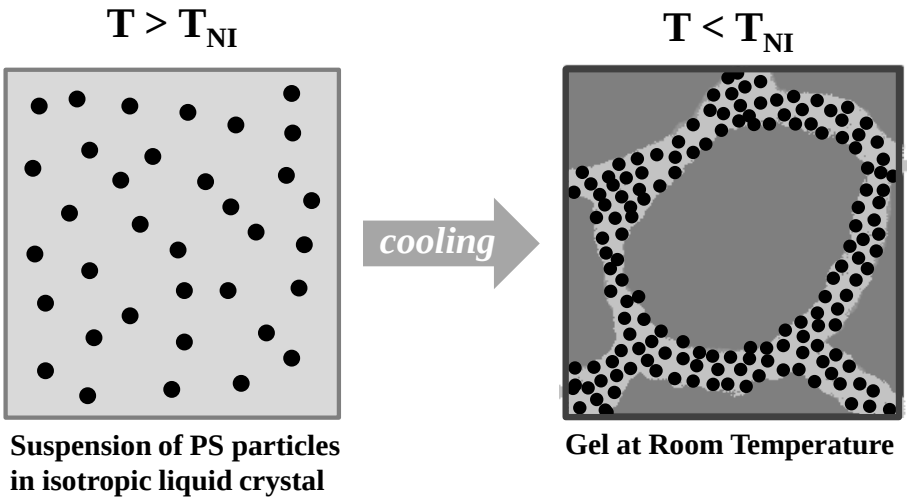

Figure 2.2 Schematic illustration of the thin films of CLC gels formed between glass slides.

2.3 Results and Discussion

2.3.1 Surface induced ordering transition of LC films in presence of LPS

Our first experiment was sought to determine the influence of LPS on the orientational ordering of E7 LC at interfaces to air and aqueous solutions. In a typical experiment, a thin film of nematic E7 LC was wicked into the pores (283 μm × 283 μm) of a 20 μm thick gold transmission electron microscopy (TEM) grid. The LC-filled grids were supported on a glass microscope slide treated with N,N-dimethyl-N-octadecyl-3 aminopropyltrimethoxysilyl chloride (DMOAP). Past studies reported that treatment of the DMOAP anchors a variety of LCs in an orientation that is perpendicular (homeotropic) to the LC-glass interface.[19] The results reported below indicate that E7 LC also assumes a homeotropic orientation at the surface of DMOAP-coated glass slide. The E7 LC filled grids were equilibrated in air for about 5 min and then immersed into an aqueous phase resulted in the formation of a stable planar interface between LC and aqueous phase.

Figure 2.3A shows optical photomicrographs (cross polars) of nematic E7 LC confined within a TEM gold grid exposed to air. Past studies have established that E7 assumes a

perpendicular (homeotropic) orientation at its free surface (LC-air interface).[28] When combined with the influence of DMOAP-coated glass slides (also causes homeotropic anchoring of the LCs as discussed above), the E7 LC film presumes a uniform orientation that is perpendicular to both the surfaces (air as well as DMOAP). This leads to dark optical appearance of the E7 LC between cross polars.

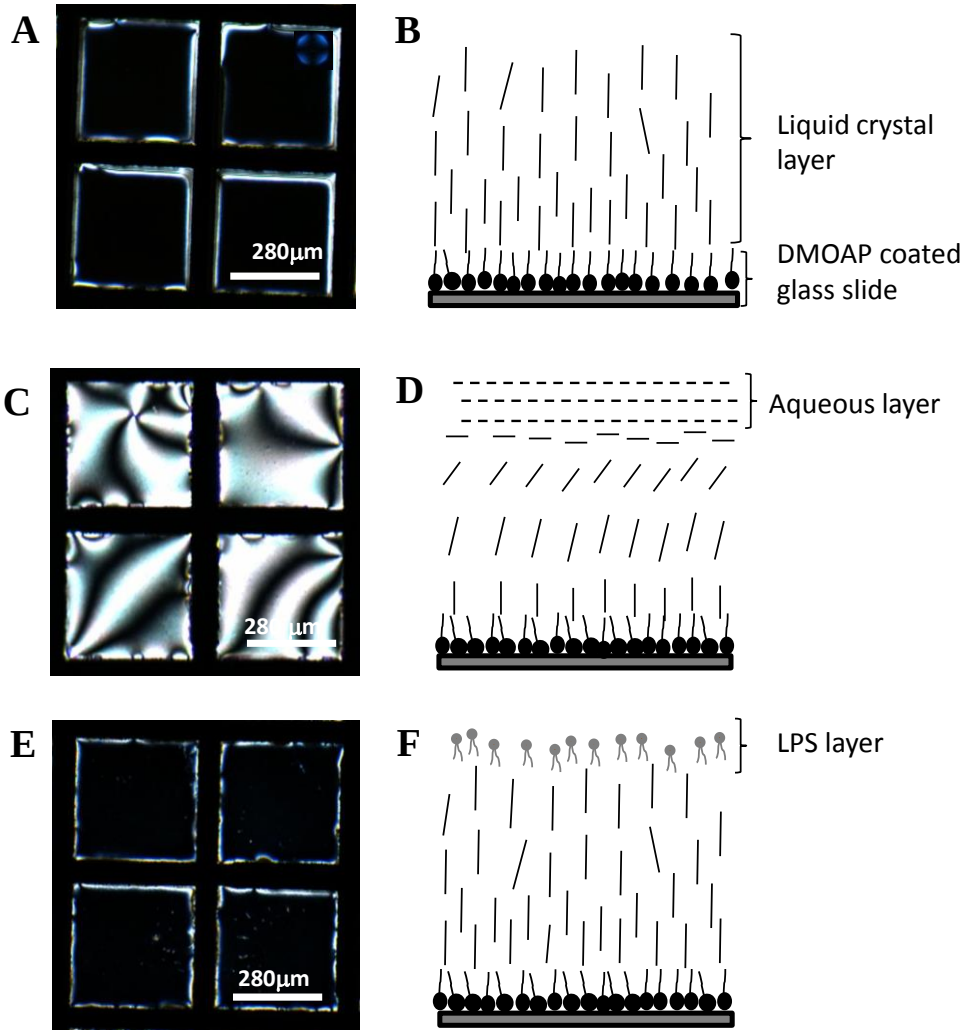

Figure 2.3 Surface induced ordering transition of LC films within TEM gold grid in response to LPS. Polarized light micrographs (cross polars) of E7 hosted in TEM gold grid supported on DMOAP-coated glass slide in contact with A) air, C) aqueous solution (DI water) and E) LPS (100 µg/mL). Cartoon representation of the anchoring of E7 exposed to B) air leading to homeotropic anchoring, D) aqueous solution leading to tilted anchoring and F) LPS (100 µg/mL) leading to homeotropic orientation of E7 LC.

The result in Figure 2.3A, when combined with conoscopic images of the LC, led us to conclude that the nematic E7 film did assume a homeotropic ordering in contact with DMOAP at one surface and air at another (the schematic profile is shown in Figure 2.3B). We note that the regions of the LCs within 10~20 μm of each grid bar assume a bright optical appearance. This is possibly due to interactions of the LCs with the hilly surfaces of the gold grid. When immersed into water, a bright optical appearance was observed (Figure 2.3C) consistent with an orientational ordering transition of the LCs in presence of water. Past studies have established that the easy axis of nematic LC is parallel to the interface with water leading to planar/tilted anchoring of the LCs. LCs undergo a continuous splay-bend distortion in order to accommodate homeotropic anchoring at DMOAP-coated glass surface and parallel anchoring at the LC-aqueous interface. The schematic representation with this new boundary condition has been shown in Figure 2.3D.

In order to see the influence of LPS on surface-induced ordering transition of LCs, we performed experiments where we added different concentrations of LPS at interfaces to aqueous solutions of LC filled TEM grid supported on DMOAP-coated glass slides (mentioned above). Past reports showed that the decoration of amphiphilic monolayers with the LC interface spontaneously give rise to change in orientation of LC due to hydrophobic interactions between hydrocarbon chains of amphiphiles and LCs.[16] To see whether LC surfaces capable of immobilizing LPS, films of nematic LC E7 were exposed to different concentrations of LPS solution. Initially in contact with aqueous solution, LC film of E7 showed bright and colorful optical appearance. In presence of LPS (100 μg/mL), the optical image of E7 evolved from bright to dark within 10 seconds (Figure 2.3E). These results indicate that adsorption of LPS at the LC-aqueous interface leads to planar-to-homeotropic orientation (the schematic representation is shown in Figure 2.3F) when the concentration of LPS is in the range of 100 μg/mL. To see what happened with lower concentrations of LPS on the orientational ordering transitions in LCs, we performed similar experiments with different concentrations of LPS. As can be seen from Figure 2.4, the ordering transition of the LC takes longer time and does not change to black completely even after 24 h in presence of 90 μg/mL of LPS solution. As expected further lower concentrations (70 μg/mL, 40 μg/mL) of LPS have very little effect on the orientational ordering transitions of LC films

(Figure 2.4B,C). Thus, we observe that the LPS induce ordering transitions in the LC at concentrations greater or equal to the value of 100 µg/mL.

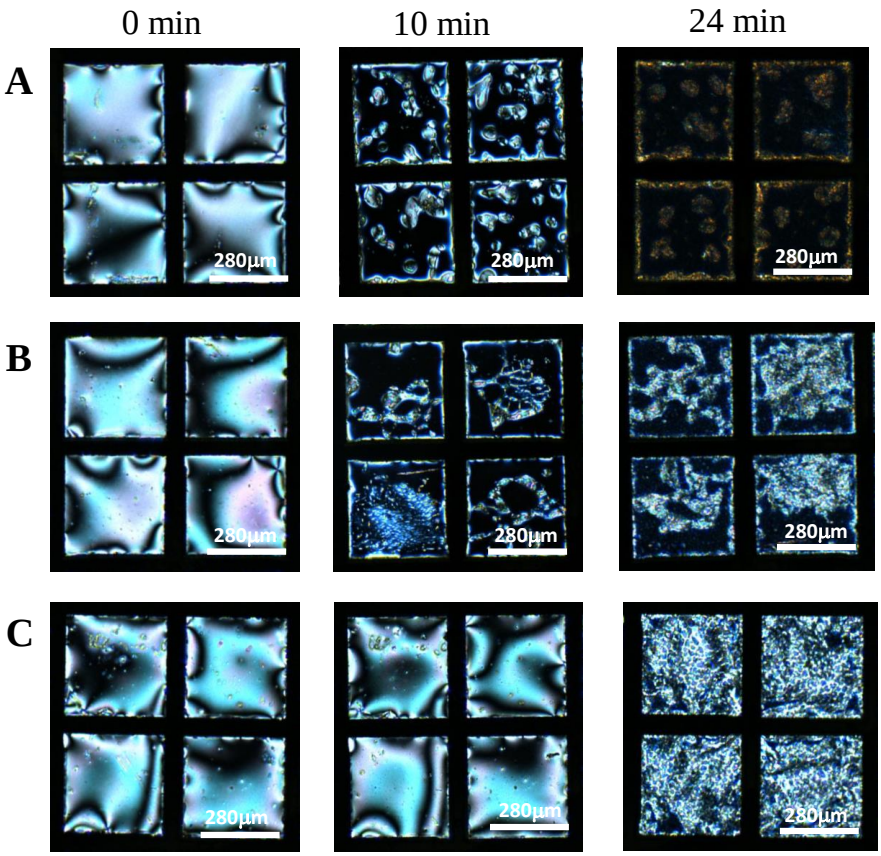

Figure 2.4 LPS induces ordering transition of LC films within gold grid at concentrations of 100 µg/mL but below this concentration no change in optical appearance is observed. Polarized light micrographs (cross polars) of the LC E7 in response to LPS of concentration A) 90 µg/mL B) 70 µg/mL C) 40 µg/mL at t = 0, 10 min and 24 h.

2.3.2 Thin films of CLC gels under water

Our next goal was sought to determine whether LPS can influence in the surface-induced ordering transition in a CLC gel containing dynamic LC domains. Past studies reported that it is possible to form thin films of CLC gels (2-4 µm) in the glass slide without disturbing their microstructure.[15] To prepare thin film of a CLC gel, a small piece of the gel was placed on a piranha cleaned glass slide and heated above the T_{NI} of E7. When the CLC gel had melted, it

was confined with another pre-warmed piranha cleaned glass slides with ~1.5 µm thick Mylar spacer spaced in between the glass slides and cooled to room temperature at a fixed rate of ~0.2 °C/min. This procedure gave very uniform dynamic domains of LC in the CLC gel. Figure 2.5 (at an objective power of 200x and 500x) show polarized light micrographs of a thin film of (15 wt. % PS particles in E7 LC). CLC gel sandwiched between two glass slides which reveal beautiful bright nematic domains of LC.

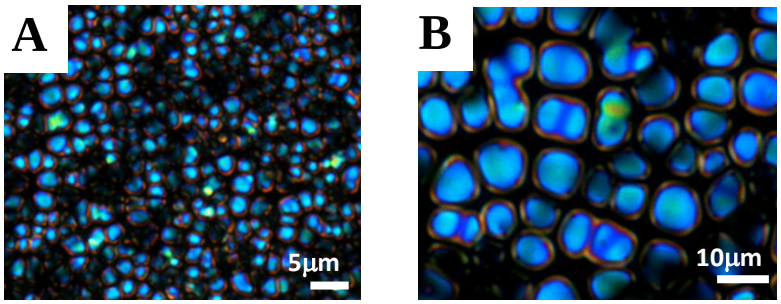

Figure 2.5 Polarized light micrographs (cross polars) of thin films of CLC gel containing 15 wt. % PS microspheres in E7 confined between two glass slides separated by ~1.5 µm thick Mylar spacer at an objective power of 200x and 500x, respectively.

After evaluating different wt. % of PS particles in E7 LC (5 wt. % and 10 wt. %), we determined that thin films of 15 wt. % gels produce large and uniform nematic domains. The approximate sizes of LC domains are of 8.46 ± 1.31 µm.

Past studies also revealed that it was possible to preserve the cellular structure of the CLC gel following detachment of the top glass slides to create an interface between gel and air.[15] Inspection of Figure 2.6 reveals that after detachment of the top glass slide thin film of CLC gel did not destroy the cellular network of the CLC gel but, led to change in the optical appearance of the CLC gel. These results together with past reports led us to conclude that LC rich domains within the CLC gel can respond to change in the boundary conditions as in the case of glass to air described above.

As noted above, thin films of CLC gels comprised of micrometer sized nematic domains of LC that are capable of being ordered by interaction of confining surfaces. This presents an

opportunity to engineer CLC gels that can optically report molecular interactions of nematic LC in the self-supporting CLC films.

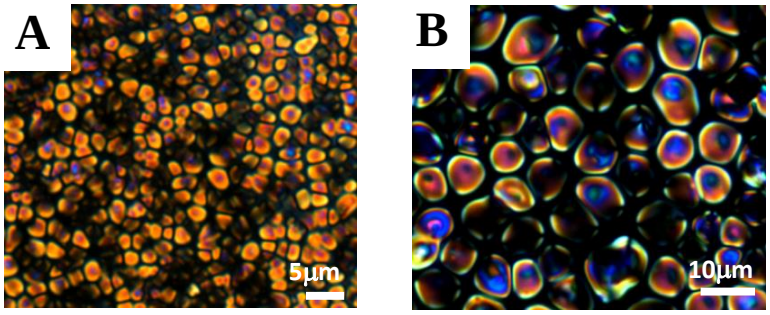

Figure 2.6 Polarized light micrographs (cross polars) of thin films of CLC gel containing 15 wt. % PS microspheres in E7 upon removal of the top glass slide at an objective power of A) 200x and B) 500x, respectively.

To determine, if it was possible to prepare the CLC gels confined by surfaces with chemical functionality suitable for adsorbtion of biological lipids, we prepared DMOAP-coated glass slides (as described above) so as to cause homeotropic orientation of E7 LC. Figure 2.7A,B show the optical appearance of 15 wt. % PS microspheres in E7 LC between two DMOAP functionalized surfaces. Inspection of Figure 2.7B reveals dark optical appearance under cross polars and only a very small amount of light scattered from the film. This observation indicates that LC was completely homeotropically aligned within the LC gel. The bright field image of the same film (Figure 2.7C) confirms the presence of micro-structured network of LC domains (~5.55 ± 1.20 µm). Combination of both polarized light and bright field micrographs led us to conclude that thin film of CLC gel has formed between two DMOAP-coated glass slides and the E7 LC within a LC rich domain of CLC gel has presumed perpendicular orientation (i.e., homeotropically aligned) consistent with the past reports observed only for nitrile containing LC systems.[29] An illustration of the potential ordering of LC in such a nematic domain of the CLC gel thin film is sketched in Figure 2.7D.

Whereas the experiments described above provide the expediency of forming thin films of CLC gels between two DMOAP-coated glass slides. In order to study the response of the gels to form LC-aqueous interface suitable for binding biological lipids, we sought to determine if

it was possible to preserve the homeotropically aligned domains following detachment of the top DMOAP-coated glass slides i.e., to create an interface between air and the CLC gel.

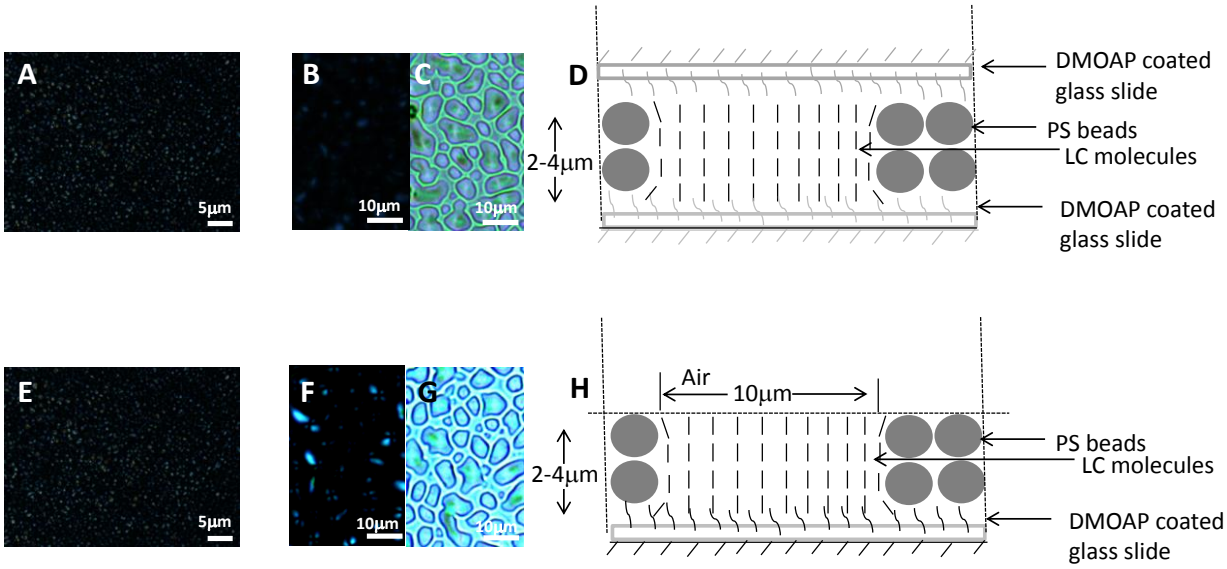

Figure 2.7 Optical micrographs of thin films of CLC gels (containing 15 wt. % PS particles in E7 LC). A, B) 15 wt. % CLC gels confined between two DMOAP-coated glass slides using 1.5 µm thick Mylar spacer at an objective power of 200x and 500x, respectively. C) A bright field image of the CLC gel film showing the microstructure network of LC rich domains. D) Schematic illustration of the ordering of LC rich domain of the CLC gel sandwiched between two DMOAP-coated surfaces. E, F) Same CLC gel film after removal of the top DMOAP-coated glass slides at an objective power of 200x and 500x, respectively. G) The bright field image of the CLC gel film showing the stability of the network of LC rich domains. H) Schematic illustration of the ordering of LC rich domain of the CLC gel after removal of the top DMOAP-coated glass slide.

Inspection of Figure 2.7E,F reveals that the CLC gel did not change the optical appearance. This is because free surface of E7 (E7-air interface) presumes same homeotropic orientation as that observed by DMOAP-functionalized glass slides. The bright field image of the same film (Figure 2.7G) confirms the presence of micro-structured network of LC domains similar to that observed in sandwiched system. A representative sketch for the director profile has been shown in Figure 2.7H. In summary, a major finding of the study reported in this work is

that it is possible to prepare thin films of CLC gels with LC rich domains that are oriented perpendicular (or homeotropically) with respect to DMOAP-functionalized glass surfaces. This also suggests that these surfaces are suitable to undergo surface-driven ordering transitions triggered by biological lipids.

2.3.3 Surface induced ordering transition of thin films of CLC gels in presence of LPS

To determine if the LC rich domains of the CLC gel supported on DMOAP-coated glass slides would undergo surface-induced ordering transitions induced by biological lipids, we first immersed a thin film of CLC gel (DMOAP-air interface) under aqueous solutions (deionized (DI) water). Inspection of Figure 2.8A reveals homeotropic orientation of LC rich domain within the CLC gel as described above. Immediately, in contact with water a bright optical appearance was observed under cross polars (Figure 2.8B). This is consistent with an orientational ordering transition induced by contact with water. The interference colors which were bright green, intense white and greyish indicate that the LCs which the CLC gel had assumed a tilted state (that is an orientational state that is distinct from that of pure E7 discussed above). Second, we investigated if E7 in the micrometer sized nematic domains of CLC gel thin films would also demonstrate ordering transitions in response to the assembly of bacterial glycolipid (similar to experiments performed with E7 as discussed above). For this, we conducted a series of experiments with LPS using LC gel-aqueous interfaces (15 wt. % PS particles in E7). As seen from Figure 2.8C in presence of LPS (30 µg/mL) a dark optical appearance was observed, thus indicate an optical amplification of LC ordering in the CLC gel at the LC-aqueous interface. In summary, a new finding of the study reported in this work, as sketched in Figure 2.8D,E is that it is possible to form thin films of CLC gels with LC rich domains that are oriented by chemically functionalized (DMOAP) glass surfaces suitable for triggering an ordering transition in presence of biological lipids at LC-aqueous interface.

Dynamic changes in the ordering of nematic LC E7 were recorded when LPS (20 µg/mL) was introduced in aqueous solution over the CLC gel. The changes in optical appearance (Figure 2.9A) of the CLC gel upon addition of LPS occurred over 15 min.

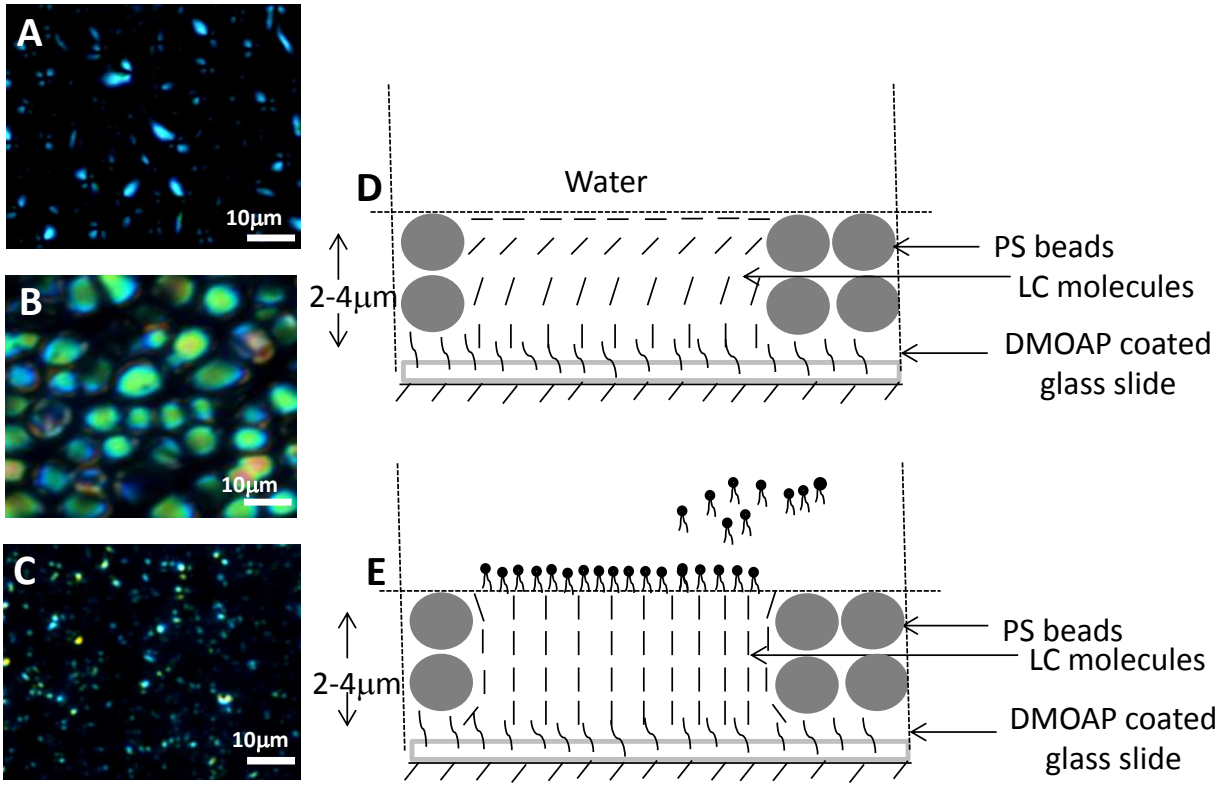

Figure 2.8 Thin films of CLC gels prepared on DMOAP-functionalized surfaces are stable when they are immersed under aqueous solutions and adsorption of LPS lead to an anchoring transition within the LC-rich domains of the gel. A) Polarized light micrograph of a CLC gel film on DMOAP-functionalized glass with one interface exposed to atmosphere observed between cross polars. B) Polarized light micrograph of CLC gel film observed between cross polars when immersed in milli-Q water and C) upon addition of LPS. D) Sketch of the orientation of LC in a LC-rich domain of CLC gel film in aqueous solution and E) in presence of LPS.

This suggests that in presence of 20 µg/mL of LPS it takes up to 15 min for the optical appearance of CLC gel to change from bright birefringent to completely dark. In order to provide insight into the dynamic response, we sought to explore not only the ordering transitions of individual domains at different point of time during 15 min time interval but also sort to find whether domains were undergoing consecutive ordering transitions in the time frame mentioned above.

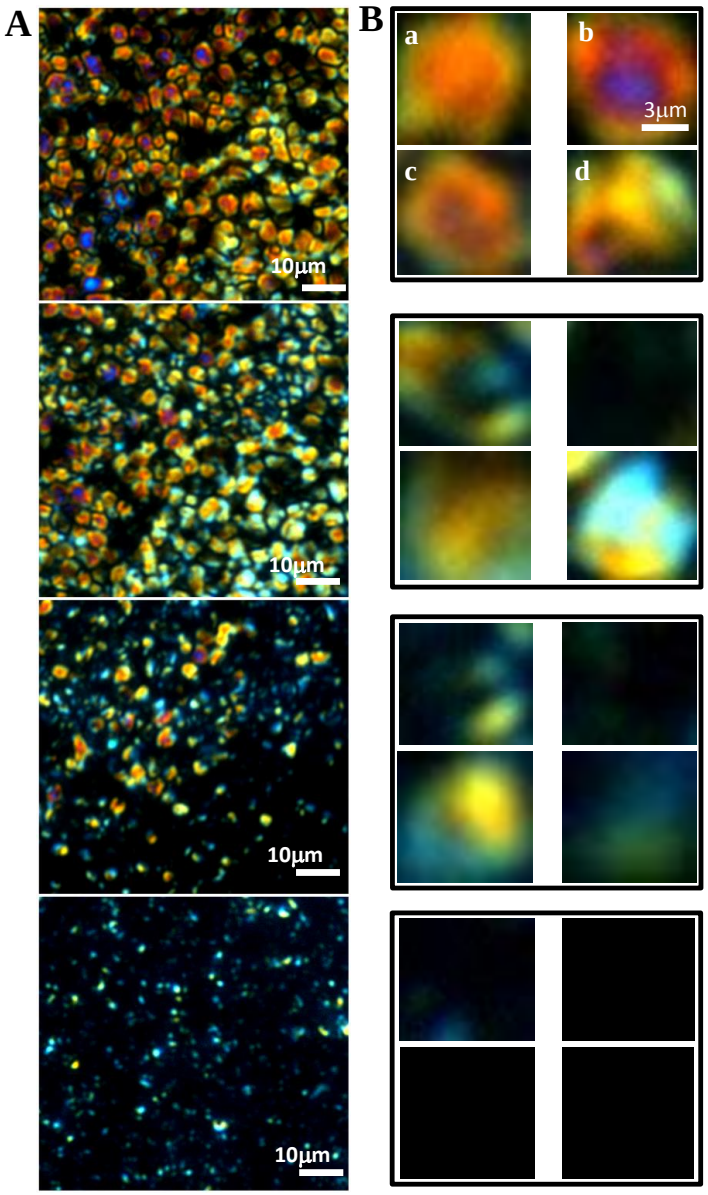

Figure 2.9 A) Polarized light micrographs of time lapse images (change in orientational ordering under cross polars) of CLC gel in response to the adsorption of LPS (20 µg/mL) at CLC-aqueous interface. B) Dynamic responses of LC rich domains (representative four domains) on DMOAP-functionalized glass at successive time points after incubating with 20 µg/mL solution of LPS.

To distinguish this, we chose four domains and measured their optical intensity at different time intervals. As seen from Figure 2.9B, the change in the optical appearance of individual domains of LC within the gel lead us to conclude that at the single-domain level, the LPS-

triggered change in optical appearance of the LC differed substantially from one domain to the next. For example, the optical intensity of some domains (e.g., a and c) decreases continuously with time. For other domains (e.g., b), the optical intensity abruptly decreases and then remains constant. Also some domains (e.g., d) exhibited a non-monotonic change in brightness (presumably due to interference effects associated with the white-light illumination). This heterogeneity in the response of the domains likely reflects variation in the sizes and shapes of the LC-rich domains in the gel and thus differences in elastic and surface anchoring energies for each domain.

The total bright light intensity from the images in Figure 2.9A and 2.9B were calculated using Image J software and plotted in Figure 2.10 and 2.11. These experiments demonstrate the progressive decrease in the brightness of the CLC gel film with time. These observations suggest that manipulation of the sizes and shapes of the LC domains may provide a means to rationally tune the response of CLC gels to interfacial adsorbates.

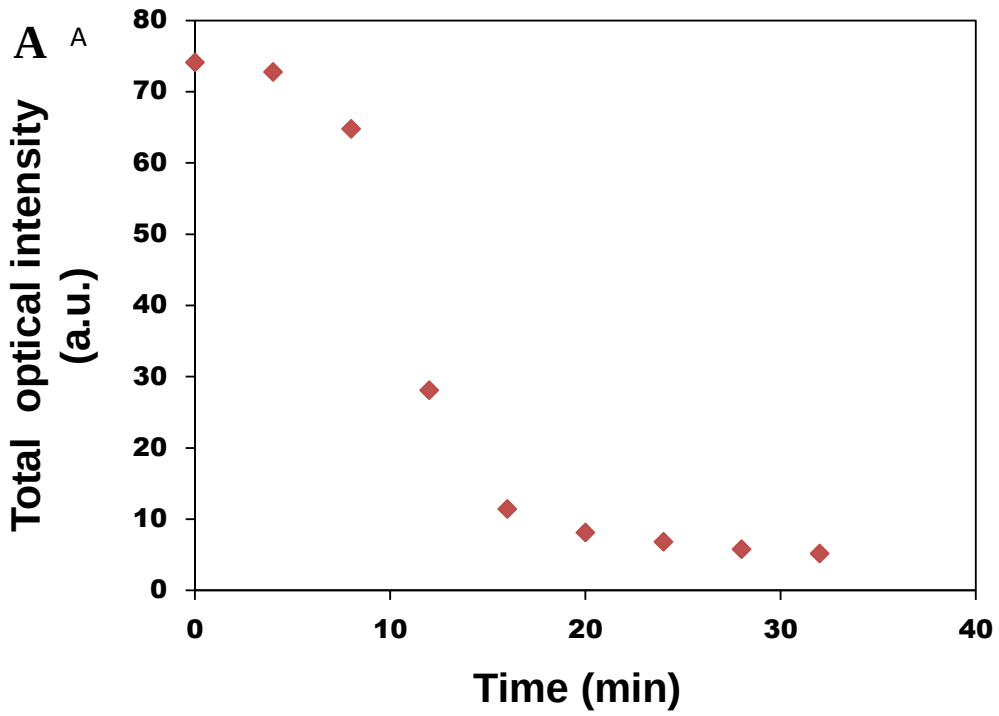

Figure 2.10 A) Total optical intensity of the polarized light images of the CLC-gel films as a function of time after incubation with LPS shown in Figure 2.9(A).

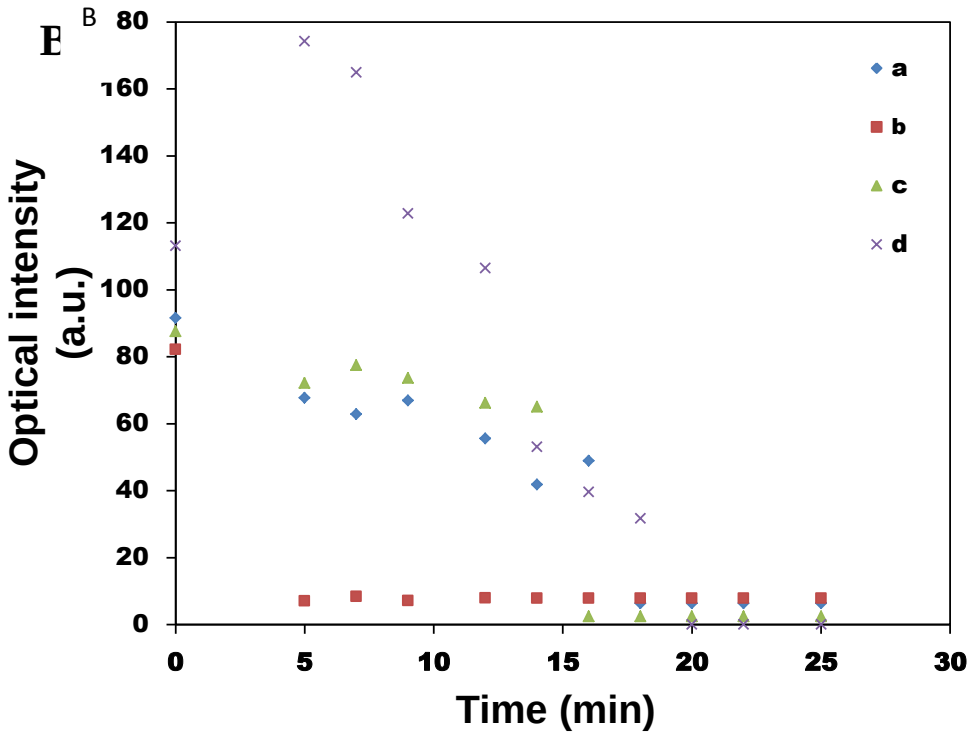

Figure 2.11 Time dependence optical appearance of the four domains shown in Figure 2.9 (B) upon addition of LPS.

The results presented above demonstrate that LPS-induced ordering transitions of E7 are not prevented by incorporation of the PS microspheres within the CLC gel. Interestingly, network of PS microspheres did not hinder the ordering transition of the LCs in the LC-rich domains in the CLC gel. In case of LC, hosted in gold grids with 283 µm square grid size (20 µm depth), it was observed that 100 µg/mL concentration of LPS would change the ordering transition of LC whereas this number became 20 in presence of CLC thin film. We note that this difference could be because of (i) significantly smaller size of LC-rich domains in CLC gels (ii) relatively thinner depth of LC domains of CLC gels (2-4 µm). The methods used to measure the CLC gel film have been described in detail elsewhere.[15] These observations indicate the ordering of LC can be synergistically by the change in its anchoring at LC-aqueous interface. Moreover, relatively thinner films and significantly smaller size of LC-rich domains compared to LC hosted in specimen grids allows dynamically faster changes in the ordering of LC in response to the orientational changes at LC-aqueous interfaces.

2.3.4 LC domain sizes *vs.* wt. % of PS particles within CLC gels

Finally, we demonstrate that the manipulation of LC domain size and shape of the CLC gels made up of E7 LC and PS particles can tune the response of the LC-based physical gels to interfacial phenomenon. For this, different wt. % of CLC gels were prepared and determined the effect of particle concentration on the cellular structure of particle LC composite. The particles used for the preparation of CLC composites were commercially available sulphate-functionalized PS microspheres. These dried PS particles were then suspended in isotropic E7 LC followed by cooling below their isotropic-nematic transition temperature (T_{NI}), they form birefringent waxy semi-solid (gel) as reported earlier.[14] Previous studies have reported the preparation of particle LC composites for a wide range of PMMA particle concentrations (3–15%).[11] In this study, we prepared 5 wt. %, 10 wt. %, 15 wt. % and 20 wt. % of PS microspheres in E7 LC. To characterize the structure of these different wt. % CLC gels, we prepared thin films of these different CLC gels on simple glass slides. From previous studies, we came to know that it is possible to form thin films of CLC gels on the glass slides without disturbing their microstructure.

To prepare a thin film of a particular CLC gel, a small piece of desired CLC gel was placed on a piranha cleaned glass slide and heated above the T_{NI} of E7. When the CLC gel had melted, it was confined with another pre-warmed piranha cleaned glass slide with ~ 1.5 μm thick Mylar spacer spaced in between the glass slides and cooled to room temperature at a fixed rate of ~ 0.2 °C min^{-1}. Using this procedure, we prepared uniform dynamic domains of LC of different wt. % of CLC gels. Polarized light micrographs of thin films of different wt. % of CLC gels showed beautiful bright nematic domains of LC but the distribution of domain sizes is found to be of different in CLC films of different particle wt.% (Figure 2.12). The domain sizes are of varying sizes in all wt. % CLC gels. For CLC gel of lowest particle concentration (5 wt. %), the majority of domains are of bigger in size and for CLC gel (20 wt. %) having highest particle concentration, the majority of domains are of smaller in size. For other wt. % CLC gels varying sizes of domains are present. From this observation, it is clear that the average size of nematic domains of E7 LC in CLC gels decrease as we increase the concentration of PS microspheres in E7 LC.

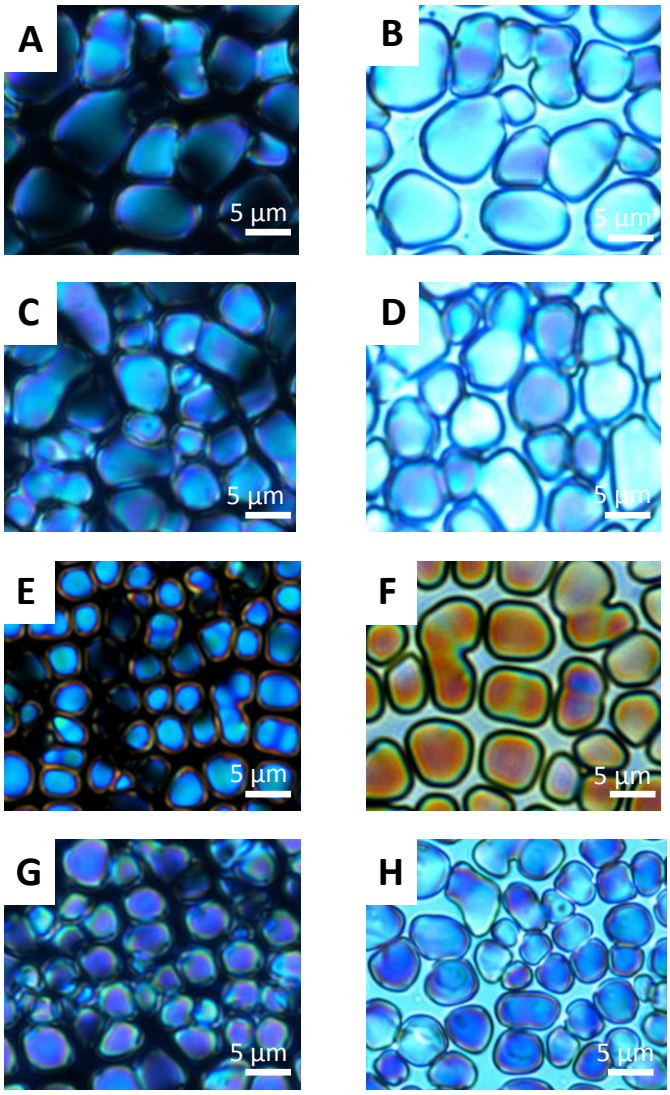

Figure 2. 12 Optical micrographs of CLC gels on simple glass slides for A) 5 wt. % at cross polars and B) its bright field image. C) 10 wt. % at cross polars and D) its bright field image. E) 15 wt. % at cross polars and F) its bright field image. G) 20 wt. % at cross polars and H) its bright field image.

Previous studies revealed that thin films of CLC gels comprised of micrometer sized domains of LC are capable of being ordered by interaction of confining surfaces. So, our next experiment was to prepare thin films of above mentioned CLC gels on DMOAP-coated glass surface and determine whether we observed the same effect of particle concentration on domain sizes as observed on simple glass slides mentioned above. For this experiment, we first prepared DMOAP-coated glass slides and then thin films of different wt. % of CLC gels

were prepared. Figure 2.13, shows the optical appearance of 5 wt. %, 10 wt. %, 15 wt. % and 20 wt. % microspheres respectively in E7 LC between two DMOAP functionalized surfaces.

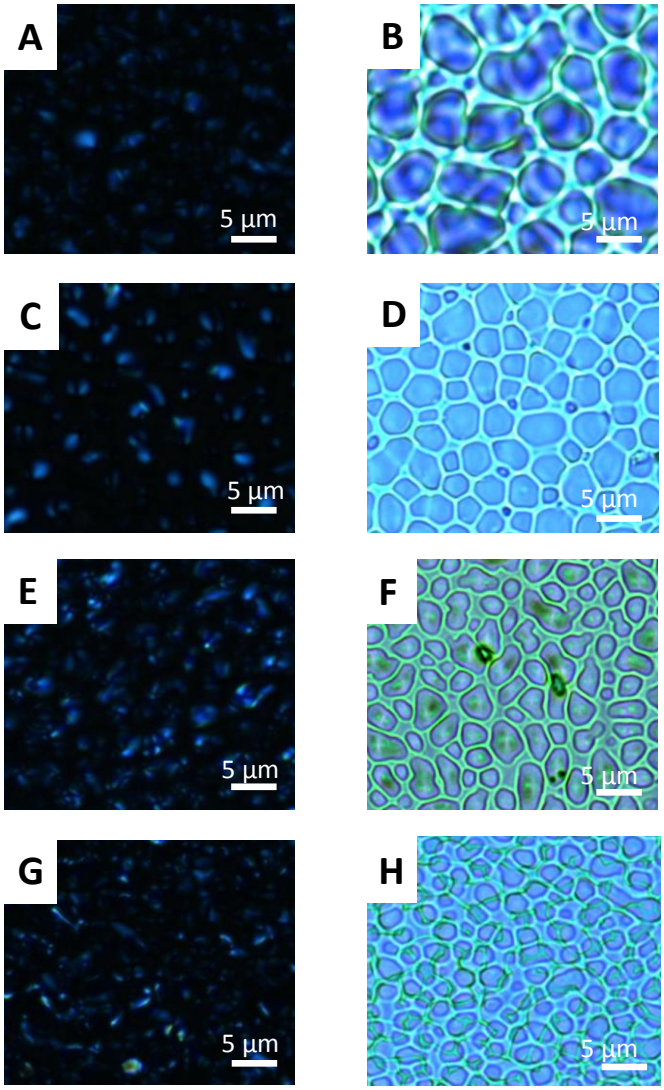

Figure 2.13 Optical micrographs of CLC gels on DMOAP-coated glass slides for A) 5 wt.% at cross polars and B) its bright field image. C) 10 wt. % at cross polars and D) its bright field image. E) 15 wt. % at cross polars and F) its bright field image. G) 20 wt. % at cross polars and H) its bright field image.

Inspection of Figure 2.13 reveals dark optical appearance under cross polars which indicates that LC was completely homeotropically aligned within the LC gel. The bright field images confirmed the presence of micro-structured networks of LC domains for the above mentioned

wt. % of CLC gels. Combination of both polarized light and bright field micrographs led us to conclude that thin film of CLC gel has formed between two DMOAP-coated glass slides and the E7 LC within an LC rich domain of CLC gel has presumed perpendicular orientation (i.e., homeotropically aligned) consistent with the past reports.[29] By evaluating the domain sizes of LC domains for different wt. % CLC gels, we determine that increasing the wt. % of PS microspheres in E7 LC gels decreases the average domain size of CLC gels on DMOAP-coated surfaces. By careful observation, we noted the difference in domain sizes on simple glass slides and on DMOAP-coated glass slides for the same wt. % gels in each case.

2.3.5 Variation of LC domain sizes *vs.* wt. % of PS particles within CLC gels

In order to validate this observation we made the quantitative measurements of the domain sizes. The optical micrograph of CLC films shows that LC domains of varying sizes are present. Accurate quantitative measurements can be made as the distribution is not too irregular and asymmetric. So, for each CLC film we calculated the average domain sizes on simple glass slides as well as on DMOAP-coated glass slide. The average sizes of LC rich domains of the CLC gels calculated for 5 wt. %, 10 wt. %, 15 wt. % and 20 wt. % CLC gels on simple glass slides are 15.36 ± 2.83 μm, 12.51 ± 2.35 μm, 8.46 ± 1.31 μm and 7.53 ± 1.48 μm respectively and on DMOAP-coated glass slide the average sizes are 7.79 ± 1.70 μm, 7.30 ± 1.89 μm, 5.55 ± 1.20 μm and 4.10 ± 1.11 μm respectively. Based on these measurements, the average sizes of LC rich domains obtained both on simple glass slides as well as on DMOAP coated glass slides were plotted against the wt. % of PS microspheres in CLC gels as shown in Figure 2.14A. Inspection of Figure 2.14A revealed a remarkable difference in domain sizes obtained on simple glass slides and on DMOAP-coated glass slides and also shows the inverse relation of domain size with particle concentration. This observation indicates that the size of the nematic LC rich domains depends on particle concentration and also on the supporting surface. We also plotted the ratio of domain sizes obtained on glass surface to that obtained on DMOAP for each wt. % CLC gels against the wt. % of PS microspheres in CLC gels. The ratio was found to be the same (~ 2 μm) for each case as shown in Figure 2.14B which indicates the variation of LC rich domains with concentration only.

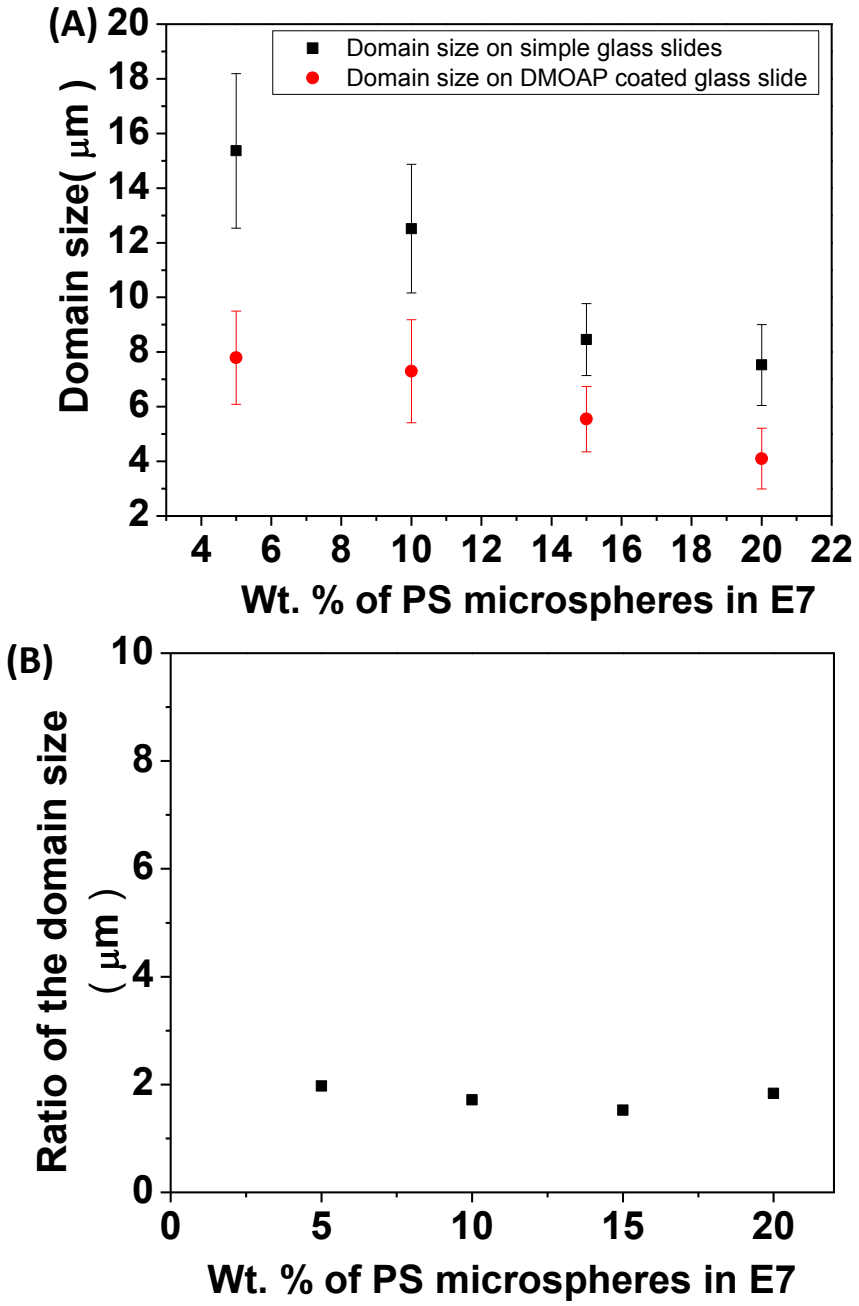

Figure 2.14 A) Plot showing the variation of domain sizes in CLC gels with increasing wt. % (5, 10, 15 and 20) of PS microspheres in E7 LC on simple glass slides and on DMOAP-coated glass slides. B) Plot showing how the ratio of domain sizes obtained on simple glass slides to that obtained on DMOAP-coated glass slide for each wt. % CLC gel (5 wt. %, 10 wt. %, 15 wt. % and 20 wt. %).

Based on the above observations, we came to know that the size of the LC rich domains depends on the concentration as well as on the interaction of LC with the supporting surface. To find out how these factors like concentration, different type of interactions of LC with the supporting surface determine the domain size, we performed another experiment in which we have tried to determine the origin of network formation in CLC composites.

2.3.6 Sensitivity of optical response of different LC domain sizes towards LPS

Now, our last goal was to determine that is there any relation between the sensitivity of optical response with the different domain sizes obtained from different wt. % of CLC gels. In the above mentioned experiment, we prepare the thin films of CLC gels with LC rich domains that are oriented perpendicular (or homeotropically) with respect to DMOAP-functionalized glass surfaces. Now, to determine if the LC rich domains of the CLC gel supported on DMOAP-coated glass slides would undergo surface induced ordering transition induced by biological lipids, we immersed thin films of CLC gels (DMOAP-air interface) under aqueous solution. Inspection of Figure 2.13 revealed the homeotropic orientation of LC rich domains within these different CLC gels as mentioned above. Immediately in contact with water a bright optical appearance was observed under cross polars. The interference colors which were bright green, pinkish, intense white and greyish indicated that the LC domains assumes tilted state within the CLC gels induced by water. Now to determine the ordering transition of E7 LC in the micrometer sized nematic domains of thin films of CLC gels in response to bacterial glycolipid (LPS from salmonella enterica), we conducted a series of experiments with LPS using CLC gel-aqueous interface and observed that all the thin films of CLC gels of different wt. % of PS appeared dark in presence of LPS. But the response time in these different above mentioned wt. % of CLC gels varied slightly. As seen from Figure 2.15, in presence of LPS (25 µg/ml), the response time of 5 wt. % CLC gel was 7 min, for 10 wt. % CLC gel it became 20-25 min, for 15 wt. %, the response time increased to 35 min and 20 wt. % CLC gel didn't show any response even after 24 h. The domain size in 5 wt. % CLC gel would found to be bigger than that of 20 wt. % CLC gel and also much greater than that of the thickness of the film. So, the biological lipid found more space to interact with the LC and gives slightly faster response. From this, we concluded that the response time decreases slightly with increase in the wt. % of CLC gels.

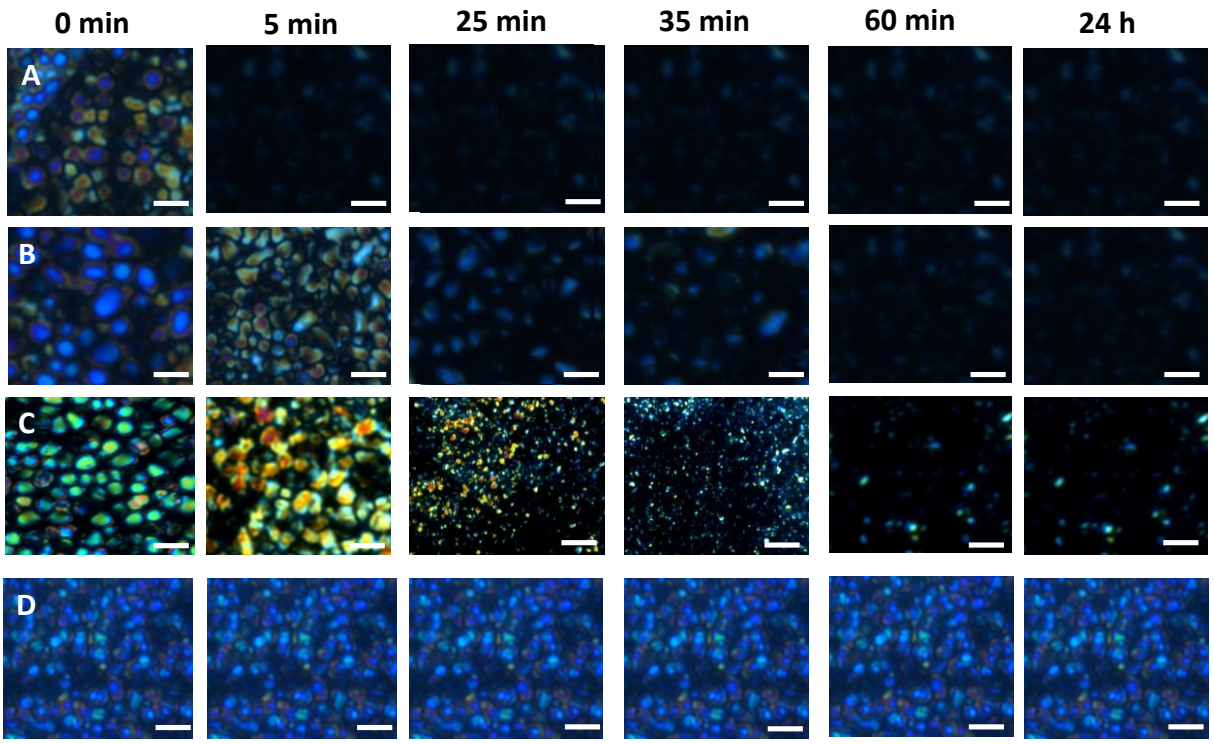

Figure 2.15 Optical micrographs of different wt. % of CLC gels upon addition of LPS (0.025 mg/ml) at 0 t, 5 min, 25 min, 35 min, 60 min and 24 h. A) For 5 wt. % CLC gel. B) For 10 wt. % CLC gel. C) For 15 wt. % CLC gel and D) For 20 wt. % CLC gel. Scale bar = 5 μm.

2. 4 Conclusions

The key result reported in this paper is that thin films of CLC gels with LC-rich domains that span the thickness of the gel are stable under water and can be used to report adsorption of LPS at LC interfaces. We observed, however, that the confinement of the LC to small domains with lateral sizes of ~10 μm lead to faster ordering of LC in response to the molecular interactions at LC-aqueous interface as compared to LCs hosted within TEM grids. We also observed that the response of individual domains of the LC within the CLC gel to vary significantly, suggesting that manipulation of domain size and shape may provide the basis of a general and facile method to tune the response of these LC composite materials to interfacial phenomena. Overall, we conclude that the CLC gels offer a general and facile approach to the preparation of "free interfaces" of LCs suitable for design of LC-based stimuli-responsive materials.

2.5 Experimental Section

2.5.1 Materials

Lipopolysaccharides (from E.coli 0111:B4 and salmonella enterica) and N,N-dimethyl-N-octadecyl-3-aminopropyltrimethoxysilyl chloride (DMOAP) were purchased from Sigma-Aldrich (St. Louis, MO). Sulfuric acid and hydrogen peroxide (30% w/v) were purchased from Merck. Ethanol was obtained from Jebsen & Jenssen GmbH and Co., Germany (Sd. fine–chem limited). The E7 LC was obtained from EMD chemicals. Sulfate coated PS microspheres (#S37498) with 1 μm diameters were obtained from Invitrogen. Deionization of a distilled water source was performed using a Milli-Q-system (Millipore, bedford, MA). Fischer's Finest Premium Grade glass microscopic slides and cover glass were obtained from Fischer Scientific (Pittsburgh, PA). Gold specimen grids (20 μm thickness, 50 μm wide bars, 283 μm grid spacing) were obtained from Electron Microscopy Sciences (Fort Washington, PA).

2.5.2 Cleaning of glass substrates

Glass microscope slides were cleaned according to published procedures using 'piranha'solution [70:30 (% v/v) H_2SO_4:H_2O_2 (30%)], as described in detail elsewhere.[14] Briefly, the glass slides were immersed in a piranha bath at 100 °C for at least 1 h and then rinsed in running deionized (DI) water for 5-10 min. Finally, the slides were rinsed sequentially in ethanol and then dried under a stream of nitrogen. The clean slides were stored in an oven at 100 °C for overnight. All other glassware was cleaned prior to use.

2.5.3 Preparation of CLC gels

The methods used to prepare CLC gels have been described in detail elsewhere.[14] Briefly, sulfate coated PS microspheres, 1 μm in diameter, were washed three times with DI water in eppendorf tubes by centrifuging for 5 min at 9000 g and suspended in fresh DI water by sonication and vortexing. The microspheres were finally washed and suspended in 200 μL in ethanol and dried in air for several days. Dried PS microspheres were weighed and suspended in isotropic E7 in an Eppendorf tube to obtain the desired wt. % of PS

microspheres in the mixture. The suspension was heated above the T_{NI} of E7 (~59 °C) in an oven and vortexed and sonicated vigorously with extensive shaking and tumbling for several hours to ensure homogeneous dispersion of colloids. The suspension was then cooled at a fixed rate (~0.2 °C/min) to room temperature in an oven where it formed a CLC gel.

2.5.4 Preparation of CLC films

To prepare thin films of CLC gels, a small piece of CLC gel prepared as described above was placed on a piranha cleaned glass slide (or chemically functionalized DMOAP coated) and heated above the T_{NI} of E7 in an oven. As the composite formed a transparent suspension, another pre-warmed glass slide (piranha cleaned or chemically functionalized DMOAP) was placed on top of the suspension and spaced from the bottom slide using a 1.5 μm thick Mylar spacer. The assembly was clamped with binder clips and cooled at a fixed rate (~0.2 °C/min) to room temperature to form a thin film of desired CLC composite. In some experiments, after cooling, the top glass slide was removed using forceps to have gel-air interface.

2.5.5 Preparation of DMOAP-coated glass slides

The cleaned glass slides were dipped into 0.1% (v/v) DMOAP solution in DI water for 5 min at room temperature and were then rinsed with DI water to remove unreacted DMOAP from the surface. The DMOAP-coated glass slides were dried under a stream of nitrogen gas and kept in oven at 100 °C for 3 h to allow crosslinking of DMOAP.

2.5.6 Preparation of aqueous dispersion of LPS

Powdered LPS was dissolved in DI water at room temperature to obtain the required concentration. The resulting solutions were then sonicated for 5 min and vortexed for 10 min at room temperature for proper mixing.

2.5.7 Preparation of LC films on TEM grids

The gold specimen grids were cleaned firstly by washing with ethanol, methanol and acetone, then dried under nitrogen gas and finally heated at 100 °C overnight. The grids were then placed on DMOAP-coated glass slides and 0.2 μL of E7 was dispensed onto grids. The

excess of LC was removed with the help of syringe to produce an approximately planar interface.

2.5.8 Optical characterization of LC films in aqueous solutions

The LC films on TEM grids (as mentioned above) were immersed into the aqueous solution. The orientational ordering of E7 was then determined under Nikon Eclipse LV100POL Polarizing Microscope using an objective power of 200x and 500x with cross polars. Orthoscopic examinations were performed with the source light intensity set to 50% of full illumination and the aperture set to 0.55 in order to collimate the incident light. In-plane birefringence was indicated by the presence of brush textures, typically four–brush textures when the sample was viewed between cross polars. All images were captured using a Q-imaging camera.

2.5.9 Optical characterization of LC films induced by LPS

A 100 μL of aqueous dispersion of LPS was added to aqueous solution of LC filled TEM grid supported on DMOAP-coated glass slide. The ordering transition was determined under polarizing microscope (as mentioned above). The bright and colorful optical appearance of LC film of E7 changed to dark which indicated the homeotropic alignment.

2.5.10 Surface-induced ordering transition of LC gels in presence of LPS

The different wt. % (5, 10, 15 and 20) of CLC gels were prepared on DMOAP-coated glass slides to obtain homeotropic alignment. These different CLC films were then immersed into aqueous solution and immediately bright optical appearance was observed under cross polars. The aqueous dispersion of required LPS concentration was added to aqueous solution of these CLC films. The dark optical appearance observed indicated the surface induced ordering transition of CLC gels in the presence of LPS.

2.5.11 Measurement of LC domain size in CLC gels

Measurements of LC domain size of desired wt. % of CLC gels were performed by measuring the domain sizes of at least 40 domains present in an image of a particular wt. %

of CLC film. And then from this calculation, the average domain size present in a particular wt. % of CLC gel was determined.

References

(1) de Gennes, P. G. The Physics of Liquid Crystals; Oxford University Press: Ely House, London, **1974**.

(2) Poulin, P.; Stark, H.; Lubensky, T. C.; Weitz, D. A. *Science* **1997**, *275*, 1770-1773.

(3) Kuskenok, O.V.; Rudwandl, R.W.; Shiyanovskii, S.V.; Terentjev, E. M. *Phys. Rev. E* **1996**, *54*, 5198-5203.

(4) Ruhwandl, R. W.; Terentjev, E. M. *Phys. Rev. E* **1997**, *56*, 5561-5565.

(5) Lubensky, T. C.; Pettey, D.; Currier, N.; Stark, H. *Phys. Rev. E* **1998**, *57*, 610-625.

(6) Stark, H. *Eur. Phys. J. B* **1999**, *10*, 311-321.

(7) Stark, H.; Stelzer, J.; Bernhard, R. *Eur. Phys. J. B* **1999**, *10*, 515-523.

(8) Andrienko, D.; Germano, G.; Allen, M. P. *Phys. Rev. E* **2001**, *63*, 041701/1-041701/7.

(9) Anderson, V. J.; Terentjev, E. M.; Meeker S. P.; Crain, J.; Poon, W. C. K. *Eur. Phys. J. E* **2001**, *4*, 21-28.

(10) Poulin P.; Weitz, D. A. *Phys. Rev. E* **1998**, *57*, 626-637.

(11) Loudet, J.; Barois, P.; Poulin, P. *Nature* **2000**, *407*, 611-613.

(12) Loudet, J.; Poulin, P. *Phys. Rev. Lett.* **2001**, *87*, 165503/1-165503/4.

(13) Meeker S. P.; Poon, W. C. K.; Crain, J.; Terentjev, E. M. *Phys. Rev. E* **2000**, *61*, R6083-R6086.

(14) Agarwal, A.; Huang, E.; Palecek, S.; Abbott, N. L. *Adv. Mater.* **2008**, *20*, 4804-4809.

(15) Pal, S. K.; Agarwal, A.; Abbott, N. L. *Small* **2009**, *5*, 2589-2596.

(16) Brake, J. M.; Daschner, M. K.; Luk, Y. Y.; Abbott, N. L. *Science* **2003**, *302*, 2094-2097.

(17) Lin, I. H.; Miller, D. S.; Bertics, P. J.; Murphy, C. J.; de Pablo, J. J.; Abbott, N. L. *Science* **2011**, *332*, 1297-1300.

(18) Gupta, J. K.; Sivakumar, S.; Caruso, F.; Abbott, N. L. *Angew. Chem. Int. Ed.* **2009**, *48*, 1652-1655.

(19) Clegg, P. S.; Birgeneau, R. J.; Park, S.; Garland, C. W.; Iannacchione, G. S.; Lehency, R. L.; Neubert, M. E. *Phys. Rev. E Stat. Nonlin. Soft Matter Phys.* **2003**, *68*, 031706/1–031706/7.

(20) Tong, X.; Chung, J. W.; Park, S. Y.; Zhao, Y. *Langmuir* **2009**, *25*, 8532-8537.

(21) Wood, T. A.; Lintuvuori, J. S.; Schofield, A. B.; Marenduzzo, D.; Poon, W. C. K. *Science* **2011**, *334*, 79-83.

(22) Raetz, C. R.; Whitfield, C. *Annu. Rev. Biochem.* **2002**, *71*, 635-700.

(23) Cohen, J. *Nature* **2002**, *420*, 885-891.

(24) Janamoto, K. *Adv. Exp. Med. Biol.* **1990**, *256*, 203-213.

(25) Warakorn, L.; Martin, H.; Panote, T.; Proespichaya, K.; Bo, M. *Anal. Bioanal. Chem.* **2007**, *389*, 517-525.

(26) Maitra, S. K.; Schotz, M. C.; Yoshikawa, T. T.; Guze, L. B. *Proc. Nat. Acad. Sci. USA* **1978**, *75*, 3993-3997.

(27) Yang, M.; Chen, J. *Anal. Lett.* **2002**, *35*, 1775-1784.

(28) Nazarenko, V.; Nych, A. *Phys. Rev. E* **1999**, *60*, R3495-R3497.

(29) Bi, X.; Hartono, D.; Yang, K. L. *Adv. Funct. Mater.* **2009**, *19*, 3760-3765.

Chapter 3

An Approach towards the Formation of Radial Nematic Droplets within a Lipid-Laden Aqueous-Liquid Crystal Interface

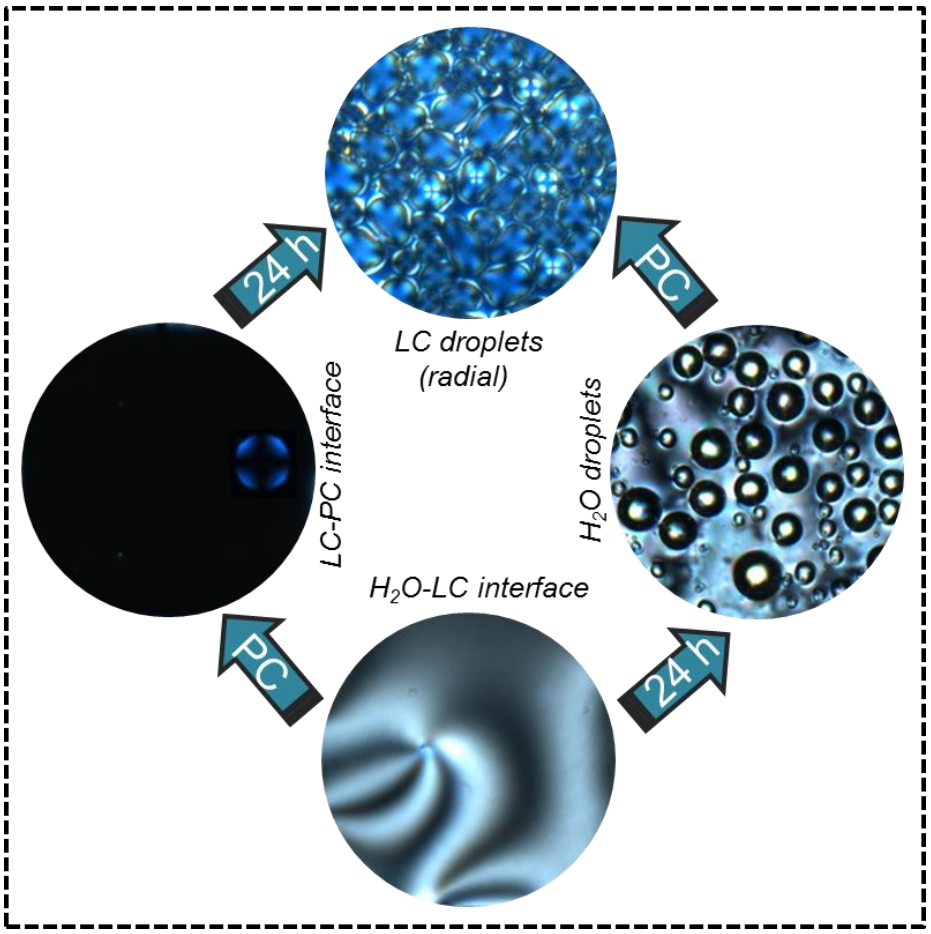

A new pathway for the formation of liquid crystal (LC) droplets with radial LC ordering in the presence of surfactants and lipids with added benefits of stability and sensitivity is reported. This study also shows that the response of these droplets due to the interactions between an enzyme and the topological defects in the LC may be exploited in applications such as sensing.

3.1 Introduction

Recently, liquid crystal (LC) droplets have been widely appreciated as a new class of functional materials due to their large surface areas, rich phases, well-defined director configurations and unique tunable optical properties.[1–10] In particular, they offer routes to design simple, economic and convenient passive sensing devices that provide a high spatial resolution of micrometers with a very high sensitivity. The director configuration of LC droplets is known to reflect the balance between the elasticity and the surface anchoring of the LC inside the droplets. It has been shown that radial and bipolar director configurations can be formed more frequently in LC droplets (Figure 3.1).[11]

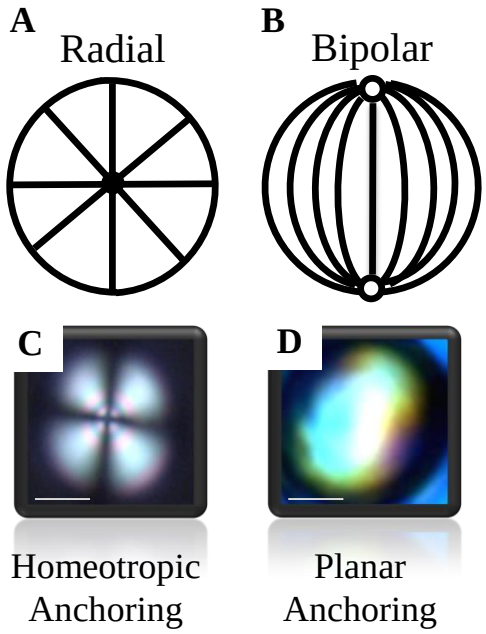

Figure 3.1 Schematic illustration of the orientational ordering of LC within a droplet in a (A) radial configuration and (B) bipolar configuration. In a radial configuration LC is oriented perpendicular to the interface of the droplet and a defect is present at the center of the droplet, whereas in a bipolar configuration LC is oriented parallel to the interface of the droplet and two diagonally opposite surface point defects are present at the poles of the droplet known as boojums. (C,D) Corresponding polarized optical textures of the LC droplets in a (C) radial configuration and (D) bipolar configuration.

The homeotropic alignment of the LC at the surface as shown in Figure 3.1A, resulting in radial droplets is characterized by a perpendicular orientation of the LC at droplet boundaries. Its configuration has a spherical symmetry with a *hedgehog* disclination at the center of droplets.[12,13] On the other hand, the planar orientation of the LC (Figure 3.1B) at the interface gives rise to bipolar droplets which are characterized by a tangential anchoring of mesogenic molecules at the droplet boundaries. Such configuration with two point defects at opposite ends of the droplet is characterized by a bend elastic deformation. Those defects are also referred to as boojums. The transition among these director configurations leads to the optical pattern change of LC droplets as shown in Figure 3.1C and 3.1D, provides a simple optical sign for the detection of chemically and biologically important species occurring at the droplet surface. Therefore, in addition to CLC gels as mentioned in Chapter 2, it is very important to explore new pathways of preparing stable and uniform LC droplets that will ultimately provide a simplified and robust LC sensing platform.

Past reports established the feasibility of forming LC droplets *via* sequential ultra-sonication and vortexing of LCs in water,[8,14] with emulsifying agents such as surfactants.[15-18] Droplets prepared by these methods have been exploited in applications such as sensing which are highly specific and sensitive to biomolecular analytes. In addition to surfactants, various other stabilizers have also been used to prepare LC droplets. Tongcher *et al.* produced stable LC droplets in aqueous solution using a hydrophobe (such as hexadecane) to suppress molecular diffusion degradation and coalescence by collision.[19] Simon *et al.* reported the dispersion and stabilization of LC droplets in aqueous solution containing water soluble polymers.[20] Tjipto *et al.* reported the polyelectrolyte multilayers (PEMs) such as polyethylene amine (PEI), poly(styrene sulfonate) (PSS) and poly-(allylamine hydrochloride) (PAH) on LC and water emulsions.[21] Similarly, Fang and his group reported polyelectrolyte multilayer-coated LC droplets.[3,10,22] These polyelectrolytes dissociate in aqueous solution making the polymers charged and thus can assemble at the interface of the LC droplet giving rise to a stable director configuration that is governed by surface anchoring and bulk elastic energies of the LC. However, droplets prepared using these methods described above have less stability and broad size distribution that limits their widespread use in real applications. To address these issues, much progress has been made to stabilize LC droplets with uniform

sizes. For example, uniform silica particles coated with polyelectrolyte multilayers (PEMs) (Figure 3.2), microfluidic devices (Figure 3.3), etc. have been used as templates for stable and uniform LC droplets.[5,23-25]

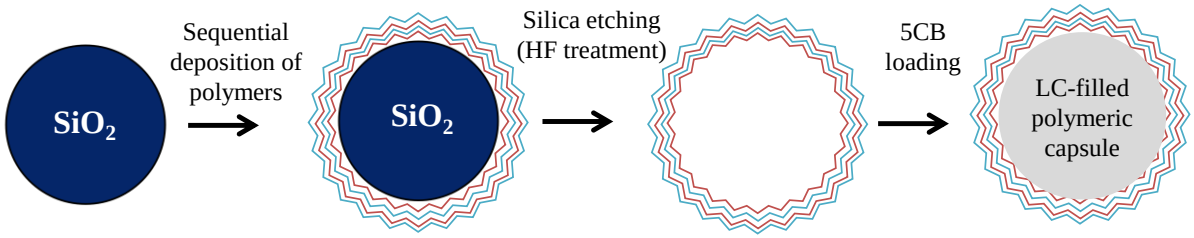

Figure 3.2 Schematic illustrations of the procedure used to prepare uniform LC droplets by the layer by-layer (LbL) adsorption of PEMs on uniform silica particles.

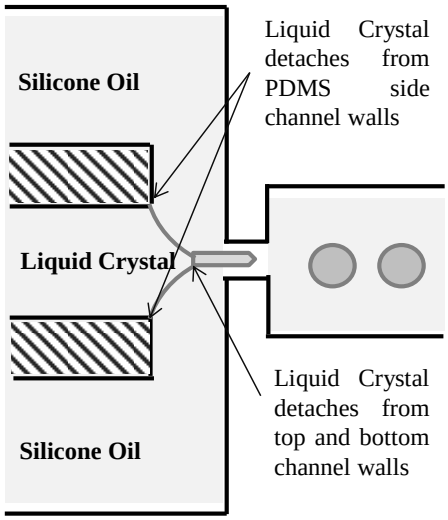

Figure 3.3 Schematic illustrations of the procedure used to prepare uniform LC droplets in microfluidic devices.

Nano size (~700 nm) LC droplets can be prepared using these methods. However, most of these techniques are either tedious or not suitable for large scale production. For instance, in this case where silica particles are coated with PEMs for the preparation of LC droplets, silica cores need to be first etched with hydrofluoric acid (HF) to achieve hollow polymeric capsules followed by filling the capsules with LCs.[5,23,24] Because of the highly corrosive nature of HF, the preparation of LC droplets becomes tedious and time consuming. Similarly,

in the case of microfluidic devices, a stream of co-flowing liquids was used to squeeze and break off LCs into spherical droplets.[25] Thus, it is difficult to customize the size of the LC droplets as they depend on the dimensions of the channel. However, all existing approaches for the preparation of LC droplets have certain limitations. Fabrication of simplified and robust LC droplet preparation is still challenging to researchers. Therefore, it is very important to explore new pathways of preparation of stable and uniform LC droplets which can be easily characterized and also provide a simplified robust LC sensing platform.

3.2 Objective

Although observations reported in the past established the feasibility of the formation of LC droplets with diameters in the micrometer-to-sub-micrometer range and their size dependent ordering,[24] direct observations of the spontaneous evolution of LC droplets with radial LC ordering in the presence of surfactants and lipids have not yet been investigated. The study reported in this work reveals the first breakthrough that shows characteristic micrometer-scale LC droplet patterns in the presence of lipids and their control over LC droplet sizes. We have also demonstrated that interactions between an enzyme and the topological defects in the LC mediate the response of these droplets and thus provide new designs for stimuli responsive soft materials. Herein, we report a new pathway for the easy formation of spontaneous uniform LC droplets. While the techniques reported in the past have resulted in the preparation of LC droplets with a life span of a few hours,[26] our approach has provided LC droplets with a stability of days to months. We observed the spontaneous formation of well-developed LC droplets with radial defects in the presence of phosphatidylcholine (PC) (Figure 3.4) within the confined boundary created by a grid system, suggesting new principles for the design of LC-based chemical and biological sensors.

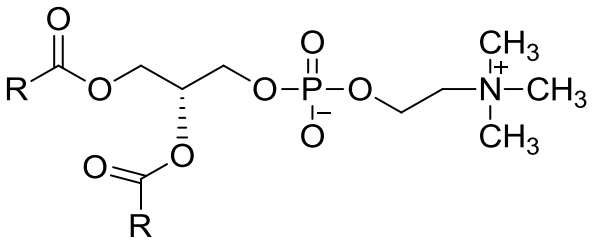

Figure 3.4 The chemical structure of L-α-Phosphatidylcholine (PC).

3.3 Results and Discussion

3.3.1 Spontaneous formation of LC droplets with radial LC ordering in presence of PC at LC-aqueous interface

We first performed an experiment to determine if the nematic ordering of 5CB (4'-pentyl-4-cyanobiphenyl) influences the organization and assembly of PC adsorbed to a 5CB-aqueous interface. We hosted 5CB in the pores of 20 μm thick electron microscopy grids supported on N,N-dimethyl-n-octadecyl-3-aminopropyltrimethoxysilyl chloride (DMOAP)-coated glass slides which induced homeotropic anchoring of the LC.[27]

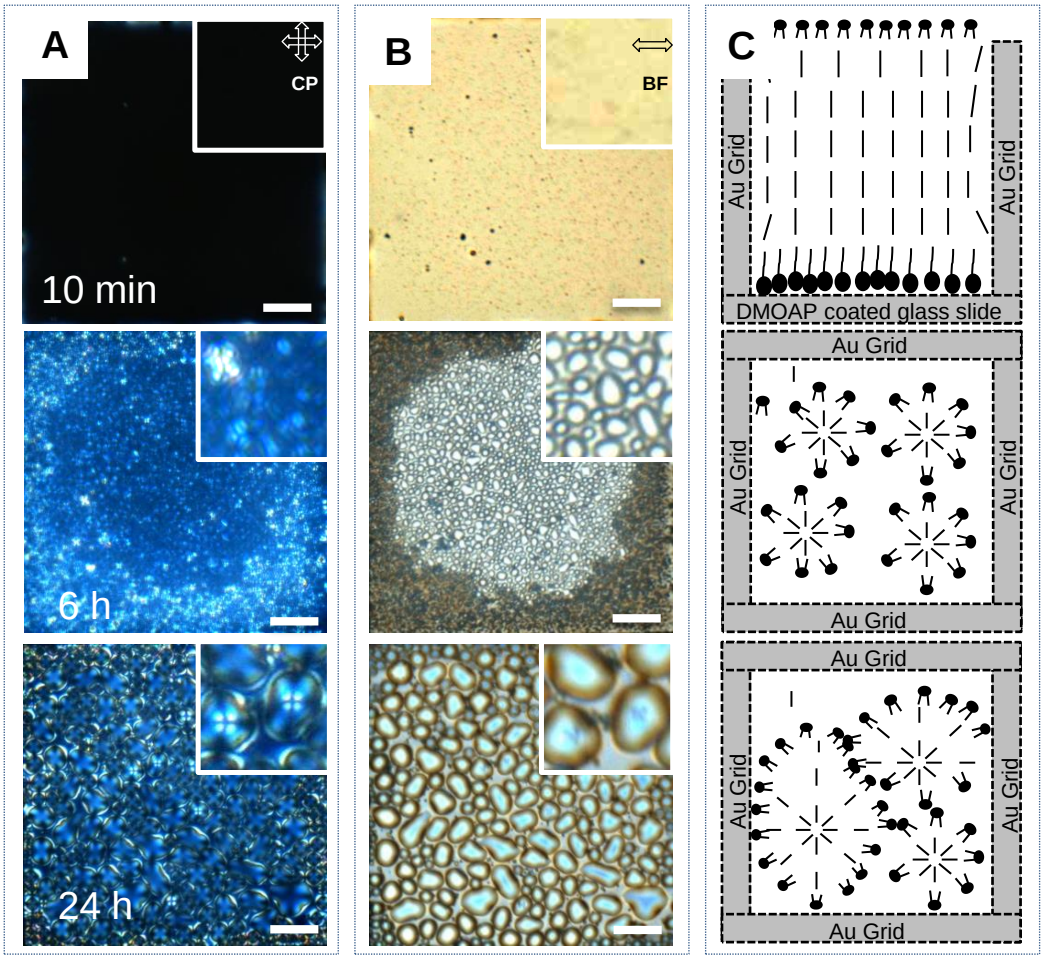

Figure 3.5 LC droplet formation within grid geometry in presence of PC. (A) Crossed polars (CP) and (B) bright field (BF) images of 5CB-aqueous interfaces within the TEM grids supported on DMOAP-coated glass slides upon exposure to 0.5 mg mL^{-1} PC after 10 min, 6 h

and 24 h. The insets (in (A) and (B)) show the corresponding high-magnification images that reveal the formation of stable and well-developed LC droplets exhibiting radial configuration. (C) Top to bottom: schematic illustration of the time dependent formation of LC droplets with radial LC ordering. Scale bar = 40 μm.

After subsequent immersion in an aqueous solution, the optical appearance of the LC became bright consistent with an orientation ordering transition induced by contact with water.[28] The results shown in Figure 3.5A were obtained by adsorbing PC (0.5 mg mL^{-1}) to the 5CB-aqueous interface which leads to a change in the optical appearance of the LC from bright to dark within a few minutes.

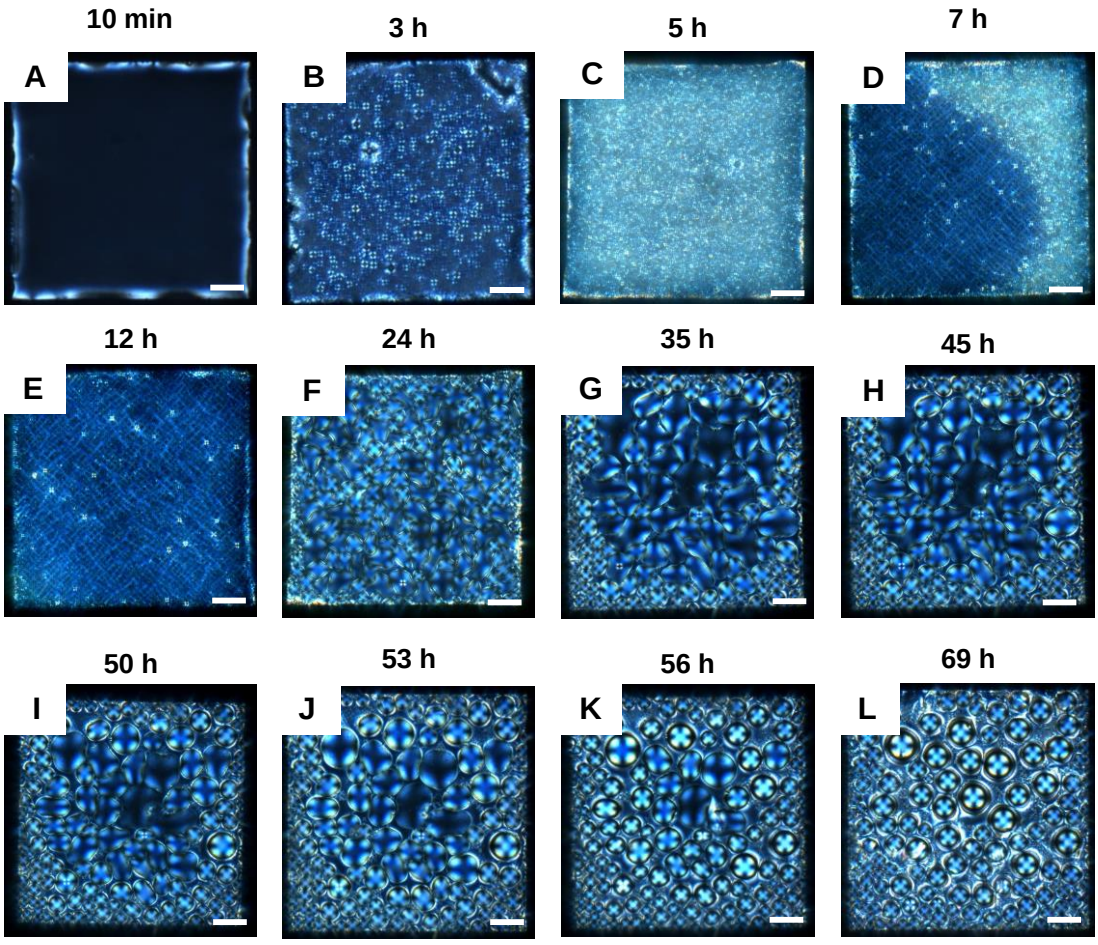

Figure 3.6 Time-dependent polarized optical micrographs (A-L) of 5CB-aqueous interfaces within TEM grids supported on DMOAP-coated glass slides upon exposure to 0.5 mg/mL phosphatidylcholine (PC). Scale bar = 40 μm.

After incubation for 3 h or more, we observed well-developed droplets which were characterized by a single point defect located at the center of the droplets shown in the bright field optical micrograph (Figure 3.5B). We hypothesized that the monolayer of PC rearranges itself around the LC resulting in the formation of LC droplets with defects (see below for details). The schematic representation and the process of the time-dependent formation of droplets are shown in Figure 3.5C and Figure 3.6.

3.3.2 Structural organization of water droplets to LC droplets with radial LC ordering in presence of PC at LC-aqueous interface

To provide an insight into whether PC is responsible for the formation of LC droplets with radial LC ordering, we first incubated a LC film (supported on DMOAP-coated glass slides) in an aqueous phase for three days followed by an exchange of the aqueous phase with the PC solution. Past investigations reported that a micrometer-thick film of the LC supported on OTS (octadecyltrichlorosilane) treated glass substrates led to the formation of water droplets when immersed under water.[29]

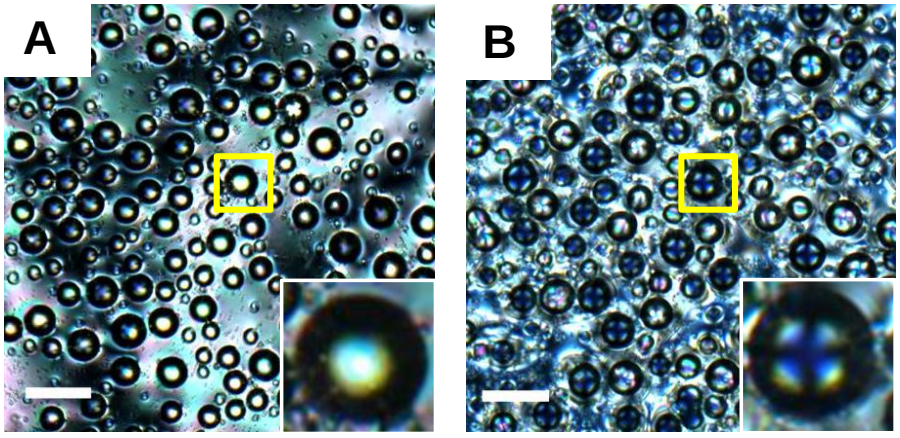

Figure 3.7 Structural organization of water droplets to LC droplets with radial LC ordering. (A) Polarized optical micrograph (crossed polars) of nematic 5CB hosted in a gold grid supported on a DMOAP-treated glass substrate after contact with water for 3 days. Water droplets formed spontaneously on the LC film. (B) Polarized optical micrograph of the 5CB-aqueous system (as in (A)) on exchanging the aqueous phase with the PC solution after 19 h. The well-developed water droplets reorganize to LC droplets with radial LC ordering. The

insets in (A) and (B) show the images of a selected water droplet and the corresponding LC droplet at high magnification, respectively. Scale bar = 40 µm.

On immersion of the LC film under water, we observed a spontaneous evolution of well-developed water droplets formed at the LC–DMOAP interface within 72 h (Figure 3.7A). Interestingly, when exchanging the aqueous phase with the PC solution we observed a topological defect formation within the droplet after 19 h.

We note two observations from Figure 3.7B. First, the regions of LCs around the droplets have transformed into a homeotropic orientation, as evidenced by the black areas. Second, LC droplets with topological defects are formed in the same location where water droplets were previously present. We do not yet fully understand the reason for the formation of LC droplets from water droplets after adding PC. It may be hypothesized that in the presence of PC, there could be a gradual replacement of water by LCs which is stabilized through topological defects. Figure 3.8 shows the time lapse images of the organization of water droplets to well-defined LC droplets.

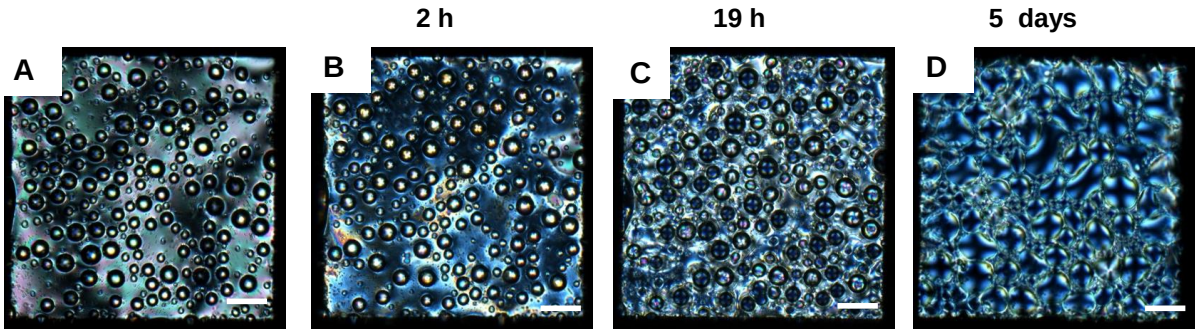

Figure 3.8 Time lapse reorganization of water droplets to LC droplets with radial LC ordering. A) Polarized optical images of 5CB within TEM grids supported on DMOAP-coated glass slides in contact with water for 3 days. (B-D) represents the time lapse polarized micrographs of 5CB-aqueous interface after exchanging the water with dispersion of PC vesicles. Scale bar = 40 µm.

The combination of the results described above leads to the following overall understanding of the LC droplet formation. During the formation of the macro emulsion, the reduction of

the interfacial tension reduces the amount of mechanical work required to break the inner phase into dispersed particles. So, the use of surfactants decreases the surface tension as well as the rate of coalescence of the dispersed LC particles by forming mechanical, steric or electrical barriers around them.

Theoretical approaches also reported the formation of an equilibrium state of a LC droplet which could be described as the minimum of the free energy functional (F), composed of both a volume (F_v) and a surface part (F_s).[30] The F_s can again be modeled as surface tension which has an isotropic part σ and an anisotropic part W_A (i.e., $Fs \sim 4\pi (\sigma r^2 + W_A r^2)$, r being the radius of the droplet). In the case of cyanobiphenyl, when the anchoring part W_A (10^{-5} to 10^{-6} J m^{-2}) is much smaller than σ (10^{-3} to 10^{-2} J m^{-2}), F_s ($4\pi\sigma r^2$) is dominated by the surface tension and thus proportional to r^2. It has been demonstrated that PC could decreases from 10^{-3} to 10^{-4} J m^{-2} which in turn decreases F_s.[31] In such cases, F is reduced to a greater extent which results in the formation of LC droplets, stabilized by topological defects. Our understanding of the formation of LC droplets is also supported by prior experiments. For example, the measured surface tension of a free interface (such as the LC–argon and LC–glycerin interface) with no surfactant is in the order of 15–20 mJ m^{-2}.[30] In contrast, the presence of a small amount of lecithin in glycerin decreases the surface tension between the LC and the glycerin to 10 mJ m^{-2} for the cholesteric (Ch) and smectic A (SmA) phase but drops to 3 mJ m^{-2} in SmA^*.[32] Kim *et al.* reported that the interface between 5CB and water + cetyl trimethylammonium bromide (CTAB) has a surface tension in the order of (1–6) mJ m^2.[33] Similarly, a plot of surface tension *vs.* temperature for 5CB–glycerin (no surfactant) showed that the values of surface tension are higher again between 20 and 15 mJ m^{-2}.[30] Of course, glycerin and water are different matrices but, adding a surfactant would generally decrease the interfacial tension between a LC and the surrounding isotropic fluid. The value inevitably depends on the concrete materials, as in the case of SmA^* it was decreased by a factor of 5–7, i.e., an order of magnitude.

In addition to the reduction of the interfacial tension, PC as reported imposes the anchoring boundary conditions for the nematic director.[34] PC, due to its hydrophobic part, interacts with the alkyl chain of 5CB and results in the homeotropic ordering of the LC. It then rearranges itself around the LC molecules and creates a radial arrangement around the LC molecules

where each droplet has a single point defect at the center (called *hedgehog*). Previous studies show the radial arrangement of the LC droplets with lecithin.[34] Past reports by Terentjev demonstrated that the stability of the nematic macro emulsions is greatly enhanced compared to that of the isotropic counterparts and thus the elastic constant of the LC and surface tension creates an energy barrier for coalescence.[35] This energy barrier of coalescence is K^2/W. With $K \sim 10^{-11}$ N and $W \sim 10^{-5}$ J m^{-2}, the energy barrier is very high ($\sim 10^{-17}$ J) compared to the typical thermal energy at room temperature.[35] Hence, it is very likely that in the presence of PC, there is an additional contribution of the elastic energy to the formation of the topological defects in the confined nematic and radial LC droplets, which prevents coagulation compared to their isotropic counterparts.

3.3.3 To characterize the location of PC within LC droplets with radial LC ordering *via* fluorescence microscopy

In order to provide a further insight into the microstructure of the LC droplets in the presence of PC, fluorescently tagged PC was used to examine the location of the surfactant (PC) in the co-assembly. Figure 3.9A shows the optical micrograph of 5CB hosted within gold grids supported on DMOAP-coated glass slides after contact with PC mixed with fluorescent PC (NBD-PC, see the Experimental section for details) for 3 days.

We observed that the fluorescence was mainly present at the boundary of (and also in between) the droplets with no fluorescence at the center of the droplets. This led us to conclude that the formation of the PC monolayer stabilizes these droplets by rearranging itself around the droplets. A bright field optical image of the same is shown in Figure 3.9B. To understand that we have LCs outside the droplet (not only inside), we performed confocal and fluorescence microscopy with a fluorescent N,N'-bis(2,5-di-tert-butylphenyl)-3,4,9,10-perylenedicarboximide (BTBP) compound which is known to align in the presence of LCs.[36] As expected from the fluorescence (Figure 3.9C) and from the confocal image (Figure 3.9E), we observed more BTBP outside the droplet. This study suggests that the background between the droplets is birefringent. Bright field fluorescence and confocal images are shown in Figure 3.9D and 3.9F, respectively.

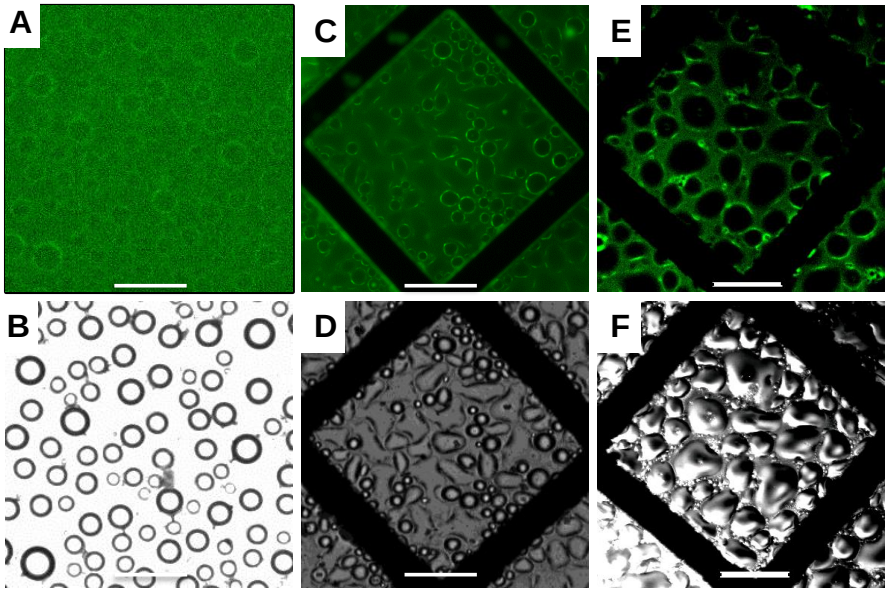

Figure 3.9 The fluorescence PC is mainly present at the boundary of the droplets. (A) Fluorescence micrograph and (B) the corresponding bright field image of nematic 5CB hosted within a gold grid supported on a DMOAP-treated glass substrate after contact with PC doped with 1 µM fluorescent PC (NBD PC) for 3 days. (C,E) represent fluorescent and confocal microscopy images of BTBP doped 5CB hosted within TEM grids after contact with PC vesicles for 5 days, respectively. (D,F) correspond to the fluorescence and confocal bright field images, respectively. Scale bar = 55 µm.

3.3.4 To determine stability of LC droplet with respect to time

Next, we sought to determine the stability of these droplets with respect to time. It was found that the droplets produced in the presence of PC are quite stable for a period of 20 days or more. As shown in Figure 3.10A, after incubation of PC at the 5CB-aqueous interface for 3 days the average droplet size reached ~ 21.34 ± 4.67 µm and remained for at least 5 days. A slight variation of the average size was observed within these days (i.e., from 21.34 ± 4.67 µm to 21.70 ± 4.70 µm). After 8 days of incubation (Figure 3.10B) the sizes increased to 32.63 ± 11.16 µm and changed continuously with time (Figure 3.10C and 3.10D). The time dependent growth of the droplet formation in the presence of PC at the 5CB-aqueous interface is shown in Figure 3.10E. We investigated and compared the stability and size distribution of the LC droplets to those of existing techniques.

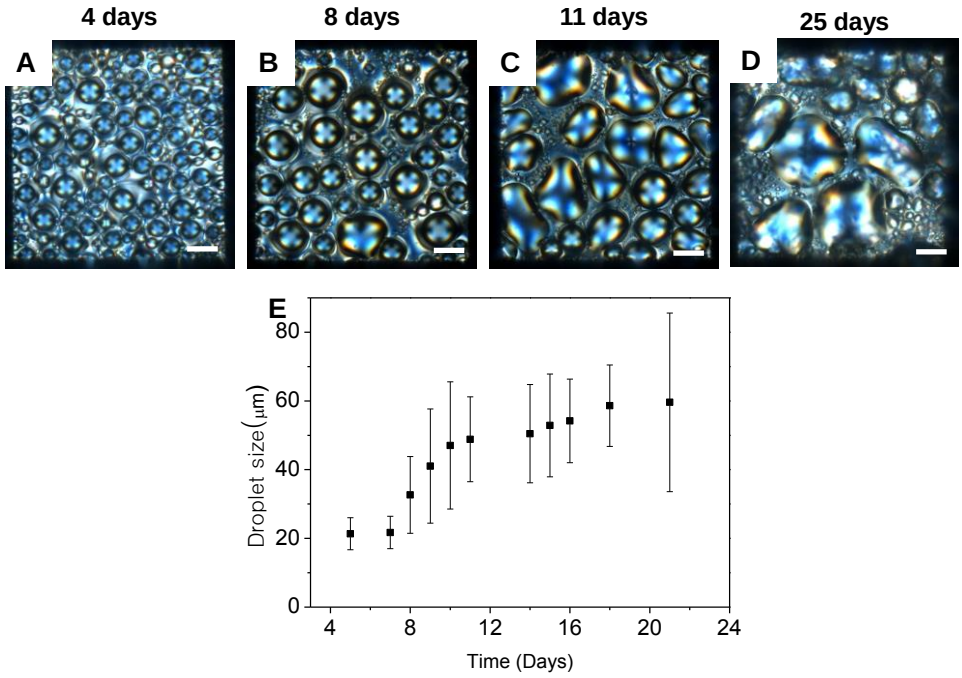

Figure 3.10 The LC droplets are stable for a period of 10 days. (A-D) Polarized optical images of time-dependent growth of 5CB droplets formed within TEM grids supported on DMOAP-coated glass slides in contact with PC (0.5 mg/mL). E) represents the time-dependent growth of domains (in μm) of 5CB droplets in presence of PC (0.5 mg/mL). Scale bar = 40 μm.

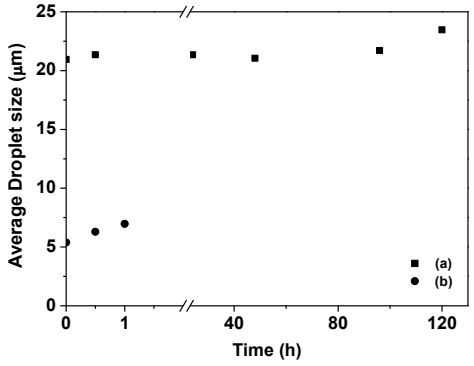

Figure 3.11 LC droplets prepared here are stable as compared to earlier reports. Stability and average size of LC droplets formed a) within TEM grids supported on DMOAP-coated glass slides in contact with PC (our approach) b) by sequential sonication and vortexing of LC in surfactant solution (past studies),[26] respectively.

Past reports quantified the size distribution (with an average diameter of ~ 6 μm) of 5CB droplets formed by sequential sonication and vortex mixing.[26] In our case, we observed an increase in the average size of the diameter of the LC droplets by approximately three times (~ 21 μm). Also, the techniques reported for the preparation of LC droplets in the past have a life span of only a few hours (Figure 3.11 and Figure 3.12).[26]

On the other hand, the droplets prepared by our method are quite stable for a period of several days. This is because in our case, the droplets formed in a confined boundary created by the grid system and thus stabilized (less mobile). These experiments also confirm the suitability of our approach towards a simple and robust platform using LC droplets for further applications.

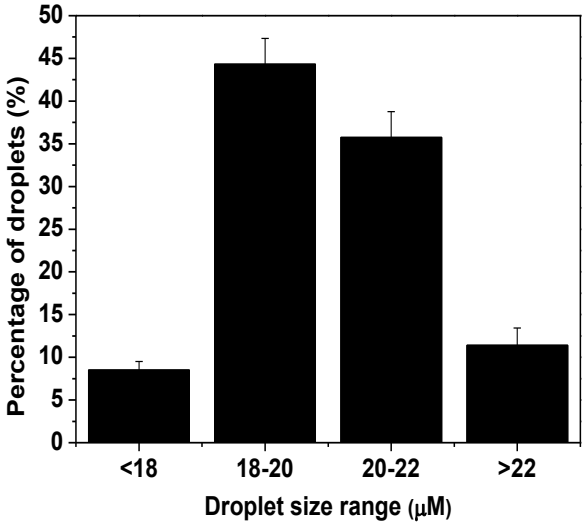

Figure 3.12 Size distribution of LC droplets formed within TEM grids supported on DMOAP-coated glass slides in contact with PC.

3.3.5 To determine stability of LC droplet with respect to temperature

Next, we examined the stability of the obtained LC droplets (with defects) below and above the nematic (N)–isotropic (I) phase transition temperature ($T_{N–I}$) of 5CB (35 ºC). Below $T_{N–I}$, the LC droplets with radial LC ordering showed a bright optical appearance under crossed polars (Figure 3.13). However, the optical response of the LC droplets exhibited a bright–

dark optical appearance after they were heated above the $T_{N–I}$ of 5CB. After cooling from the isotropic temperature to the N phase, we observed a bright optical appearance of the LC droplets followed by the appearance of the topological defects within these droplets. These results indicate that the LC droplets (with radial configuration) were quite stable and reversible i.e., the optical responses remain unchanged by the temperature-induced phase transition of the LCs.

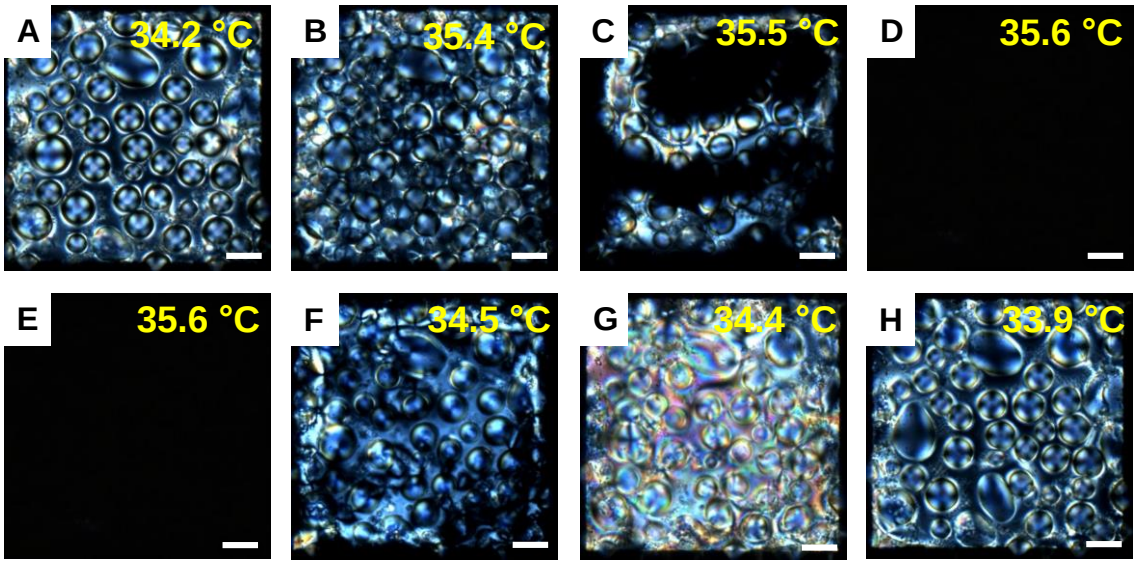

Figure 3.13 The optical responses of LC droplets remain unchanged by the temperature-induced phase transition of the LCs. Optical images under crossed polarizers of 5CB within TEM grids supported on DMOAP-coated glass slides in contact with aqueous dispersion of PC (0.5 mg/mL) vesicles after incubation for 3 days followed by heating above and below the phase transition temperature (T_{N-I} ~ 35 °C) of 5CB between nematic and isotropic states. The top rows (A-D) and the bottom rows (E-H) show the LC droplet patterns on heating above and cooling below the T_{N-I}, respectively. Scale bar = 40 μm.

3.3.6 To determine the effect of other surfactants/lipids on the spontaneous formation of LC droplets within confined boundaries

In addition to PC, which induces the formation of stable droplets with radial LC configuration, we investigated the role of other surfactants and lipids and explored their behavior on incubation at 5CB-aqueous interfaces. We have chosen sodium dodecyl sulfate

(SDS), CTAB, lysophosphatidic acid (LPA), 1,2- dilauroyl-sn-glycero-3-phosphocholine (DLPC) and lipopolysaccharide (LPS) and studied their behavior at 5CB-aquoeus interfaces. The chemical structure of these selected lipids and surfactants are shown in Figure 3.14. The goal of this experiment is mainly twofold. First, we sought to find out whether other lipids are also suitable for the spontaneous formation of LC droplets in addition to PC as described above. Second, we sought to demonstrate any additional parameter which can advance our understanding in the formation of droplets.

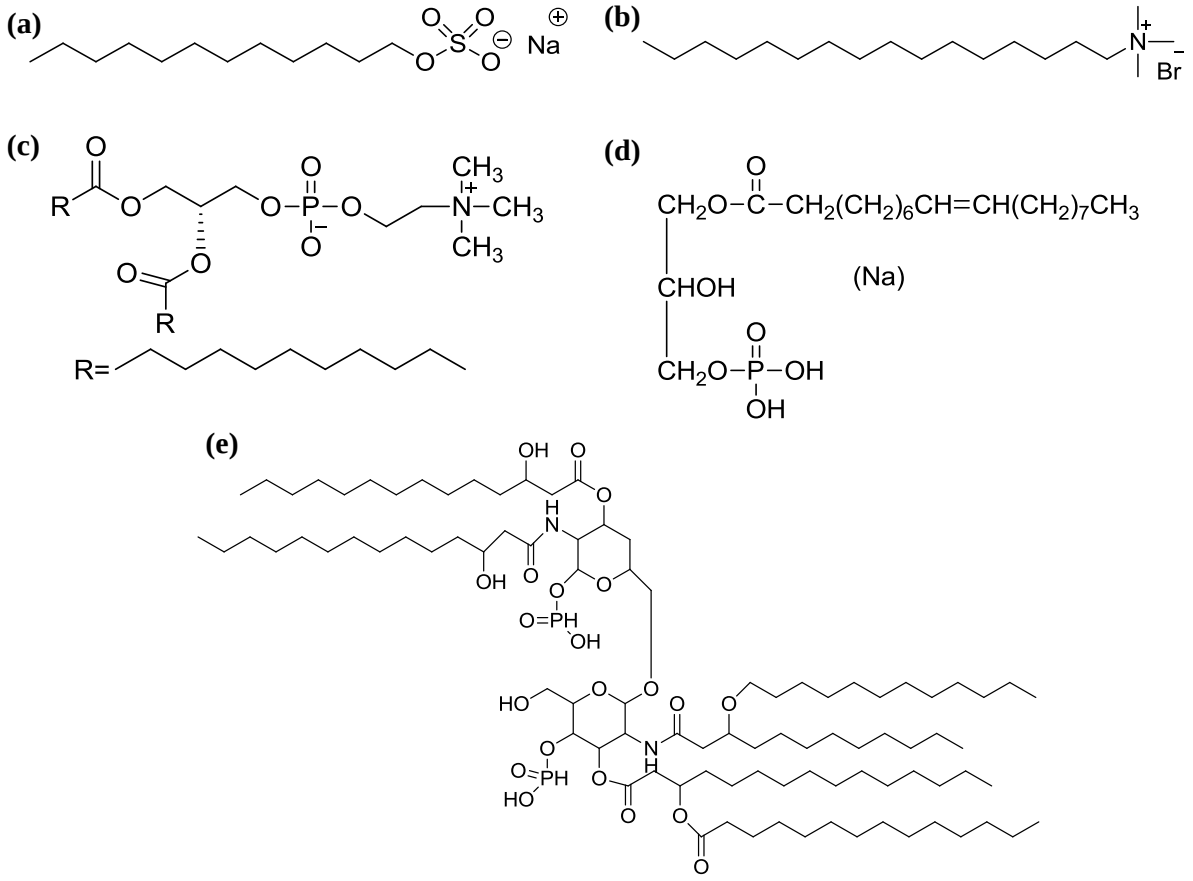

Figure 3.14 The chemical structures of (a) SDS, (b) CTAB, (c) DLPC, (d) LPA and (e) Lipid A part of LPS.

All the surfactants we have chosen are ionic and therefore, can stabilize the droplets electrostatically. Figure 3.15 shows the optical images of nematic 5CB hosted within gold grids supported on DMOAP-coated glass slides in contact with CTAB, DLPC, SDS, LPS and LPA with respect to time. We monitored these systems carefully for 15 days and observed

the following two key points. First, within 3 days of incubation, both CTAB and DLPC resulted in the formation of nice and well developed droplets with radial LC ordering. Second, LPA does not lead to the formation of stable droplets whereas no droplet formation was observed in the presence of LPS and SDS.

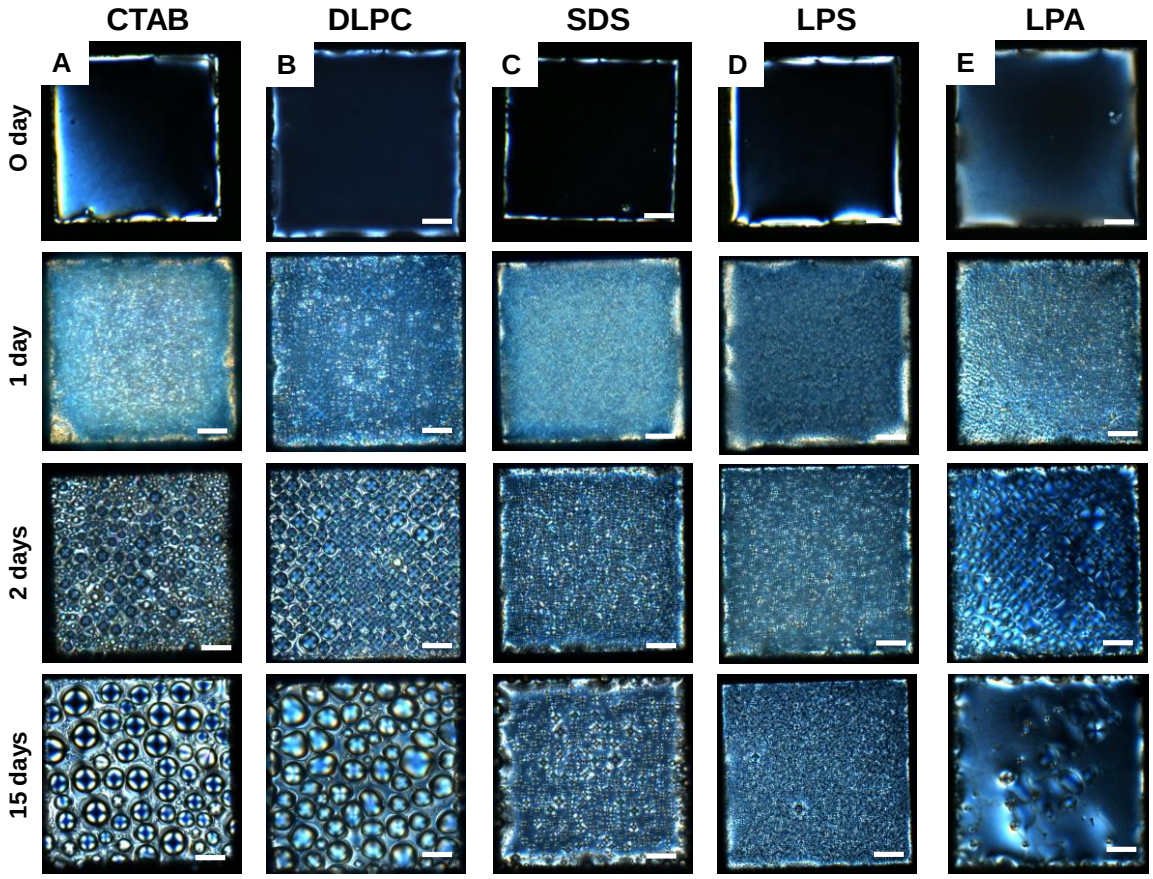

Figure 3.15 The positively or zwitterionic surface active surfactants and lipids (CTAB and DLPC) resulted in the spontaneous LC droplets formation. Time-dependent optical images under crossed polarizers of 5CB within TEM grids supported on DMOAP-coated glass slides after exposure of 5CB-aqueous interface to A) positively charged hexadecyltrimethyl ammonium bromide (0.1 μM CTAB), B) zwitterionic 1,2-dilauroyl-sn-glycero-3-phosphocholine (0.5 mg/mL DLPC), C) negatively charged sodium dodecylsulfate (2 μM SDS), D) negatively charged lipopolysaccharides (0.5 mg/mL LPS) and E) negatively charged oleoyl-L-α lysophosphatidic acid sodium salt (40 μM LPA). Scale bar = 40 μm.

These results indicate that (i) CTAB and DLPC are more surface active (in comparison to SDS and the others) and thus resulted in a more efficient reduction in surface tension.[5,31,37] (ii) Past reports also demonstrated that the LC droplets formed in water remained stable due to the adsorption of hydroxide ions at the LC–water interface.[38] This hydroxide ion adsorption makes the LC droplet surface negatively charged. So, it can be concluded that in addition to an efficient reduction in surface tension, an electrostatic attraction in the presence of DLPC and CTAB (DLPC is zwitterionic and CTAB is positively charged) at the LC interface (negatively charged) stabilized the LC droplets compared to SDS, LPA and LPS (being negatively charged). Also a negative surface charge density on DMOAP-coated surfaces stabilizes the positive and zwitterionic droplets. These results reveal for the first time that, in addition to inducing homeotropic alignment of the LC, the ionic charge in the lipids can play an important role for the spontaneous formation of LC droplets.

3.3.7 Using these spontaneously prepared LC droplets for detecting biomolecules (e.g., LPS)

The observations reported above are interesting to consider based on prior studies on the topological ordering of LCs within droplets to report interfacial enzymatic reactions.[5] Past reports established that PLA_2 triggers a transformation of the LC droplet from a radial configuration to a bipolar configuration decorated with L-DLPC.[5] Motivated by this, we investigated the topological states encountered in the LC droplets during enzymatic degradation of PC using PLA_2.

Figure 3.16 shows the corresponding polarized light micrograph of the LC droplets in response to the adsorption of PLA_2 (150 nM). Interestingly, upon introduction of PLA_2, an anchoring transition of the LC was observed from an initially homeotropic orientation (radial configuration in the presence of PC) to a planar orientation with a bipolar topological defect. These bipolar droplets were then further explored in detecting various bio-molecules such as bacterial phospholipids (LPS). Past reports demonstrated that LPS induced an ordering transition in LC droplets from a bipolar to radial configuration.[8] This ordering transition is not mediated by surface anchoring energy but rather consistent with the association of LPS with defects.

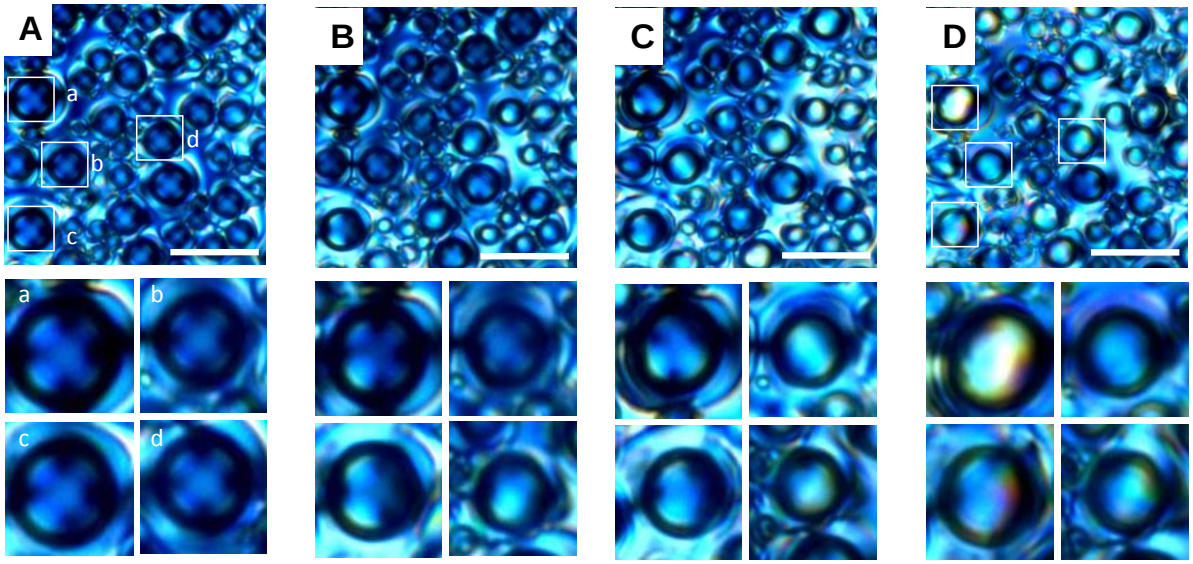

Figure 3.16 Enzymatic degradation of PC decorated LC droplets using PLA_2 triggers a transformation of the LC droplet from a radial to a bipolar configuration. Top row: (A–D) optical images (crossed polars) of 5CB droplets covered with DLPC upon exposure of 150 nM PLA_2 into an aqueous solution of TBS (pH = 8.9) containing 10 mM $CaCl_2$. These droplets with a radial defect were formed by contacting the 5CB interface laden with DLPC (0.1 mg mL^{-1}) at an incubation period of 2 days. The second row depicts the change in the anchoring transition of the representative region of the four selected droplets (a–d) from radial to bipolar upon adsorption of PLA_2. Scale bar = 40 µm.

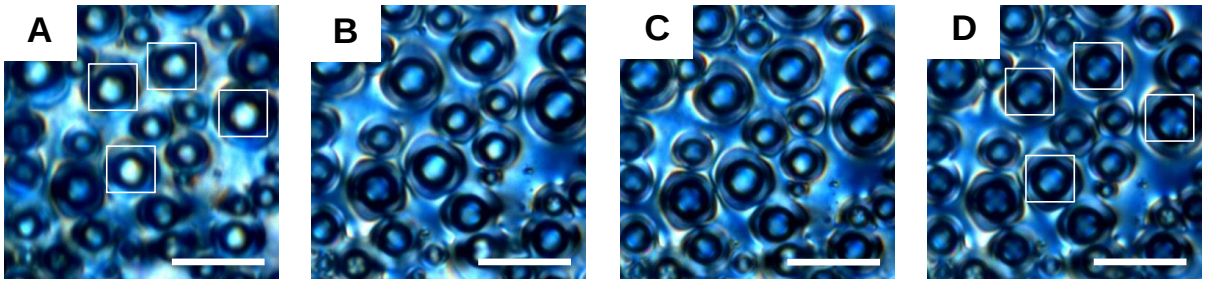

Figure 3.17 Represents change in anchoring transition of LC droplets from bipolar to radial upon adsorption of LPS. A) Polarized optical image of 5CB droplets covered with DLPC upon exposure of 150 nM PLA_2 containing 10 mM $CaCl_2$ into an aqueous solution of TBS (pH = 8.9). (B-D) represents the time lapse polarized micrographs of 5CB-aqueous interface following contact with 100 µg/mL aqueous LPS. Scale bar = 40 µm.

We investigated this phenomenon with LC droplets formed through enzymatic degradation of PLA_2 (bipolar) and observed a structural transformation to radial configuration. The optical response of these LC droplets with a bipolar configuration to radial configuration after the adsorption of LPS is shown in Figure 3.17. This result, we believe in principle, enables new pathways to exploit interfacial adsorbate-induced properties of LC droplets.

3.4 Conclusions

In conclusion, the study establishes first to reveal direct observations of the spontaneous evolution of LC droplets with radial LC ordering in the presence of surfactants and lipids. The formations of stable LC droplets are not only due to the reduction of the interfacial tension between the LC and the surrounding isotropic fluid but also have an additional stability mechanism (against coagulation) associated with the internal elasticity. Our observations also affirm that ionic charge can play an important role in the spontaneous formation of LC droplets with topological defects. Finally, we have shown that interactions of an enzyme with the topological defects in the LC droplets can provide means for developing new responsive soft materials.

3.5 Experimental Section

3.5.1 Materials

L- α- Phosphatidylcholine (PC), oleoyl-L-α-Lyso phosphatidic acid sodium salt (LPA), hexadecyltrimethylammonium bromide (CTAB), lipopolysaccharides (from E.coli 0111:B4), N,N'-Bis(2,5-di-tert-butylphenyl)-3,4,9,10-perylenedicarboximide (BTBP), N,N dimethyl-N-octadecyl-3-aminopropyltrimethoxysilyl chloride (DMOAP) and sodium dodecylsulfate (SDS) were purchased from Sigma-Aldrich (St. Louis, MO). 1,2-dilauroyl-snglycero- 3-phosphocholine (DLPC) and 1-Palmitoyl-2-{12-[(7-nitro-2-1,3-bezoxadiazol-4-yl) amino] dodecanoyl-sn-glycero-3-phosphocholine (NBD PC) were purchased from Avanti Polar Lipids Inc. Phospholipase A_2 from naja mossambica mossambica was purchased from Sigma- Aldrich (St. Louis, MO). Sulfuric acid, chloroform and hydrogen peroxide (30% w/v) were purchased from Merck (Mumbai, India). Ethanol was obtained from Jebsen & Jenssen GmbH and Co., Germany (s d. fine–chem limited). 4-cyano-4'-pentylbiphenyl (5CB) was

obtained from Sigma-Aldrich (St. Louis, MO). Deionization of a distilled water (DI water) source was performed using a Milli-Q-system (Millipore, bedford, MA). Fisher's Finest Premium Grade glass microscopic slides and cover glass were obtained from Fischer Scientific (Pittsburgh, PA). Gold specimen grids (20 μm thickness, 50 μm wide bars, 283 μm grid spacing) were obtained from Electron Microscopy Sciences (Fort Washington, PA).

3.5.2 Preparation of LC films in TEM grids

Glass slides were cleaned with piranha solution (70:30 (% v/v) H_2SO_4:H_2O_2) for 1 h at 100 °C according to the published procedures.[39] Briefly, the glass slides were immersed in a piranha bath at 100 °C for at least 1 h and then rinsed in running deionized (DI) water for 5-10 min. Finally, the slides were rinsed sequentially in ethanol and then dried under a stream of nitrogen. The clean slides were stored in an oven at 100 °C for overnight. These cleaned glass slides were then dipped into 0.1% (v/v) DMOAP solutions in DI for 5 min at room temperature and rinsed with DI to remove the unreacted DMOAP from the surface. The DMOAP-coated glass slides were dried under a stream of nitrogen gas and kept in oven at 100 °C for 3 h.

Cleaned gold specimen grids were placed on DMOAP-coated glass slides. The grids were filled with approximately 0.2 μL of 5CB and the excess of LC was removed with the help of syringe to produce a planar interface.

3.5.3 Preparation of vesicles

Vesicles were prepared according to the published procedures.[5] Briefly, the lipids were dissolved in chloroform (0.5 mL) and dispensed into round bottomed flask. Prior to re-suspension, the chloroform was evaporated from the flask under vacuum for at least 2 h until it formed a thin film along the inner walls of the flask. The lipid film formed in the flask was then placed under a stream of nitrogen for 30 min. The dried lipid was then hydrated in the aqueous solution (DI water) for at least 1h and vortexed for 1 min. This results in the cloudy solution indicative of large multi-lamellar vesicles. Subsequent sonication of lipid suspension using a probe ultra-sonicator (1 x 15 min at 25 W) resulted in a clear solution. Vesicles size was determined by DAWN8$^+$ dynamic light scattering instrument (Figure 3.18).

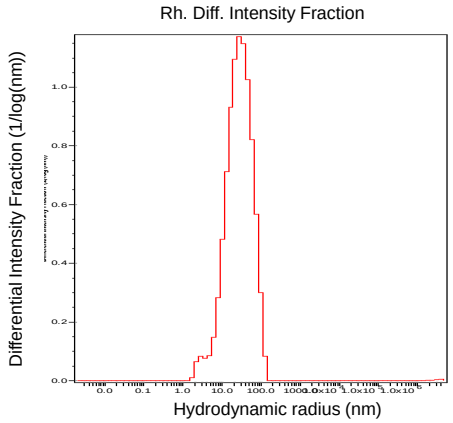

Figure 3.18. Plot showing the PC vesicle size distribution using dynamic light scattering.

Prior to dynamic light scattering measurements, the solution of PC vesicles was filtered twice using 0.22 μm filter. The vesicles were used within 24 h of their preparation.

3.5.4 Formation of LC droplets with radial defects

The DMOAP-coated glass surface supported LC-filled grid was submerged into glass wells containing 3 mL of distilled water. 1 mL of PC lipid solution was added to the aqueous solution to make a final concentration of 0.5 mg/mL (Figure 3.19). The LC-filled grid in PC solution was then allowed to incubate for 48 h. Paraffin was placed over the top of the glass well to prevent evaporation of water.

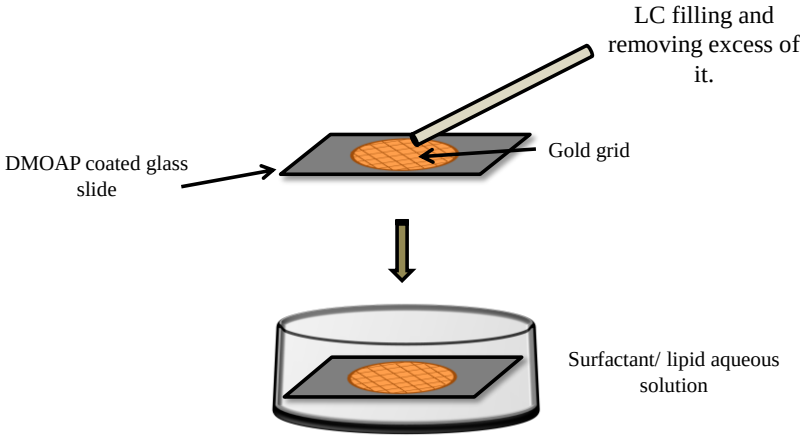

Figure 3.19 Schematic illustrations of the experimental setup for the preparation of LC droplets within confined boundaries created by grid system.

3.5.5 Optical characterization of LC droplets with radial defects

The orientational ordering of LC droplets was determined under Nikon Eclipse LV100POL Polarizing Microscope using an objective power of 200x with cross polars. Orthoscopic examinations were performed with the source light intensity set to 50% of full illumination and the aperture set to 0.45 in order to collimate the incident light. All the images were captured using a Q-imaging camera.

3.5.6 Fluorescence imaging

The LC-filled grid was incubated under lipid solution containing 1 μM 1-Palmitoyl-2-{12-[(7-nitro-2-1,3-bezoxadiazol-4-yl) amino] dodecanoyl-sn-glycero-3-phosphocholine (NBD-PC) for 48 h. After incubation the solution was then exchanged with distilled water thrice to remove the excess of NBD-PC from the bulk solution. The LC-filled grid supported on DMOAP-coated surfaces was then removed from the solution and placed over a glass slide. Few drops of distilled water was poured over it and covered with a cover slip keeping a distance of 0.2 cm from the sample. Fluorescence imaging was performed with Zeiss (Scope. A1) fluorescence microscope. The samples were viewed using a fluorescence filter cube with a 460 nm excitation filter and a 534 nm emission filter. Images were obtained with Axio cam camera.

References

(1) Alino, V. J.; Pang, J.; Yang, K.-L. *Langmuir* **2011**, *27*, 11784–11789.

(2) Alino, V. J.; Tay, K. X.; Khan, S. A.; Yang, K.-L. *Langmuir* **2012**, *28*, 14540–14546.

(3) Bera, T.; Fang, J. *J. Mater. Chem.* **2012**, *22*, 6807–6812.

(4) Bera, T.; Fang, J. *Langmuir* **2013**, *29*, 387–392.

(5) Gupta, J. K.; Zimmerman, J. S.; de Pablo, J. J.; Caruso, F.; Abbott, N. L. *Langmuir* **2009**, *25*, 9016–9024.

(6) Khan, W.; Choi, J. H.; Kim, G. M.; Park, S.-Y. *Lab Chip* **2011**, *11*, 3493–3498.

(7) Kinsinger, M. I.; Buck, M. E.; Abbott, N. L.; Lynn, D. M. *Langmuir*, **2010**, *26*, 10234–10242.

(8) Lin, I.-H.; Miller, D. S.; Bertics, P. J.; Murphy, C. J.; de Pablo, J. J.; Abbott, N. L. *Science* **2011**, *332*, 1297–1300.

(9) Sivakumar, S.; Wark, K. L.; Gupta, J. K.; Abbott, N. L.; Caruso, F. *Adv. Funct. Mater*. **2009**, *19*, 2260–2265.

(10) Zou, J.; Bera, T.; Davis, A. A.; Liang, W.; Fang, J. *J. Phy. Chem. B* **2011**, *115*, 8970–8974.

(11) Volovik, G. E.; Lavrentovich, O. D. *Sov. Phys. JETP* **1983**, *58*, 1159−1167.

(12) Xie, A.; Higgins, D. A. *Appl. Phys. Lett.* **2004**, *84*, 4014-4016.

(13) Groot, D.; Eleanor, M.; Fuller, G. G. *Liq. Cryst.* **1997**, *23*, 113-126.

(14) Miller, D. S.; Wang, X.; Buchen, J.; Lavrentovich, O. D.; Abbott, N. L. *Anal. Chem.* **2013**, *85*, 10296−10303.

(15) Loudet, J. C.; Richard, H.; Sigaud, G.; Poulin, P. *Langmuir* **2000**, *16*, 6724-6730.

(16) Nicoletta, F. P.; Lanzo, J.; Filpo, G. D.; Chidichimo, G. *Langmuir* **2001**, *17*, 534-536.

(17) Butler, M. H.; Williamson, A.-M.; Terentjev, E. M. *Liq. Cryst.* **2005**, *32*, 77-84.

(18) Tixier, T.; Butler, M. H.; Terentjev, E. M. *Langmuir* **2006**, *22*, 2365-2370.

(19) Tongcher, O.; Sigel, R.; Landfester, K. *Langmuir* **2006**, *22*, 4504-4511.

(20) Simon, K. A.; Sejwal, P.; Gerecht, R. B.; Luk, Y-Y. *Langmuir* **2007**, *23*, 1453-1458.

(21) Tjipto, E.; Cadwell, K. D.; Quinn, J. F.; Johnston, A. P. R.; Abbott, N. L.; Caruso, F. *Nano Lett*. **2006**, *6*, 2243-2248.

(22) Zou, J.; Fang, J. *Langmuir* **2010**, *26*, 7025–7028.

(23) Sivakumar, S.; Gupta, J. K.; Abbott, N. L.; Caruso, F. *Chem. Mater*. **2008**, *20*, 2063–2065.

(24) Gupta, J. K.; Sivakumar, S.; Caruso, F.; Abbott, N. L. *Angew. Chem. Int. Ed.* **2009**, *48*, 1652–1655.

(25) Umbanhowar, P.; Prasad, V.; Weitz, D. *Langmuir* **2000**, *16*, 347–351.

(26) Miller, D. S.; Abbott, N. L. *Soft Matter* **2013**, *9*, 374–382.

(27) Bi, X.; Huang, S.; Hartono, D.; Yang, K.-L. *Sens. Actuators B* **2007**, *127*, 406–413.

(28) Brake, J. M.; Daschner, M. K.; Luk, Y.-Y.; Abbott, N. L. *Science* **2003**, *302*, 2094–2097.

(29) Yang, Z.; Abbott, N. L. *Langmuir* **2010**, *26*, 13797–13804.

(30) Lavrentovich, O. D. *Liq. Cryst.* **1998**, *24*, 117–126.

(31) Harrison, D.; Fisch, M. R. *Liq.Cryst.* **2000**, *27*, 737–742.

(32) Lavrentovich, O. D.; Nastishin, Y. A.; Kulishov, V. I.; Narkevich, Y. S.; Tolochko, A. S.; Shiyanovskii, S. V. *Europhys. Lett.* **1990**, *13*, 313–318.

(33) Kim, J.-W.; Kim, H.; Lee, M.; Magda, J. J. *Langmuir* **2004**, *20*, 8110–8113.

(34) Prischepa, O. O.; Shabanov, A. V.; Zyryanov, V. Y. *Mol. Cryst. Liq. Cryst.* **2005**, *438*, 141/[1705]–1150/[1714].

(35) Terentjev, E. M. *Europhys. Lett.* **1995**, *32*, 607–612.

(36) Lavrentovich, O. D. *Contemp. Math.* **2012**, *577*, 25–46.

(37) Sohrabi, B.; Gharibi, H.; Tajik, B.; Javadian, S.; Hashemianzadeh, M. *J. Phys. Chem. B* **2008**, *112*, 14869–14876.

(38) Marinova, K. G.; Alargova, R. G.; Denkov, N. D.; Velev, O. D.; Petsev, D. N.; Ivanov, I. B.; Borwankar, R. P. *Langmuir* **1996**, *12*, 2045–2051.

(39) Brake, J. M.; Abbott, N. L. *Langmuir* **2002**, *18*, 6101-6109.

Chapter 4

pH-Driven Ordering Transitions in Liquid Crystal Induced by Conformational Changes of Cardiolipin

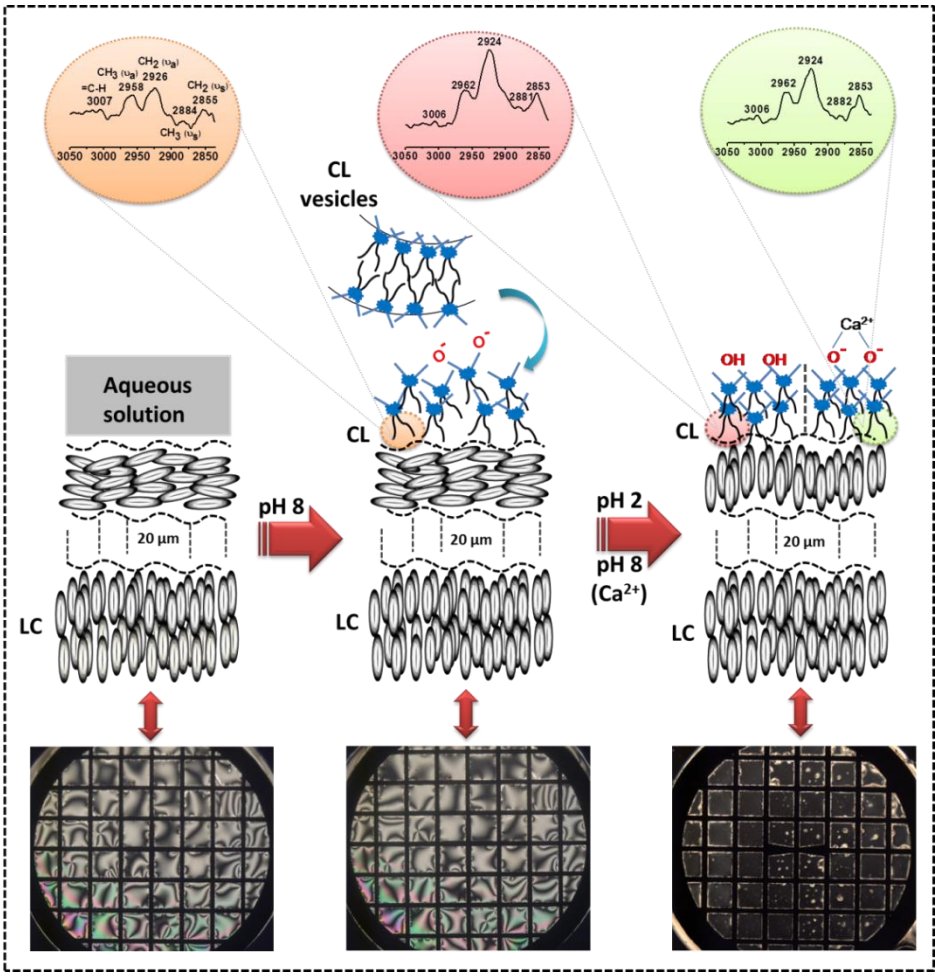

Interfacial phenomena occurring at liquid crystal (LC)-aqueous interfaces that trigger an orientational ordering transition of the LC in the presence of cardiolipin (CL) by varying pH, salt concentration and valence. In particular, LCs offer a promising approach to differentiate different conformations (label free detection) of the CL through ordering transition of the LC at LC-aqueous interfaces.

4.1 Introduction

Cardiolipin (CL), the signature phospholipid of a mitochondrion, has broad and complex implications in the function of oxidative phosphorylation and other mitochondrial activities.[1,2] In particular, CL has been shown to play a key role in the maintenance of optimal activity of a number of major integral proteins in energy-transducing membranes.[3–7] This unique lipid is a dimeric phospholipid with two phosphatidyl moieties linked *via* a central glycerol group. It has four unsaturated acyl chains of varying lengths and a polar head group with two negative charges (Figure 4.1).

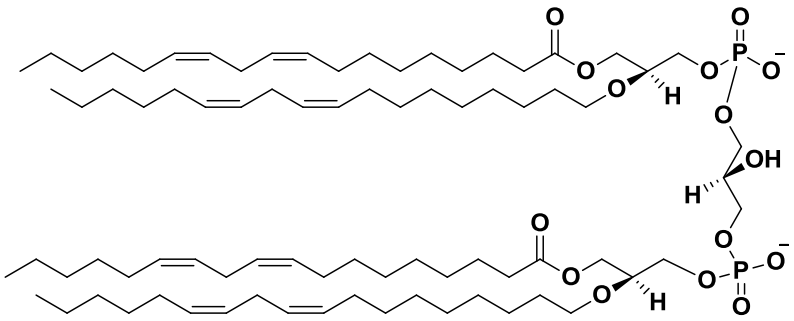

Figure 4.1 Chemical structure of cardiolipin [(1,3-bis(sn-3'-phosphatidyl)-sn-glycerol].

However, these phosphate groups have different pK_a values (pK_1< 4.0 and pK_2> 7.0). This has been attributed to an intramolecular hydrogen bond with the centered glycerol's hydroxyl group thus resulting in the formation of a bicyclic resonance structure.[8] CL is able to form different conformational forms in aqueous dispersions depending on pH and ionic strength (Figure 4.2).[9–11] Because of this unique structure, CL is virtually the only negatively charged lipid in the inner mitochondrial membrane[12] where a chemical gradient of protons is used in the respiratory chain to restore the fundamental energy currency of the living cell ATP. It should be noted that the CL contributes in modulating surface properties of membranes.[13,14] This property of CL is known to determine the interactions between CL and many CL requiring membrane enzymes.[7] In human mitochondria, the inner mitochondrial membrane is rich in CL (9.2% by mole).[15]

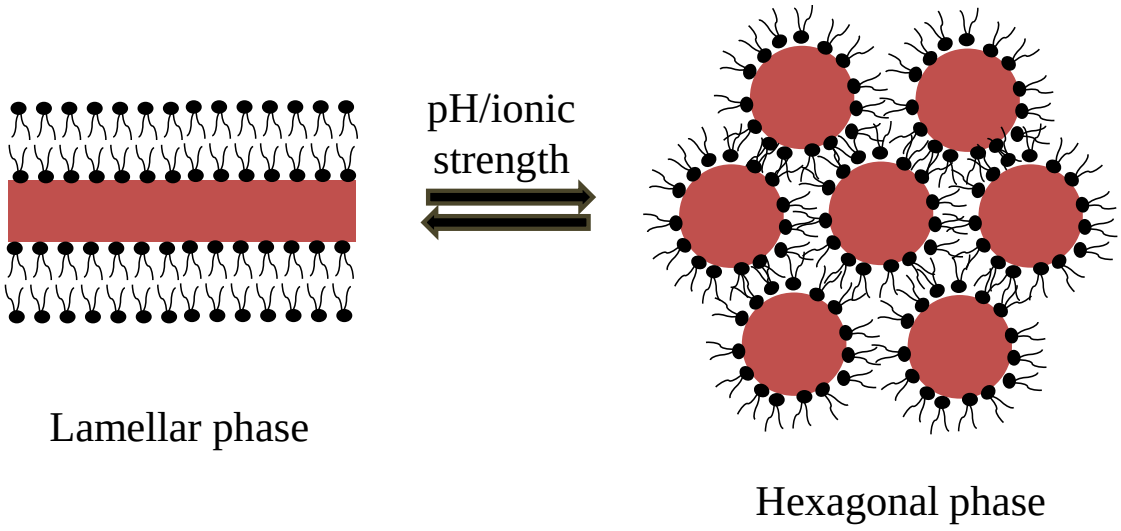

Figure 4.2 Schematic illustrations of different conformational forms (lamellar and hexagonal) of CL in aqueous dispersions, depending on pH and ionic strength.

Consequently, being an exclusive mitochondrial inner membrane phospholipid involved in various mitochondrial functions, marked change in the polymorphic behavior of the CL is known to affect a range of cellular processes. Therefore, the structural behavior of the CL acts as a biomarker for understanding the clinical investigation of mitochondrial related problems like heart failure, myopathy, Tangier, Barth syndrome, HIV-1 and cancers.[16] Thus, the study of the different conformers of the CL is potentially important for therapeutical and clinical point of view.

To date, extensively used procedures for location and quantitative analysis of CL have been done using fluorescent probes. The fluorescent dye 10-N-nonyl acridine orange (NAO) is used, which upon binding with CL-containing membranes results decrease in fluorescence that enables the detection and quantification of the CL.[17] But, this method is highly nonspecific, involves tortuous steps and poor water solubility of NAO makes it less appealing to be used in biological systems.[17] In addition, NAO is influenced by membrane potential and spatial arrangement of CL[18-20] and thus limits its widespread use for CL and mitochondria based quantitative studies. Significant progress has been made in the development of fluorescent based strategies, like derivatization of CL in a total lipid extract with 1-pyrenyldiazomethane (PDAM) to form stable fluorescent 1-pyrenylmethyl esters[21] or

use of aggregation induced emission (AIE) luminogens[22] or surface modified quantum dots[23] as a fluorescent probe for the detection of CL. In addition to this, lipidomics profiling by high resolution LC-MS has recently been developed for quantitative analysis of CL.[24] However, these methods lack simplicity, sensitivity and require sophisticated instrumentation which limits the scope of their application. In this study, we have used intrinsic cooperative behavior associated with the long-range orientational order of the liquid crystal (LC) phase as a probe to study the different polymorphic behaviors of CL. The methodology in our study eliminates the need for biochemical amplification, labeling or expensive instrumentation.

LC-based sensing techniques at LC-aqueous interfaces in addition to LC droplets as discussed in Chapter 3 have drawn widespread interest for the sensitive amplification of amphiphiles, such as phospholipids[25,31,32] and surfactants.[27,30] These adsorbed surfaces make them attractive for a number of potential applications involving more complex interfacial phenomena, such as high-throughput screening of enzymatic activity[37](as mentioned in Chapter 3) and molecular binding events,[38-44] through LC reorientations driven by chemical or physical events that perturb the organization of the monolayer interfaces. For example, Schwartz and his co-workers reported that DNA hybridization causes a dynamic LC reorientation at a surfactant laden LC-aqueous interface.[30] In another study, they found that conformational change of an aptamer from a relaxed random coil to more intricate secondary structures upon target binding led to LC reorientation at the surfactant-laden LC-aqueous interface.[45] Thus, orientation of LC responded directly with the binding events associated with nucleic acid conformational change at the surfactant laden LC-aqueous interface. The study reported in this paper builds on the results by these prior investigations which suggest that LC-aqueous interfaces demonstrate a promising class of biomolecular interfaces for reporting interfacial phenomena. Herein, we report an investigation to the development of a new design of such interfaces for the detection of CL.

4.2 Objective

The study was motivated by two broad goals. First, we sought to establish a methodology to create an LC-aqueous interface that would be responsive in the presence of the CL. It should be noted that unlike other lipids (such as DLPC), anchoring transition of LCs remains

invariant through adsorption of CL at these interfaces (at pH 7.4, see Results and Discussion for details). Second, we sought to determine how different conformers (controlled by change in pH, see next paragraph) of the CL would impact (e.g., modify interactions) the orientational ordering of LCs at aqueous interfaces. In particular, we sought to develop a design that would distinguish different conformers of the CL based on LC ordering transition with these interfaces. It should be noted that ionization levels of the head group of CL are strongly dependent on pH and therefore, a change in pH can easily get reflected in the protonation state of the two phosphate group of each CL derivative.[8] The very different pK_a values of these phosphate groups (pK_1< 4 and pK_2> 8.0) can be attributed to an intramolecular hydrogen bond with the 2′- hydroxyl group found on the glycerol linker in between the two phospholipids. For example, it has been demonstrated that at higher pH (such as pH 9.0) CL assumes to exhibit mostly an open conformation (A^{2-}) because of strong electrostatic repulsions between the two head groups (Figure 4.3a).[9–11] At pH 5.5, repulsions between the two head groups are minimized through the formation of a bicyclic/closed structure (HA^-), stabilized by intramolecular H-bonding (Figure 4.3b). Further lowering the pH (at pH < 2.8 or so), CL mostly exists in an undissociated form (H_2A, both the phosphate groups are protonated) having the least repulsions between the two head groups (Figure 4.3c). Consequently, the variation of pH modifies the charge−charge interaction in the lipid head groups which in turn affects the packing of lipids.[46] Keeping this idea in mind, we hypothesized that a particular form of CL could strongly couple to the ordering of LCs at LC-aqueous interfaces and that the presence and organization of these conformers can be reported through changes in the optical appearance of the LC. A key finding of the study reported in this paper is that the interactions of CL at LC-aqueous interfaces mainly depend on the different conformational forms of the CL acquired due to varied pH conditions. In addition to pH, we also find evidence that the LC ordering transitions have a strong influence on the phase preference of the CL which can form either lamellar or inverted hexagonal structures depending on the ionic strength, salt concentration and valence of the cations (monovalent or divalent). Overall, the results of the study explore the sensitivity of the LC-aqueous interface toward different conformational forms of CL through the LC ordering transition which provides application in clinical diagnosis and understanding of the organization of the CL at the molecular level.

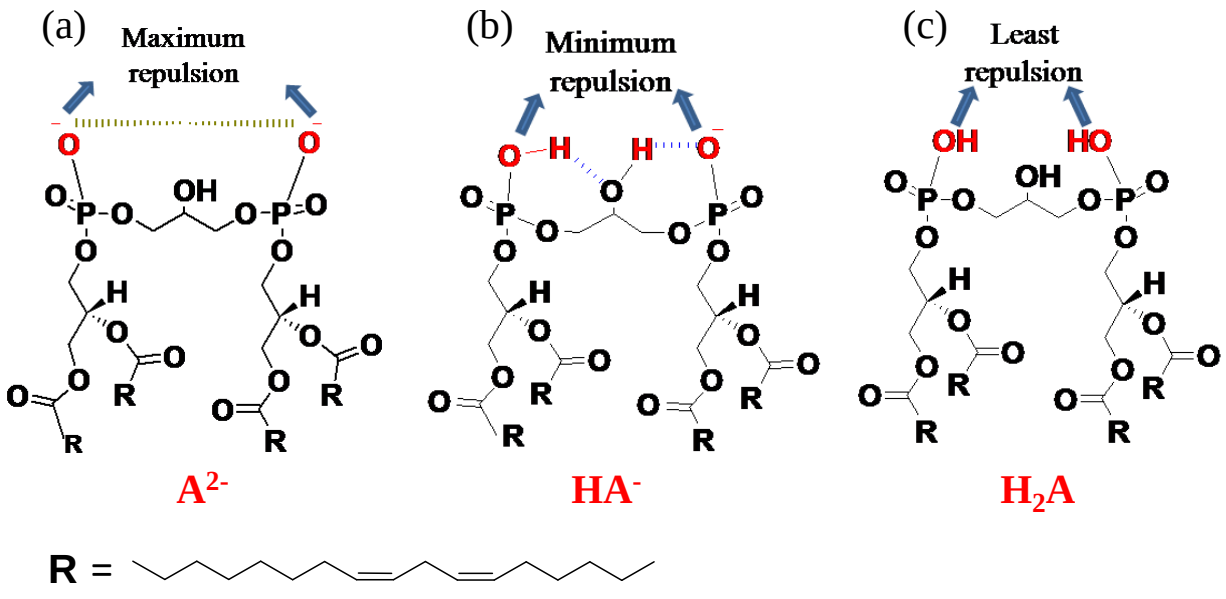

Figure 4.3 Molecular conformations of CL at different pH conditions. (a) Open form, (b) bicyclic/closed form and (c) undissociated form.

4.3 Results and Discussion

4.3.1 LC ordering transition induced by CL at different pH conditions

Our first set of experiments employed polarizing optical microscopy to determine whether the CL influences the orientational ordering of the 4-cyano-4'-n-pentyl-biphenyl (5CB) LCs at LC-aqueous interfaces. Figure 4.4A shows the optical micrograph (crossed polars) of 5CB confined within a gold grid supported on DMOAP-coated glass slides in contact with an aqueous solution. As expected, in contact with water, the optical appearance of the 5CB LCs became bright, which was associated with a planar/tilted orientation of the LC. It should be noted that the nematic 5CB (exposed to air) assumes homeotropic anchoring at the DMOAP-treated glass surface, leading to a dark optical appearance between cross polars. Interestingly, on introduction of 0.5 mM CL solution, the optical appearance of the 5CB film remained bright under cross polars (Figure 4.4B). These results indicate that there is not enough strong coupling between the ordering of 5CB and the organization of assemblies of CL molecules at 5CB-aqueous interfaces.

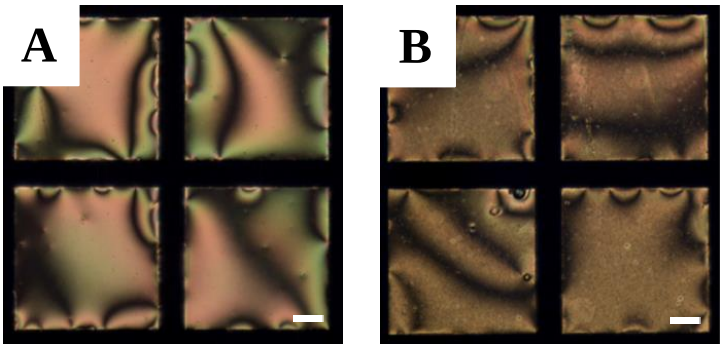

Figure 4.4 CL is unable to show the orientational ordering transition of LCs at aqueous interfaces. Optical micrographs (crossed polars) of 5CB hosted in gold grids supported on DMOAP-treated glass slides in contact with A) water B) aqueous solution of 0.5 mM CL vesicles. Scale bar = 40 μm.

Past reports have shown that alkyl chains of lipids interact with 5CB molecules and cause the homeotropic orientation of 5CB at the LC-aqueous interface.[25] Surprisingly, being an amphiphilic molecule with four long alkyl chains, CL is unable to show the orientational ordering transition of LCs at aqueous interfaces. We hypothesized that the alkyl chains of the CL molecules might have different spatial conformations that impede them from self-assembly at LC−aqueous interfaces and thus make the LC ordering insensitive toward CL. This made us explore other conformations (H_2A, HA^- and A^{2-}) of the CL molecules in which it may couple strongly with the LC ordering at the LC-aqueous interfaces and could result in an orientational ordering transition of the LCs.

To investigate the influence of other conformers of the CL on the orientational ordering of LC at LC-aqueous interfaces, we studied the optical response of the LC toward CL at different pH conditions. As described in the introduction, due to very different pK_a values of the two phosphate groups, CL exists in three different equilibrium species (H_2A, HA^- and A^{2-}; see Figure 4.3). At very low pH (pH < 2.8), the dominant species is H_2A (both the phosphate groups are protonated) and as the pH is gradually increased (pH ~ 5.5), first cyclic/ closed form (HA^-) becomes predominant followed by the open conformer (pH > 7, A^{2-}). The concentration of each conformers present at given pH can be determined using

general dibasic acid calculations (see appendix A). Figure 4.5 represents the speciation curves (changing concentration of varying forms) for the aqueous CL as a function of pH.

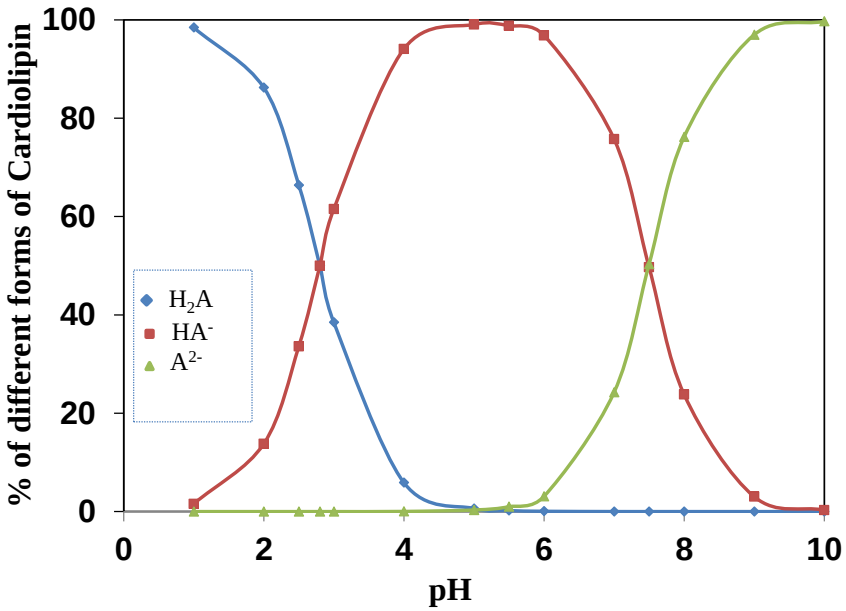

Figure 4.5 Represents the speciation curves for aqueous CL as a function of pH. The blue curve corresponds to undissociated (H_2A) CL in solution. The red and green curves correspond to cyclic/closed (HA^-) and open form (A^{2-}), respectively.

These three different forms (conformers) of the CL differ on their surface charge and therefore they exist at different ratios at different pH values. For our experiments, we chose three different pH (i.e., pH = 2, 4, 8) in which CL molecules adopt mostly one of the conformations at each pH. The results reported below demonstrate the self-assembly of the CL at LC-aqueous interfaces with varying pH and their coupling to the orientational ordering transition of LCs.

Figure 4.6A shows the optical micrograph (crossed polars) of nematic 5CB confined within a gold grid upon immersion under the aqueous Tris buffer of pH 8. It exhibited bright optical appearance which indicates that LCs had assumed a planar/ tilted state. Figure 4.6B shows the optical appearance of the same film in contact with an aqueous solution of 0.5 mM of CL at LC-aqueous interfaces. Inspection of Figure 4.6B reveals no ordering transition of the LC in contact with CL at pH 8 in which CL exists mostly in the open form (A^{2-}). The tilted

orientation of the LCs, when combined with the observation over a period of hours or so, suggests that this form of CL was unable to induce an ordering transition of 5CB at LC-aqueous interfaces. This observation leads us to hypothesize that head group−head group repulsion of the CL can alter the conformation of phosphate moieties of the polar head group and thus changes the orientation of the alkyl chains. These results also suggest that due to this structural conformation, CL molecules do not couple strongly with 5CB, resulting in no change in the orientational ordering transition of LC.

Next, we sought to investigate the influence of CL on the orientational ordering of 5CB at interfaces to air and aqueous buffer solutions at pH 4. It should be noted that at pH 4, CL exists predominantly in bicyclic form. In a typical experiment, thin film of 5CB supported on DMOAP-coated glass slides was immersed under the aqueous citric acid buffer of pH 4 and subsequently contacted with an aqueous solution of 0.5 mM CL. We observed a rapid change in the optical appearance of the LC from bright to dark (Figure 4.6C,D) consistent with an orientational ordering transition at pH 4. It is noteworthy, however, that without CL, 5CB remains bright at pH 4 citric acid buffer indicating planar orientation (Figure 4.6C). The change in the orientation of LC from planar to homeotropic indicates the self-assembly of CL at the LC-aqueous interface at pH 4. This observation also demonstrates that change in pH from 8 to 4, which induces the change in the structural conformation of CL from open to bicyclic is mainly responsible for the LC ordering transition. We speculate that reduction in head group−head group repulsion of the CL (due to the bicyclic form) at pH 4 may be playing a role in the efficient packing of alkyl chains of the CL at these interfaces leading to orientational ordering transitions in LCs.

In the next experiment, we contacted 5CB with aqueous solution at pH 2 and then investigated the response of the CL. Figure 4.6E,F showed the optical appearance of the LC in aqueous Tris buffer solution at pH 2 and in contact with 0.5 mM of CL solution, respectively. An orientational ordering transition was observed from planar (bright optical appearance) to homeotropic corresponding to a change in optical appearance to a dark state. This result further supports our proposition that with decrease in pH, efficient packing geometry of the lipid head group to the hydrophobic tail length is mainly responsible for the ordering transition. As noted earlier, at pH 2, CL is mostly in undissociated form having the

least head group−head group repulsion. This results in an effective monolayer at LC-aqueous interfaces and thus an ordering transition of the LC was detected.

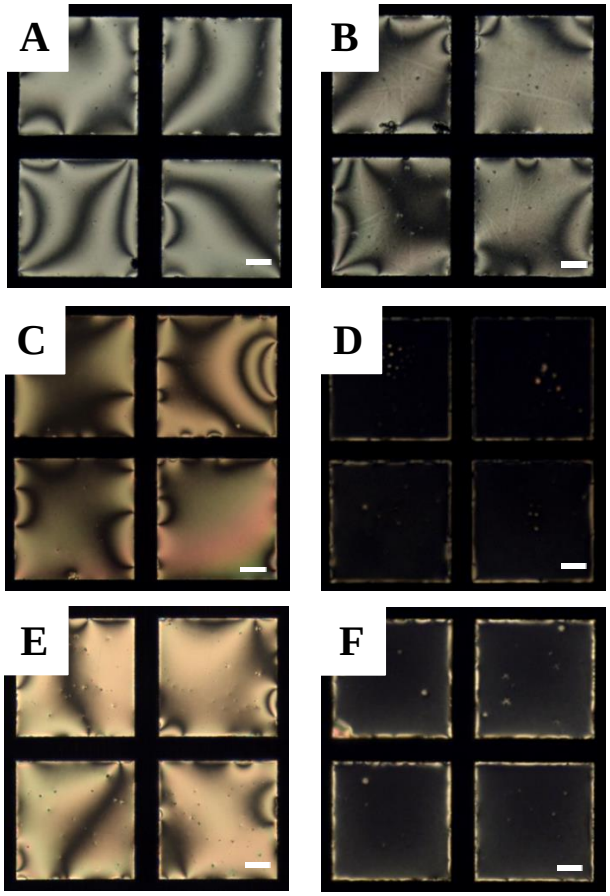

Figure 4.6 CL induces ordering transitions of LC at aqueous interfaces by varying pH of the solution. Cross-polarized optical images of 5CB films (A) with Tris buffer (pH = 8), C) with citric acid buffer (pH = 4) and (E) with citric acid buffer (pH = 2). Panels B, D, and F represent the corresponding optical micrographs of 5CB films after addition of an aqueous solution of 0.5 mM CL immersed in buffer of pH 8, 4, and 2, respectively. Scale bar = 40 μm.

To verify and provide further support to our above proposition, we sought to determine whether the ordering transition was perturbed or preserved upon contact with highly acidic and basic aqueous solutions. We performed two additional experiments to establish the role of pH at these interfaces in the above-described response of the LC to CL. First, we observed that there was no optical response (Figure 4.7A,B) when LC supported on DMOAP-treated

glass slides under 0.1 mM aqueous NaOH solution was in contact with 0.5 mM CL. The optical appearance of the LC remains bright even after 12 h of incubation of CL at these interfaces suggesting that at basic pH, LC is unable to undergo an ordering transition in the presence of CL. Second, we observed an immediate change in the optical appearance of the LC from bright to dark following the addition of 0.1 mM of CL to the 0.1 mM aqueous HCl solution (Figure 4.7C,D). In summary, these results provide evidence that CL-induced ordering transitions can be driven at LC-aqueous interfaces by varying pH of the solution in which either bicyclic or undissociated rich conformers of the CL are responsible for the observed LC ordering.

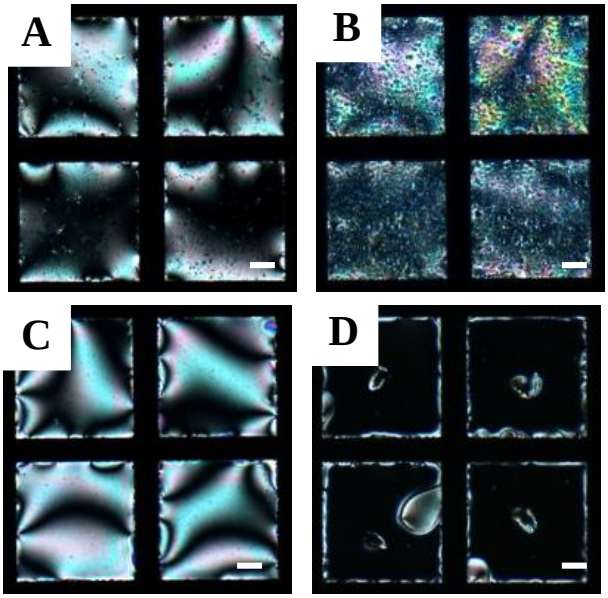

Figure 4.7 Cross-polarized optical images of 5CB films with an aqueous solution of (A) 0.1 mM NaOH) and (C) 0.1 mM HCl. (B) and (D) represent the 12 h incubation and immediately effect of 5CB films corresponds to A and B respectively after addition of an aqueous solution of 0.5 mM CL. Scale bar = 40 μm.

As noted above, the change in the optical appearance of the LC upon exposure to CL occurred by varying pH of the system. To provide further insight into the origins of this pH dependent response, we sought to perform a detailed study by varying concentration of the CL in a wide range of pH at LC-aqueous interfaces. The study was motivated by two main goals. First, we sought to demonstrate the coupling of the CL with the LC ordering at LC-

aqueous interfaces at different pH conditions. It is noteworthy that the anchoring transitions in LCs at LC-aqueous interfaces directly correlate with changing the percentage of the three different conformational forms of the CL present at a particular pH. Second, we sought to determine the sensitivity of CL through surface-driven ordering transition in LCs at LC-aqueous interfaces. To this end, we sequentially varied the concentrations of CL at LC-aqueous interfaces starting from pH 2 to pH 7. We found that on decreasing the concentration of the CL at LC-aqueous interfaces at different pH conditions, the sensitivity of the CL became more pronounced at lower pH and therefore led to an ordering transition in the LC. Figure 4.8A-F shows the optical images of the LCs at LC-aqueous interfaces in contact with 0.1 mM CL at varying pH (pH 2 to pH 7).

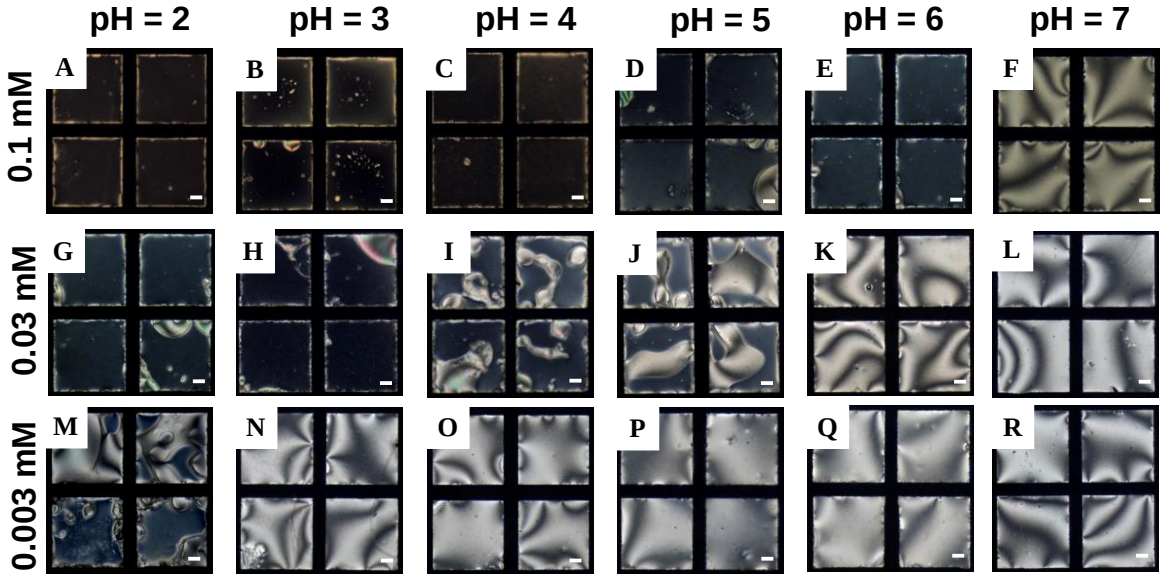

Figure 4.8 CL detection at LC-aqueous interface is in the micromolar range (0−10 μM) at lower pH. Optical micrographs (crossed polars) of 5CB films in contact with an aqueous solution of CL of A-F) 0.1 mM, G-L) 0.03 mM and M-R) 0.003 mM at pH 2 – pH 7. Scale bar = 40 μm.

At 0.1 mM concentration of CL up to pH 6, a change in the optical appearance of LC from bright to dark was observed. Above pH 6, no change in optical appearance of the LC was found even after keeping the aqueous solution of 0.1 mM CL at LC-aqueous interfaces over a period of 1 h. On decreasing the concentration to 0.03 mM CL, we observed an immediate

change in the optical appearance of the LC to a dark state at pH 2 and pH 3 (Figure 4.8G-H). Interestingly, at pH 4 and pH 5 the anchoring transition of the LC in the presence of CL resulted in a partial dark optical appearance of LC even after an incubation of CL for a period of 30 min (Figure 4.8I-J). Further increasing the pH to 6 (or more), no obvious change in the optical appearance of the LC was observed in the presence of 0.03 mM of CL (Figure 4.8K-L). The film was anchored parallel to the aqueous interface. When the concentration of CL was further decreased to 0.003 mM or lower, we observed the 5CB to undergo a transition in optical appearance at pH 2 (Figure 4.8M) and no change in anchoring transition was observed at other pHs (pH 3 to pH 7) for a period of 30 min or more incubation of the CL (Figure 4.8N-R). In summary, a key finding of the study reported in this paper is that pH can drive the ordering transitions in LCs by conformational changes of CL. This also supports our earlier proposition that among the three conformational forms of the CL, the undissociated and the bicyclic conformations lead to self-assembly of CL alkyl chains at LC-aqueous interfaces and thus tune the ordering transition of the LCs.

As described above, in the presence of 0.1 mM of CL the ordering transition of the LC is observed up to pH 6 (containing approximately 97% bicyclic form of CL), while at the pH > 6 no change in optical appearance of LC was observed. This is probably because at pH > 6 the concentration of the bicyclic form of CL is decreased (from approximately 97% to 75%) and adopts open conformation (~22%), making it insensitive toward ordering transition of the LC. This is also in good agreement with the fact that when the concentration of CL was decreased from 0.1 mM to 0.03 mM, both pH 7 and pH 6 conditions are unable to make any optical response of the LC. In contrast, at lower pH (pH 2 to pH 5) the change in the optical appearance of the LC was observed due to contribution of undissociated form in addition to bicyclic form of CL. Another key observation of this study was that with increase in undissociated form of CL (i.e., at lower pH) the sensitivity and the response time increases toward orientational ordering transition of the LC at LC-aqueous interfaces. This can be said to have a strong influence on the phase preference (results hexagonal conformation of CL from lamellar) of the lipid at $pK_a < 2.8$ that led to more ordered monolayer of CL at LC-aqueous interfaces.[9] As a consequence, a very low concentration of CL (0.003 mM) is able to induce the ordering transition of LC at pH 2 which results highly responsive and label-free

identification of CL at LC-aqueous interfaces. This high sensitivity of CL detection at LC-aqueous interface is in the micromolar range (0−10 μM) which lies in the physiological range of CL in mitochondrial membrane providing a simple, rapid and accessible method for the detection of CL. Therefore, the LC-based design may offer a facile approach for the detection of CL in addition to other past studies reported earlier.[17-24,47]

4.3.2 Quantification and influence of CL density on the LC ordering transition (*via* fluorescence measurements)

In order to provide further insights to the above described proposition, we performed a series of fluorescence measurements to determine the extent to which CL adsorbs at aqueous interfaces of nematic 5CB from the bulk aqueous solutions at different pH conditions. Figure 4.9 shows the change in fluorescence intensity of BODIPY-CL at the LC-aqueous interfaces following incubation against dispersions of CL vesicles as a function of pH. Inspection of Figure 4.9 reveals that the interface that was incubated against the solution containing BODIPY-CL at pH 7 (Figure 4.9A) exhibited a fluorescence intensity comparable to the control but lower than an aqueous solution of CL at pH 2 (Figure 4.9B). This confirms that CL adsorbed onto LC-aqueous interfaces at pH 2 instead of pH 7. This result supported the above-described hypothesis. These observations also show that the favorable head group conformation of CL at pH 2 leads to self-assembly of CL alkyl chains onto LC-aqueous interfaces and therefore induces an ordering transition of LCs. Figure 4.9C,D show the corresponding crossed polars of CL at pH 7 and pH 2, respectively. We have also quantified the fluorescence intensity by varying the effect of incubation time of BODIPY-CL on the resulting density of CL adsorbed onto the LC-aqueous interfaces. Figure 4.9E shows that the fluorescence intensity of an aqueous solution of BODIPY-CL at pH 2 and pH 4 at the LC interface increases with increase in incubation period but at pH 7 the fluorescence increases relatively minimum. This result also confirms that the pH-dependent conformational forms of CL have different abilities to self-assemble at LC−aqueous interfaces leading to ordering transition of LC to a different extent at different pH values.

To further support the above-described phenomena that the ordering transition of the LC at LC-aqueous interfaces was explicitly controlled by the change in the conformations adopted

by the CL (at different pHs) and not by the unequal surface density of the CL, we performed several other control experiments.

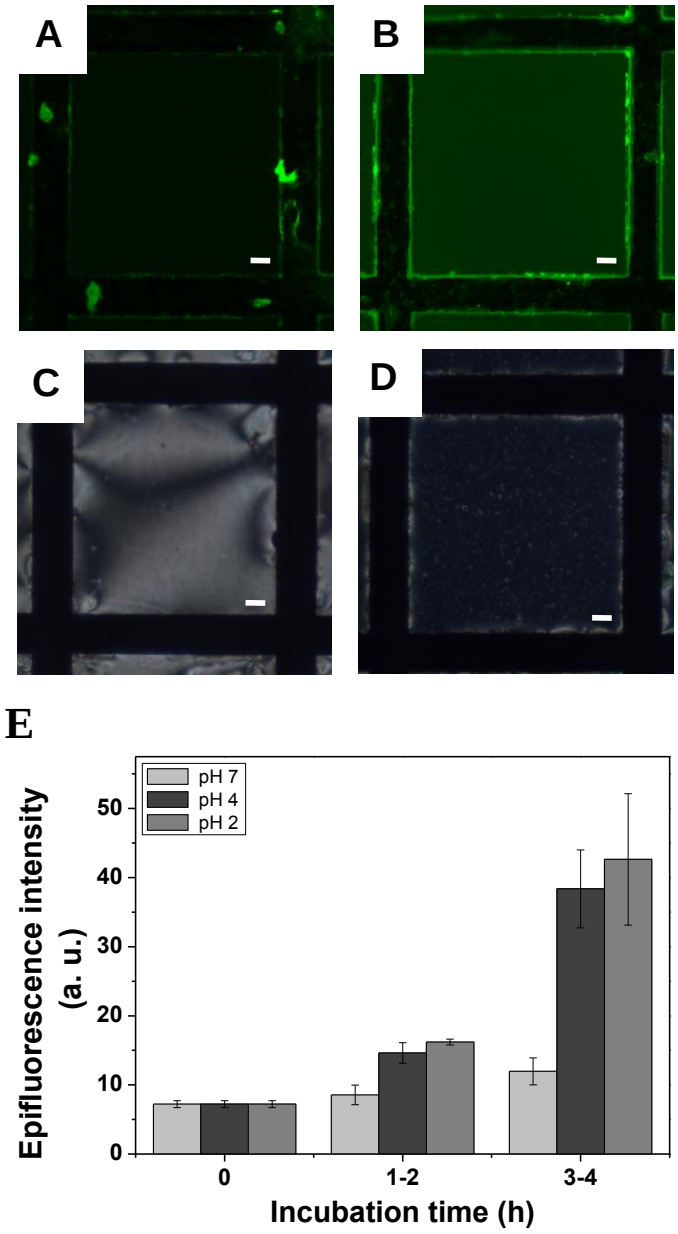

Figure 4.9 pH-dependent conformational forms of CL have different abilities to self-assemble at LC−aqueous interfaces. Epifluorescence micrographs of CL laden 5CB-aqueous interface (containing 0.03 mM CL and 0.025 mol % BODIPY-CL) following 90 min incubation against (A) an aqueous buffer of pH 7 (10 mM Tris) and (B) an aqueous buffer of pH 2 (10 mM citric acid). Corresponding micrographs (crossed polarizers) of the nematic

5CB film are shown in panels C and D, respectively. Scale bar = 40 μm. (E) Plot of epifluorescence intensity of BODIPY-CL at the LC-aqueous interface without and with CL vesicles against an aqueous buffer of pH 7, 4 and 2 at different incubation periods.

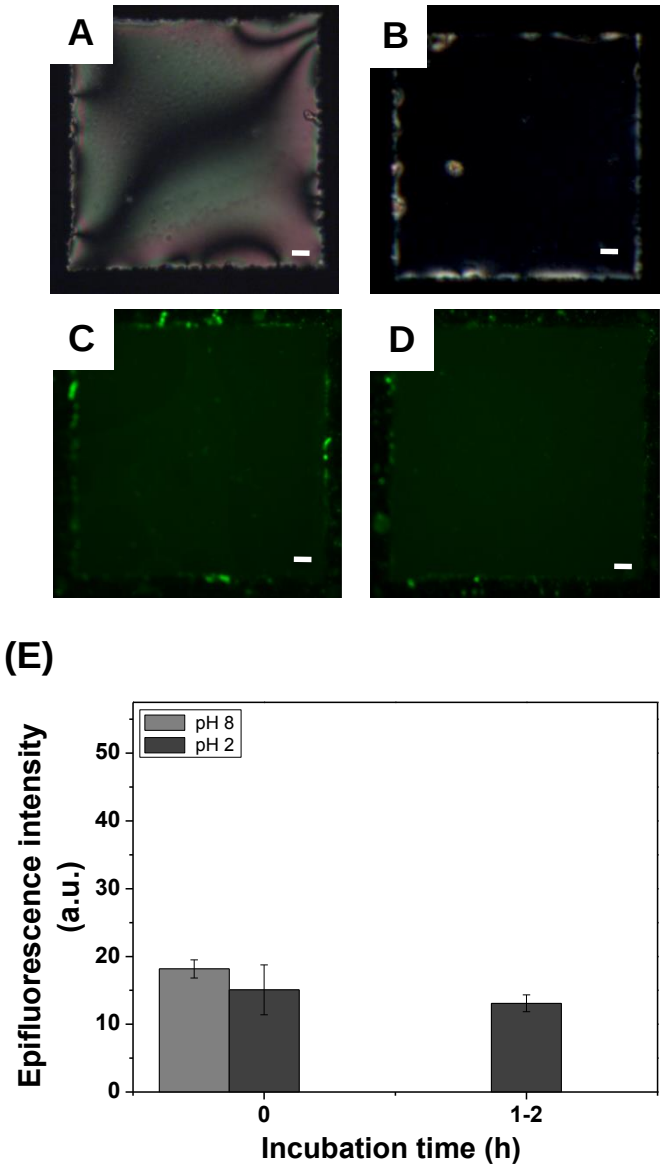

Figure 4.10 The optical response of the LC at LC-aqueous interfaces was independent on the surface density of the CL. Optical micrographs (crossed polars) of CL laden 5CB-aqueous interface following 90 min incubation against (A) an aqueous buffer of pH 8 (10 mM Tris) and (B) after exchanging the same CL laden nematic 5CB film with aqueous buffer of pH 2 (10 mM citric acid). Corresponding epifluorescence micrographs of the nematic 5CB film

(containing 0.3 mM CL and 0.025 mol % BODIPY-CL) are shown in panels C and D, respectively. (E) Scale bar = 40 μm. Plot of epifluorescence intensity of BODIPY-CL at the LC-aqueous interface, with CL vesicles against an aqueous buffer of pH 8 and on exchange with pH 2 (immediately and after 90 min of incubation period).

First, we observed that the ordering of the LC remained invariant (bright) when an LC-aqueous interface (that shows also bright optical appearance) supported on DMOAP-treated glass slides was in contact with the CL (0.3 mM) at pH 8 (10 mM Tris buffer) on incubation for 90 min or more (Figure 4.10A). In contrast, there was an immediate change in the optical response of the LC from bright to dark (Figure 4.10B) when the same LC-filled grid (in contact with 0.3 mM solution of CL) at pH 8 was transferred to a buffer solution (CL free) at pH 2 (10 mM citric acid). It may be hypothesized that during this transfer process, the surface density of the CL remained unchanged at both pH 8 and pH 2. This result is consistent with our observation that the change in the molecular conformations of the CL play the key role (not the interfacial density of the CL) in determining the ordering transitions of the LCs (driven by pH). Second, during this transfer process (from pH 8 to pH 2), we observed no visual change in the epifluorescence micrographs of the nematic 5CB film (containing 0.3 mM CL and 0.025 mol % BODIPY-CL) at LC-aqueous interfaces (Figure 4.10C,D). The epi-fluorescence (which remains unchanged) was also conveniently quantified (Figure 4.10E) by measurement of the fluorescent intensity at pH 8 (in the presence of 0.3 mM CL solution) followed by the transfer of the LC-filled grid at pH 2 on incubation for 90 min or more. These experiments provide further support that the interfacial surface density of the CL does not contribute to the observed ordering transitions at different pHs.

4.3.3 Effect of head group−head group repulsion in determining LC ordering transition *via* effect of ions

The results above suggest that the change in the anchoring of 5CB with CL is determined by a particular conformation of the CL. Therefore, in order to provide an additional perspective on the effectiveness of head group−head group repulsion in determining the response of different conformational forms of the CL toward LC, we performed some additional

experiments. First, we sought to observe the orientational ordering transition of 5CB in response to the CL at pH 7 in the presence of different ions. As discussed earlier, CL at pH 7 is insensitive toward LC ordering at LC-aqueous interfaces and carries potentially large negative charge of the phosphatidyl head groups. Therefore, it may be hypothesized that at pH 7, positively charged ions can interact strongly with the negatively charged head groups of the CL, which could reduce the head group−head group repulsion of the phosphatidyl groups and subsequently an ordering transition of LC can be realized. We have chosen both divalent (such as Ca^{2+} and Mg^{2+}) and monovalent (such as Na^{+}) cations to investigate the above proposition. It should be noted that CL can readily form inverted hexagonal structure depending on the salt concentration and the valence of the ions (mono- or di-).[9] Figure 4.11A−F represents the change in the optical appearance of the LC in contact with CL at pH 7 after addition of Ca^{2+}, Mg^{2+} and Na^{+} ions, respectively.

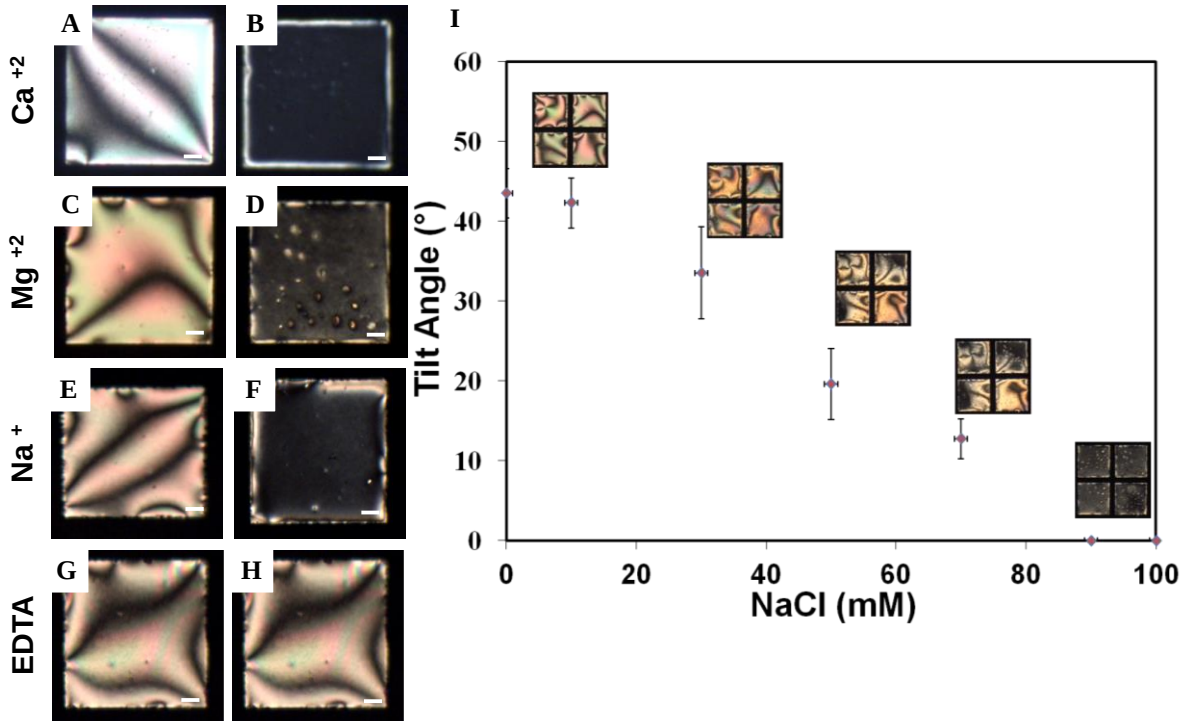

Figure 4.11 The optical response of 5CB in response to the CL at pH 7 is observed in the presence of different positively charged ions. Optical images (crossed polars) of 5CB hosted in gold grids supported on DMOAP-coated glass slides and placed into contact with aqueous solution of Tris buffer (pH = 7) followed by (A, C, E, G) introduction with an 0.1 mM CL

and (B, D, F, H) contacting a CL-laden interface with 100 mM aqueous solution of Ca^{2+}, Mg^{2+}, Na^{+} and EDTA, respectively. Scale bar = 40 μm. (I) Graph showing the continuous change in the tilt angle of the 5CB at CL laden LC-aqueous interface on exposure with increasing NaCl concentration.

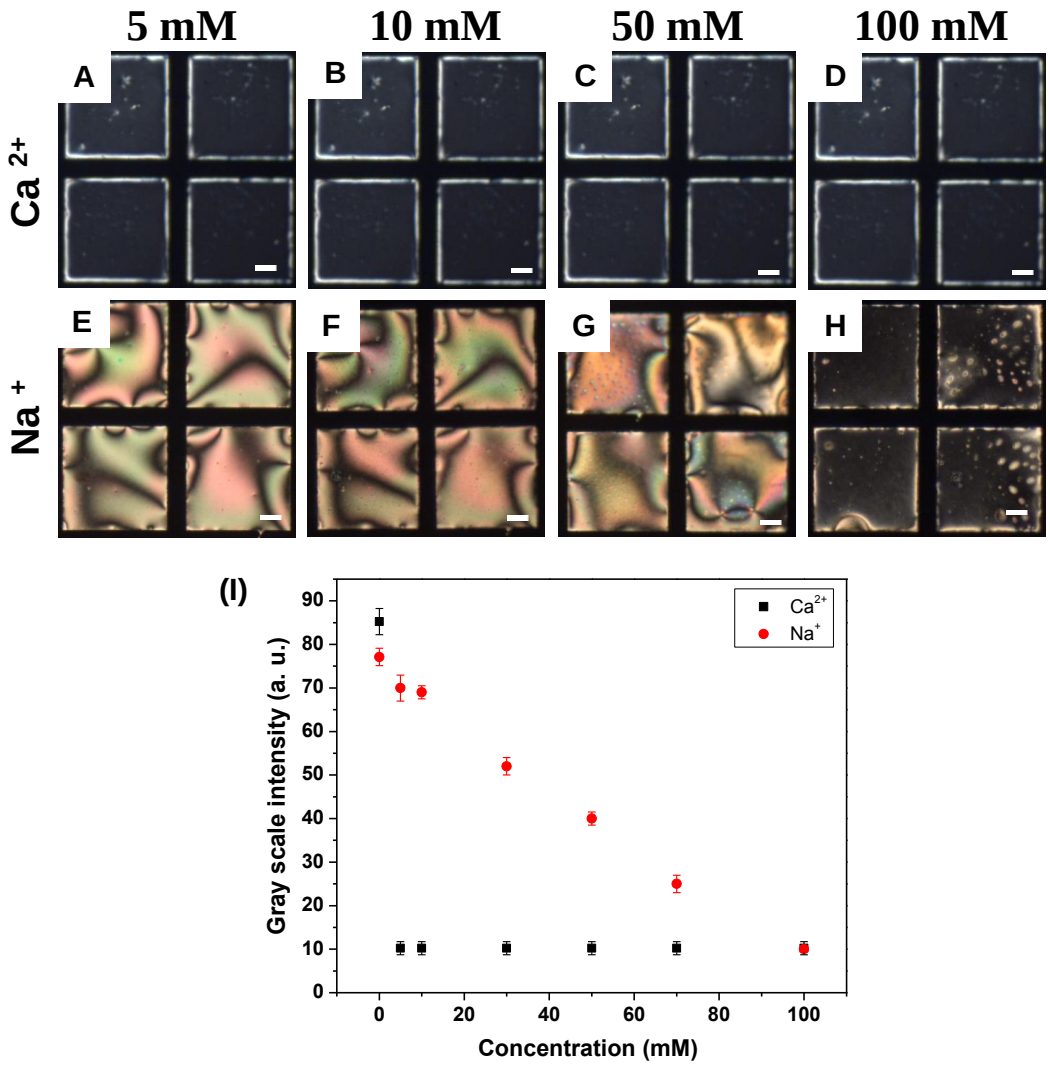

Figure 4.12 The optical response of 5CB in response to the CL at pH 7 is faster in presence of divalent cations compared to monovalent cations. Optical micrographs (crossed polars) of 5CB films in contact with a buffer solution (pH = 7) of 0.1 mM CL with A, E) 5 mM, B, F) 10 mM, C, G) 50 mM and D, H) 100 mM aqueous solution of Ca^{2+} and Na^{+}, respectively. Graph showing the average gray scale intensity of optical images of 5CB at CL laden LC-

aqueous interface on exposure with increasing $CaCl_2$ and NaCl concentration. Scale bar = 40 μm.

The change in optical appearance of LC from bright to dark on addition of these ions onto a CL-laden LC-aqueous interface clearly depicts that compensation of head group−head group charge of the phosphatidyl groups alters the conformations of two phosphate groups and results in the formation of an ordered monolayer formation at LC-aqueous interfaces. In addition, we have compared the effect of divalent (such as Ca^{2+}) and monovalent (such as Na^{+}) cations on the screening of negative charge on the CL head groups. Figure 4.12 depicts the change in ordering transition of LC at pH 7 in the presence of Ca^{2+} and Na^{+} as a function of concentration. This reflects stronger binding affinity (i.e., higher electrostatic shielding capabilities) of the divalent cations than monovalent cations toward the head group of the CL. We performed one additional control experiment to establish the role of anions in the above-described response of the LC to CL. We observed no change in the optical appearance of the LC film hosted on DMOAP-coated glass slides when it was exposed to EDTA (Figure 4.11G-H) at LC-aqueous interfaces. This is not surprising, as EDTA, being negatively charged, could not alter the conformations of the CL at these interfaces and therefore resulted in the bright optical appearance of the LC. We have also measured the optical retardance of the LC within the LC at LC-aqueous interfaces to quantify the tilt of the LC as a function of the concentration of the ions. The results are shown in Figure 4.11I for the LC hosted within a TEM grid with increasing concentration of NaCl solution at LC-aqueous interfaces. We note that the tilt of the LC continuously decreases as a function of increasing NaCl concentration at LC-aqueous interfaces. This tilt angle is calculated with the assumption that surface anchoring of the LC at DMOAP-coated glass slides remains homeotropic during the entire experiment.

Finally, we demonstrate that the orientation of the LC in the presence of CL is dependent on the strength of the buffer capacity at the LC-aqueous interface. In this experiment, we first incubated LC against an aqueous Tris buffer solution at pH 7 in the presence of 0.5 mM of CL followed by gradual increase in the concentration of the buffer solution. As discussed earlier, no ordering transition of the LC was observed in the presence of CL at pH 7 buffer solution (Figure 4.13A, planar anchoring). Inspection of Figure 4.13A−D shows the optical

appearance of the LC as a function of increase in the concentration of the buffer strength. We observed that LC undergo an anchoring transition in the presence of 0.5 mM CL at a buffer strength of 80−100 mM, consistent with the formation of a monolayer of CL at the aqueous interfaces of the LC (and thus homeotropic anchoring). Figure 4.13E shows the quantified measurement of the intensity of the light transmitted through the LC (crossed polars) by varying ionic strength adsorption of CL at the LC-aqueous interface. As the LC is imaged with the white light under crossed polars, we observed interference phenomena to cause changes in the average gray-scale intensity of the optical images.

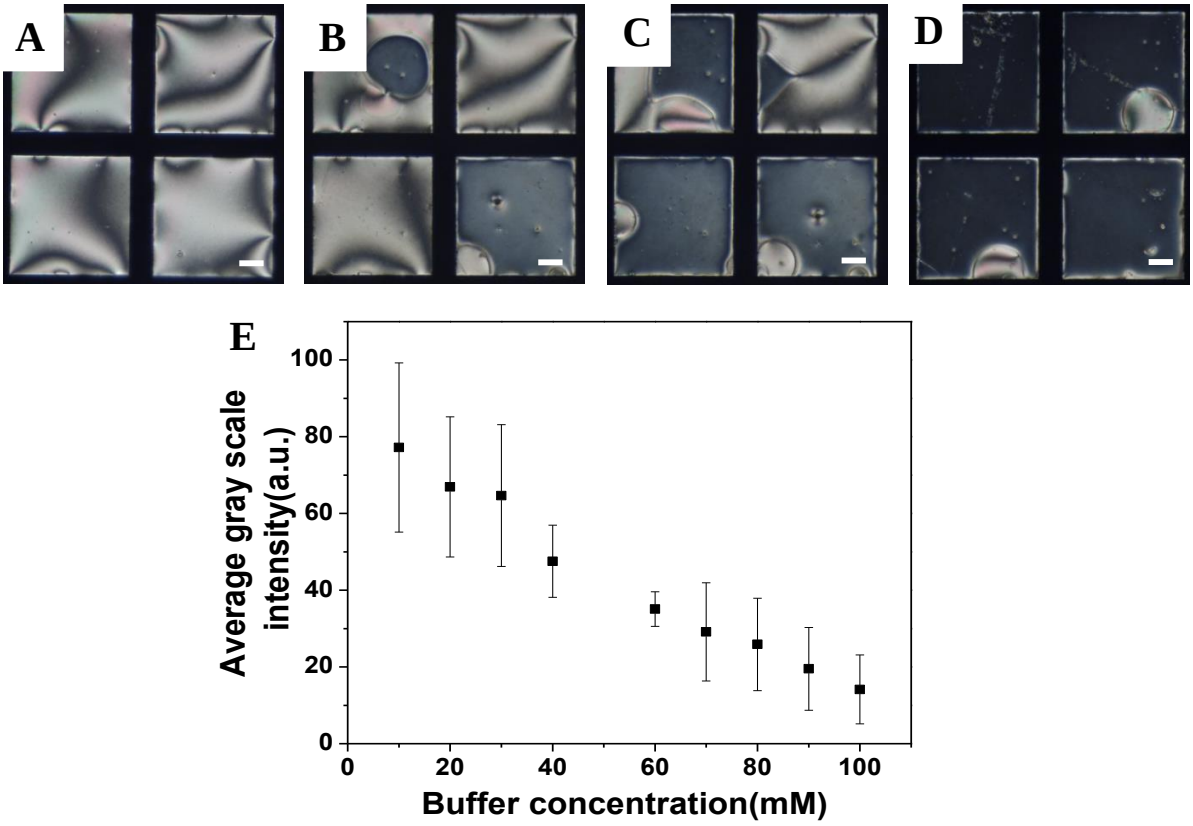

Figure 4.13 The optical response of 5CB in response to the CL at pH 7 is observed on increasing ionic strength. Polarizing optical micrographs of 5CB films placed into contact with a CL-laden aqueous interface at pH = 7, followed by increasing Tris buffer concentration of (A) 10 mM, (B) 40 mM, (C) 70 mM and (D) 100 mM. (E) Representation of the average gray scale intensity of optical images of 5CB films as a function of varying concentrations of Tris buffer on a CL-decorated 5CB-aqueous interface. Scale bar = 40 μm.

While the gray scale intensity of the LC changed continuously with increase in concentration of buffer at pH 7, we noted two additional observations regarding the ordering of the LCs at CL-laden LC-aqueous interfaces. First, an increase in ionic strength from 60 to 80 or 100 mM, achieved by the addition of higher concentration of buffer reduces the electrostatic repulsive forces between the two phosphatidyl head group, and thus LC exhibits a dark optical appearance in the presence of CL at pH 7. Second, the reduction in head group−head group repulsion is achieved not only due to decrease in pH but also with increasing ionic strength that results in a stable CL conformer at these interfaces. In summary, these results provide evidence that the concentration of ionic strength of the aqueous buffer solution also plays an important role in determining CL conformations which influences the LC ordering transition.

4.3.4 Effect of CL alkyl chain packing and conformation at different pH and ionic conditions *via* Langmuir− Blodgett and PM-IRRAS measurements

The results reported above provide evidence that restricting the conformation of phosphate groups of the CL (by reducing head group−head group repulsions) is the central factor in determining the LC ordering transition in the presence of CL. Inspired by this, next we sought to determine the influence of head group−head group repulsions of the CL on alkyl chains organizations at the molecular level.

We prepared and studied monolayer film properties of the CL at the air−water interface (Langmuir film) and the air−solid interface (Langmuir−Blodgett film) by varying pHs and in the presence of ions. It should be noted that monolayer films of phospholipids at air−water interfaces have been widely used as primitive models of biological membranes in order to study lipid organization and biomolecular interactions that occur at membrane surfaces.[48] Figure 4.14 A,B,C shows the surface pressure versus area isotherms of CL monolayers at pH 2, pH 8 and at pH 8 in the presence of Ca^{2+} ions, respectively.

Careful inspection of Figure 4.14 reveals two important messages. First, we observed no significant change in the collapse pressure (~42 ± 2 mN/ m) for the CL monolayer either at pH 2 or at pH 8. Interestingly, a notable change was observed at the limiting area per

molecule at those pHs (~235.1 ± 0.9 Å^2 at pH 8 *vs* 220.5 ± 0.3 Å^2 at pH 2). We hypothesized that the increased area per molecule at pH 8 than pH 2 could be due to less efficient packing arrangements. Second, in the presence of Ca^{2+} ions at pH 8, the limiting area per molecule was found to be almost the same (216.5 ± 0.9) to that of pH 2. These results provide evidence that head group−head group repulsion of the CL determines the lipid packing efficiency, which largely dictates the resulting ordering transition of the LC.

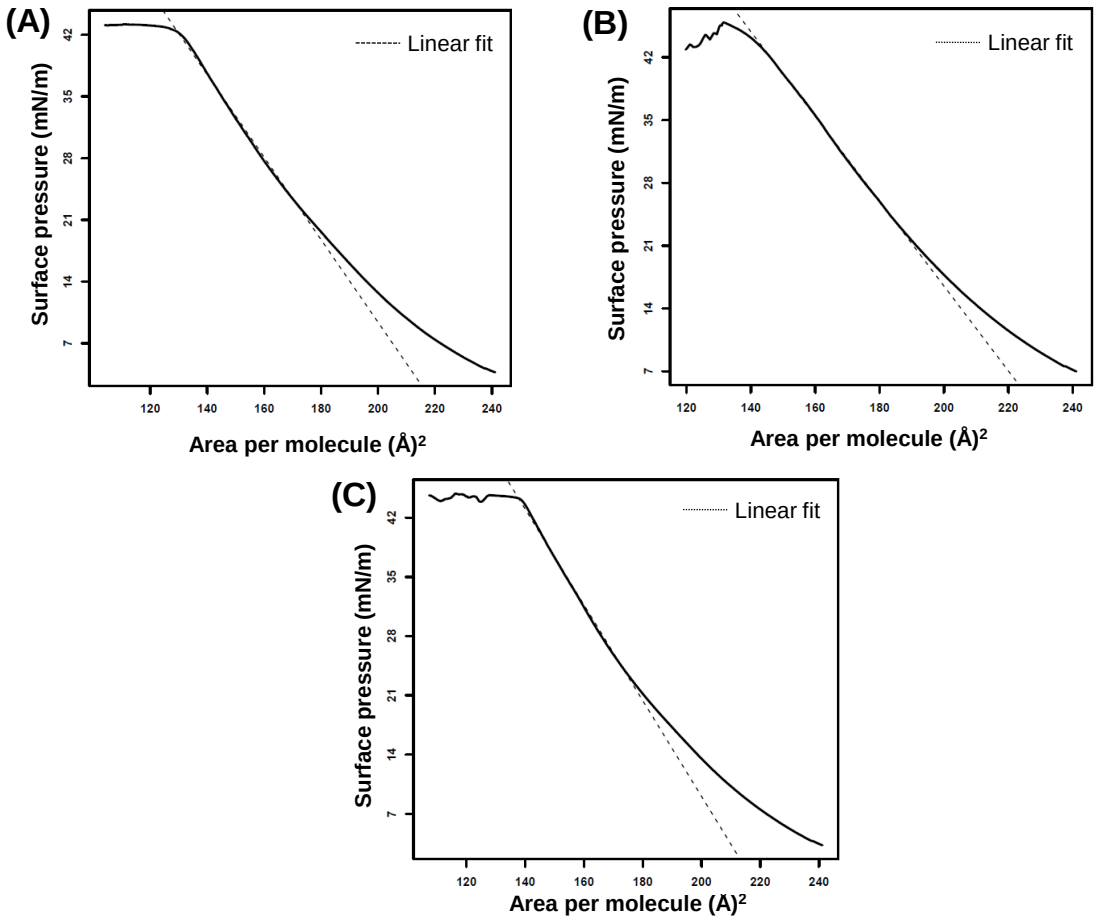

Figure 4.14 The limiting area per molecule was found to be higher in case of CL at pH 2 to that of CL at pH 8. Surface pressure (π)-area per molecule (A_m) isotherm for CL on A) pH 2, B) pH 8 and C) pH 8 (5 mM Ca^{2+}) based sub-phase at 25 °C.

In order to provide further insight that the ordering transition of the LC occurs only at specific conditions which can be attributed to change in the molecular conformations, we performed Fourier transform PM-IRRAS to characterize the influence of pH on the

molecular conformations occurring within a thin film of CL. As PM-IRRAS is used to evaluate the structural and conformational features of organic films,[49] we speculate that, using PM-IRRAS, a detailed conformational feature of the CL films could be obtained at different pH and ionic conditions.

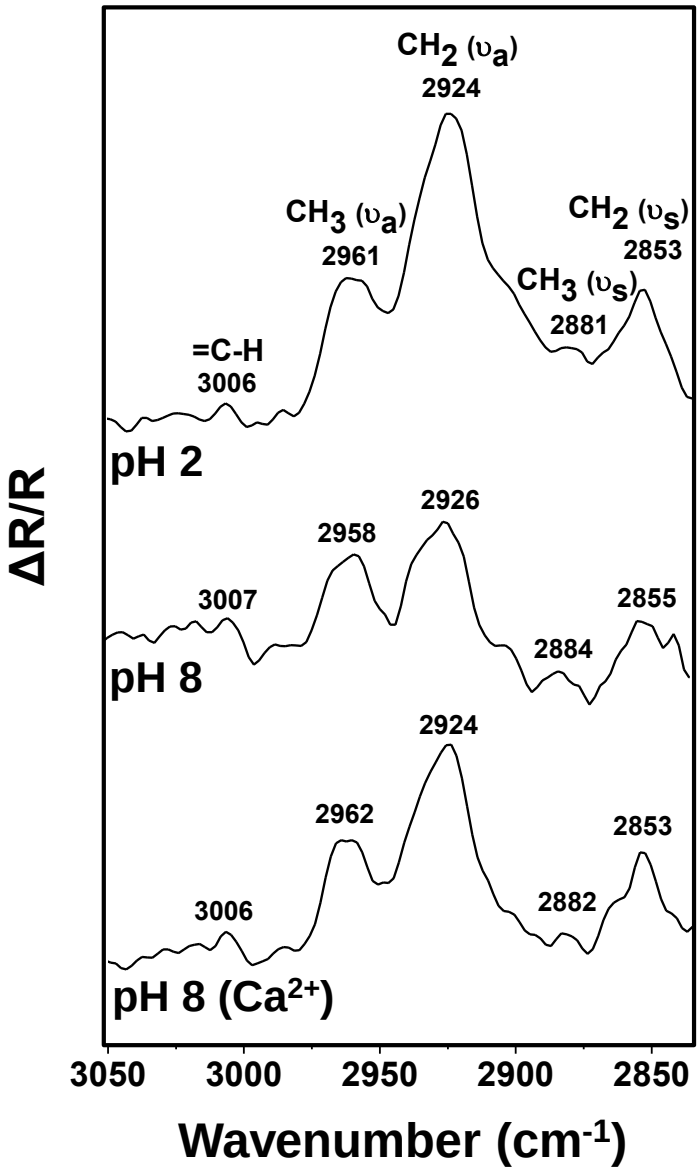

Figure 4.15 A significant change in the peak intensity is observed for both $-CH_3$ and $-CH_2$ bands in case of CL at pH 2 to that of CL at pH 8. PM-IRRAS spectra generated from alkyl region of CL monolayers prepared at pH 2, pH 8 and pH 8 in the presence of Ca^{2+} onto SAM prepared using mercaptohexanoic acid supported on a uniformly deposited gold film.

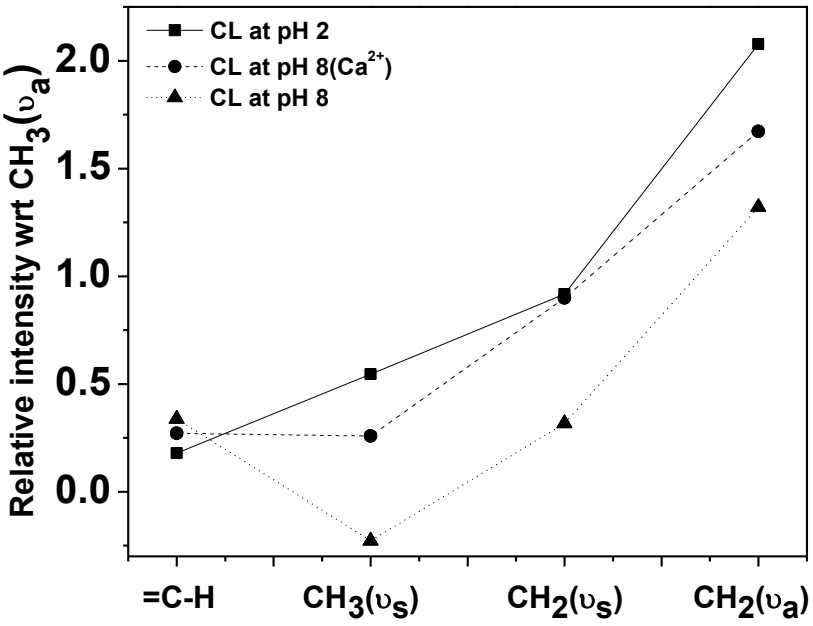

Figure 4.16 Relative intensity of $-CH_3$ and $-CH_2$ bands of the alkyl region of CL monolayers prepared at pH 2, pH 8 and pH 8 in the presence of Ca^{2+} onto a SAM prepared using mercaptohexanoic acid supported on a uniformly deposited film of gold as measured by PM-IRRAS.

First, the monolayer film of CL (as discussed above) was transferred onto gold surfaces-coated with self-assembled monolayers of mercaptohexanoic acid using LB technique at different pH conditions. Next, we sought to evaluate the structural and conformational features of these organic thin films within the PM-IRRAS instrument and obtained the IR spectra using polarization modulation at different pH (i.e., at pH 2 and pH 8). Figure 4.15, Figure 4.16 and Figure 4.17 showed that the C−H stretching, C=O stretching, and asymmetric phosphate O−P−O stretching regions can be distinguished in IR spectra at pH 2 and pH 8 using polarization modulation. These regions encode information about hydrocarbon chain conformation, hydration and hydrocarbon chain packing interactions and the polarity of the phosphate polar head groups, respectively. In particular, we observed that the frequency, intensity and bandwidth of the methylene C−H stretching region are highly sensitive to the conformational order of the films at different pH. At pH 2, the absorption spectra are characterized by two intense bands corresponding to the asymmetric and

symmetric CH_2 vibrations of the lipid hydrocarbon chains that appear at 2924 and 2853 cm^{-1}, respectively (Figure 4.15). The other peaks at 2881 and 2961 cm^{-1} are due to the symmetric and antisymmetric CH_3 stretching modes, respectively. Moreover, due to the high degree of unsaturation of the acyl chains, an absorption peak at 3006 cm^{-1} is evident and represents the (= CH) stretch. The high frequency values of the CH stretching absorption peaks are consistent with a high degree of gauche conformers in the methylene groups of the acyl chains.[50]

In contrast, at pH 8, a significant change in the peak intensity (see also Figure 4.16 for relative intensity) was observed for both $-CH_3$ and $-CH_2$ bands. Also, these bands were found to become broadened with a change in the peak frequency at pH 8. From the spectroscopic data we found that the absolute value of the $-CH_2$ (ν_a) absorption frequencies of CL at pH 8 and pH 2 are 2926 and 2924 cm^{-1}, respectively. Additionally, comparison of full width half maxima showed a higher value for both $-CH_3$ and $-CH_2$ bands at pH 8 than pH 2. In particular, at pH 8 we observed an increase of the peak width of approximately 2 and 6 cm^{-1} for $-CH_2$ (ν_a) and $-CH_3$ (ν_a), respectively.

We hypothesized that in addition to a significant change in the peak intensity, the increase in the frequency of about 2 cm^{-1} for the $-CH_2$ (ν_s and ν_a) at pH 8 could be due to an enhanced state of disorder of the acyl chains of the CL as pointed out by others in past studies.[50,51] However, in the presence of Ca^{2+} at pH 8, peaks appear at the same position as those in the presence of pH 2 (see below for details). Therefore, it may be hypothesized that at pH 8, the packing efficiency of the CL is lower than at pH 2 due to the formation of unoccupied inter chain space. We also find evidence in the change in the carbonyl and P−O vibration modes of the CL in between 1200 and 1800 cm^{-1} (Figure 4.17) at different pHs. We noted two important observations from Figure 4.17. First, we observed a substantial increase in the peak intensity of both −C=O and P−O stretching modes at pH 8 than pH 2. Second, these peaks were seen to shift considerably to the higher wavenumber at pH 8. This clearly signifies a distinct variation of the head group conformations of the CL at varying pH. Figure 4.18a,b shows the deconvoluted spectra in the interfacial C=O stretching region of the CL at pH 2 and pH 7, respectively.

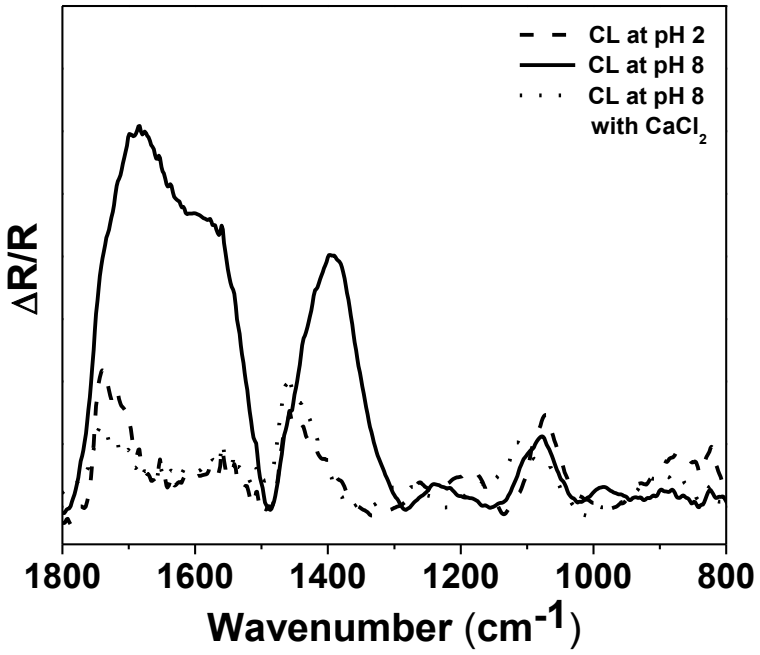

Figure 4.17 PM-IRRAS spectra generated from head group region of CL monolayers prepared at pH 2, pH 8 and pH 8 in presence of Ca^{2+} onto SAM prepared using mercaptohexanoic acid supported on a uniformly deposited gold film.

At pH 2, three prominent peaks were observed in the interfacial C=O stretching region (1650−1800 cm^{-1}) at 1742, 1715, and 1669 cm^{-1}, which are marked to change in their integrated band intensities at pH 8. For example, the relative integrated intensities of the bands at 1742 and 1740 cm^{-1} (assigned to the carbonyl groups of the CL),[52] relative to the intensity of the entire carbonyl region (calculated from cumulative fit, see appendix A) are 29% and 8.5% at pH 2 and pH 8, respectively. The peak at around 1715 and 1696 cm^{-1} at pH 2 and pH 8, respectively, can be attributed to the hydrogen bonded carbonyl groups (Figure 4.18c) at the surface of SAMs as demonstrated in earlier reports.[53]

All these results indicate a conformational change in the CL in the interfacial region at different pHs. We believe that this conformational change leads to buckling of the alkyl chains of the CL which is responsible for the different orientational behavior of the 5CB LC. On LC-aqueous interfaces at pH 2, 5CB exhibits homeotropic anchoring in the presence of CL while on surfaces at pH 8 5CB exhibits planar (tilted) anchoring. Interestingly, at pH 8 in

the presence of Ca^{2+} ions both peak intensity and position of different vibrational bands appear similar to that in the presence of pH 2 (Figure 4.15 and Figure 4.17).

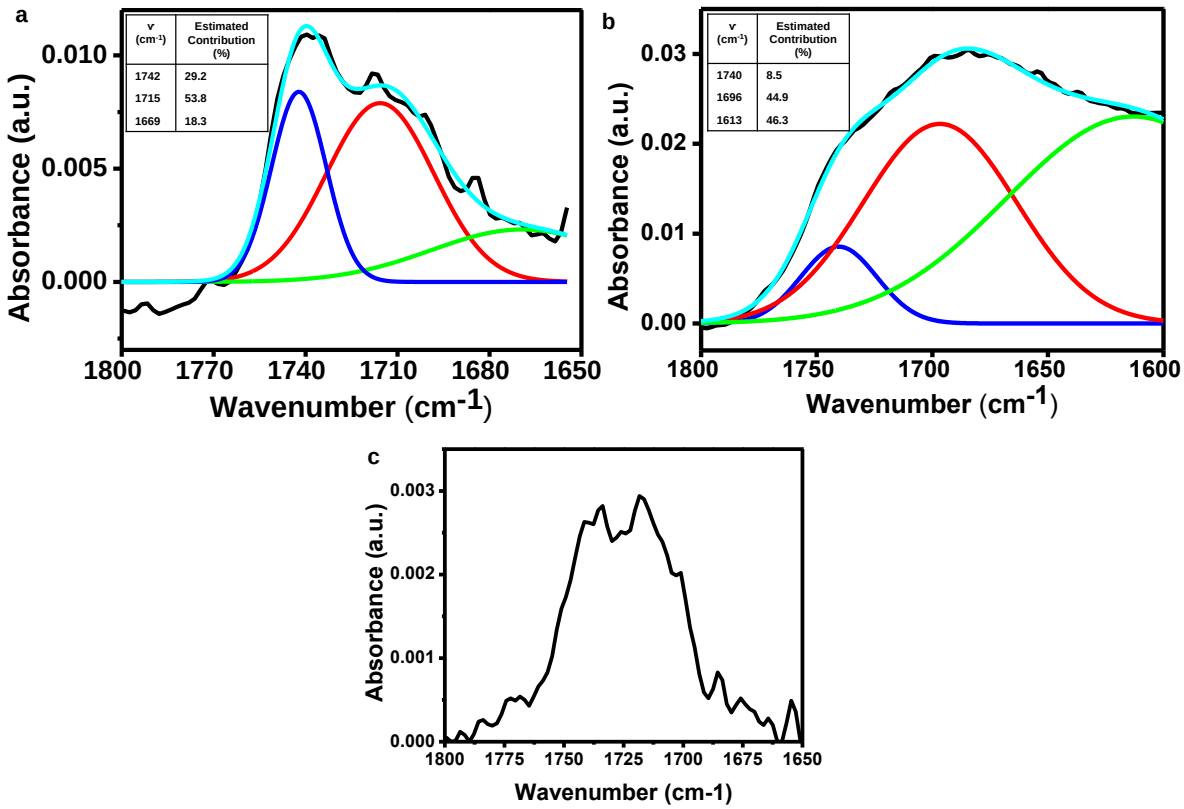

Figure 4.18 Deconvoluted spectra in the interfacial C=O stretching region of the CL at (a) pH 2 and (b) pH 8. (c) PM-IRRAS of 6-mercaptohexanoic acid terminated SAMs indicating a mixture of non-hydrogen bonded (1736 cm^{-1}) and hydrogen-bonded (1716 cm^{-1}) carbonyl groups at the surface of SAMs.

This is due to the complexation of Ca^{2+} ions with the negatively charged head groups of the CL that changes the molecular conformations back as it was for pH 2 and therefore, an ordering transition of LC is realized. These experiments clearly established that the change in the surface charge of the CL head group through change in pH or addition of cations causes significant conformational changes of the acyl chains of CL and thus attributes different ordering transitions of the LCs at different pHs at LC-aqueous interfaces. Overall, the results in our study suggest that LCs can offer a novel tool for fundamental understanding of CL-

induced ordering of LC and in particular they offer new methods to report different conformational forms of the CL at LC-aqueous interfaces.

4.4 Conclusions

The key result in this paper is that the response of LC in the presence of CL at LC-aqueous interface is determined by the molecular-level self-assembly of the CL. Specifically, we observed that the response of nematic 5CB varies significantly in the presence of different conformational forms (undissociated form, bicyclic/closed form and open form) of the CL with varying pH. In particular, the change in head group−head group repulsion of the central phosphatidyl groups in different conformations of the CL plays a key role in tuning the lipid packing efficiency which alters the response to interfacial phenomena. Finally, we also found that the orientational ordering of the LC is strongly influenced by the ionic strength of the buffer solution in which head group−head group repulsions of the CL can be adjusted. Our results also demonstrate that head group−head group repulsion could alter the conformation of the central glycerol and the phosphate moieties of the polar head group, which ultimately leads to alterations in conformation of alkyl groups. Overall, this approach provides evidence that conformational change of CL induces a predictable LC anchoring transition and offers the basis of novel strategy that can provide fundamental insights into the CL molecular structure through LC anchoring transition at LC-aqueous interfaces.

4.5 Experimental Section

4.5.1 Materials

Cardiolipin sodium salt (from bovine heart), citric acid, Tris (hydroxyl methyl) amino-methane, N,N-dimethyl-Noctadecyl- 3-aminopropyltrimethoxysilyl chloride (DMOAP), ethylenediaminetetra acetic acid, hydrochloric acid, sodium hydroxide, magnesium chloride, sodium chloride, and calcium chloride were purchased from Sigma-Aldrich (St. Louis, MO). Sulfuric acid, chloroform and hydrogen peroxide (30% w/v) were purchased from Merck (Mumbai, India). Ethanol was obtained from Jebsen & Jenssen GmbH and Co., Germany (S D Fine-Chem, Ltd.). 4-cyano-4-pentylbiphenyl (5CB) was obtained from Sigma-Aldrich (St. Louis, MO). Deionization of a distilled water (DI water) source was performed using a Milli-

Q-system (Millipore, bedford, MA). Fisher's Finest Premium grade glass microscopic slides and cover glass were obtained from Fischer Scientific (Pittsburgh, PA). Gold specimen grids (20 μm thickness, 50 μm wide bars, 283 μm grid spacing) were obtained from Electron Microscopy Sciences (Fort Washington, PA). Sodium citrate (pH 2−6) and Tris-HCl (pH 7−8) were used for buffer preparations. All the pH buffers were made freshly and adjusted by adding 1 N HCl or NaOH prior to every pH titrations experiments.

4.5.2 Preparation of LC films in TEM grids

Glass slides were cleaned with piranha solution (70:30 (% v/v) H_2SO_4:H_2O_2) for 1 h at 100 °C according to the published procedures.[25] Briefly, the glass slides were immersed in a piranha bath at 100 °C for at least 1 h and then rinsed in running deionized (DI) water for 5-10 min. Finally, the slides were rinsed sequentially in ethanol and then dried under a stream of nitrogen. The clean slides were stored in an oven at 100 °C for overnight. These cleaned glass slides were then dipped into 0.1% (v/v) DMOAP solutions in DI water for 5 min at room temperature and rinsed with DI to remove the unreacted DMOAP from the surface. The DMOAP-coated glass slides were dried under a stream of nitrogen gas and kept in an oven at 100 °C for 3 h.

Cleaned gold specimen grids were placed on DMOAP-coated glass slides. The grids were filled with approximately 0.2 μL of 5CB and the excess LC was removed with the help of a syringe to produce a planar interface. The grids containing LCs were then put on the optical wells containing samples of interest kept at room temperature (25 °C). This optical cell was then ready for examination under crossed polarizers.

4.5.3 Preparation of CL vesicles

Vesicles were prepared according to the published procedures.[36] Briefly, the lipids (CL, BODIPY-CL) were dissolved in chloroform (0.5 mL) and dispensed into round bottomed flask. Prior to resuspension, the chloroform was evaporated from the flask under vacuum for at least 2 h until it formed a thin film along the inner walls of the flask. The lipid film formed in the flask was then placed under a stream of nitrogen for 30 min. The dried lipid was then hydrated in the required solution of interest (e.g. DI water, buffer solution of different pH)

and vortexed for 1 min. This resulted in the cloudy solution indicative of large multilamellar vesicles. Subsequent sonication of lipid suspension using a probe ultrasonicator (1 × 15 min at 25 W) resulted in a clear solution. The vesicles were used within 24 h of their preparation.

4.5.4 Optical characterization of LC films in response to CL aqueous solutions

The orientational ordering of the LC was determined using a Nikon Eclipse LV100POL polarizing microscope using an objective power of 200x with cross polars. Orthoscopic examinations were performed with the source light intensity set to 50% of full illumination and the aperture set to 0.45 in order to collimate the incident light. All the images were captured using a Q-imaging camera.

4.5.5 Epifluorescence imaging of 5CB-aqueous interface

The LC-filled grid was incubated under CL vesicle solution containing 0.025 mol % of BODIPY-CL. After incubation, the solution was then exchanged with distilled water thrice to remove the excess of BODIPY-CL from the bulk solution. The LC-filled grid supported on DMOAP-coated surfaces was then removed from the solution and placed over a glass slide. Fluorescence imaging was performed with a Zeiss (Scope. A1) fluorescence microscope. The samples were viewed using a fluorescence filter cube with a 460 nm excitation filter and a 534 nm emission filter. Images were obtained with an Axio cam camera. All fluorescence intensity measurements were determined using ImageJ (public-domain image processing software by the U.S. National Institute of Health).

4.5.6 Tilt angle measurements

The optical retardance of LCs was measured using a tilting compensator (type 2357 K, equipped with a calcite compensator plate, Leitz, Germany). The retardance values reported in this paper are the average obtained within four squares of the gold specimen grid used to host the LCs. For a thin film of nematic LCs with strong homeotropic anchoring (θ_1 = 0°) at the OTS-treated glass interface and a tilt of angle of θ_2 away from the surface normal at the LC-aqueous interface, the tilt of LCs across the film varies linearly with position so as to minimize the elastic energy of the LC film (assuming splay and bend elastic constants of the

LCs to be equal). This result permits the establishment of a relationship between optical retardance (Δr) of the film of LCs and the tilt of the director at the LC-aqueous interface (θ_S), namely

$$\Delta r \approx \int_0^d \left(\frac{n_e n_o}{\sqrt{n_o^2 sin^2\left(\frac{z}{d}\theta_s\right) + n_e^2 cos^2\left(\frac{z}{d}\theta_s\right)}} - n_o \right) dz \qquad (1)$$

where n_e and n_o are the indices of refraction parallel (so-called extraordinary refractive index) and perpendicular (ordinary refractive index) to the optical axis of the LCs, respectively and θ_s is the tilt angle of LCs measured relative to the surface normal.[54] The retardance values (measured using the Scope. A1) were used to calculate the tilt angle of LCs at the LC-aqueous interface by numerically solving equation 1. The indices of refraction of 5CB were taken to be $n_e = 1.71$ and $n_o = 1.52$ ($\lambda = 632$ nm at 25 °C).

4.5.7 Uniform deposition of gold films

The gold films with thicknesses of ≥ 2000 Å were deposited onto silicon wafers mounted on rotating planetaries (no preferred direction or angle of incidence) by using thermal evaporator (Excel Instruments, India). A layer of titanium (thickness∼ 100 Å) was used to promote adhesion between the silicon wafer and the film of gold. The rates of deposition of gold and titanium were ∼1 Å/s. The pressure in the evaporator was close to 9×10^{-7} Torr before and during each deposition.

4.5.8 Formation of self-assembled monolayers (SAMs)

SAMs were formed on the surfaces of gold films by immersing the gold films in ethanolic solutions containing 2 mM of 6-mercaptohexanoic acid for 12 h. After being rinsed in ethanol, the COOH-terminated SAMs were dried under a stream of nitrogen.

4.5.9 Preparation of CL monolayers

The surface manometry (surface pressure (π)−area per molecule (A_m) isotherm) experiments were carried out in a LB trough. CL monolayers at different pH conditions were prepared at

the air−water interface. The surface pressure (π) was measured using the standard Wilhelmy plate technique in a trough (MINITROUGH, KSV, Finland) enclosed in a Plexiglas box to reduce surface contamination. The sub phase of the trough was filled with either Tris buffer of pH 8 or citric acid buffer of pH 2 or Tris buffer of pH 8 in the presence of 5 mM $CaCl_2$. Using a microsyringe, 25 μL of a CL solution (1 mg/mL) was carefully spread onto the aqueous sub phase at different pH conditions. After spreading, the film was left for 20 min, allowing the solvent to evaporate. The π− A_m isotherms were obtained by symmetric compression of the barriers with a constant compression rate of 10 mm min^{-1}. Surface pressure and trough area were recorded simultaneously using Nima software. Based upon the volume deposited, the average molecular weight, and concentration of solution, the average area per molecule was calculated. All the measurements were performed at a room temperature of 25.0 ± 1 °C. Once deposited and transferred (with a transfer ratio of 0.9) onto the COOH-terminated SAMs supported on gold films at a surface pressure of 35 mN m^{-1}, these supported CL monolayers were kept under vacuum for polarization modulation infrared reflection absorption spectroscopy (PM-IRRAS) study.

4.5.10. Polarization modulation infrared reflection absorption spectroscopy (PM-IRRAS)

Deposited monolayers of CL onto a SAM ($HS(CH_2)_6COOH$) supported on a uniformly deposited film of gold (2000 Å) were examined by using PM-IRRAS. A Bruker PMA 50 connected to the external beam port of a Bruker Tensor 27 FT-IR spectrometer was used for PM-IRRAS measurements. The deposited CL monolayer on a gold sample was mounted on an attachment for PM-IRRAS measurements within the PMA 50 compartment. After reflection of the polarized light incident on the substrate at an angle of incidence of 82° from the surface normal, the IR beam was focused on a liquid nitrogen-cooled photovoltaic MCT detector in the PMA 50 cabinet. A photo elastic modulator (Hinds, PEM 90) was used to modulate the polarization of the light at a frequency of 50 kHz. Demodulation was performed with a lock-in-amplifier (Standford Research Systems, SR830 DSP). Before measurements, the spectrometer was allowed for a complete purge with nitrogen for at least 30 min. Each spectrum is the sum of 100 individual spectra collected at a resolution of 4 cm^{-1} with photo

elastic modulator (ZnSe, 42 kHz, AR-coated) set to 1600 cm^{-1}. Data was collected as differential reflectance ($\Delta R/R$) versus wavenumber.

References

(1) Claypool, S. M.; Koehler, C. M. *Trends Biochem. Sci.* **2012**, *37*, 32−41.

(2) Osman, C.; Voelker, D. R.; Langer, T. J. *Cell Biol.* **2011**, *192*, 7−16.

(3) Dowhan, W. *Annu. Rev. Biochem.* **1997**, *66*, 199−232.

(4) Hoch, F. L. *Biochim. Biophys. Acta* **1992**, *1113*, 71−133.

(5) Awasti, Y. C.; Chuang, T. F.; Keenan, T. W.; Crane, F. L. *Biochim. Biophys. Acta* **1971**, *226*, 42−52.

(6) Robinson, N. C. *Biochemistry* **1982**, *21*, 184−188.

(7) McAuley, K. E.; Fyfe, P. K.; Ridge, J. P.; Isaacs, N. W.; Cogdell, R. J.; Jones, M. R. *Proc. Natl. Acad. Sci. U.S.A.* **1999**, *96*, 14706−14711.

(8) Haines, T. H.; Dencher, N. A. *FEBS Lett.* **2002**, *528*, 35−39.

(9) Seddon, J. M.; Kaye, R. D.; Marsh, D. *Biochim. Biophys. Acta* **1983**, *734*, 347−352.

(10) Powell, G. L.; Marsh, D. *Biochemistry* **1985**, *24*, 2902−2908.

(11) Schlame, M.; Rua, D.; Greenberg, M. L. *Lipid Res.* **2000**, *39*, 257−288.

(12) Hovius, R.; Lambrechts, H.; Nicolay, K.; de Kruijff, B. *Biochim. Biophys. Acta* **1990**, *1021*, 217−226.

(13) Rawicz, W.; Olbrich, K. C.; McIntosh, T.; Needham, D.; Evans, E. *Biophys. J.* **2000**, *79*, 328−339.

(14) Shoemaker, S.; Vanderlick, T. K. *Biophys. J.* **2002**, *83*, 2007−2014.

(15) Gomez, B.; Robinson, N. C. *Anal. Biochem.* **1999**, *267*, 212−216.

(16) Houtkooper, R. H.; Vaz, F. M. *Cell. Mol. Life Sci.* **2008**, *65*, 2493−2506.

(17) Mileykovskaya, E.; Dowhan, W.; Birke, R. L.; Zheng, D.; Lutterodt, L.; Haines, T. H. *FEBS Lett.* **2001**, *507*, 187−190.

(18) Garciafernandez, M.; Ceccarelli, D.; Muscatello, U. *Anal. Biochem.* **2004**, *328*, 174−180.

(19) Jacobson, J.; Duchen, M. R.; Heales, S. J. *J. Neurochem.* **2002**, *82*, 224−233.

(20) Keij, J. F.; Bell-Prince, C.; Steinkamp, J. A. *Cytometry* **2000**, *39*, 203−210.

(21) Ritov, V. B.; Menshikova, E. V.; Kelley, D. E. *J. Chromatogr. B* **2006**, *831*, 63−71.

(22) Leung, C. W. T.; Hong, Y.; Hanske, J.; Zhao, E.; Chen, S.; Pletneva, E. V.; Tang, B. Z. *Anal. Chem.* **2014**, *86*, 1263−1268.

(23) Zhao, W.; Fung, Y.; Waisum, O.; Cheung, M. P. *Anal. Sci.* **2010**, *26*, 879−884.

(24) Bird, S. S.; Marur, V. R.; Sniatynski, M. J.; Greenberg, H. K.; Kristal, B. S. *Anal. Chem.* **2011**, *83*, 940−949.

(25) Brake, J. M.; Daschner, M. K.; Luk, Y.-Y.; Abbott, N. L. *Science* **2003**, *302*, 2094−2097.

(26) Lin, I. H.; Miller, D. S.; Bertics, P. J.; Murphy, C. J.; de Pablo, J. J.; Abbott, N. L. *Science* **2011**, *332*, 1297−1300.

(27) Brake, J. M.; Abbott, N. L. *Langmuir* **2002**, *18*, 6101−6109.

(28) Brake, J. M.; Mezera, A. D.; Abbott, N. L. *Langmuir* **2003**, *19*, 6436−6442.

(29) Lockwood, N. A.; de Pablo, J. J.; Abbott, N. L. *Langmuir* **2005**, *21*, 6805−6814.

(30) Price, A. D.; Schwartz, D. K. *J. Am. Chem. Soc.* **2008**, *130*, 8188−8194.

(31) Brake, J. M.; Daschner, M. K.; Abbott, N. L. *Langmuir* **2005**, *21*, 2218−2228.

(32) Lockwood, N. A.; Mohr, J. C.; Ji, L.; Murphy, C. J.; Palecek, S. R.; de Pablo, J. J.; Abbott, N. L. *Adv. Funct. Mater.* **2006**, *16*, 618−624.

(33) Agarwal, A.; Sidiq, S.; Setia, S.; Bukusoglu, E.; de Pablo, J. J.; Pal, S. K.; Abbott, N. L. *Small* **2013**, *9*, 2785−2792.

(34) Sivakumar, S.; Wark, K. L.; Gupta, J. K.; Abbott, N. L.; Caruso, F. *Adv. Funct. Mater.* **2009**, *19*, 2260−2265.

(35) Sidiq, S.; Das, D.; Pal, S. K. *RSC Adv.* **2014**, *4*, 18889−18893.

(36) Gupta, J. K.; Zimmerman, J. S.; de Pablo, J. J.; Caruso, F.; Abbott, N. L. *Langmuir* **2009**, *25*, 9016−9024.

(37) Park, J.-S.; Abbott, N. L. *Adv. Mater.* **2008**, *20*, 1185−1190.

(38) Hu, Q.-Z.; Jang, C. H. *ACS Appl. Mater. Interfaces* **2012**, *4*, 1791−1795.

(39) Hartono, D.; Xue, C.-Y.; Yang, K.-L.; Lanry Yung, L.-Y. *Adv. Funct. Mater.* **2009**, *19*, 3574−3579.

(40) Tan, L. N.; Orler, V. J.; Abbott, N. L. *Langmuir* **2012**, *28*, 6364−6376.

(41) Liu, D.; Hu, Q. Z.; Jang, C. H. *Colloids Surf. B: Biointerfaces* **2013**, *108*, 142−146.

(42) Hu, Q. Z.; Jang, C. H. *Analyst* **2012**, 137, 567−570.

(43) Das, D.; Sidiq, S.; Pal, S. K. *ChemPhysChem* **2015**, 16, 753–760.

(44) Sidiq, S.; Pal, S. K. *AIP Conf. Proc.* **2014**, *1591*, 33−35.

(45) Noonan, P. S.; Roberts, R. H.; Schwartz, D. K. *J. Am. Chem. Soc.* **2013**, *135*, 5183−5189.

(46) Khalifat, N.; Fournier, J.-B.; Angelova, M. I.; Puff, N. *Biochim. Biophys. Acta* **2011**, *1808*, 2724−2733.

(47) In past studies, mostly fluorescent based techniques have been used for the detection of CL. These techniques involves the interaction of CL with different fluorescence probes such as 10-N-nonyl acridine orange (NAO) and its analogues, pyrene methyl esters, luminogens, surface modified quantum dots, and so on.[17-24] The fluorescence enhancement in most of these methods is in a linear fashion of the CL concentration in the range of 0−10 μM. However, the procedures for preparation of fluorescence probes are complex, time-consuming involving several derivatization and purification steps. Recently, LC-MS has been used for quantitative analysis of CL. Most of these processes require laborious techniques and a laboratory-based analytical apparatus, which thus limits their widespread use.

(48) Sackmann, E. *Science* **1996**, *271*, 43−48.

(49) Frey, B. L.; Corn, R. M.; Weibel, S. C. Polarization−Modulation Approaches to Reflection−Absorbtion Spectroscopy. In Handbook of Vibrational Spectroscopy; Chalmers, J., Griffins, P. R., Eds.; John Wiley & Sons: Chichester, U.K., **2001**; Vol. *2*, p 1042.

(50) Casal, H. L.; Mantsch, H. H. *Biochim. Biophys. Acta* **1984**, *779*, 381−401.

(51) Alessandrini, A.; Muscatello, U. *J. Phys. Chem. B* **2009**, *113*, 3437−3444.

(52) Choi, S.; Swanson, J. M. *Biophys. Chem.* **1995**, *54*, 271−278.

(53) Luk, Y.-Y.; Yang, K.-L.; Cadwell, K.; Abbott, N. L. *Surf. Sci.* **2004**, *570*, 43−56.

(54) Lockwood, N. A.; Gupta, J. K.; Abbott, N. L. *Surf. Sci. Rep.* **2008**, *63*, 255−293.

Chapter 5

Cell-Surface Sensors by Probing Poly (L-lysine)-Liquid Crystal Interactions that can Monitor Cellular Environment

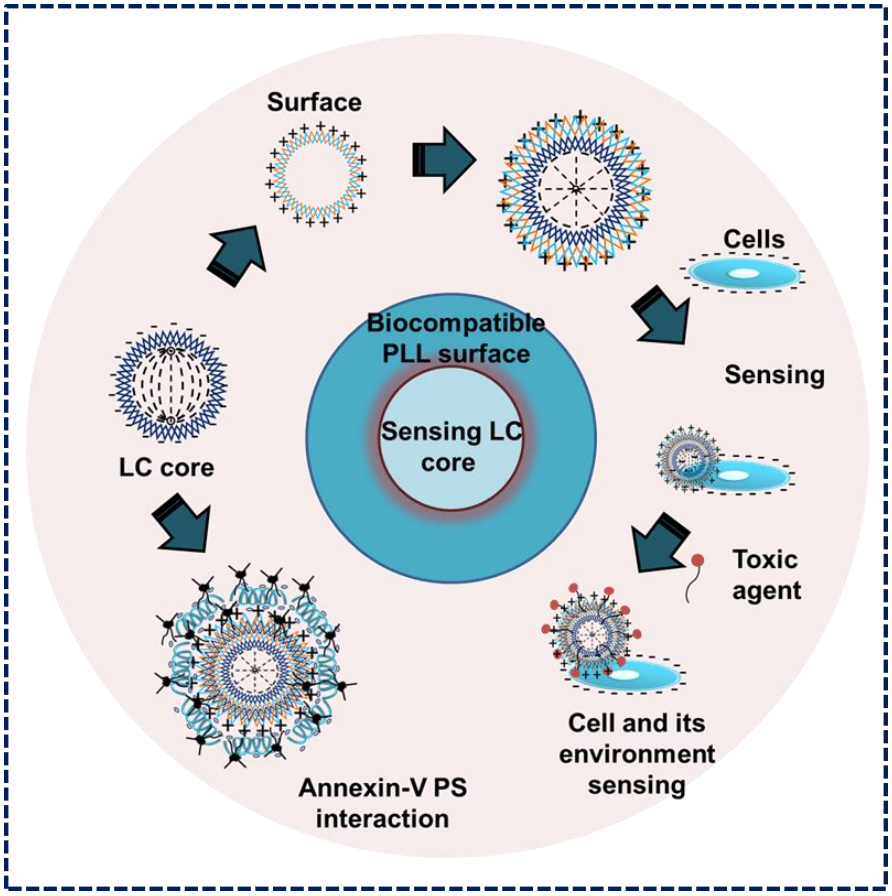

Although much effort has been devoted to the development of cell signaling for understanding cell biology, design of a new principle by probing direct protein-LC interactions (in aqueous media) that can mimic chemico-biological interactions at cellular level remains elusive. Here, we report a simple methodology to produce biocompatible LC droplets through Poly (L-lysine)-LC interactions in situ for reporting presence of cells and to monitor the interaction of cells with their environments in real time that are mediated by topological defects in those droplets.

5.1 Introduction

Recently, investigations on the director configuration transition of liquid crystals (LCs) to the surface anchoring have been emerged as optical amplification medium to be highly sensitive towards small changes in external conditions making them phenomenologically attractive for the study of interfacial interactions of biomolecules in biological systems.[1-7] The surface energetics that control these configurational transitions within the LC materials has shown to be influenced by a variety of interfacial interactions such as, hydrogen bonding,[8-10] metal−ligand coordination,[11] vander waals forces,[12] electrical double layers[8,13] and other intermolecular interactions.[14,15] Understanding these interactions at nanometer scale by designing surfaces with regular nanoscale features and defined chemistries can lead to control the ordering of the LCs at those interfaces.[8,13,16-21] Past studies demonstrated a wide range of surface interactions involving lipids, polymers, surfactants that strongly couple to the ordering of the LCs, providing the basis of a general and facile method to tune the response of the LCs at LC-aqueous interfaces.[8,13,16-30] In addition, a substantial effort has been pursued that report proteins captured on solid surfaces through specific interactions using LCs. For example, it has been demonstrated that nanometer scale surface topography of self-assembled monolayers (SAMs) on gold-coated surfaces presenting bound proteins govern the response of the LCs to protein decorated interfaces.[18,22,31-38] For example, Skaife *et al.* have shown that biotinylated SAMs supported on obliquely deposited gold lead to an observable change in the alignment of the LC through binding of avidin and anti-biotin IgG to these surfaces.[32] Luk *et al.* studied the binding ability of immobilized protein (ribonuclease A) with its ribonuclease inhibitor protein on SAMs surfaces with different orientations using LCs.[35] Govindaraju *et al.* studied the anti-phosphotrysine antibody binding to EGFR peptides decorated SAMs surfaces through measurement of the anchoring energies of LCs on these surfaces.[38] The measurement of changes in the orientational order of the LC as a result of these protein captured surfaces occurs *via* specific biomolecular binding event like specific protein-protein or protein–lipids interactions at those interfaces. However, design of a new principle by probing direct protein-LC interactions in aqueous media that can mimic chemico-biological interactions remains elusive. Advances in dealing with these processes are anticipated to result from better mechanistic understanding of the interactions of proteins

with LCs (as described for cardiolipin LC interactions in aqueous in Chapter 4) that provide a gateway for building fundamental *in vitro* and *in vivo* studies to the development of effective therapeutics.

In this study, we report that interaction of Poly-L-lysine (PLL) and LC in aqueous environment could fulfil the significant knowledge gap in understanding the intermolecular interactions that underlie the direct ordering of LCs with protein-decorated surfaces and hold great promise to provide LCs as cell surface sensors. PLL is a natural homo-polymer of the essential amino-acid L-lysine. It belongs to the group of cationic polymers contains a positively charged hydrophilic amino group. PLL is known to adsorb electrostatically to the negatively charged cell surface, DNA etc. PLL is one of the most important linear polyisopeptides which has been widely used to functionalize a range of surfaces as a promotion of cellular adhesion and drug delivery applications because of their functional versatility, biodegradability and biocompatibility.[39,40]

5.2 Objective

Inspired by this, we sought to explore if the intermolecular interactions between PLL and LC can provide a dynamic LC response (in a manner analogous to cooperative association of amphiphiles) in aqueous media which can offer the possibility of expanding these systems to communicate and interact to a diverse range of targets in the cellular environment. The approach revolves around the preparation of micrometer-scale LC droplets[41] that interact with PLL and can trigger the configurational transitions of the droplets which can be detected as changes in optical appearance of the LC. A key finding of the study reported here is that protein binding events involving PLL at LC-aqueous interface can trigger a LC reorientation at the cell surface in real time using polarized light.[26] This study also advances in mechanistic understanding of the intermolecular interactions at PLL-laden LC-aqueous interface that can be effectively applied as a simple entry for producing biocompatible LC surfaces. Our approach provides new methods for the design of LC chemical sensors for μm scale detection of toxic agents located in the surrounding media of a cell surface. Although the promise of topological defects mediated by LC materials on the μm scale have been used directly on the surface of cells, the possibility of using free-floating biocompatible LC

droplets through PLL-LC interactions *in situ* for reporting presence of cells has not been explored. Finally, our study further demonstrates the interaction between Annexin-V with phosphatidylserine (PS), as a tool to measure apoptosis, and an example of how this approach can be used for further biomedical applications.

5.3 Results and Discussion

5.3.1 Intermolecular interactions between nematic 5CB and PLL laden surfaces

Our first set of experiments employed polarizing optical microscopy (POM) to investigate if PLL was able to induce an ordering transition to nematic 4'-pentyl-4-cyanobiphenyl (5CB) molecule at LC-aqueous interfaces. We hypothesized that due to the presence of a protonated side chain amino group in each L-lysine residues (at physiological pH) they can have intermolecular interactions with the polar head group of 5CB (-CN in this case). These interactions can vary depending on the number of homopolymeric lysine units (e.g., molecular weight (M. wt.)). Keeping this in mind, we sought to investigate the ordering of 5CB by adsorbing the low and high molecular weight PLL (~3.5 kDa and 225 kDa) at 5CB-aqueous interface. For this, we hosted 5CB in the pores of electron microscopy grids supported on N,N-dimethyl-*n*-octadecyl-3-aminopropyltrimethoxysilyl chloride (DMOAP) treated glass slides. The DMOAP treatment of the glass anchors 5CB in an orientation that is perpendicular (homeotropic) to the LC-glass interface.[28] Subsequently, in contact with aqueous solutions (Figure 5.1a), the optical appearance of the LC became bright, consistent with an ordering transition of the LC induced by water[1]. Interestingly, when we introduced PLL (M. wt. 225 kDa) into this an ordering transition was observed within a minute leading to dark optical appearance of the LC (Figure 5.1b).

In contrast, with low molecular weight PLL solution (M. wt. 3.5 kDa) the optical appearance of the LC remains invariant (Figure 5.2b). These observations suggest that high M. wt. PLL is likely adsorbed and pre-organized at the interface to the aqueous phase of 5CB, thereby, allowing a rapid ordering transition. On the other hand, low M. wt. PLL is not able to organize itself at the LC-aqueous interface consistent with prior reports.[25]

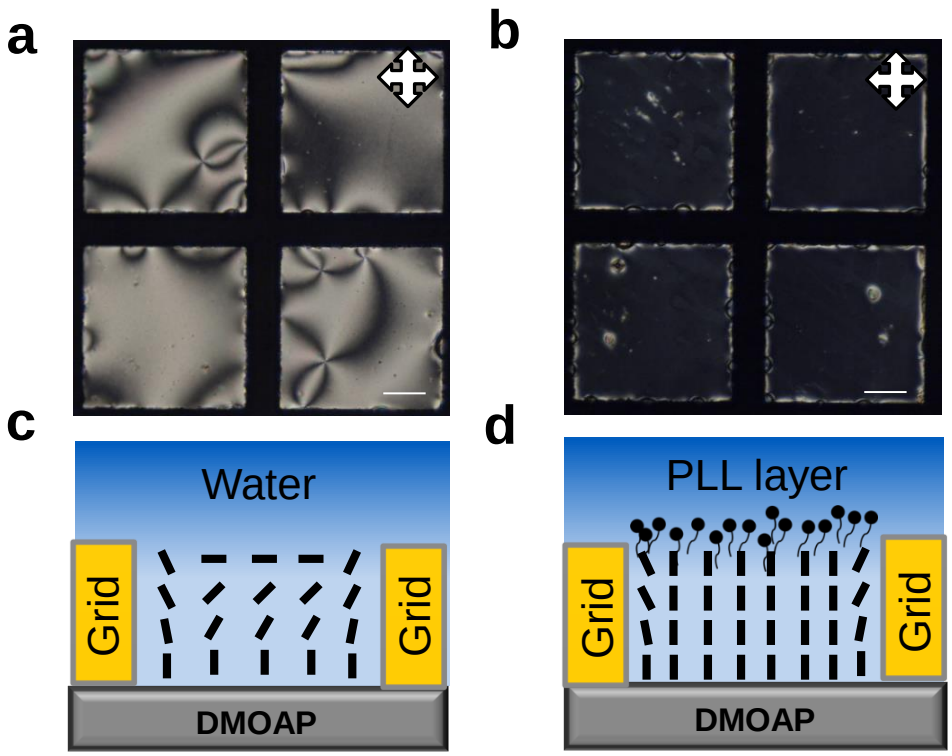

Figure 5.1 Polarized light micrographs (a, b) and corresponding schematic side views of 5CB (c, d) confined to a gold grid on DMOAP-coated surfaces in contact with aqueous phase (a, c) and after addition of 0.5 mg/mL of PLL (225 kDa) solution (b, d). Scale bar = 40 µm.

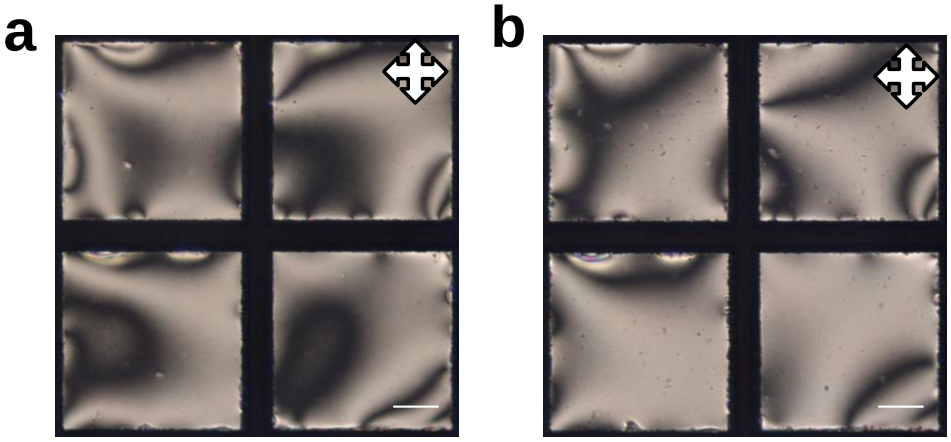

Figure 5.2 Polarized light micrographs of 5CB confined to a gold grid on DMOAP-coated surfaces in contact with aqueous phase (a) and after addition of 1 mg/mL of PLL (3.5 kDa) solution (b). Scale bar = 40 µm.

We hypothesized that modulation of the reactive sites of the PLL caused by the increase in the number of polypeptide units and the accompanying changes in overall balance of intermolecular interactions between 5CB and PLL molecules likely play an important role in governing the ordering of the LC at those interfaces.

In order to provide additional insight into the above described ordering of the LCs that can be attributed due to intermolecular interactions between PLL and 5CB, we performed Fourier transform polarization modulation infrared reflection absorption spectroscopy measurements (PM-IRRAS) to characterize the thin films of PLL decorated with 5CB.[42] Prior to PM-IRRAS measurements, VCD spectrum was taken to determine the structural conformation of the PLL at physiological pH. Figure 5.3a shows the amide I VCD spectra for PLL (in D_2O at pH 7) that exhibits VCD couplets at about 1650 cm^{-1}. This corresponds to the random coil conformation[43] consistent with the observed CD spectra of the PLL as shown in the Figure 5.3b.

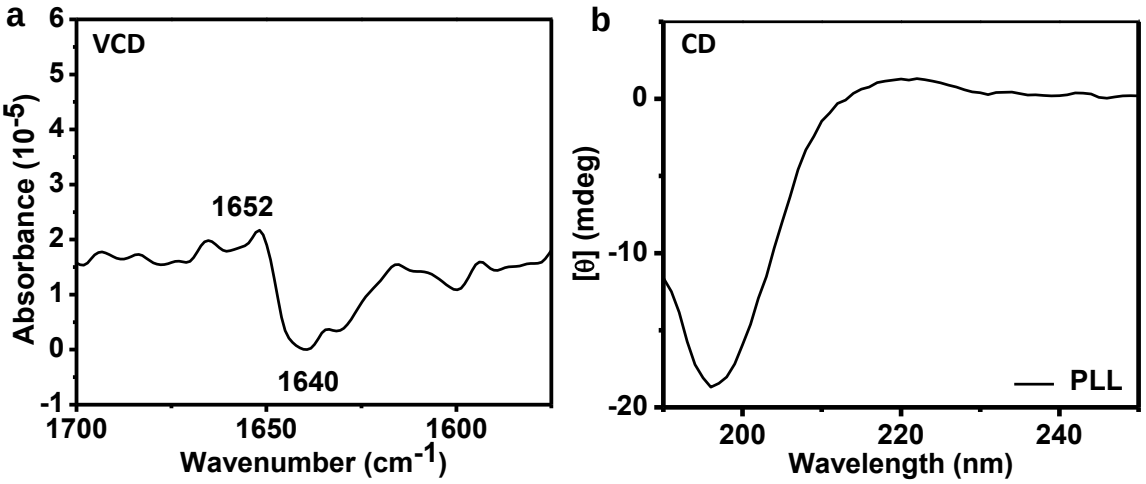

Figure 5.3 a) PLL VCD spectra in the amide region at pH 7.4 (random coil) and b) shows the CD spectra of PLL in the water under neutral pH conditions [PLL] 0.15 mg mL^{-1}.

Next, we performed PM-IRRAS measurements using PLL deposited on gold-coated surfaces and sought to determine any significant change in the observed spectrum in presence of 5CB at those interfaces (see experimental section for details).

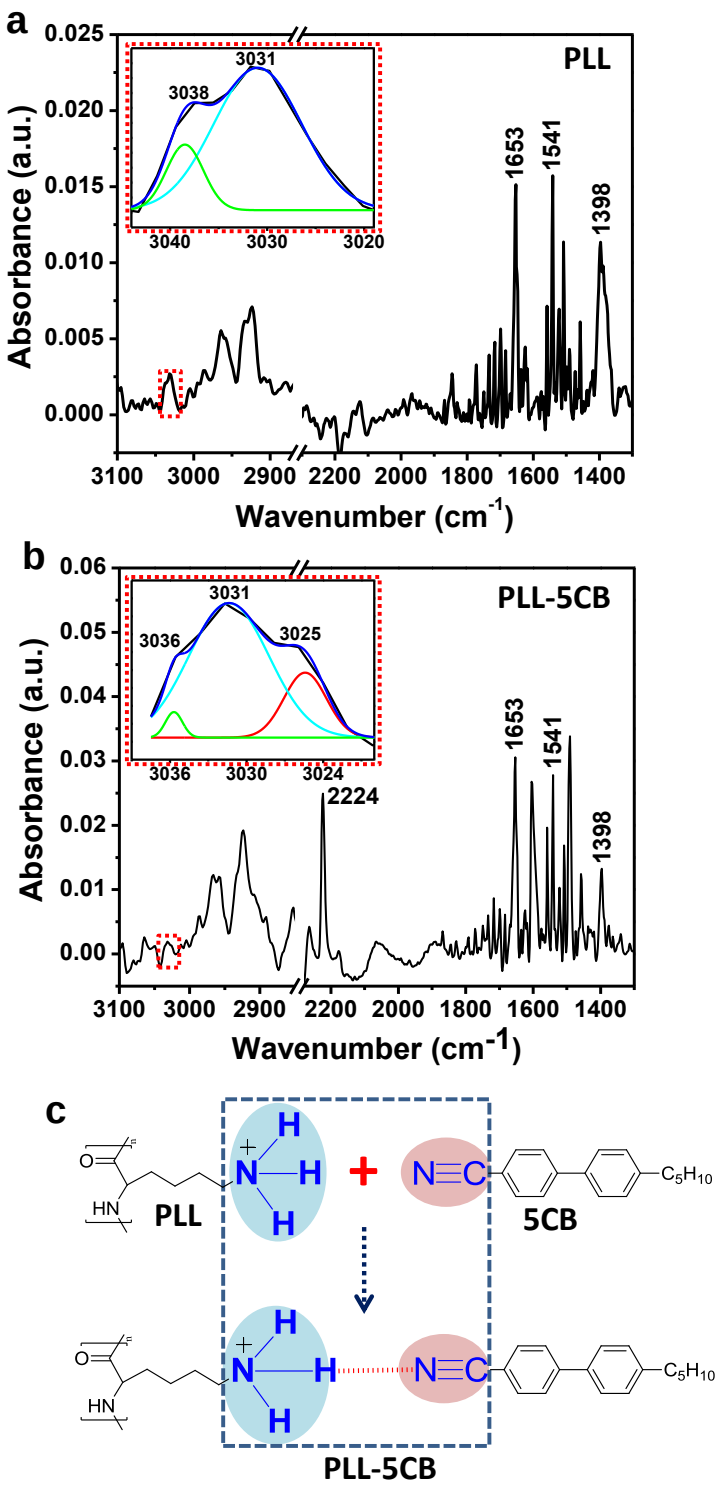

Figure 5.4 Characterizing the interaction of LC with PLL through PM-IRRAS measurements. (a and b) PM-IRRAS spectra of PLL monolayers that are adsorbed on a)

micro-pillars-coated with a uniformly deposited film of gold and b) 5CB films on the DMOAP-coated micro-pillars. The insets of a) and b) showing deconvolution of the band for protonated side chain NH_3^+ groups of PLL on gold surfaces and 5CB films respectively. c) Schematic illustration of the coordination interactions exhibit between 5CB and PLL.

First, examination of the wavenumber spectrum (1400-3100 cm^{-1}, Figure 5.4a) on PLL-laden interface reveals a significant band at 3030 cm^{-1} that corresponds to the free N-H stretch of the side chain NH_3^+ groups. The spectrum is associated with three other characteristic bands at 1653, 1541 and 1396 cm^{-1} of which first two are assigned to the amide I and amide II stretch, respectively and third one corresponds to the COO^- symmetric carboxyl stretch of PLL.[44,45] Second, in presence of 5CB, in the PM-IRRAS spectrum, we observed a strong peak at 2224 cm^{-1} corresponds to -C≡N stretch with four other additional bands for PLL (above described phenomena) consistent with the adsorption of PLL on 5CB films (Figure 5.4b). Careful inspection of Figure 5.4a and 5.4b reveals a significant change in the observed stretching (N-H) mode of the side chain of NH_3^+ groups (~ 3030 cm^{-1}) between PLL and PLL supported on 5CB films.

Table 5.1 Vibrational frequency (cm^{-1}) assignments for PLL and 5CB-laden PLL monolayers using PM-IRRAS.

Frequency (cm^{-1})	Vibrational assignment	Frequency (cm^{-1})	Vibrational assignment
	PLL Monolayer		**Monolayer of PLL-Modified 5CB**
3037, 3030	ν (N-H) mode of protonated NH_3^+ side chain group	**3037, 3030, 3025**	ν (N-H) mode of protonated NH_3^+ side chain group
2964, 2924	ν (C−H) symmetric and asymmetric stretching	**2964, 2924**	ν (C−H) symmetric and asymmetric stretching
1653	ν (C=O) amide I (carbonyl stretch)	**2224**	ν (C≡N) stretch
1541	ν (C-N) + amide II (CN stretch and NH bend) ν (N-H)	**1653**	ν (C=O) amide I (carbonyl stretch)
1398	ν_s (COO^-) symmetric carboxylate stretch	**1605**	ν (C–C) stretch
		1558, 1541	ν (C-N) + amide II (CN stretch and NH bend) ν (N-H)
		1398	ν_s (COO^-) symmetric carboxylate stretch

We note that the complex shape of this band in PLL clearly contains two components (3031 cm^{-1} and 3038 cm^{-1}) whereas in case of PLL on 5CB films, an additional weak band appears

at 3025 cm^{-1} that can be illustrated by the deconvolution of the band at 3030 cm^{-1} as shown in the inset of Figure 5.4a and Figure 5.4b, respectively. The new peak at 3025 cm^{-1} which we assigned due to the participation of the $-NH_3^+$ to the intermolecular hydrogen bonding with -C≡N groups of 5CB, suggests a strong evidence for the coordination interactions between 5CB and PLL as shown schematically in Figure 5.4c.

The observed downshift is consistent with previous studies that reported hydrogen bonding, in general, typically shifts the amide bands to the lower frequencies.[46,47] A summary of spectral assignments used in this study can be noted down in Table 5.1 for convenience. The other possible contributions include the change in the conformation of the polypeptide (PLL) in presence of 5CB but, the amide I position remains within the limits of a random coil (1653 cm^{-1}) as present in the aqueous form of PLL. Overall, the results described above are consistent with our hypothesis that intermolecular hydrogen bonding between 5CB and PLL is responsible for the observed ordering transition.

5.3.2 PLL-coated LC droplets as a biomarker for cell and its interactions with environment

Inspired by our preliminary studies that employed PLL induced ordering of LCs, our next goal is to design a simple but useful advance of an experimental system that can exploit the speed and sensitivity of droplet based LC sensors[41] for the manipulation and immobilization on the surface of cells. The approach that we report below revolves around the spontaneous adsorption of poly(styrene sulfonate) (PSS, Figure 5.5a) and poly(L-lysine) (PLL, Figure 5.5a) on LC droplets by using layer-by-layer technique. We have chosen E7 because (i) the T_{N-I} of E7 is well above the optimal temperature (37 ℃) for mammalian cell culture and (ii) it is not as cytotoxic as 5CB. We fabricated films composed of four PSS/PLL bilayers on LC droplets with outermost layer being PLL. Figure 5.5b illustrates the director profile of E7 within PSS and PLL encapsulated LC droplets during the progression of multilayer films. The PSS-coated LC emulsion droplets exhibited a bipolar configuration (similar to bare E7 droplets in aqueous media) with two point defects at opposite poles of the droplet surface as characterized by using polarized optical microscopy under crossed polars (Figure 5.6a) and bright field observation (Figure 5.6b).

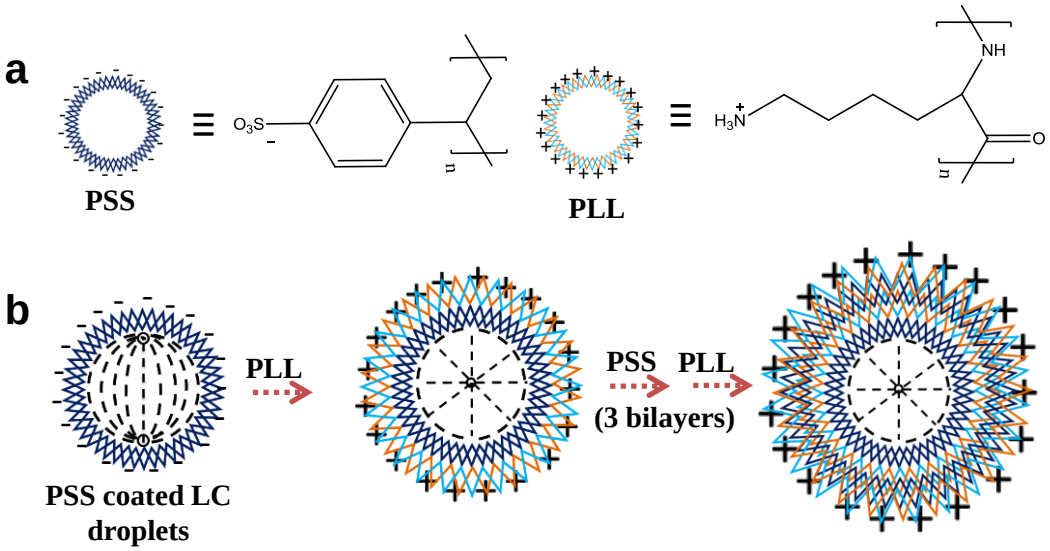

Figure 5.5 a) Chemical structures of PSS and PLL. b) Schematic showing the director profile of PLL/PSS multilayers adsorption on LC droplets.

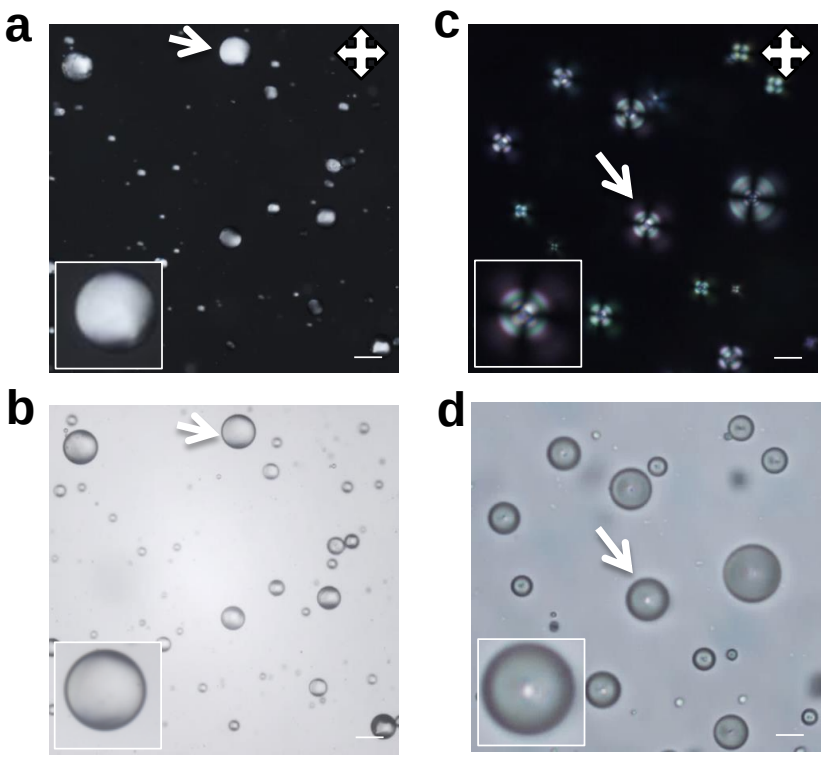

Figure 5.6 Polarized light and corresponding bright-field microscopy images of PSS (a,b) and PLL (c,d) coated droplets of E7, respectively. PSS-coated droplets exhibited a bipolar

configuration with two point defects at opposite poles of the droplet surface whereas in PLL radial configuration is achieved as characterized by a single point defect (cross-like appearance) at the center of the droplet which can be shown which can also be observed in a bright-field micrograph (as shown by a white arrow in d). The insets within (a-d) illustrates the higher magnification version of the arrow marked LC droplet. Scale bar = 10 µm.

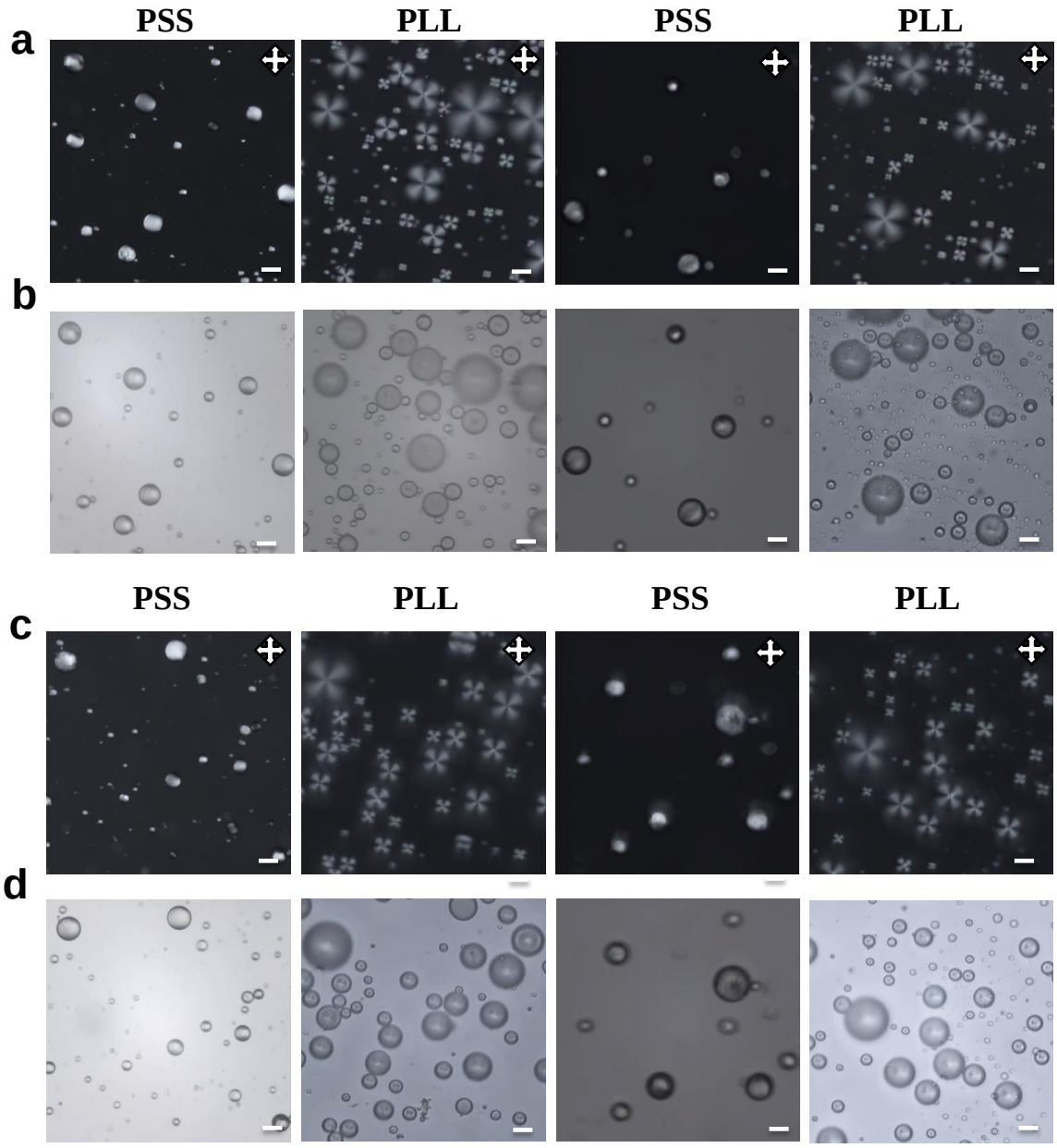

Figure 5.7 Polarized optical microscopic characterization of polyelectrolyte multilayer of LC droplets build up. (a,c) Polarized optical micrographs of PSS-coated LC droplets as a

function of the number of deposition steps. (b,d) Corresponding bright field micrographs. The first deposition is PLL followed by PSS. [PLL], [PSS] = 1mg/mL. The scale bar= 40 µm.

In presence of PLL, these droplets undergo an ordering transition from a bipolar to radial configuration as characterized by a single point defect (cross-like appearance) at the center of the droplet (Figure 5.6c) which can also be observed in a bright-field micrograph (as shown by a white arrow in Figure 5.6d) consistent with the homeotropic anchoring of the LC at PLL laden LC-aqueous interface. The polarized optical micrographs and their bright field images after the addition of each polyelectrolyte layer (4 bilayers) to E7 droplets were shown in Figure 5.7. The building up of PSS/PLL multilayer films on E7 LC droplets were also investigated by ζ-potential measurements. The ζ -potentials of PSS and PLL-coated droplets in water at pH 7.4 were measured to be -45 mV and +55 mV, respectively. Alternating ζ -potentials for PSS and PLL-coated LC droplets during layer-by-layer (between -45 mV and +50 mV) as shown in Figure 5.8 deposition is consistent with the stepwise adsorption of anionic PSS and cationic PLL, respectively.

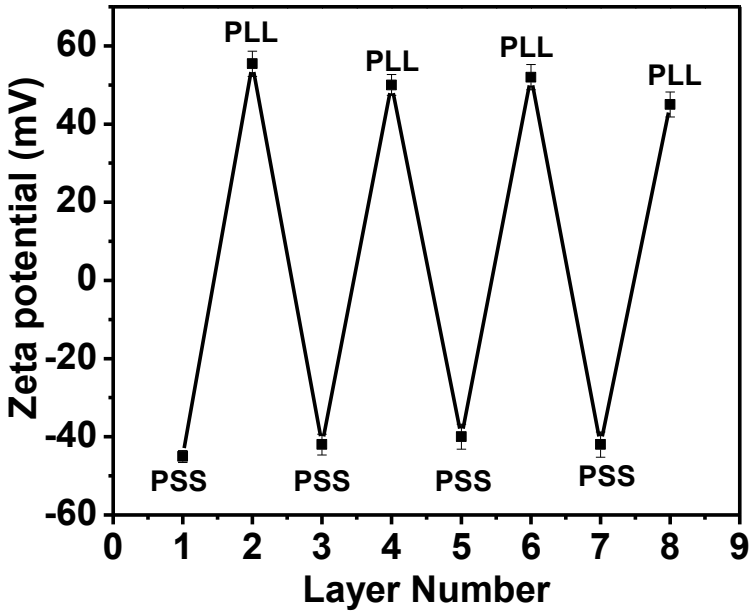

Figure 5.8 Progression of multilayer of LC droplets formation. Zeta-potential of four bilayers of (PLL/PSS)-coated E7-PSS emulsions as a function of layer number, with

outermost being PLL. The measurements were taken after deposition of each layer (PSS/PLL layer) corresponds positive values (+50 mV) for PLL adsorption and negative values (-45 mV) for PSS deposition. The zeta-potential measurements were taken in water (pH 7.4).

Next, we performed a series of experiments to determine whether these PLL-coated LC micro-droplets would mechanically support and could be immobilized on the surfaces of cells, yet retain their responsiveness to changes in the chemical environment on interactions with the cells. We have chosen adherent T84 (ATCC) cell line for this study as a proof-of-concept. Prior to expose to cells, PLL encapsulated LC droplets were suspended into Dulbecco's modified Eagle's medium (DMEM) medium used for cell culture. Inspection of crossed polarizer and bright field images (Figure 5.9a,b) reveal that, following incubation in DMEM medium, LC micro-droplets remained stable and their structure was not perturbed in contact with culture media (retain radial configuration). These polarized-light and bright field micrographs, when combined, suggest that it may be possible to exploit the reordering of these PLL-laden LC droplets to report mechanical interactions with cell surfaces.

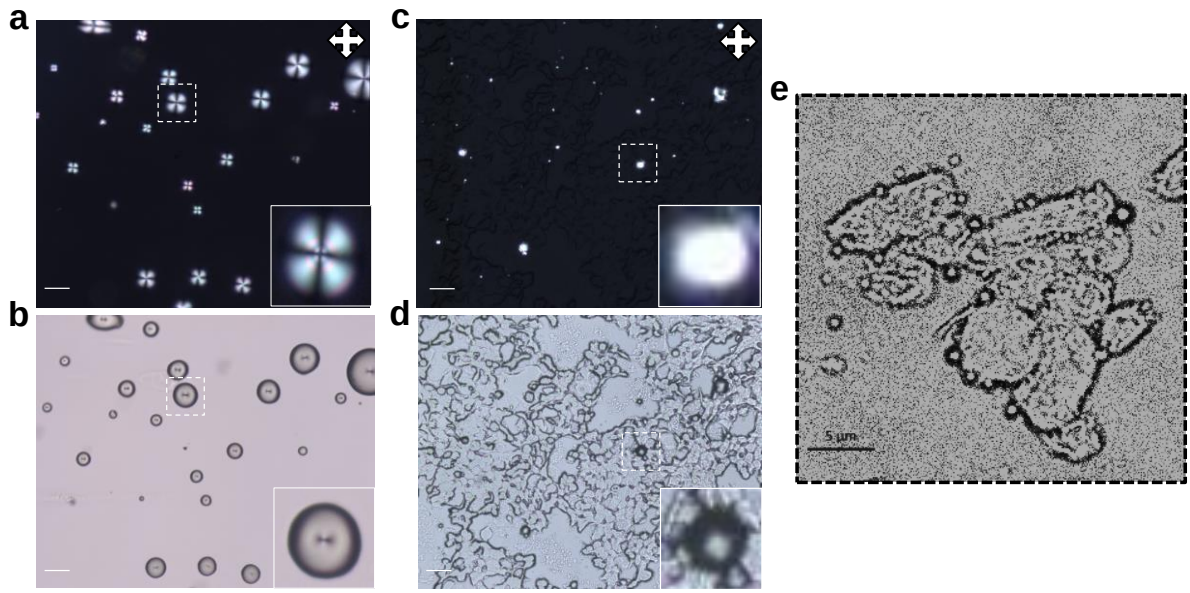

Figure 5.9 Interaction of cells with PLL-coated LC droplets. Polarized optical and bright-field micrographs images of PLL-coated LC droplets: (a,b) suspended in DMEM (c,d) in contact with cells. The LC droplets were in radial states (a) before but transitioned to bipolar state (c) after anchored to cells. The insets show the magnified version of selected LC

droplet. e) The bright field micrograph of PLL-coated LC droplets adhered to cells at an objective power of (640x), clearly depicting the attachment of PLL-coated LC to cell boundary. Scale bars are 50 µm.

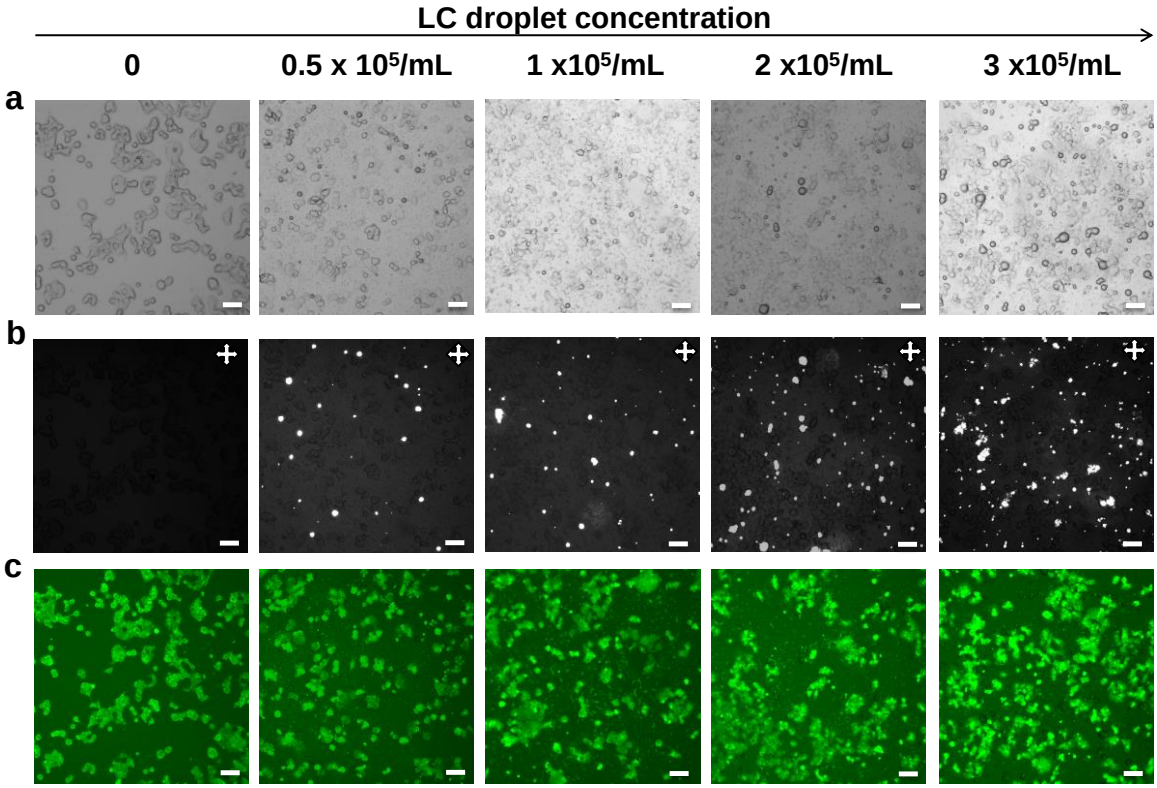

Figure 5.10 Optimization of PLL-coated LC droplet concentration for cell adherence. a) bright field, b) crossed polars and c) epi-fluorescence (cells stain with calcein–AM) microscopic images of cell adhered PLL-coated LC droplets on incubation of 0, 10^4/mL, 1 x 10^5/mL, 2 x 10^5/mL and 3 x 10^5/mL concentration of PLL-coated LC droplets in contact with cells. The increasing concentration of droplets resulting more number of droplets attached to cells without affect the cell viability. The green fluorescence corresponds to the cells stain with calcein–AM as a marker of cell viability. Scale bar = 40 µm.

Next, the PLL-coated droplets were placed into culture media and incubated with cells for a period of 1 h. Figure 5.9c and 5.9d shows the polarized light and bright field micrographs after incubation of PLL-coated droplets in contact with cells, respectively. Interestingly, in contact with cells, PLL-coated droplets resulted a rapid change from the radial state to the so-

called bipolar configuration that confirms the cell-adhesive nature of these droplets. We performed two additional control experiments to establish the role of PLL encapsulated droplets in the above described phenomenon. First, we observed that with systematic increase in the concentration of PLL-coated LC droplets resulted more number of droplets to get attached to cells without affecting the cell viability as shown in Figure 5.10. Second, we observed no attachment of LC droplets (Figure 5.11) with cells by using bare E7 droplets (i.e. uncoated). Careful analysis of bright field and polarized micrographs (Figure 5.11a and Figure 5.11c) revealed that bare E7 droplets were not remain associated with cells and completely washed away by removing media and manually rinsing with buffer. In contrast, PLL-coated LC droplets remained associated with cells and were not removed from the cell surface by manual rinsing.

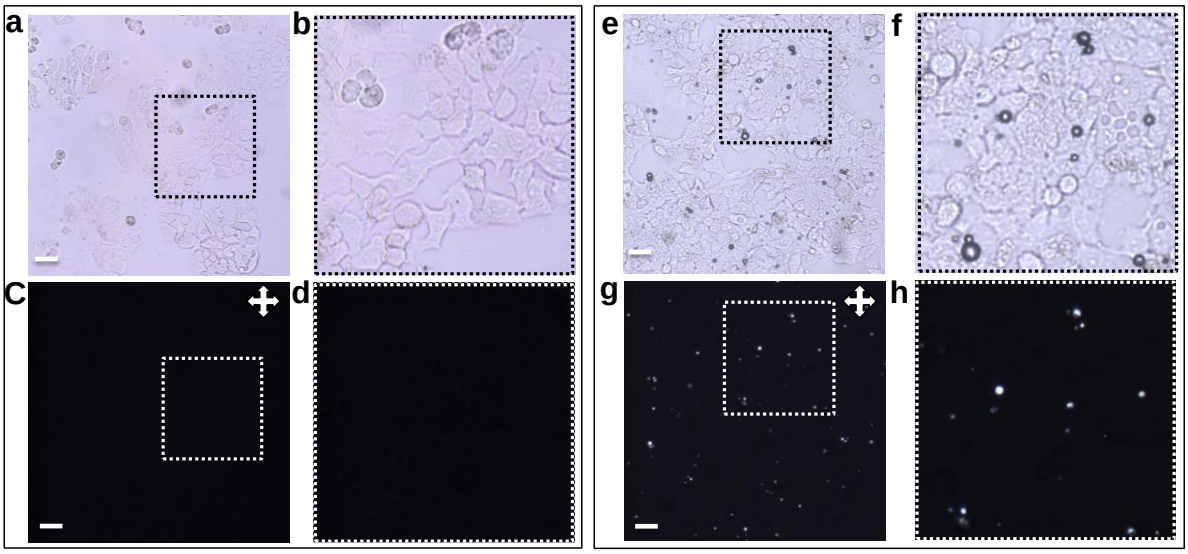

Figure 5.11 Cell adherence towards PLL-coated/uncoated LC droplets. (a,e) Bright field and (c,g) corresponding polarized light microscopy images of bare and PLL-coated LC droplets in contact with cells for 1 h incubation, respectively. (b,d,f,h) are the zoomed portions of the insets shown in images (a,e,c,g). The PLL-coated LC droplets adhered strongly to the surface of cells while bare droplets are completely removed in washing step. Scale bar = 40 µm.

These results clearly established that 1) PLL-coated LC droplets get anchored strongly on cells plausibly through ionic interaction of positively charged PLL with negatively charged cell membranes and 2) contact of the PLL-coated LC droplets with cell surface promote

change in the orientation of LC droplet configuration from radial to bipolar. We believe that the observed change in the optical appearance of the droplets (i.e., radial to bipolar configuration) is likely due to the interaction of these PLL-coated LC droplets with cells that disturbs the intermolecular interactions of PLL with the LC.

Motivated by the above-described results, we sought to determine whether the cell-anchored PLL-coated LC droplets can report in real-time on the presence of toxic agents. We selected HTAB, a small surfactant and a well-known toxic agent to the cells.[48] To investigate the effect of toxic agent on the orientation of cell-anchored PLL-coated LC droplets (shown in Figure 5.12a and 5.12b), a concentrated solution of HTAB was added carefully to the culture well containing the droplets.

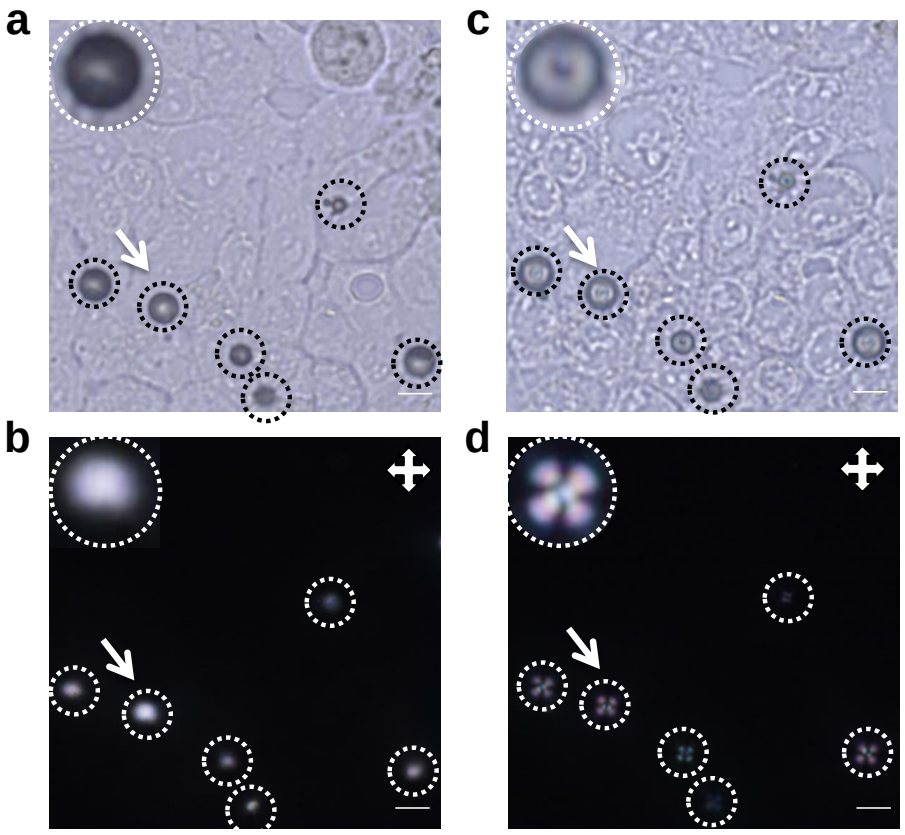

Figure 5.12 Ordering response of cell anchored PLL-coated LC droplets in addition to cytotoxic agents (HTAB). (a,b) Bright-field and polarized microscopic images of PLL-coated LC droplets anchored on cells. (c,d) Corresponding bright and polarized microscopic images after addition of HTAB (100 μM). The director configuration of PLL-coated LC droplets

attached with cells change from bipolar to radial after adsorption of HTAB through PLL layer and then interacts with LC. The insets show the magnified version of configuration transition of arrow marked PLL-coated LC droplet anchored on cells before and after addition of HTAB. Scale bar = 10 µm.

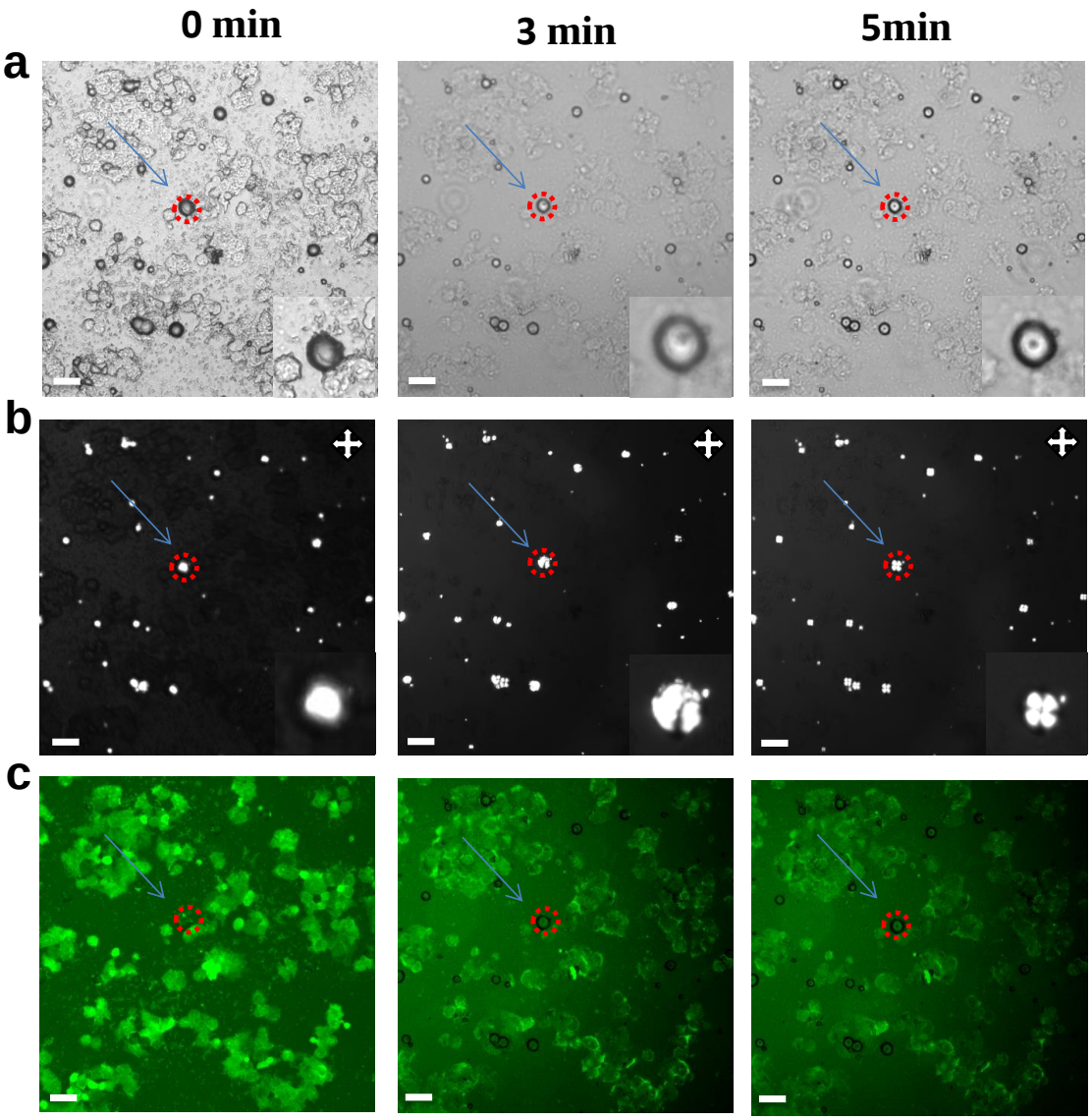

Figure 5.13 Continuous change in ordering transition of cell anchored PLL-coated LC droplets in addition to cytotoxic agents (HTAB). a) Bright-field and b) polarized microscopic images of PLL-coated LC droplets anchored on cells after addition of HTAB (100 µM) at different point intervals of 0, 3 min and 5 min, respectively. The insets show the magnified version of continuous configuration transition of arrow marked PLL-coated LC droplet

anchored on cells after addition of HTAB. c) Corresponding epi-fluorescence images of cells attached with PLL-coated LC droplets. Scale bar = 40 µm.

Inspection of the bright field and polarized micrographs (as shown in Figure 5.12c and 5.12d, respectively) revealed a change in the configuration of cell-attached droplets from bipolar to radial in contact with 100 µM HTAB. A lower concentration 60 µM of HTAB was added to monitor the time dependent changes in the orientational order of the LC droplets as shown in Figure 5.13. Systematic observation of Figure 5.13 showed that the ordering of LCs within droplets changes from bipolar to pre-radial and then to a radial ordering as a function of time at a fixed concentration of HTAB in cell culture well. The epi-fluorescence micrographs shown in Figure 5.13c demonstrated that PLL-coated LC droplets can detect the presence of HTAB in significantly lower concentration much below the toxic level of HTAB to cells. In summary, these results provide the sensitivity of PLL-coated LC droplets in response to cells and cell-attached LC droplets can act an excellent optical biomarker for cells and cell based interactions.

5.3.3 Biocompatibility of PLL-coated LC droplets for cellular environments

Biocompatibility is the major requirement for using PLL-coated LC droplets to promote cell substrate interaction for cell based studies. To explore whether PLL-coated LC droplets are biocompatible, we carried out flow cytometry based experiment with the use of calcein AM and propidium iodide (PI) staining. Calcein AM is a cell membrane permeable dye that converts into green fluorescent calcein by intracellular esterases. As esterase activity is a function of live cells, only live cells show green fluorescence. On the other hand, PI is a membrane impermeable dye and only can enter into the cell through the damaged or compromised membrane of apoptotic or dead cells. PI fluoresce red when it binds to nucleic acids. Therefore, by calcein AM and PI staining cell viability can be accurately estimated.

For this, cells (T84) were treated with different concentrations of PLL-coated LC droplets. The incubation time for different concentrations of PLL-coated LC droplets to cells was 45 min for all cell based experiments. Following incubation treated cells were stained with calcein AM and PI (see experimental section for detailed procedure) and analyzed by flow

cytometry. Live cells showed green fluorescent calcein staining which was analyzed in FL1 channel and dead or damaged cells showed PI staining which was analyzed in FL2 channel. Quantification of cell viability was performed by dot plot analysis of the flow cytometry data with quadrant gate. Interestingly, treated cells showed decrease in calcein fluorescence and increase in PI uptake with increasing concentration of the PLL-coated LC droplet treatment (Figure 5.14). From the quadrant gate analysis of the dot plot it is evident that Q3 of buffer treated cells show more calcein+ve cells (65.5%) compared to PLL-coated LC droplet-treated cells (64.3%, 53.6% and 32.1%) with increasing doses (Figure 5.14a).

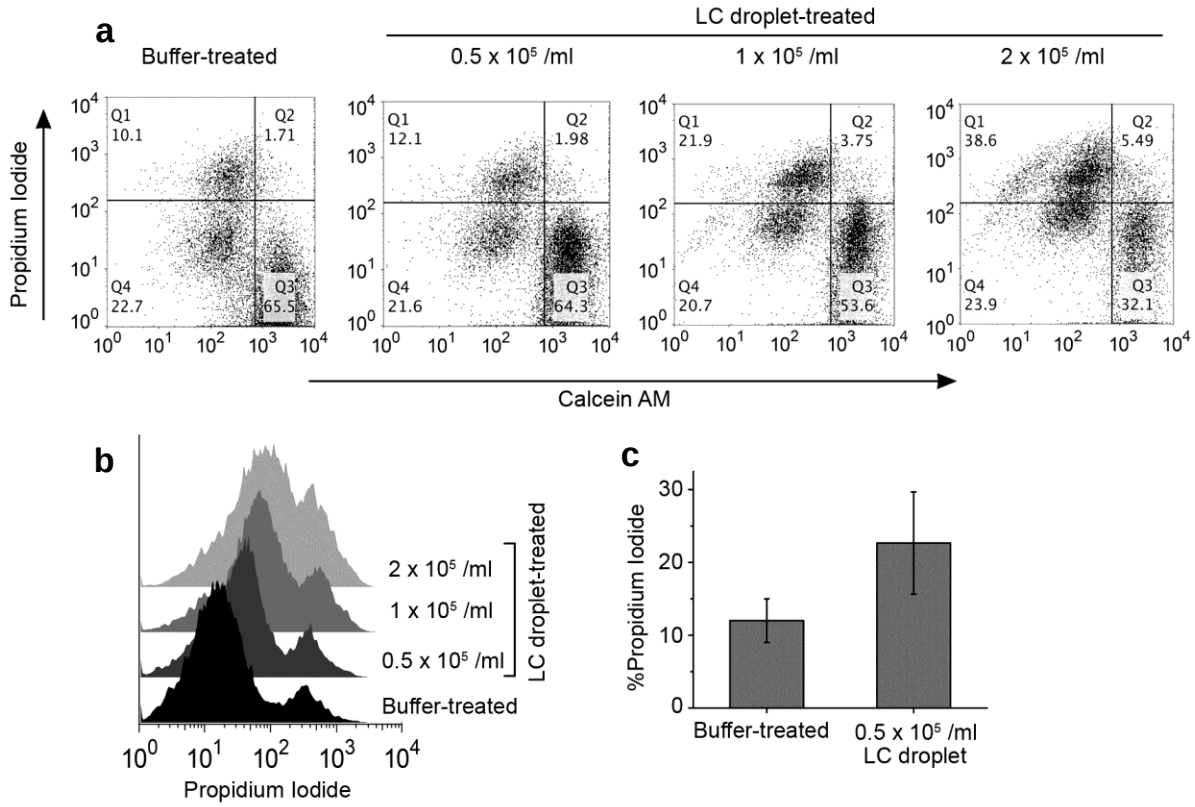

Figure 5.14 Cell viability is minimally affected by $5x10^4$/mL PLL-coated LC droplet treatment. T84 cells were treated with $5x10^4$/mL, $1x10^5$/mL or $2x10^5$ cells/mL PLL-coated LC droplets or buffer and incubated for 45 min. Following incubation cells were stained with calcein AM and PI and analysed by flow cytometry. The experiments were repeated for more than three times. (a) Dot plot analysis with quadrant gate showing increase in PI positive cells (Q1) and decrease in calcein positive cells (Q3) with increase in treatment doses compared to buffer-treated control. (b) Offset histogram showing increase in PI positive cells

with increasing concentration of LC droplet treatment. (c) Bar-graph showing comparison of PI positive population between buffer-treated cells and $5x10^4$/mL LC droplet-treated cells. Difference between these two population found to be non-significant ($p<0.075$) by unpaired Student's t-test.

Further, it is very clear from the plot that the numbers of cells failing to get calcein staining are the same population of cells incorporating PI in the DNA (Figure 5.14a). The cells in the Q1 are the PI+ve cells and there is around 10.1% cells in Q1 for buffer-treated control but there is an increase in dead cell population (12.1%, 21.9% and 38.6%) were observed with increase in doses of LC-droplet treatment (Figure 5.14a). The cells in the Q4 of the quadrant are the Cal-ve and PI-ve population, means those cells who are dying but not yet dead (Figure 5.14a). The Q4 population is same across all the treatment suggesting that LC droplet treatment is inducing death to the cells as the percentage of PI+ve cells (Q1) are only increasing (Figure 5.14a). Further, the offset histogram is showing an increase in PI-staining with increase in doses of PLL-coated LC droplet treatment (Figure 5.14b).

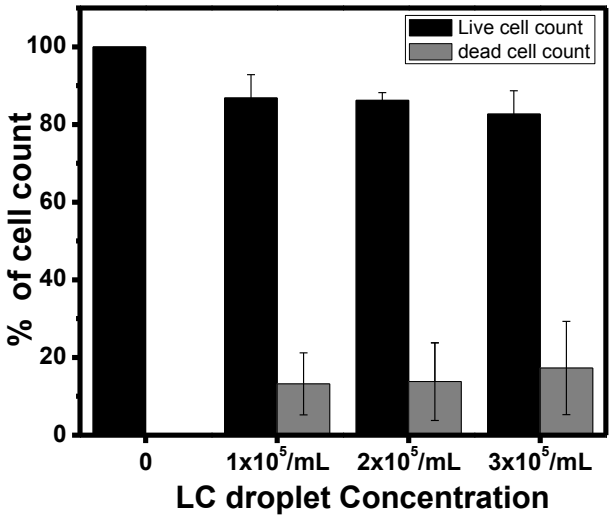

Figure 5.15 Quantification of PLL-coated LC droplets anchored on T-84 cell survival using Trypan blue exclusion assay. The graph represents the live and dead cell count percentage with increasing concentration of PLL-coated LC droplets. The relative change in the number of live and dead cell count after PLL-coated LC droplet treatments was slight even at $3x10^5$/mL.

Interestingly, the PI uptake of cells treated with $5x10^4$/mL ($0.5x10^5$/mL) concentration of PLL-coated droplets appeared to be little higher than untreated cells (Figure 5.14c). The difference is statistically insignificant ($p<0.075$). The gradual induction of cell death rises beyond $5x10^4$/mL concentration of PLL-coated LC droplets with increase in concentration. This data suggests that $5x10^4$/mL LC droplet is biocompatible and can be used for cell based studies.

In addition, we have performed Trypan blue exclusion assay for assessing biocompatibility. Trypan blue, a diazo dye, is only permeable to cells with compromised membranes, therefore, dead cells are stained while live remain colorless. The amount of cell death was determined using light microscopy (see experimental section for detailed procedure). Figure 5.15 represents the graph of the live and dead cell count percentage with increasing concentration of PLL-coated LC droplets. The relative change in the number of live and dead cell count after PLL-coated LC droplet treatments was slight even at $3x10^5$/mL concentration in contrast to relative change observed using flow cytometry staining assay. In combination, these two results exemplify that the PLL-coated droplets are biocompatible to cells up-to 10^5/mL level, consistent to the optimum level of droplet concentration used for cell based study.

5.3.4 Utilization of PLL-coated LC droplets for studying other interactions (e.g., Annexin-V–PS interactions)

Finally, we sought to explore PLL-coated LC droplets as a template for studying other important biological interactions. Apoptosis is considered as a vital component of various processes including normal cell turnover, proper development and functioning of the immune system, hormone-dependent atrophy, embryonic development and chemical-induced cell death. Inappropriate apoptosis (either too little or too much) is a factor in many human conditions including neurodegenerative diseases, ischemic damage, autoimmune disorders and many types of cancers. The ability to modulate the life or death of a cell is recognized for its immense therapeutic potential. Apoptosis is accompanied by various morphological changes including nuclear condensation, DNA fragmentation and cell surface changes. The significant change in cell surface is the loss of cell membrane asymmetry which leads to a

consequence that PS normally present in the inner cell membrane is redistributed out to the cell surface.[49] The PS was found to specifically bind to a protein named Annexin-V in the presence of Ca^{2+}. For that purpose, calcium dependent Annexin-V protein interaction with PS used as a reliable marker for monitoring the progression stages of apoptosis is selected as a proof of example.[49] Here in, we have prepared PLL-coated LC droplets as described above and exposed to an aqueous solution of 0.1mg/mL Annexin-V protein for 10 min incubation. The polarized and bright field micrographs of PLL-coated LC droplets in Hepes buffer at pH 7.4 before and after adsorption of Annexin-V shown in Figure 5.16a,b and Figure 5.16c,d, respectively demonstrate a radial-to-bipolar configuration transition of E7 inside the droplets.

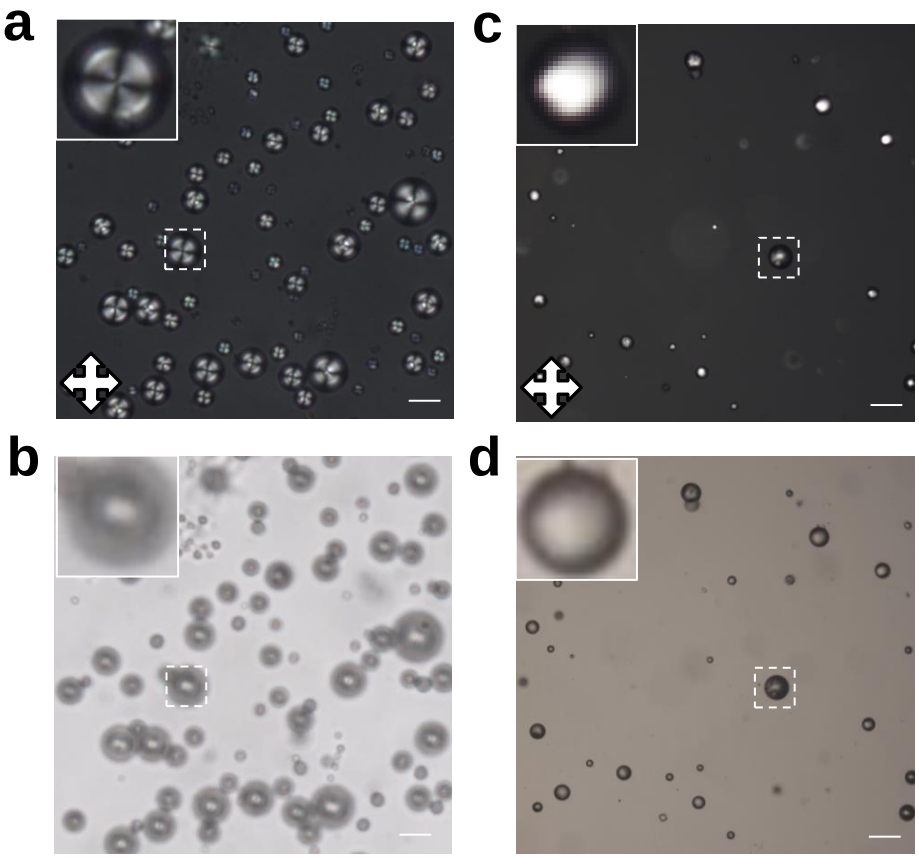

Figure 5.16 (a,b) Polarized and bright-field optical microscopic images of PLL-coated LC droplets and (c,d) corresponding images after coating of these capsules with Annexin-V solution. The absorption of Annexin-V over PLL-coated droplets is depicted through change

in ordering transition of LC droplets from radial to bipolar on interaction of Annexin-V with PLL. The insets show the magnified version of selected LC droplet. Scale bar = 40 µm.

Annexin-V protein is a negatively charged protein, adsorbs on the surface of positively charged PLL-coated LC droplets likely through the electrostatic interaction and is responsible for this configurational transition of these LC droplets.

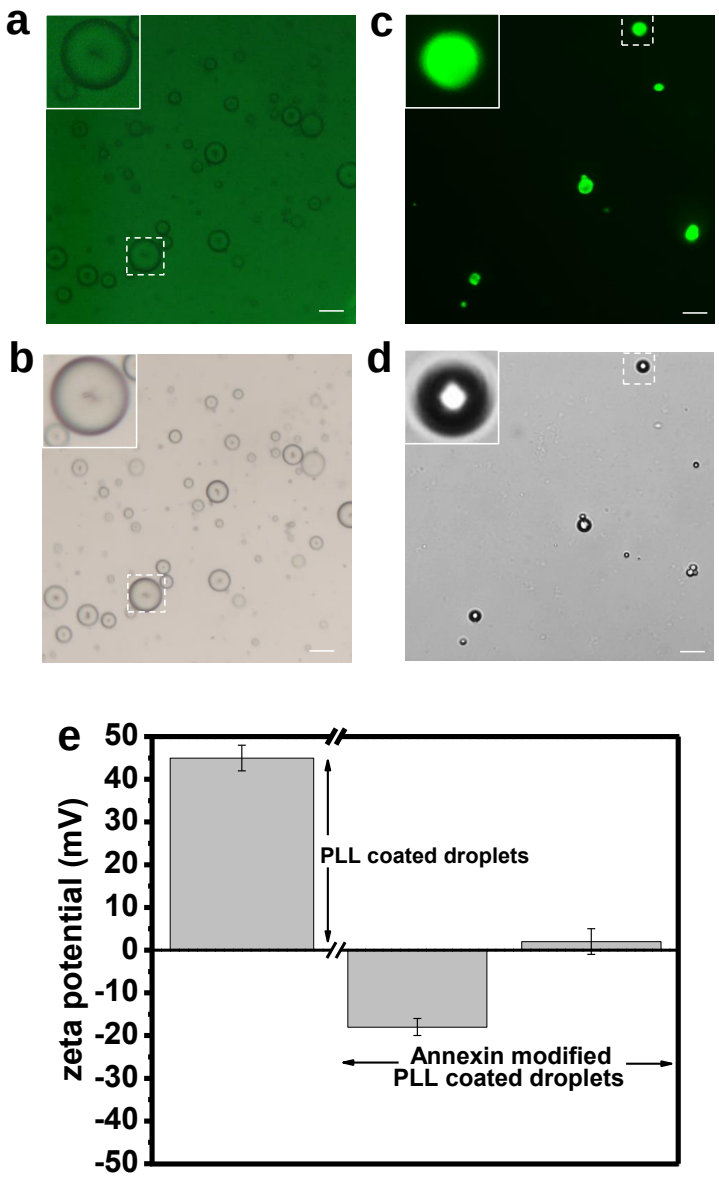

Figure 5.17 Epi-fluorescence microscopic images of PLL-coated LC droplets before a) and after c) adsorption of Annexin (FITC-Annexin). (b,d) corresponding bright field images of a)

and c) respectively. The insets show the magnified version of selected LC droplet. Scale bar = 40 µm. (e) Zeta potential of PLL-coated droplets showing the absorption of negatively charged Annexin-V over positively charged PLL-coated LC droplets on changing the zeta-potential from positive to negative.

The fluorescent microscopy confirms the adsorption of Annexin-V on the PLL-coated LC droplets is responsible for the radial to bipolar configurational transition. As can be seen in Figure 5.17c, the surface of the bipolar Annexin-V-coated PLL E7 droplets shows strong fluorescence in contrast to PLL-coated LC droplets (Figure 5.17a), confirming the adsorption of FITC-Annexin-V on PLL-coated LC droplets. Figure 5.17e shows the drop of zeta potential of PLL-coated LC droplets from 45 mV to -18 mV after addition of Annexin-V further suggesting the adsorption of negatively charged Annexin-V on the PLL-coated LC droplets. The two values of zeta potential (-18 mV and 2 mV) of Annexin-V-coated LC droplets obtained is likely due to the non-uniform adsorption of Annexin-V.

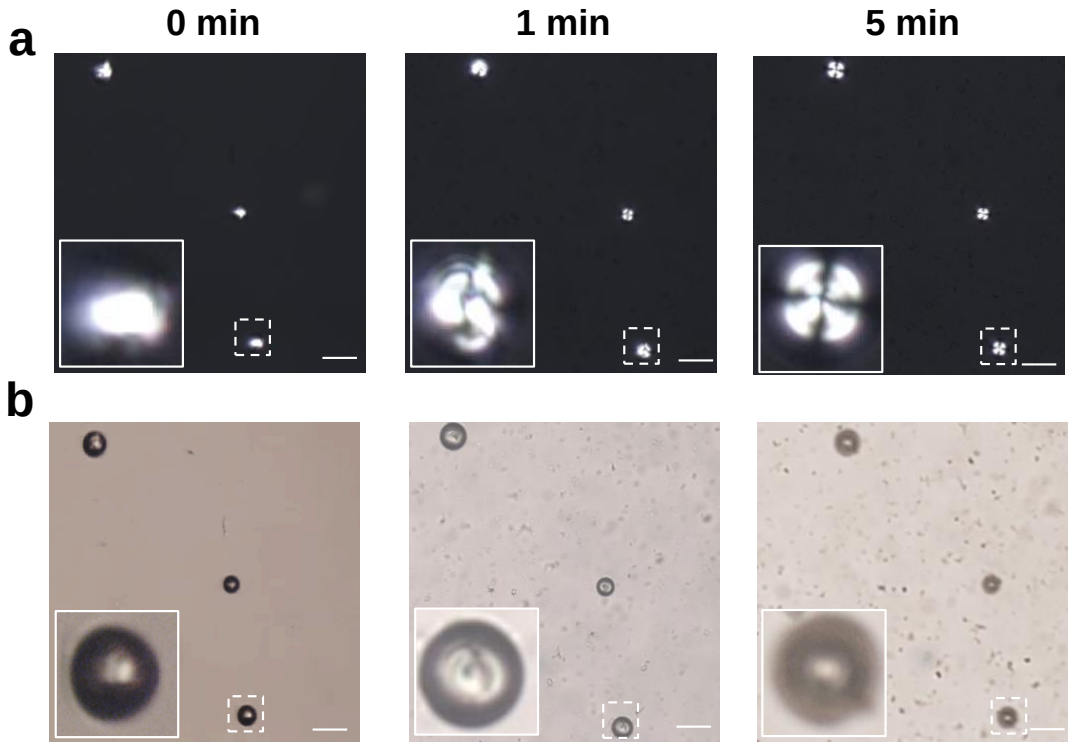

Figure 5.18 Study of Annexin-V and PS interaction on PLL-coated LC droplets. a) represents the time lapse polarized micrographs and its corresponding bright field

micrographs (b) of Annexin-V-coated LC droplets in response to PS vesicles in the presence of 10 mM $CaCl_2$. The insets show the magnified version of selected LC droplet. Scale bar = 40 µm.

To investigate the interaction of PS on the Annexin-V-coated LC droplets, we exposed the Annexin adsorbed PLL-LC droplets in contact with an aqueous solution of 10 mM $CaCl_2$ with 0.2 mg/mL of PS vesicles. Figure 5.18a represents the time lapse polarized micrographs and its corresponding bright field micrographs (Figure 5.18b) of Annexin-V-coated LC droplets in response to PS vesicles. We observed a rapid change in ordering transition (within couple of minutes) in the orientation from bipolar to pre-radial and then ultimately to radial in response to PS vesicles.

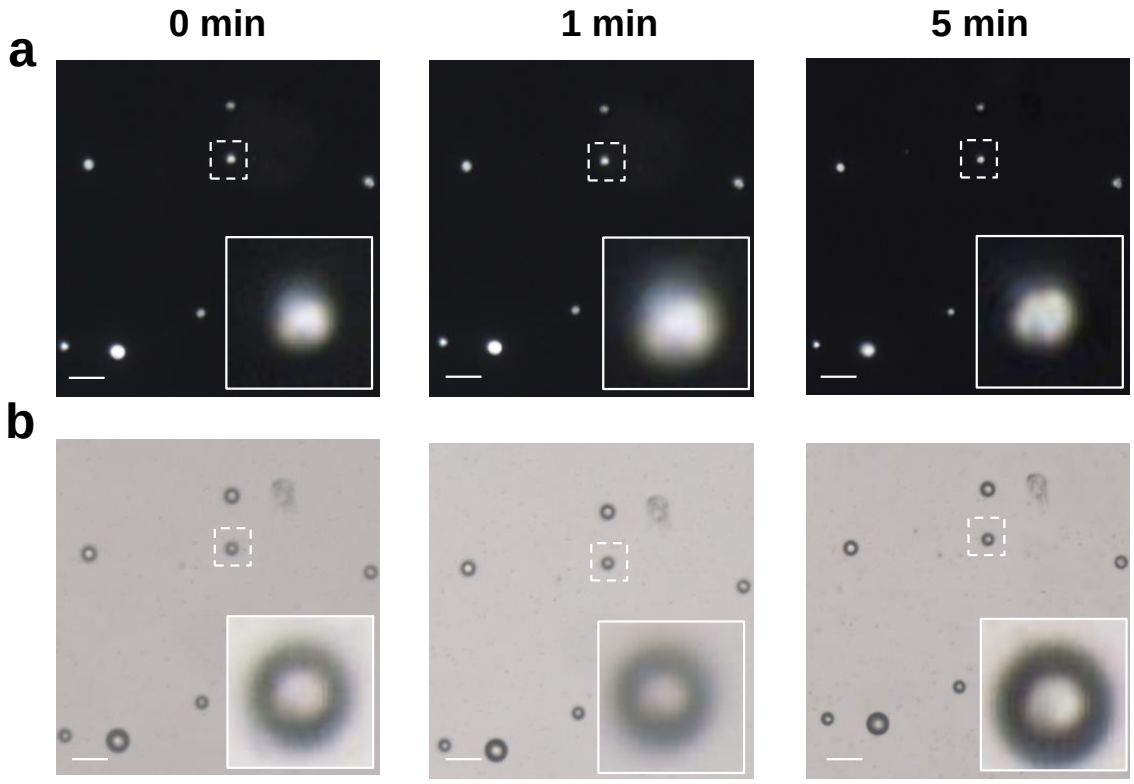

Figure 5.19 a) Represents the time lapse polarized micrographs and its corresponding bright field micrographs (b) of Annexin-V-coated LC droplets in response to PS vesicles in the absence of $CaCl_2$. The insets show the magnified version of selected LC droplet. Scale bar = 40 µm.

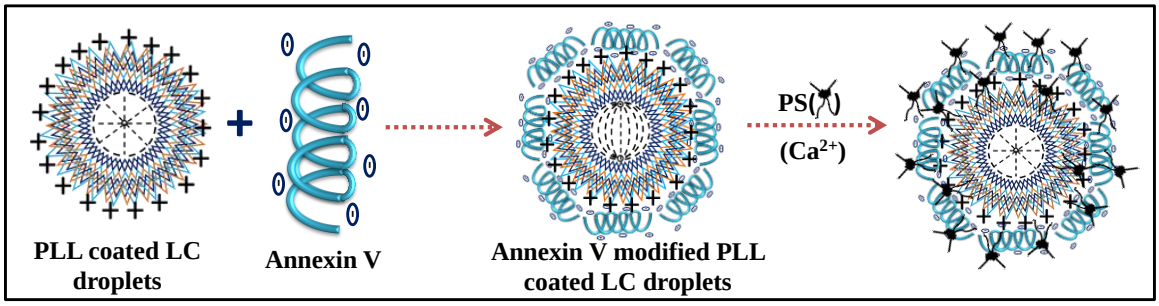

Figure 5.20 Schematic illustrations of the Annexin-V and PS interaction on PLL-coated LC droplets.

We propose that the due to the interaction of Annexin-V with PS in presence of Ca^{2+}, the PS molecules get adsorbed and permeate through the polyelectrolyte multilayers to interact with the LC core of the droplets. This leads to causing the changes in the LC orientation within the droplets. In contrast, in absence of Ca^{2+}, the LC orientation remains invariant (i.e., bipolar, Figure 5.19). The adsorption of PS on the Annexin-V-coated LC droplets get slowed down in the absence of Ca^{2+} due to which LC droplet were unable to show the change within this time frame. This result further confirms that the change is due to the formation of the Annexin-V-PS binding on the surface of the LC droplets. The schematic corresponding to the change in the director profile of PLL-coated LC droplets due to the interaction of Annexin-V with PS is shown in Figure 5.20. These results show that it is possible to exploit PLL-coated LC droplets in cell based apoptosis detection which are currently in progress.

5.4 Conclusions

In summary, the methodology developed in this work not only achieves, for the first time, an efficient and simple design for cell-based sensors using biocompatible LC droplets *via* direct PLL-LC interactions at aqueous interfaces but also, it provides to detect the presence of toxic agents in terms of healthcare applications. In addition, we have established that hydrogen bonding between protonated side chain amino group in each L-lysine residues of PLL with the polar head group of 5CB plays a central role in determining the orientations of LC at PLL laden LC-aqueous interfaces. Our finding further demonstrated the use of PLL droplets to study other biological interactions in particular, Annexin V-PS, a tool to measure apoptosis,

which thereby opens up unique opportunities for discovering several interfacial phenomena related to cell biology.

5.5 Experimental Section

5.5.1 Materials

Poly-L-lysine (PLL) solution 0.1 % (w/v) in H_2O, poly(4-styrenesulfonic acid) sodium salt (PSS), Dulbecco's modified Eagle's medium (DMEM), propidium iodide, Annexin V, FITC-Annexin, hexadecyltrimethylammonium bromide (HTAB), tris (hydroxyl methyl) amino-methane, N,N-dimethyl-N-octadecyl-3-aminopropyltrimethoxysilyl chloride (DMOAP), hydrochloric acid, sodium hydroxide and calcium chloride were purchased from Sigma-Aldrich (St. Louis, MO). Opti-MEM cell culture medium, phosphate-buffered saline (PBS), fetal bovine serum (FBS), trypan blue and calcein AM were purchased from Invitrogen (Carlsbad, CA). The thermotropic liquid crystal (LC) E7, sulfuric acid, chloroform and hydrogen peroxide (30% w/v) were purchased from Merck (Mumbai, India). Ethanol was obtained from Jebsen & Jenssen GmbH and Co., Germany (s d. fine–chem limited). 4-cyano-4'-pentylbiphenyl (5CB) was obtained from Sigma-Aldrich (St. Louis, MO). Deionization of a distilled water (DI water) source was performed using a Milli-Q-system (Millipore, bedford, MA). All materials were used as received without further purification.

5.5.2 Preparation and characterization of Optical Cells

Procedure used to prepare and examine the LC films in TEM grids within optical cells have been described in detail elsewhere[1]. Briefly, glass slides were cleaned with piranha solution (70:30 (% v/v) H_2SO_4:H_2O_2) for 1 h at 100 °C and coated with DMOAP. Cleaned gold specimen grids were placed on DMOAP-coated glass slides. The grids were filled with approximately 0.2 µL of 5CB and the excess of LC was removed with the help of syringe to produce a planar interface.

The orientational ordering of the LC films within TEM grids was determined under (Zeiss, Axio Scope. A1, Germany) polarizing microscope (serial no. 430035-9290-000) using an objective power of 200x with cross polars. Orthoscopic examinations were performed with

the source light intensity set to 50% of full illumination and the aperture set to 0.45 in order to collimate the incident light. All the images were captured using a Q-imaging camera.

5.5.3 Polarization modulation infrared reflection absorption spectroscopy (PM-IRRAS)

The gold films with thicknesses of ~ 2000 Å were deposited onto micro-pillars (array of nickel (Ni) micro-pillars electroplated on glass substrate fabricated) mounted on rotating planetaries (no preferred direction or angle of incidence) by using thermal evaporator (Excel Instruments, India). These gold-coated micro-pillars were dipped into 0.1% (v/v) DMOAP solution in DI water for 5 min at room temperature and were then rinsed with DI water to remove unreacted DMOAP from the surface (see Appendix B). The DMOAP-coated micro-pillars were dried under a stream of nitrogen gas and kept in oven at 100 ºC. Then, 5CB was dispersed onto the micro-pillars.

Deposited PLL laden 5CB films onto DMOAP supported on micro-pillars[50] coated with a uniformly deposited film of gold (~2000 Å) were examined by using PM-IRRAS. The deposited surface on a gold sample was mounted on an attachment for PM-IRRAS measurements within the PMA 50 compartment connected to the external beam port of a Bruker Tensor 27 FT-IR spectrometer. After reflection of the polarized light incident on the substrate at an angle of incidence of 82° from the surface normal, the IR beam was focused on a liquid nitrogen-cooled photovoltaic MCT detector in the PMA 50 cabinet. A photoelastic modulator (Hinds, PEM 90) was used to modulate the polarization of the light at a frequency of 84 kHz. Demodulation was performed with a lock-in-amplifier (Standford Research Systems, SR830 DSP).

Before measurements, the spectrometer was allowed for a complete purge with nitrogen for at least 30 min. Each spectrum is the sum of 100 individual spectra collected at a resolution of 4 cm^{-1} with photoelastic modulator (ZnSe, 42 kHz, AR-coated) set to 1600 cm^{-1}. Data was collected as differential reflectance ($\Delta R/R$)/absorbance versus wavenumbers. Deconvolution of PM-IRRAS spectra were carried out using the peak analyzer option (listed in the peak and baseline analysis) available in the Origin Pro version 8.5 software (see Appendix A for details).

5.5.4 Vibrational circular dichroism (VCD) and circular dichroism (CD) measurements

The VCD spectra were measured in the 1800-800 cm^{-1} range using a Bruker FT-IR spectrometer equipped with the Bruker polarization modulation accessory PMA 50. In the PMA 50 module, the light beam is focused onto the sample passing through an optical low pass filter (blocking wavenumbers >1800 cm^{-1}), a KRS-5 wire grid polarizer, and a ZnSe Photoelastic Modulator (PEM) with an oscillation frequency of 42 kHz. The light is focused by a ZnSe lens to a MCT detector. The detector signal comprises two components: a low-frequency modulation which corresponds to the IR absorption bands, i.e., the A signal, and a high-frequency modulated signal (42 kHz) corresponding to the dichroic absorptions, i.e., the ΔA signal. Additionally, the reference signal direct from the PEM (42 kHz) is mixed to the high-frequency modulated detector signal. These two high-frequency modulated signals are demodulated by an internal synchronous demodulator integrated in the electronic units of the TENSOR and VERTEX series FTIR spectrometers. The VCD spectra were recorded with 1 h data collection time at 4 cm^{-1} resolution. The sample was held in demountable cell with CaF_2 windows and a 25 μm spacer. Spectra were measured in D_2O solvent at a concentration of 10 mg/mL. For each measurement, the intensity calibration factor was obtained using a multiple-wave retardation plate combined with the second wire grid polarizer, whereby the system tuning was exactly the same as for the sample measurement. The spectra were corrected by subtracting the absorption (or VCD) of the corresponding solvent and were plotted in Origin 8 software.

The CD spectra were acquired using a Chirascan Spectrophotometer (Applied Photophysics, UK) in a 1 mm path length quartz cell with a scan range of 190–260 nm and 1 nm as step size. The spectra were corrected for the buffer signal.

5.5.5 Emulsion Preparation

The LC emulsions were formed by mixing 10 μL of E7 in 1 mL of PSS (1 mg mL^{-1}) with bath sonication for 15 minutes. The PSS-LC droplets were confirmed to exhibit bipolar configurations following sonication.

5.5.6 Fabrication of PLL-coated LC droplets using layer by layer technique

We fabricated these LC droplets with PSS and PLL polyelectrolyte multilayer by layer-by-layer (LbL) technique.[3] 5CB-PSS emulsions were first washed with millipore water thrice. The tube containing 1 mL of emulsion was agitated with a vortex mixer and then centrifuged at 5000 g for 5 min. This resulted in a pellet forming at the bottom of the tube. Approximately 0.5 mL of the supernatant was removed and replaced with water. This was repeated twice to remove excess PSS polyelectrolyte coating. After washing, the second layer of the polyelectrolyte film was then deposited by adding 1 mL of PLL solution (0.8 mg/mL) was added to 0.1 mL of the emulsion. The mixture was agitated with a vortex mixer and allowed to incubate for 15 min to allow sufficient time for PLL adsorption. After adsorption, the dispersions were centrifuged (at 5000 g, 5 min), after which the supernatant was removed and replaced by water. Washing was performed 1 time, followed by adsorption of the next polyelectrolyte. The entire process was repeated until the four bilayers of (PLL/PSS)-coated 5CB-PSS emulsions as a function of layer number, with outermost being PLL.

5.5.7 Cell based assays

5.5.7.1 Cell line and culture conditions

The human colon adenocarcinoma cell line T84 (ATCC) were maintained in Dulbecco's Modified Eagle's Medium (DMEM) supplemented with 10% (v/v) fetal bovine serum, 100 U/mL penicillin and 100 U/ml streptomycin (Invitrogen Life Technologies, Carlsbad, CA, USA) at 37 °C in a 5% CO_2 humidified incubator. Cells at a confluency of 80% were used for all the experiments.

5.5.7.2 Bright-field, polarized optical and fluorescence microscopy

Cells were seeded on sterile cover slips at a density of $0.1x10^6$ cells/ml/well in a 24-well plate and allowed to grow overnight at 37 °C. Following incubation growth medium was aspirated and replaced with 500 µL of fresh media. Further, cells in the different wells were treated with varying concentrations of PLL-coated LC droplets and incubated for 45 minutes. After incubation the excess and unbound LC droplets were removed along with the media from the

treated wells. The cover slips containing LC droplets anchored cells were put in the fresh media (DMEM) or media containing 100 μM hexadecyltrimethylammonium bromide (HTAB, company name) and then imaged using bright-field and polarized optical microscopy (Zeiss, Axio Scope. A1, Germany).

For fluorescence microscopy, calcein AM was used to stain the live cells. Before addition of the dye, the serum supplemented growth media was replaced with phosphate-buffered saline (PBS, pH 7.4) as the serum esterases can hydrolyze calcein AM resulting in augmented extracellular fluorescence. Calcien AM (5 μM in PBS) was added to the cells treated with PLL-coated LC droplets and incubated for 15 minutes at 37 °C in the dark. Following incubation, cells were washed with PBS (twice) and imaged using fluorescence microscope (Zeiss, Axio Scope. A1, Germany).

5.5.8 Biocompatibility assessment

Biocompatible potential of PLL-coated LC droplets in regard to cell viability was assessed using calcein AM and PI staining and trypan blue exclusion assay.

5.5.8.1 Flow cytometry experiment for Calcein AM and Propidium Iodide (PI) staining to assess the cytotoxicity of PLL-coated LC droplet

Cytotoxicity assessment of PLL-coated LC droplets was carried out in T84 cells. Cells were plated at a density of $1x10^6$ cells/mL/well in a 24-well plate and incubated at 37 °C for overnight. Next day varying concentrations of PLL-coated LC droplets (0, $5x10^4$/mL, $1x10^5$/mL and $2x10^5$/mL) were added at cells in different wells and incubated for 45 minutes at 37 °C. After incubation, unbound LC droplets were removed along with media and washed with PBS (twice).

Cells were then harvested using trypsin and following washing with (PBS). Cells were stained with calcein AM (10 μM) (see Appendix B) and PI (8 μM) for 15 min at room temperature. Stained cells were washed with PBS (once) and were acquired by flow cytometer BD FACSCalibur (BD Biosciences, San Jose, CA, USA). Flow cytometry analysis was performed using FlowJo (Tree Star).

5.5.8.2 Trypan blue exclusion assay

Viability of T84 cells exposed to PLL-coated LC droplets was determined by trypan blue dye exclusion assay. Briefly $1x10^6$ cells/ml were plated and treated with different concentrations (0, $1x10^5$/mL, $2x10^5$/mL and $3x10^5$/mL) of PLL-coated LC droplets and incubated for 45 minutes 37 °C. Exposed cells were harvested, washed with PBS, and mixed with equal volume of 0.25% trypan blue dye solution and incubated for 5 minutes at room temperature. 10 μL of this suspension was loaded onto a hemocytometer (Invitrogen, UK) and viable cells were counted manually. Loss in viability was expressed as percent dead cells.

5.5.9 Zeta potential measurements

A Malvern Zetasizer Nano ZS90 instrument (Malvern Instruments, Southborough, Massachusetts) was used to measure zeta potential at 25 °C for LC emulsions. The DLS instrument was operated under the following conditions: temperature: 25 °C, detector angle: 90 incident laser wavelength: 632 nm, and laser power: 4 mW. Samples prepared were loaded into a pre-rinsed zeta potential cell for measurements. Approximately 5 μL of 1 vol. % emulsions was added to 2.5 mL of millipore water. The quoted values were calculated by taking the average of 5 successive measurements.

5.5.10 Polarized and fluorescence microscopy

The PLL-coated LC droplets treated cells were examined with bright field, plane –polarized in transmission mode on a (Zeiss, Scope A1, Germany) polarizing optical microscope using an objective power of 200x and 500x. The orientation of the LC within droplets was examined with plane-polarized light in transmission mode with crossed polarizers. Cells were characterized with bright field, phase contrast and fluorescence microscopy. Fluorescence imaging was performed with (Zeiss, Axio Scope A1, Germany) fluorescence microscope equipped with a 100 W mercury lamp. The samples were viewed using a fluorescence filter cube with a 460 nm excitation filter and a 534 nm emission filter. Images were obtained with Axio cam camera.

References

(1) Brake, J. M.; Daschner, M. K.; Luk, Y.-Y.; Abbott, N. L. *Science* **2003**, *302*, 2094-2097.

(2) Price, A. D.; Schwartz, D. K. *J. Am. Chem. Soc.* **2008**, *130*, 8188−8194.

(3) Sivakumar, S.; Wark, K. L.; Gupta, J. K.; Abbott, N. L.; Caruso, F. *Adv. Funct. Mater.* **2009**, *19*, 2260−2265.

(4) Lin, I. H.; Miller, D. S.; Bertics, P. J.; Murphy, C. J.; de Pablo, J. J.; Abbott, N. L. *Science* **2011**, *332*, 1297−1300.

(5) Bai, Y.; Abbasi, R.; Wang, C.; Abbott, N. L. *Angew. Chem. Int. Ed.* **2014**, *53*, 8079-8083.

(6) Sadati, M.; Apik, A. I.; Armas-Perez, J. C.; Martinez-Gonzalez, J.; Hernandez-Ortiz, J. P.; Abbott, N. L.; de Pablo, J. J. *Adv. Funct. Mater.* **2015**, *25*, 6050–6060.

(7) Sidiq, S.; Verma, I.; Pal, S. K. *Langmuir* **2015**, *31*, 4741-4751.

(8) Shah, R. R.; Abbott, N. L. *J. Am. Chem. Soc.* **1999**, *121*, 11300-11310.

(9) Luk, Y.-Y.; Yang, K.-L.; Cadwell, K.; Abbott, N. L. *Surf. Sci.* **2004**, *570*, 43-56.

(10) Bai, Y.; Abbott, N. L. *J. Am. Chem. Soc.* **2012**, *134*, 548-558.

(11) Cadwell, K. D.; Alf, M. E.; Abbott, N. L. *J. Phys. Chem. B* **2006**, *110*, 26081-26088.

(12) Follonier, S.; Miller, W. J. W.; Abbott, N. L.; Knoesen, A. *Langmuir* **2003**, *19*, 10501-10509.

(13) Shah, R. R.; Abbott, N. L. *J. Phys. Chem. B* **2001**, *105*, 4936-4950.

(14) Gupta, V. K.; Abbott, N. L. *Langmuir* **1996**, *12*, 2587-2593.

(15) Gupta, V. K.; Abbott, N. L. *Phys. Rev. E*. **1996**, *54*, R4540-R4543.

(16) Gibbons, W. M.; Shannon, P. J.; Sun, S.-T.; Swetlin, B. J. *Nature* **1991**, *351*, 49-50.

(17) Toney, M. F.; Russell, T. P.; Logan, J. A.; Kikuchi, H.; Sands, J. M.; Kumar, S. K. *Nature* **1995**, *374*, 709-711.

(18) Gupta, V. K.; Skaife, J. J.; Dubrovsky, T. B.; Abbott, N. L. *Science* **1998**, *279*, 2077-2080.

(19) Stohr, J.; Samant, M. G.; Luning, J.; Callegari, A. C.; Chaudhari, P.; Doyle, J. P.; Lacey, J. A.; Lien, S. A.; Purushothaman, S.; Speidell, J. L. *Science* **2001**, *292*, 2299-2302.

(20) Luk, Y. Y.; Abbott, N. L. *Science* **2003**, *301*, 623-626.

(21) Clare, B. H.; Efimenko, K.; Fischer, D. A.; Genzer, J.; Abbott, N. L. *Chem. Mater.* **2006**, *18*, 2357-2363.

(22) Park, J.-S.; Abbott, N. L. *Adv. Mater.* **2008**, *20*, 1185−1190.

(23) Hartono, D.; Xue, C.-Y.; Yang, K.-L.; Lanry Yung, L.-Y. *Adv. Funct. Mater.* **2009**, *19*, 3574−3579.

(24) Tan, L. N.; Bertics, P. J.; Abbott, N. L. *Langmuir* **2011**, *27*, 1419-1429.

(25) Hu, Q. Z.; Jang, C. H. *Analyst* **2012**, *137*, 567−570.

(26) Hu, Q.-Z.; Jang, C. H. *ACS Appl. Mater. Interfaces* **2012**, *4*, 1791−1795.

(27) Tan, L. N.; Orler, V. J.; Abbott, N. L. *Langmuir* **2012**, *28*, 6364−6376.

(28) Agarwal, A.; Sidiq, S.; Setia, S.; Bukusoglu, E.; de Pablo, J. J.; Pal, S. K.; Abbott, N. L. *Small* **2013**, *9*, 2785−2792.

(29) Liu, D.; Hu, Q. Z.; Jang, C. H. *Colloids Surf. B: Biointerfaces* **2013**, *108*, 142−146.

(30) Das, D.; Sidiq, S.; Pal, S. K. *ChemPhysChem* **2015**, *16*, 753–760.

(31) Skaife, J. J.; Abbott, N. L. *Langmuir* **2000**, *16*, 3529-3536.

(32) Skaife, J. J.; Abbott, N. L. *Langmuir* **2001**, *17*, 5595-5604.

(33) Skaife, J. J.; Brake, J. M.; Abbott, N. L. *Langmuir* **2001**, *17*, 5448-5457.

(34) Luk, Y.-Y.; Tingey, M. L.; Hall, D. J.; Israel, B. A.; Murphy, C. J.; Bertics, P. J.; Abbott, N. L. *Langmuir* **2003**, *19*, 1671-1680.

(35) Luk, Y.-Y.; Tingey, M. L.; Dickson, K. A.; Raines, R. T.; Abbott, N. L. *J. Am. Chem. Soc.* **2004**, *126*, 9024-9032.

(36) Clare, B. H.; Abbott, N. L. *Langmuir* **2005**, *21*, 6451-6461.

(37) Jang, C.-H.; Tingey, M. L.; Korpi, N. L.; Wiepz, G. J.; Schiller, J. H.; Bertics, P. J.; Abbott, N. L. *J. Am. Chem. Soc.* **2005**, *127*, 8912-8913.

(38) Govindaraju, T.; Bertics, P. J.; Raines, R. T.; Abbott, N. L. *J. Am. Chem. Soc.* **2007**, *129*, 11223-11231.

(39) Luo, R.; Neu, B.; Venkatraman, S. S. *Small* **2012**, *8*, 2585-2594.

(40) Ayyappan, J. P.; Sami, H.; Rajalekshmi1, D. C.; Sivakumar, S.; Abraham, A. *Chem. Biol. Drug Des.* **2014**, *84*, 292–299.

(41) Manna, U.; Zayas-Gonzalez, Y. M.; Carlton, R. J.; Caruso, F.; Abbott, N. L.; Lynn, D. M. *Angew. Chem. Int. Ed.* **2013**, *52*, 14011–14015.

(42) Frey, B. L.; Corn, R. M.; Weibel, S. C. Polarization−Modulation Approaches to Reflection−Absorbtion Spectroscopy. In Handbook of Vibrational Spectroscopy; Chalmers, J., Griffins, P. R., Eds.; John Wiley & Sons: Chichester, U.K., **2006**.

(43) Keiderling, T. A. *Nature* **1986**, *322*, 851-852.

(44) Frey, B. L.; Corn, R. M. *Anal. Chem*. **1996**, *68*, 3187-3193.

(45) Rozenberg, M.; Shoham, G. *Biophys. Chem.* **2007**, *125*, 166-171.

(46) Rozenberg, M. 1.; Shoham, G.; Reva, I.; Fausto, R. *Phys. Chem. Chem. Phys.* **2005**, *7*, 2376-2383.

(47) Dos, A.; Schimming, V.; Tosoni, S.; Limbach, H.-H. *J. Phys. Chem. B* **2008**, *112*, 15604–15615.

(48) Inácio, Â. S; Costa, G. N.; Domingues, N. S.; Santos, M. S.; Moreno, A. J. M.; Vaz, W. L. C.; Vieira, O. V. *Antimicrob. Agents Chemother.* **2013**, *57*, 2631–2639.

(49) Blankenberg, F. G. *J. Nucl. Med.* **2008**, *49*, 81S-95S.

(50) Cheng, D.; Sridharamurthy, S. S.; Hunter, J. T.; Park, J.-S.; Abbott, N. L.; Jiang, H. *J. Microelectromech. Syst.* **2009**, *18*, 973–982.

Chapter 6

PLL-coated LC droplets as a Template for Selective and Sensitive Detection of Heparin and Protamine

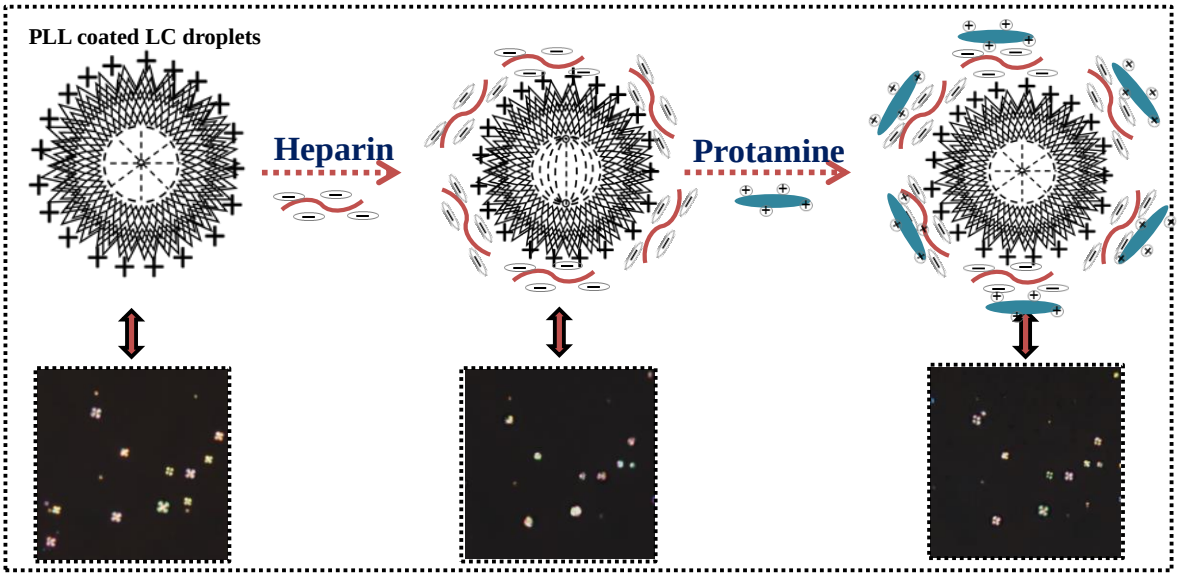

The PLL modified LC emulsion droplets can act as a potential tool for sensitive and selective detection of heparin and protamine for laboratory and bedside diagnosis.

6.1 Introduction

Heparin and protamine are the two important poly-ionic drugs in biological systems which are widely used in surgical procedures.[1-4] Heparin is the most charge dense naturally occurring mainly in the lungs, intestine and liver of a variety of mammals. Heparin is richly found intracellularly in mucosal mast cells, connective tissue mast cells and basophilic leukocytes.[5] Based on the structural features, heparin is an anionic rod-like polysaccharide (copolymer of uronic/iduronic acids alternating with sulfated glucosamine residues) with an average molecular weight of approximately 15 kDa[6] as shown in Figure 6.1. The high content of negatively charged sulfo and carboxyl groups endows heparin with the highest negative charge density of any known biological macromolecule.[7] Heparin can play a vital role in biological systems and interacts with a wide range of protein targets.[7,8] Heparin binds to the small protein anti-thrombin which is an inhibitor for thrombin and as a consequence, is responsible for preventing blood clotting cascade.[2,9,10]

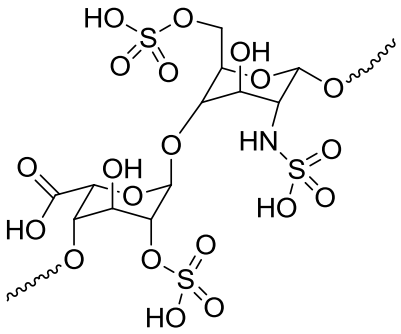

Heparin

Figure 6.1 Chemical structure of heparin.

Clinically, heparin has been widely used as an anticoagulant during cardiovascular surgery or used to avoid thrombosis.[11] Although anticoagulation is the major pharmacological activity, heparin has many other functions. Heparin inhibits the proliferation of vascular smooth muscle cells and renal mesengial cells,[12] suppresses the delayed-type hyper sensitivity[13] and inhibits angiogenes.[14] Other pharmacological functions of heparin include antithrombotic effect,[15] antibacterial,[16] antivirus[17] and antitumor angiogenesis, particularly in combination

with cortisone.[18] As a result of its clinical importance, monitoring the heparin concentration in plasma during the surgery and the anticoagulant therapy is of crucial significance. For example, heparin overdose can induce some complications like hemorrhages and heparin-induced thrombocytopenia.[19]

In contrast, protamines are the family of small arginine-rich cationic proteins extracted from salmon roe. Protamine has a low molecular weight (ca. 4500 Da) and 20 positive charges (with an isoelectric point of 13.8 pH) in physiological condition for its high content of basic arginine residues.[20-22] The chemical structure of protamine is shown in Figure 6.2. The guanidinium groups of protamine can bind to heparin specifically by electrostatic attraction to form a stable ion pair complex. Due to strong binding of protamine to heparin, it displaces anti-thrombin from heparin–anti-thrombin complex thus reverses the anticoagulant effects of heparin.[23] Therefore, it acts an antidote for heparin to overcome the risk of heparin-induced bleeding.[1] Besides, it also has the ability to prolong the insulin release in diabetes mellitus therapy.[24]

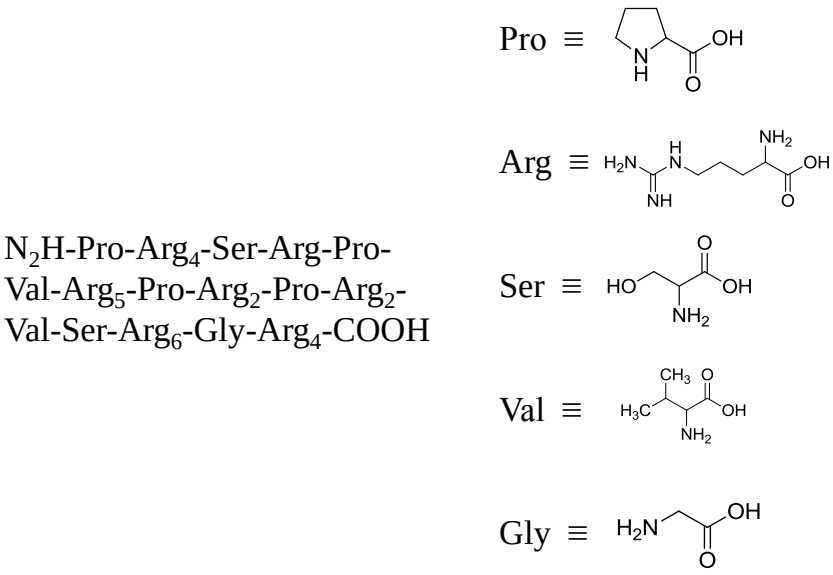

Figure 6.2 Chemical structure of protamine.

As a result of the biomedical importance of these heparin and protamine poly-ionic drugs especially during clinical procedures, there has been a surge of interest in developing a sensing methodology which is selective and operates under biological conditions. To date, a

wide range of methods has been reported for heparin and heparin-protamine sensing. For example, Egawa *et al.* report a fluorescent determination of heparin based on self-quenching of fluorescein-labeled protamine.[25] Moreover, Smith's group recently reported the facile synthesis of cationic dye, mallard blue which exhibits high affinity for heparin.[26] Chem *et al.* developed a fluorescence turn-on method for detection of protamine and heparin by making use of aggregation-induced emission enhancement of silole (silacyclopentadiene) molecules.[27] Further, tripodal boronic acid,[28,29] heparin specific peptide,[30] fluorescent copolymers with binding sites tailored for sulfated sugars[31] or polycationic calix[8]arenes,[32] benzimidazolium dyes[33] and polymethinium salts[34] have also been reported for heparin sensing. In addition, Wang's group designed a surface-enhanced Raman scattering (SERS) platform for the detection of heparin based on anti-aggregation of 4-mercaptopyridine functionalized silver nanoparticles.[35] A robust reversed-phase high-performance liquid chromatography method was also developed to quantify protamine sulfate.[36] But, sensitive sensors for heparin and protamine which can be easily accessible and can be used for direct monitoring of heparin and protamine in biological conditions (i.e., human serum), still remain rare. Therefore, development of simple and reliable method for heparin and protamine detection has attracted immense interest. Herein, we report a sensitive, rapid and simple label free sensor based on poly-L-lysine (PLL) coated liquid crystal (LC) micro-droplets for heparin and protamine detection at aqueous interfaces.

LC micro-droplets dispersed in aqueous solution are emerging as a new class of biosensors for the detection of interfacial interactions of chemicals or biomolecules in biological systems due to their large surface areas, tunable surface properties and well-defined director configurations.[37-48] The director configuration of LC micro-droplets is highly sensitive to the interfacial interactions. It has been shown that LC droplets typically exhibit either a radial or bipolar director configurations in response to external stimuli. In recent studies, LC droplet-based sensors have been used to detect and differentiate between types of bacteria and viruses,[47] to report immunoassays,[37] endotoxin at ppm level,[44] KB cancer cells,[48] lithocholic acid[40] and many more.[49-51] Though the interfacial interactions of LC materials have been made specific to bind antibodies, bacteria and viruses by using specific ligands but, there is

no report for the detection of heparin and protamine using E7 LC micro-droplets emulsion that has been prepared using PLL multilayer.

6.2 Objective

The study is motivated by the use of PLL-decorated LC capsules for sensitive and selective detection of heparin and protamine for laboratory and bedside diagnosis. Inspired by this, we sought to design (E7) LC droplets dispersed in aqueous solution using PLL at the E7-water interface that would be responsive in the presence of the heparin and protamine. The approach involves PLL because of two reasons. (1) As reported in our earlier study (Chapter 5), PLL provide a dynamic LC response and provide the possibility of using free-floating biocompatible LC droplets through PLL-LC interactions for communicate and interact to a diverse range of targets in biological environment. (2) PLL, a poly-cationic isopolypeptide, is known to have high affinity for poly-ionic drug heparin through electrostatic attraction.[52] The advantage of using PLL as the recognition molecules to decorate the LC micro-droplets acts as mediator to induce configurational transitions in LC micro-droplets for the detection of heparin and protamine.

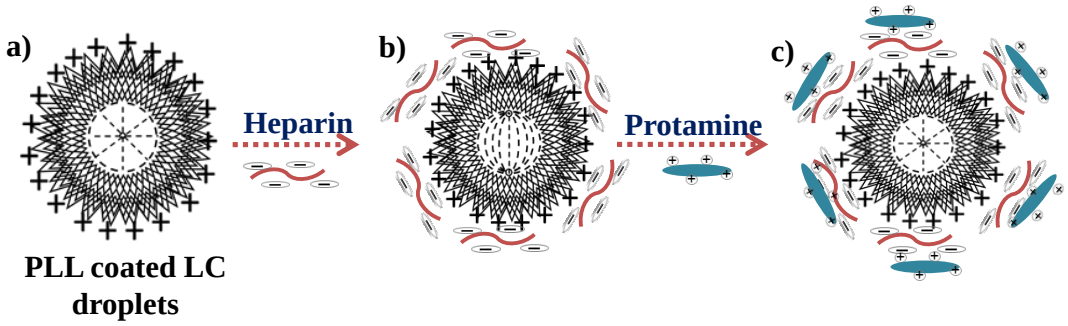

Scheme 6.1 Schematic illustration of the orientation of the LC droplets coupled to the addition of heparin and protamine onto the positively charged PLL-coated LC droplet surface: a) Director profile of PLL-coated LC droplets, leading to radial (homeotropic) anchoring, b) the PLL-coated LC droplets exposed to heparin leading to bipolar (planar) anchoring and then, c) heparin adsorbed PLL-coated LC droplets exposed to protamine leading to radial (homeotropic) anchoring of LC droplets.

A key finding in this study is that the poly-anionic heparin molecules adsorb on positively charged PLL-coated LC droplets *via* electrostatic interactions trigger a LC configurational change from radial to bipolar within LC droplets using polarized light. This study also provides selective heparin binding over PLL-coated LC droplets in competitive conditions. Further, this study demonstrates that protamine addition to the heparin adsorbed PLL-coated LC droplets cause a reordering of the LCs due to the stronger affinity of heparin to protamine. A schematic representation of the anchoring transitions of the PLL-coated LC droplets in the presence of heparin and protamine is shown in Scheme 6.1.

6.3 Results and Discussion

6.3.1 Optical behavior of PLL-coated LC droplets in response to heparin

Our first experiments employed the preparation of PLL-coated LC droplets. The approach involves the adsorption of poly(styrene sulfonate) (PSS) and PLL on LC droplets *via* layer by layer technique. The chemical structures of PSS and PLL are shown in Figure 6.3. The PSS is negatively charged polyelectrolyte and PLL is a positively charged polyelectrolyte. The E7 droplets are formed by sonication in deionized water at pH 7.4 in the presence of PSS. The adsorption of negatively charged PSS at the E7-water interface stabilizes the E7 droplets in deionized water and exhibited a bipolar configuration with two point defects at opposite poles of the droplet surface.

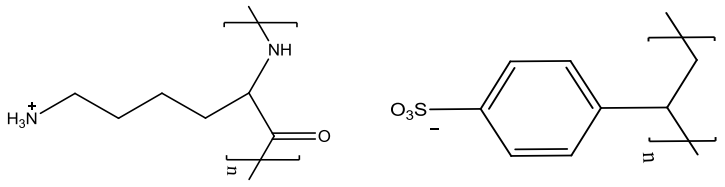

PLL **PSS**

Figure 6.3 Chemical structure of Poly-*L*-Lysine (PLL) and polystyrene sulfonate (PSS).

Next, we prepared films composed of four PSS/PLL bilayers on LC droplets with outermost layer being PLL. The adsorption of positively charged PLL exhibited a radial configuration as characterized by a single point defect (cross-like appearance) at the center of the droplet (see chapter 5, Figure 5.6). Figure 6.4a shows a polarizing optical micrograph of PLL-coated

E7 droplets in deionized water at pH 7.4. The corresponding bright-field micrograph (Figure 6.4b) consistent with the homeotropic anchoring of the LC at PLL laden LC-aqueous interface as characterized by a single point defect at the center of the droplet. Next, the PLL-coated LC droplets were exploited to study the detection of heparin. For this, PLL-coated LC droplets were exposed with 50 µM of heparin solution at pH 7.4 for 10 min.

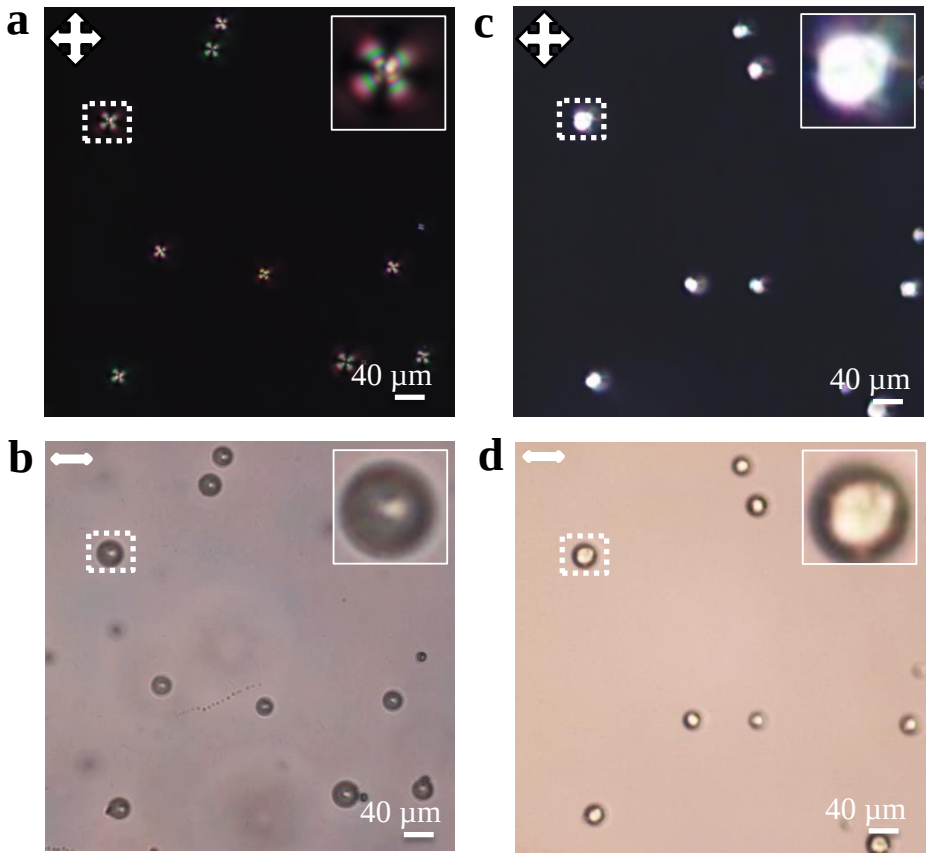

Figure 6.4 Polarized optical and bright-field micrographs images of PLL-coated LC droplets: (a,b) suspended in Tris buffer and (c, d) corresponding polarized and bright-field micrographs of PLL-coated LC droplets in contact with heparin. The LC droplets were in radial states (a) before but transitioned to bipolar state (c) after addition of heparin. The insets show the magnified version of selected LC droplet.

The polarized and bright field micrographs of PLL-coated LC droplets in Tris buffer at pH 7.4 after adsorption of heparin are shown in Figure 6.4c and 6.4d, respectively, demonstrating a radial-to-bipolar configuration transition of E7 inside the droplets. Since,

heparin is a negatively charged protein it adsorbs on the surface of positively charged PLL-coated LC droplets likely through the electrostatic interaction and is responsible for this configurational transition of these LC droplets.

6.3.2 Characterization of heparin adsorption on PLL-coated LC droplets

To confirm the adsorption of heparin-triggered configuration transition of the E7 inside the PLL-coated LC droplets, we carried out fluorescence microscopy studies and zeta potential measurements. For fluorescent microscopy studies, PLL-coated LC droplets were incubated with 0.1mg/mL fluorescent (fluorescein isothiocyanate) heparin in Tris buffer at pH 7 for 30 min. The epi-fluorescence micrograph and its bright field image after the addition of fluorescent heparin to PLL-coated LC droplets were shown in Figure 6.5a and 6.5b. Inspection of epi-fluorescence micrograph (Figure 6.5a) of the heparin adsorbed PLL-coated E7 droplets shows strong fluorescence confirming the adsorption of fluorescent heparin on PLL-coated LC droplets. Also, the bright field micrograph (Figure 6.5b) confirms the bipolar configuration of PLL-coated droplets after addition of heparin. This result suggests that the adsorption of heparin on the PLL-coated LC droplets is responsible for the radial to bipolar configurational transition within the LC droplets. The zeta potential was measured positive (40.13 mV) for PLL-coated LC droplets and negative (-41.43 mV) for heparin adsorbed PLL-coated LC droplets as shown in Figure 6.5c. The drop of zeta potential of PLL-coated LC droplets from 40.13 mV to -41.43 mV after addition of heparin further suggesting the adsorption of negatively charged heparin on the positively charged PLL-coated LC droplets. Thus, the heparin-induced radial-to-bipolar transition of the E7 LC in the PLL-coated droplets allows us to rapidly detect the heparin concentration in aqueous solution with a polarizing optical microscope.

We find that the concentration of heparin required to trigger the configuration transition of PLL-coated LC droplets depends on the number of droplets and also on the number of the layers of PSS/PLL on LC droplets. However, the percentage of PLL-coated E7 droplets changed from radial to bipolar configuration increases rapidly as the function of heparin concentration.

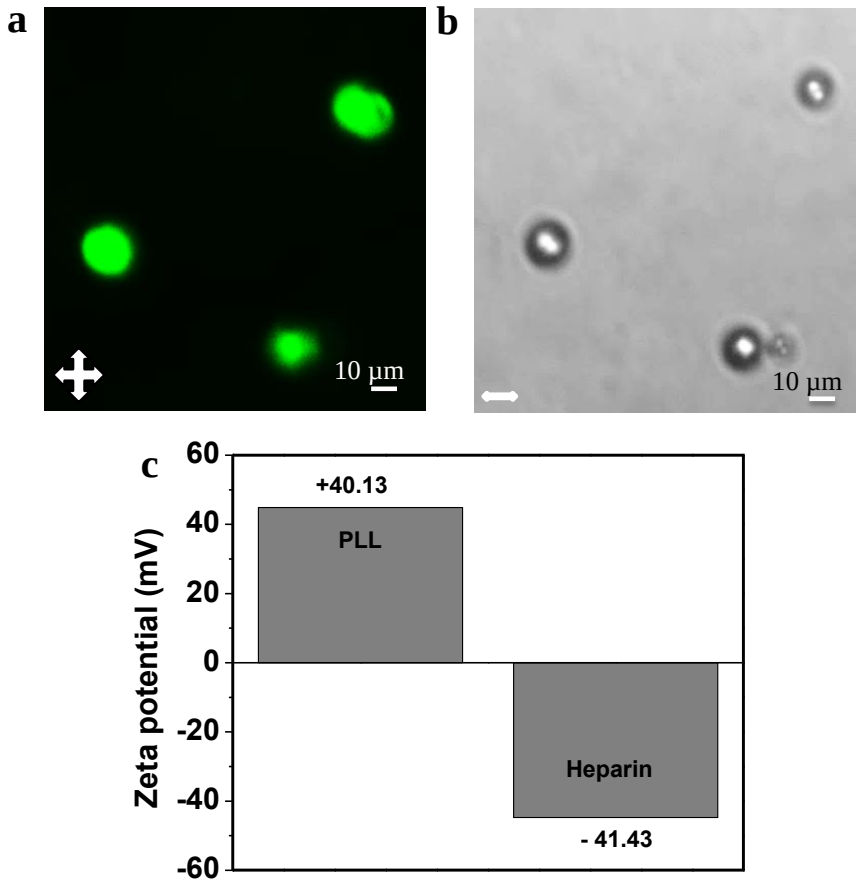

Figure 6.5 Epi-fluorescence microscopic images of PLL-coated LC droplets after (a) adsorption of fluorescent heparin and its (b) corresponding bright field image. (c) Zeta potential of PLL-coated droplets showing the absorption of negatively charged heparin over positively charged PLL-coated LC droplets on changing the zeta-potential from positive (40.13 mV) to negative (-41.43 mV).

However, the detection limit of PLL-coated E7 droplets for heparin rapidly drops to 5 µM when the number of droplets is reduced. The droplets concentration used was close to 4.2 x 10^4 mL^{-1}.The total number of PLL-coated E7 droplets used in the detection of heparin was estimated by putting a drop of a known dilution of PLL-coated E7 droplet solution on a glass slide. Then, a series of optical microscopy images were taken to ensure the whole sample was represented. From these micrographs the number of PLL-coated E7 droplets was carefully counted. The further reduction in the detection limit of PLL-coated E7 droplets for heparin rapidly drops to 5 µM to 0.5 µM when the bilayers of PEMs is reduced from 4 to 1,

in which the total number of droplets is kept the same (~4.2 x 10^4 mL^{-1}). By controlling these factors we reached up to 50 nM detection limit of PLL-coated E7 droplets for heparin. During cardiovascular surgery the recommended therapeutic dosing level of heparin is 2-8 U/mL (17-67 μM) while 0.2-1.2 U/mL (1.7-10 μM) is required in case of postoperative and long term care.[53] From these results, we conclude that the detection limit of PLL-coated E7 droplets for heparin were much lower than the clinical demanded concentration of heparin.

6.3.3 Selectivity

Our next goal was to determine the selectivity which is the greatest challenges for any heparin sensor operating in biological media. Since heparin coexists with other glycosaminoglycams in biological fluids, the presence of other electrolytes and polyanions may also interfere in the detection of PLL-coated LC droplets for heparin. The glycosaminoglycams are the potential competitors for heparin binding due to their similar structure. For this study, heparin sulfate (HS) and chondroitin sulfate (CS) were selected to probe their binding interactions for PLL-coated LC droplets relative to heparin and hence determine the degree of selectivity. The chemical structure of heparin, CS and HS are shown in Figure 6.6.

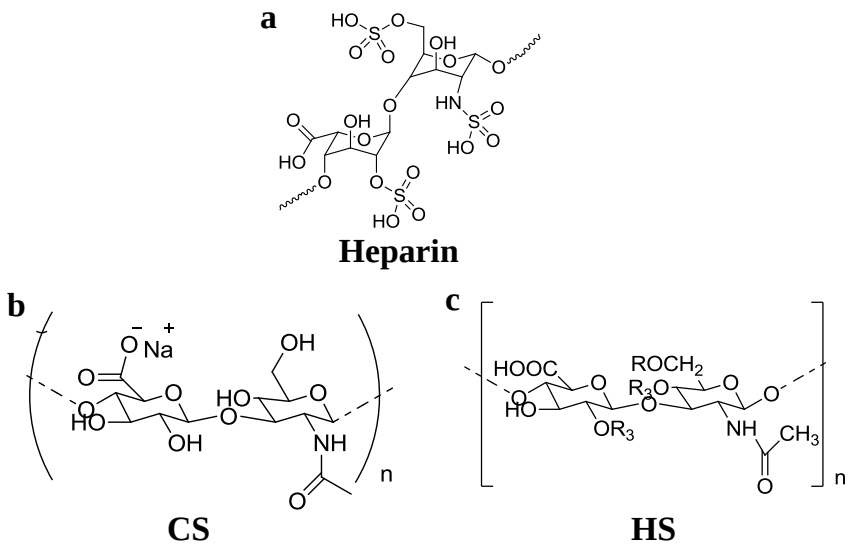

Figure 6.6 Chemical structure of a) heparin, b) chondroitin sulfate (CS) and c) heparin sulfate (HS).

Like heparin, both HS and CS are able to trigger a radial-to-bipolar transition of LC inside the PLL-coated LC droplets. However, PLL-coated LC droplets are less sensitive to HS and CS, compared to heparin. The PLL coated LC droplets with four bilayers were exposed to HS and CS solutions with concentrations up to 5 μM.

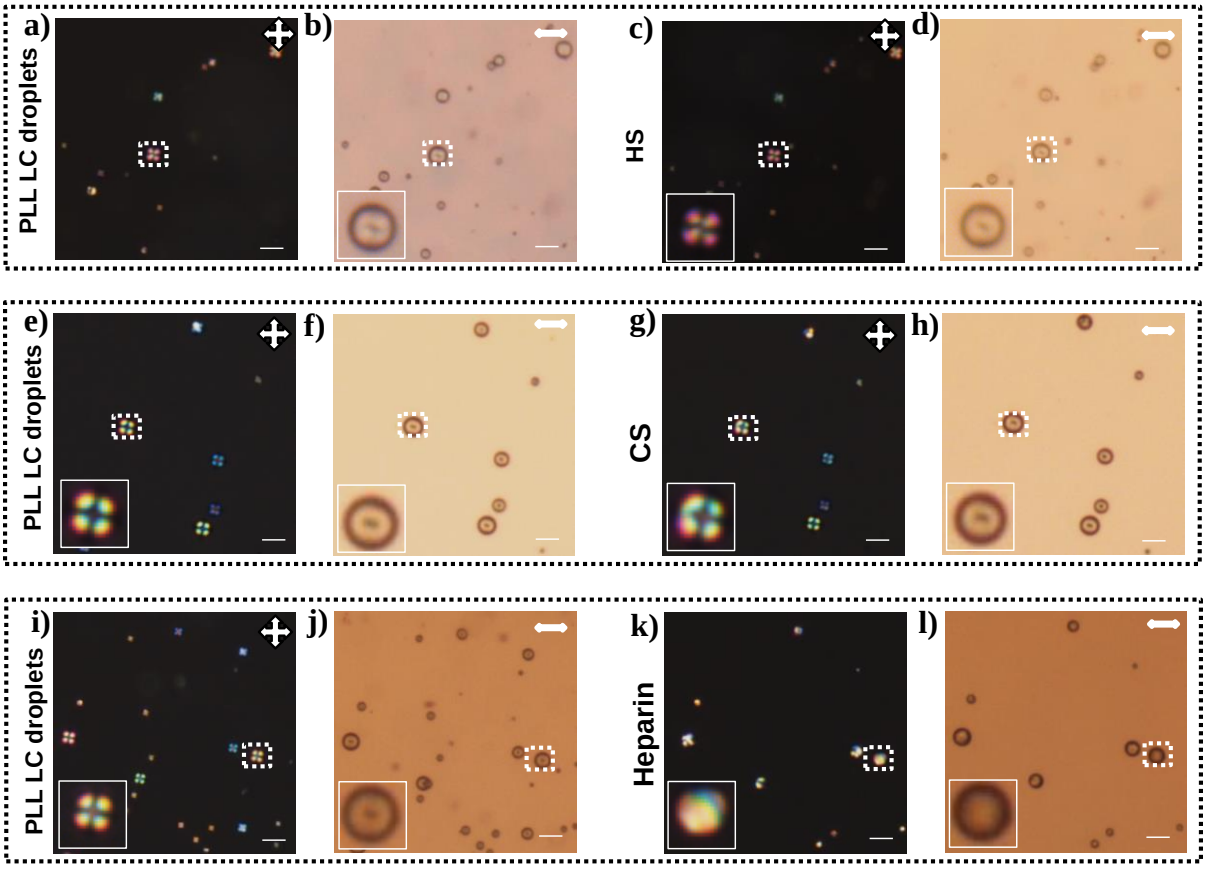

Figure 6.7 (a,b) Polarized and bright-field optical microscopic images of PLL-coated LC droplets and (c,d) corresponding images after coating of these capsules with heparin sulfate (HS). (e,f) Polarized and bright-field optical microscopic images of PLL-coated LC droplets and (g,h) corresponding images after coating of these capsules with chondroitin sulfate (CS). (i,j) Polarized and bright-field optical microscopic images of PLL-coated LC droplets and (k,l) corresponding images after coating of these capsules with heparin. The insets show the magnified version of selected LC droplet. Scale bar = 40 μm.

Inspection of optical polarized micrographs (Figure 6.7a,c and 6.7e,g) and their bright field images (Figure 6.7b, d and 6.7f, h) of PLL-coated LC droplets before and after addition of

HS and CS, respectively, show no configuration transition of LC droplets. In contrast, we find that heparin is able to induce the configuration transition of PLL-coated LC droplets at this particular concentration (Figure 6.7i-l). This may be either a consequence of heparin containing sulfate groups or, more likely, the overall greater anionic charge density of heparin compared to HS and CS. Therefore, this study indicates that PLL-coated LC droplets act as a selective sensor for heparin over potentially competitive glycosaminoglycams (HS and CS).

6.3.4 Optical detection of protamine on heparin adsorbed PLL-coated LC droplets

Next, we sought to determine whether heparin adsorbed PLL-coated LC droplets can be further exploited for the detection of protamine. Protamine is a positively charged peptide showing high affinity for heparin and can be used to sequester heparin and release anti-thrombin.

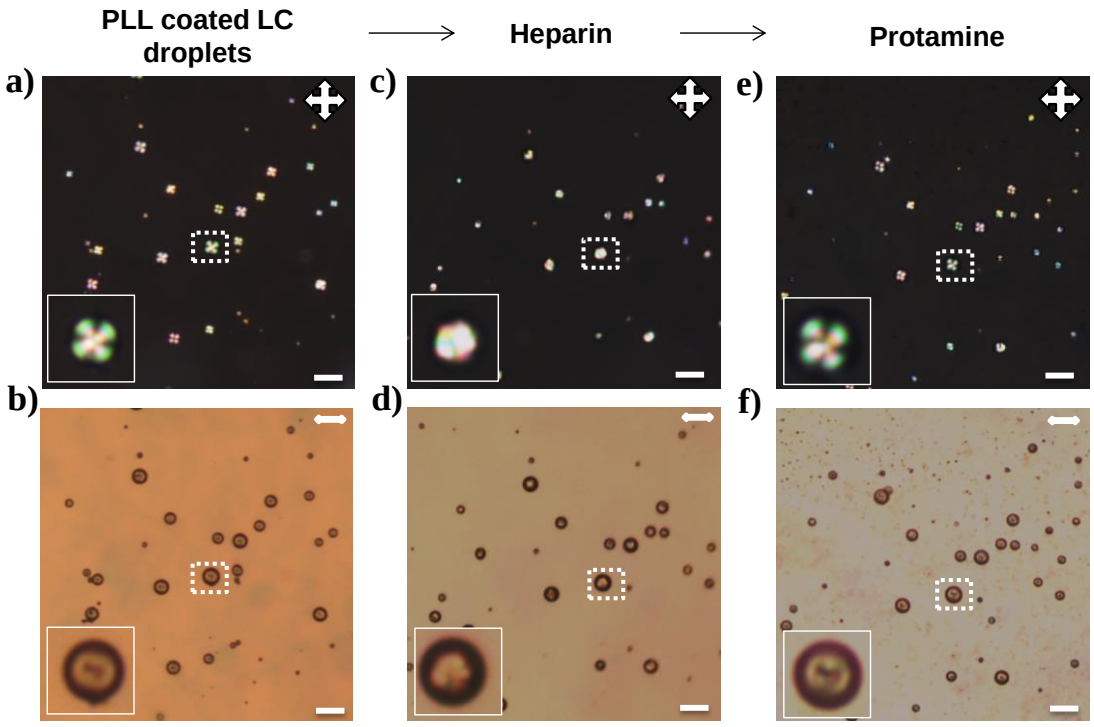

Figure 6.8 (a,b) Polarized and bright-field optical microscopic images of PLL-coated LC droplets and (c,d) corresponding images after coating of these capsules with heparin and (e,f) after addition of protamine to these heparin adsorbed PLL-coated LC droplets. The insets show the magnified version of selected LC droplet. Scale bar = 40 µm.

It is expected that the configurational transition of heparin adsorbed PLL-coated LC droplets would occur after addition of protamine, since protamine can strongly bind with heparin to weaken the interaction of heparin with PLL (see scheme 6.1). This is indeed in agreement with the experimental findings as shown in Figure 6.8. Figure 6.8a,b and 6.8c,d show the polarized and bright field micrographs of PLL-coated LC droplets before and after addition of 5 μM heparin. Then, these heparin adsorbed bipolar PLL-coated LC droplets were exposed with 0.1 mg/mL protamine solution in Tris buffer at pH 7.4. Inspection of polarized (Figure 6.8c, e) and bright field (Figure 6.8d, f) micrographs reveal that configurational transition of heparin adsorbed PLL-coated LC droplets changes from bipolar to radial after addition of protamine. Since, protamine is a positively charged protein, it adsorbs on the surface of negatively charged heparin adsorbed PLL-coated LC droplets, likely, through the electrostatic interaction and is responsible for the ordering transition within LC droplets. The adsorption of protamine on heparin adsorbed PLL-coated LC droplets was confirmed using zeta potential measurements. The zeta potential was measured negative (-41.43 mV) for heparin adsorbed PLL-coated LC droplets and positive (18.80 mV) after addition of protamine as shown in Figure 6.9a.

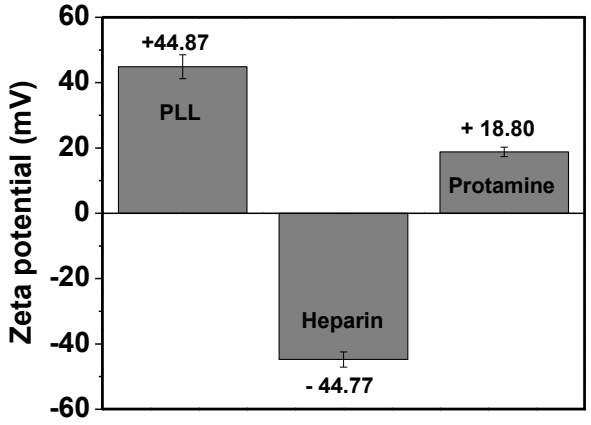

Figure 6.9 Zeta potential of PLL-coated LC droplets showing the absorption of positively charged protamine over negatively charged heparin adsorbed on positively charged PLL-coated LC droplets. The zeta potential changing from positive (40.13 mV) for PLL-coated LC droplets to negative (-41.43 mV) after heparin adsorption and then to positive (18.80 mV) after protamine addition.

The variation of zeta potential of heparin adsorbed PLL-coated LC droplets from -41.43 mV to 18.80 mV after addition of protamine further suggesting the adsorption of positively charged protamine on the negatively charged heparin adsorbed PLL-coated LC droplets.

To provide further insight whether the ordering transition within the LC droplets is due to heparin-protamine binding, we performed two additional control experiments. First, we determine the direct interaction of protamine with LC. For this, we prepared E7 droplets by sonication in deionized water at pH 7.4. The bare E7 droplets in aqueous media exhibited a bipolar configuration with two point defects at opposite poles of the droplet surface as characterized by using polarized optical microscopy under crossed polars (Figure 6.10a) and bright field observation (Figure 6.10b).

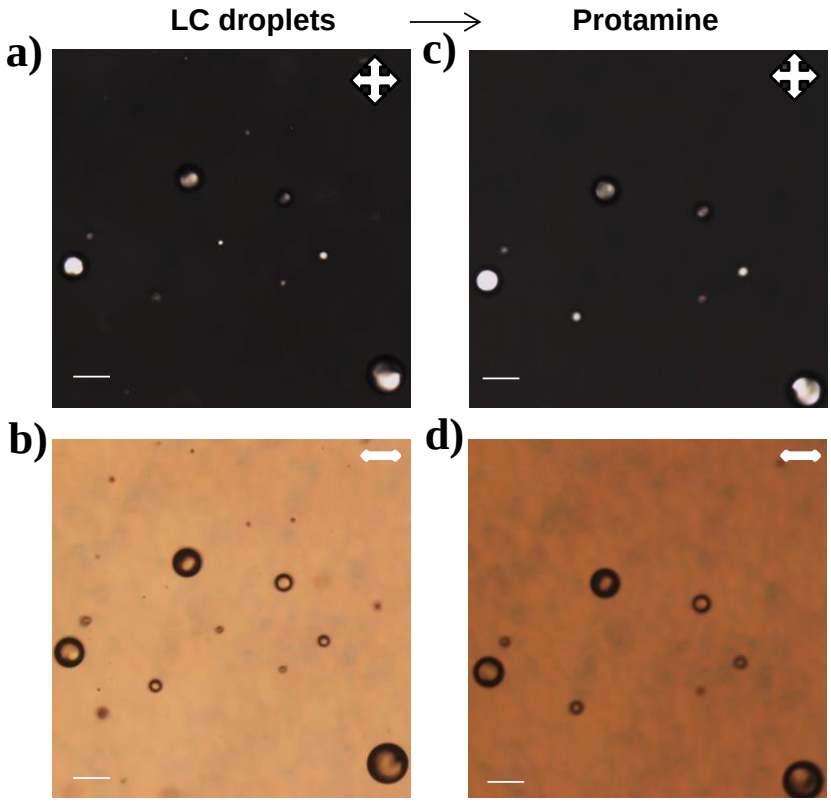

Figure 6.10 (a,b) Polarized and bright-field optical microscopic images E7 LC droplets in aqueous solution and (c,d) corresponding images after addition of protamine. Scale bar = 40 µm.

However, after the exposure of E7 LC droplets to protamine solution, we find that there occurs no change in the director configuration of the E7 LC droplets (Figure 6.10c,d), reflecting no interaction of protamine with E7.

Second, we have performed another control experiment to determine the specificity of heparin for the configurational change of PLL-coated LC droplets (Figure 6.11a,b) in response to protamine. For this, we have used BSA, a negatively charged protein instead of heparin for the detection of protamine. Figure 6.11 represents the polarized optical micrographs under crossed polars (Figure 6.11c) and bright field micrographs (Figure 6.11d) of PLL-coated LC droplets after exposure to an aqueous solution of 0.1mg/mL BSA solution at pH 7.4.

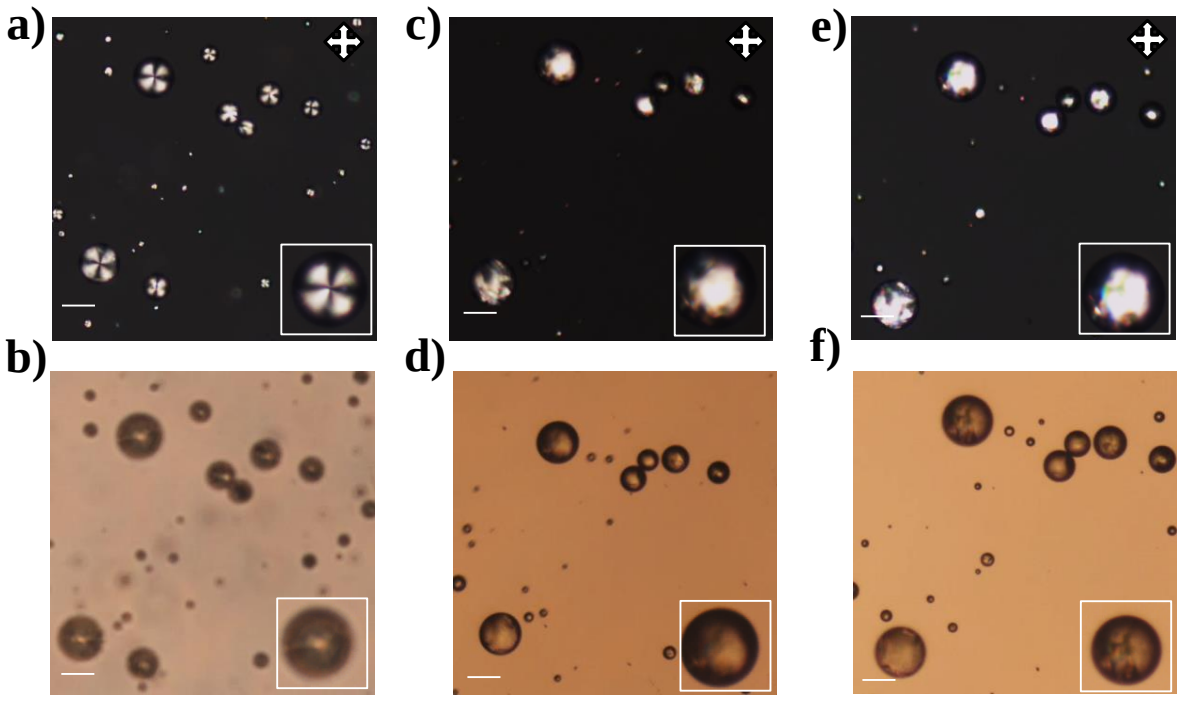

Figure 6.11 (a,b) Polarized and bright-field optical microscopic images of PLL-coated LC droplets and (c,d) corresponding images after coating of these capsules with BSA and (e,f) after addition of protamine to these BSA adsorbed PLL-coated LC droplets. The insets show the magnified version of selected LC droplet. Scale bar = 40μm.

This results reveal that adsorption of BSA on PLL-coated LC droplets induces radial to bipolar configurational transition of LC droplets. Since, BSA is a negatively charged protein, adsorbs on the surface of positively charged PLL-coated LC droplets (similar to heparin adsorption) likely through the electrostatic interaction and is responsible for this configurational transition of these LC droplets. Then, protamine of 0.1mg/mL was added to the BSA adsorbed PLL-coated droplets as shown in Figure 6.11e,f. The polarized (Figure 6.11e) and bright field micrographs (Figure 6.11f) of BSA adsorbed PLL-coated LC droplets demonstrate that the director profile of BSA adsorbed PLL-coated LC droplets remains unchanged after addition of protamine. Thus, no adsorption of protamine occurs on the BSA adsorbed PLL-coated LC droplets due to which LC droplets were unable to show the ordering transition. These results confirm that the configurational transition of heparin adsorbed PLL-coated LC droplets after addition of protamine occurs due to the specific heparin-protamine binding on the surface of the LC droplets.

6.3.5 Mechanistic insight into PLL-coated LC droplet-based detection of heparin protamine interactions

We have performed several experiments regarding the possible origin of this preferential orientation of PLL-coated LC droplets in presence of heparin and protamine. First, we have performed circular dichroism (CD) experiments to confirm the conformations of PLL in response to heparin and protamine. It is reported that heparin changes the random coil conformation of PLL to α-helical at neutral pH which is attributed to the charge neutralization on the basic polypeptides. Figure 6.12 shows the CD spectra of PLL, PLL-heparin and PLL-heparin-protamine aqueous solutions. The CD spectra show that the PLL is in random coil conformation but, after addition of heparin the conformation of PLL changed to helical one. Next, we added protamine to the PLL-heparin complex. The addition of protamine precipitates the PLL–heparin solution. This observation has also been found when we have added protamine to heparin adsorbed PLL-coated LC droplets. Thus, CD experiment of supernatant has been performed after centrifuging protamine-heparin PLL solution. The CD spectrum was observed to be similar to random coil but the ellipticity decreases to a large extent. The CD spectra of heparin and protamine are shown in Figure 6.13. From these results, we speculate that the addition of protamine might result in protamine-heparin

complex which results in precipitation and some of the PLL likely gets free from heparin which shows random coil conformation. Prior studies report that both PLL and protamine can result nanoparticle formation with heparin but depending upon the concentration, the size of the nanoparticle varies. Also, the interaction of heparin with PLL is stronger as compared to protamine. Therefore, in order to show the interaction of heparin with protamine on PLL-coated surfaces, concentration of protamine has to be increased. Interestingly, this observation is consistent with what we have observed in POM experiments for protamine detection. To show the presence of protamine on heparin-coated PLL-LC droplets through configurational transition of LC droplets, higher concentration of protamine than heparin is required.

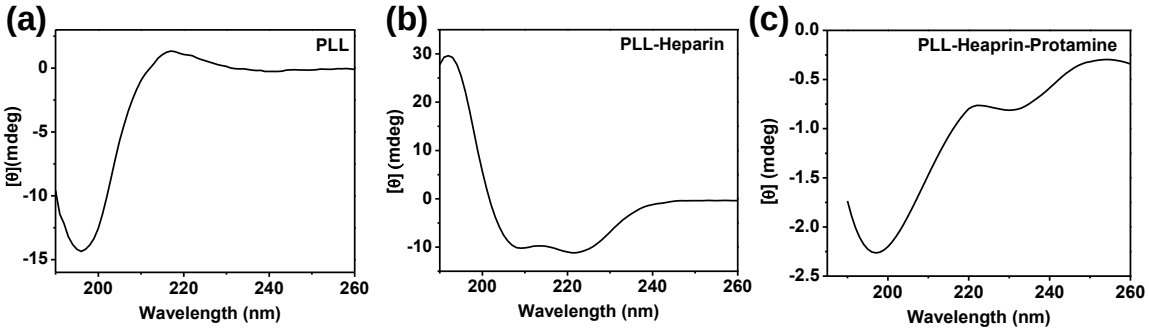

Figure 6.12 Conformational change of PLL (0.15 mg/mL) aqueous solution in presence of heparin and protamine. Circular dichroism of PLL (a) PLL-heparin solution (b) and supernatant of PLL-heparin-protamine solution.

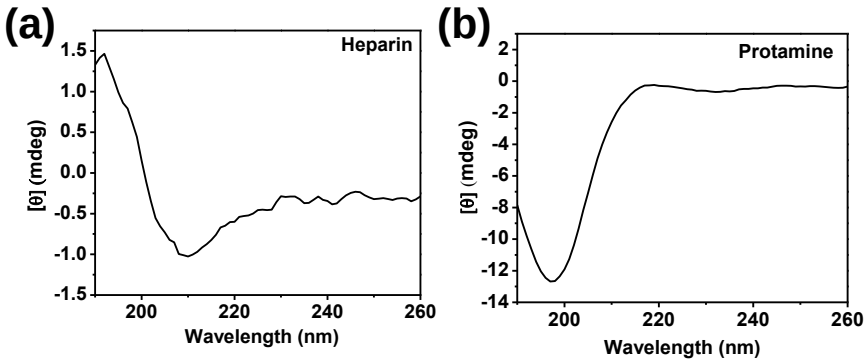

Figure 6.13 (a,b) Circular dichroism of heparin and protamine solution, respectively.

Besides CD, we have also further elucidated the conformations of PLL in presence of heparin and protamine using vibrational circular dichroism (VCD) measurements. Figure 6.14 shows the VCD spectra of PLL, heparin-PLL and protamine-heparin-PLL solution in D_2O. As a control, we have performed VCD spectra of heparin and protamine. It has been observed from Figure 6.14 that the amide I VCD spectrum for PLL (in D_2O at pH 7) exhibits VCD couplets at about 1650 cm^{-1}. This corresponds to the random coil conformation[55] amide stretch consistent with the observed CD spectrum of the PLL as shown in Figure 6.12a. In addition to heparin, the VCD couplets at about 1650 cm^{-1} reverses its direction corresponding to the α-helix conformation of PLL. Interestingly, the VCD couplets at about 1650 cm^{-1} has found to be in positive direction again for protamine-heparin PLL supernatant solution corresponding to random coil conformation.

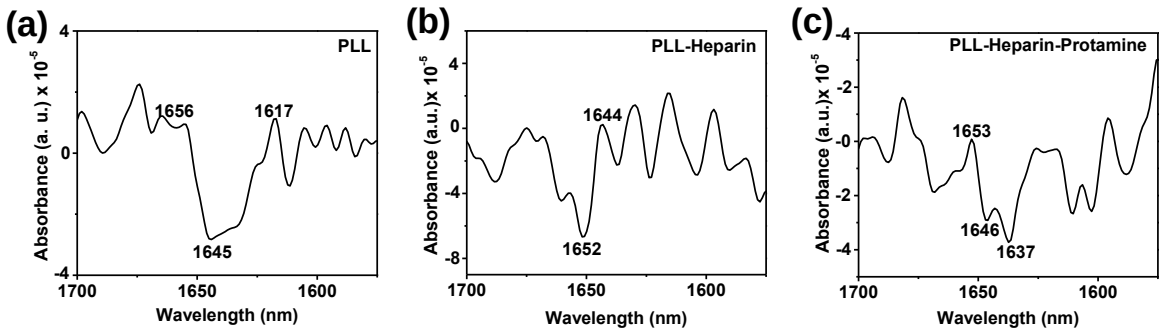

Figure 6.14 Conformational change of PLL (0.15 mg/mL) aqueous solution in presence of heparin and protamine. Vibrational circular dichroism of PLL (a), PLL-heparin solution (b) and supernatant of PLL-heparin-protamine solution.

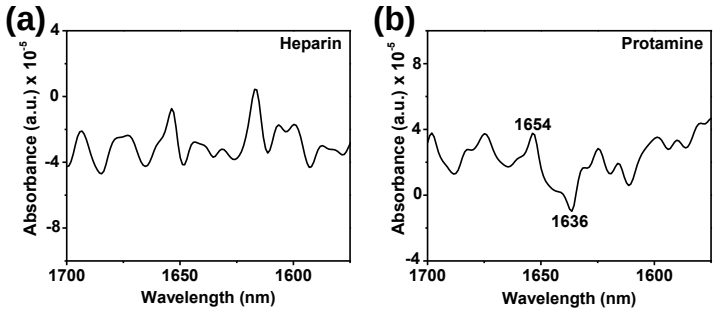

Figure 6.15 (a,b) Vibrational circular dichroism of heparin and protamine solution, respectively.

These experiments are in consistent with the observed CD spectrum of the PLL as shown in Figure 6.12 confirming that the PLL undergoes conformational changes in presence of poly-ionic drugs (heparin and protamine).

Next, we sought to determine the conformational changes of PLL at LC-aqueous interfaces in response to heparin and protamine. This would provide additional attribute towards mechanism of detection of poly-ionic drugs induced configurational transition of PLL-coated LC droplets. For this, we have performed PM-IRRAS measurements using PLL laden 5CB gold-coated surfaces and sought to determine any significant change in the observed spectrum in presence of heparin and protamine at these LC-aqueous interfaces (see experimental section for details). For PM-IRRAS, first we functionalized gold coated micro-pillars (2–4 μm) with DMOAP. Next, we poured the 5CB into the DMOAP coated micro-pillars. Then, we immersed the 5CB films on DMOAP coated micro-pillars in an aqueous solution of PLL for 4 h at room temperature and dried under vacuum. Figure 6.16a shows the PM-IRRAS spectrum of the PLL laden 5CB films. We have observed the appearance of bands corresponding to PLL adsorption on 5CB films. Based on the examination of spectrum, we assign the peaks at 1654cm^{-1} and 1558 cm^{-1} to amide I and amide II bands of PLL. In addition, we observed a peak at (1603 cm^{-1}) corresponding to the aromatic C–C stretching of 5CB. Next, we incubate these films on heparin solution in order to observe the conformational change within amide region of PLL at these surfaces. Figure 16b shows the PM-IRRAS spectrum of the heparin incubated PLL-laden 5CB films. We observed the appearance of new bands corresponding to heparin adsorption. Heparin is rich in carboxyl (−COOH) and sulfonic groups (−SO_3). From PM-IRRAS spectrum, we observed a strong peak at 1600 cm^{-1}, corresponding to COO^- carboxyl stretch with characteristic bands present within 1200-1100 cm^{-1}for C−O−S, S=O and C−O−C bonds which demonstrates the adsorption of heparin on PLL laden 5CB films (Figure 6.17). Careful inspection of Figure 16a and 16b reveals a significant change in the amide I stretching between PLL and heparin adsorbed PLL-laden surfaces. We note that the amide I in PLL clearly contains single peak (1654cm^{-1}) corresponding to random coil whereas in case of heparin adsorbed PLL laden surfaces, an additional peak appears at 1637 cm^{-1} corresponding to the helical conformation of PLL.

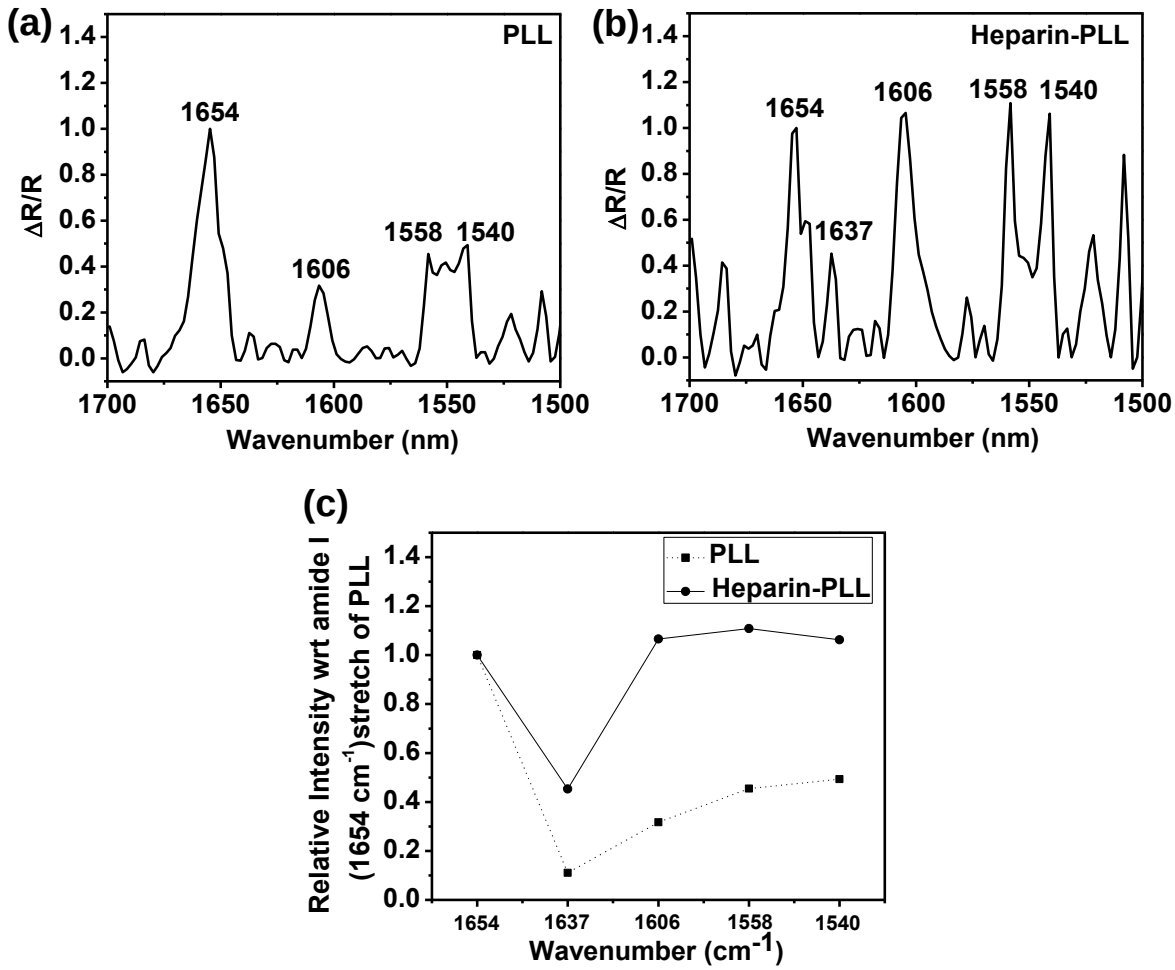

Figure 6.16 Characterizing the interaction of PLL with heparin through PM-IRRAS measurements. (a and b) PM-IRRAS spectra of PLL monolayers that are adsorbed on a) micro-pillars coated with a uniformly deposited film of gold and b) heparin adsorbed on PLL-coated micro-pillars. (c) Relative intensity of amide stretching region of PLL coated surfaces in presence and absence of heparin supported on a uniformly deposited film of gold as measured by PM-IRRAS.

In particular, a significant change in peak intensity was observed in the relative intensity ratio of amide I stretch of PLL (1654 cm^{-1} : 1637 cm^{-1}) for PLL-laden surfaces and heparin adsorbed PLL-laden surfaces (Figure 6.16c). The ratio of amide I stretch of PLL (1654 cm^{-1} : 1637 cm^{-1}) for PLL-laden surfaces in the absence and presence of heparin corresponds to (1:0.1) and (1:0.45), respectively. These results speculate that in presence of heparin; almost

50% of the PLL molecules undergo conformational change from random to helical even at these interfaces. Next, we want to determine the effect of protamine to these surfaces but we were unable to get any information from PM-IRRAS. This might be due to the following reasons: (1) The monolayer doesn't remain stable after 3-4 incubations. (2) The protamine-heparin complex formation which results precipitation might accompanied with displacements of complex from the surfaces and also intern disturb the PLL surfaces which makes it difficult to study using PM-IRRAS.

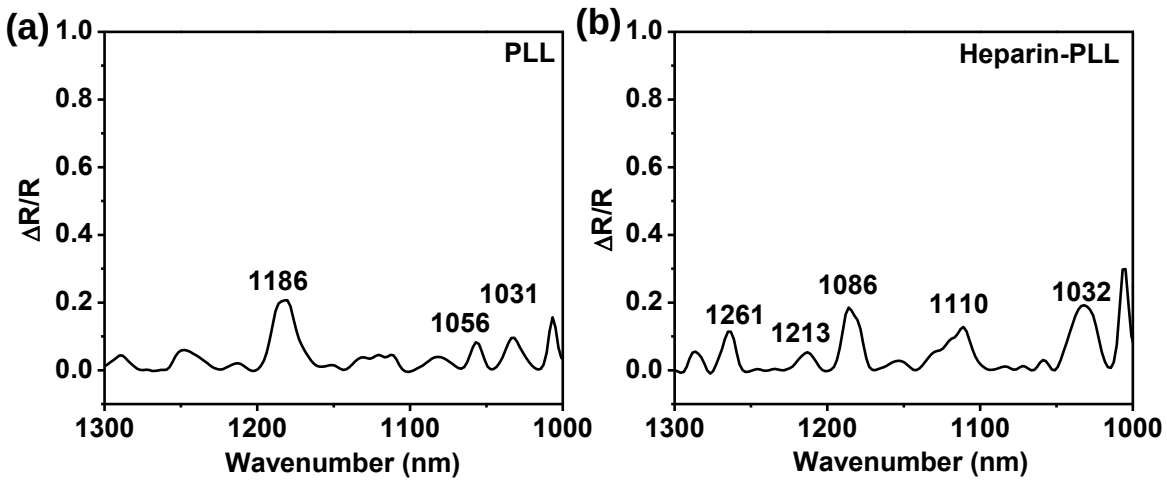

Figure 6.17 Characterizing the heparin adsorption through PM-IRRAS measurements. (a and b) PM-IRRAS spectra of PLL monolayers that are adsorbed on a) micro-pillars coated with a uniformly deposited film of gold and b) heparin adsorbed on PLL-coated micro-pillars.

In order to provide further insight to investigate whether protamine driven reorientation of heparin adsorbed PLL-coated LC droplets (*via* binding of the protamine to the heparin-decorated surfaces) was accompanied by redistribution or displacement of the heparin-protamine complex from the interface, we have performed epi-fluorescence microscopy. For this, PLL-coated LC droplets have been incubated in 5 μM of heparin doped with fluorescent (fluorescein isothiocyanate) heparin in Tris buffer at pH 7 for 30 min. The epi-fluorescence micrograph (Figure 6.18) of heparin adsorbed PLL-coated surfaces showed a well-defined uniform ring fluorescence of the droplet surface.

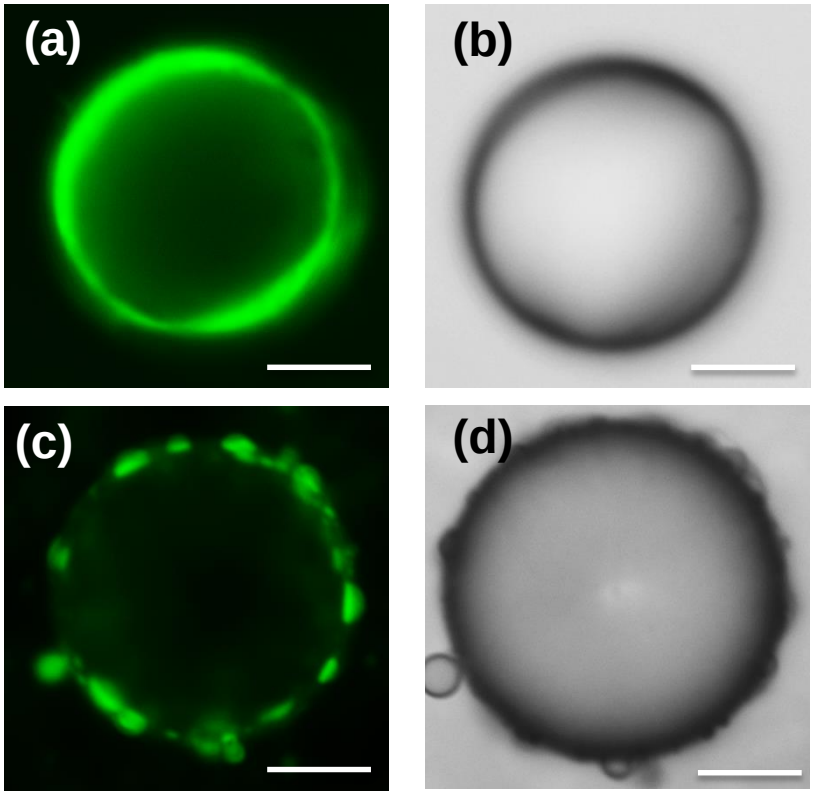

Figure 6.18 Epi-fluorescence microscopic images of fluorescent heparin adsorbed PLL-coated LC droplets before a) and after c) addition of protamine (b,d) corresponding bright field images of a) and c) respectively. Scale bar =10 µm.

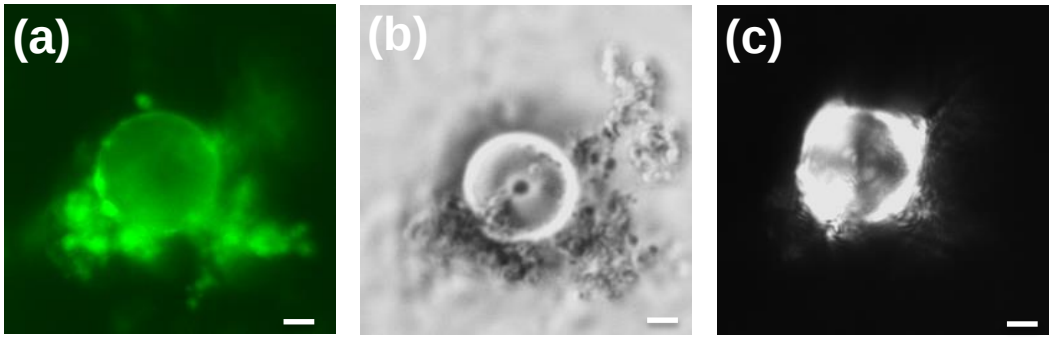

Figure 6.19 a) Epi-fluorescence microscopic images of FITC-heparin adsorbed PLL coated LC droplets after addition of protamine and its (c, d) corresponding bright field and polarized images, respectively. Scale bar = 10 µm.

Further, 1 mg/mL aqueous solution of protamine was added to these fluorescently labelled heparin-coated droplets and incubated for a period of 15 min. Inspection of epi-fluorescence micrograph reveals that the interfacial density of fluorescence decreases at the surface as shown in Figure 6.18. However, some aggregate like structures has been found around and outside the droplet surface as shown in Figure 6.18c and Figure 6.19a, respectively. These structures might be heparin-protamine complex aggregates and result in change in bipolar to radial confirmation of heparin-coated PLL-LC droplets. Bright and polarized light micrographs shown in Figure 6.18 and Figure 6.19 confirm the radial orientational ordering of the LC droplets indicating that PLL reorganizes at the LC droplet surface to radial ordering after heparin protamine complex formation. Since, the concentration for heparin and protamine used in these experiments was kept higher in order to see these structures under fluorescence microscope. From these results, we conclude that the conformational switching of PLL in addition to electrostatic interaction likely plays a role in detection of heparin and protamine on PLL-coated LC droplets through LC ordering transition. Overall, the results presented here suggested that PLL-coated LC droplets could offer not only the basis of a sensitive and selective sensor for heparin and selective protamine detection in biological conditions but also, provides fundamental insight towards interactions of PLL with heparin and protamine.

6.4 Conclusions

We demonstrate here that micrometer-scale droplets of thermotropic LCs modified with PLL in aqueous media can act as exquisitely sensitive reporters for the selective detection of heparin and protamine. The polyanionic heparin molecules adsorb on positively charged PLL-coated LC droplets *via* electrostatic interactions which results a configurational change from radial to bipolar within LC droplets under crossed polarizers in polarized optical microscopy. Heparin binding over PLL-coated LC droplets has been shown to be selective over other glycosaminoglycans, such as hyaluronic acid and chondroitin-4-sulfate. Further, addition of protamine over heparin adsorbed PLL-coated LC droplets change the director profile of LC droplets back to radial configuration due to the stronger affinity of heparin to protamine. The adsorption of heparin and protamine on the PLL-coated LC droplets is confirmed using fluorescence microscopy and zeta potential measurements. CD, VCD, PM-

IRRAS and fluorescence experiments has been performed which provided some mechanistic approach of these interactions (PLL-heparin and heparin-protamine) to undergo predictable LC ordering. Using this approach heparin and protamine can be detected within clinical demanded concentration in biological conditions. Thus, PLL-coated LC droplets act as a potential tool for sensitive and selective detection of heparin and protamine for laboratory and bedside diagnosis.

6.5 Experimental Section

6.5.1 Materials

Poly-L-lysine (PLL) solution 0.1 % (w/v) in H_2O, poly(4-styrenesulfonic acid) sodium salt (PSS), heparin sodium salt from porcine intestinal mucosa, BSA, protamine sulfate salt from salmon, heparin sulfate (HS) and chondroitin-4 sulfate sodium salt from bovine trachea (CS), tris (hydroxyl methyl) amino-methane, N,N-dimethyl-N-octadecyl-3-aminopropyltrimethoxysilyl chloride (DMOAP), hydrochloric acid and sodium hydroxide were purchased from Sigma-Aldrich (St. Louis, MO). Fluorescent heparin (Fluorescein Isothiocyanate) was purchased from Polysciences, Inc., USA. The thermotropic liquid crystal (LC) E7 was purchased from Merck (Mumbai, India). Deionization of a distilled water (DI water) source was performed using a Milli-Q-system (Millipore, bedford, MA). All materials were used as received without further purification.

6.5.2 PLL-coated LC droplets using layer by layer technique

The LC emulsions were formed by mixing 10 μL of E7 in 1 mL of PSS (1 mg mL^{-1}) with bath sonication for 15 minutes. The PSS-LC droplets were confirmed to exhibit bipolar configurations following sonication.

We fabricated these LC droplets with PSS and PLL polyelectrolyte multilayer by layer-by-layer (LbL) technique.[54] E7-PSS emulsions were first washed with millipore water thrice. The tube containing 1 mL of emulsion was agitated with a vortex mixer and then centrifuged at 5000 g for 5 min. This resulted in a pellet forming at the bottom of the tube. Approximately 0.5 mL of the supernatant was removed and replaced with water. This was

repeated twice to remove excess PSS polyelectrolyte coating. After washing, the second layer of the polyelectrolyte film was then deposited by adding 1 mL of PLL solution (0.8 mg/mL) was added to 0.1 mL of the emulsion. The mixture was agitated with a vortex mixer and allowed to incubate for 15 min to allow sufficient time for PLL adsorption. After adsorption, the dispersions were centrifuged (at 5000 g, 5 min), after which the supernatant was removed and replaced by water. Washing was performed 1 time, followed by adsorption of the next polyelectrolyte. The entire process was repeated until the four bilayers of (PLL/PSS)-coated E7-PSS emulsions as a function of layer number, with outermost being PLL.

6.5.3 Preparation of aqueous solutions of heparin, protamine, heparin sulfate and chondroitin sulfate

All the solutions were made in Tris buffer at pH 7.4. The calculated amount of biomolecule was dissolved in tris buffer at room temperature to obtain the required concentration of particular compound. The resulting solutions were directly used for experiment of interest.

6.5.4 Zeta potential measurements

A Malvern Zetasizer Nano ZS90 instrument (Malvern Instruments, Southborough, Massachusetts) was used to measure zeta potential at 25 °C for LC emulsions. The DLS instrument was operated under the following conditions: temperature: 25 °C, detector angle: 90 incident laser wavelength: 632 nm, and laser power: 4 mW. Samples prepared were loaded into a pre-rinsed zeta potential cell for measurements. Approximately 5 μL of 1 vol. % emulsions was added to 2.5 mL of millipore water. The quoted values were calculated by taking the average of 5 successive measurements.

6.5.5 Polarized and fluorescence microscopy

The PLL coated LC droplets treated with heparin and protamine was examined with bright field, plane–polarized in transmission mode on a (Zeiss, Scope A1, Germany) polarizing optical microscope using an objective power of 200x and 500x. The orientation of the LC within droplets was examined with plane-polarized light in transmission mode with crossed polarizers. Fluorescently labelled LC droplets were characterized with fluorescence

microscopy. Fluorescence imaging was performed with (Zeiss, Axio Scope A1, Germany) fluorescence microscope equipped with a 100 W mercury lamp. The samples were viewed using a fluorescence filter cube with a 491 nm excitation filter and a 516 nm emission filter. Images were obtained with Axio cam camera.

6.5.6 Circular dichroism (CD) and Vibrational circular dichroism (VCD) measurements

The CD spectra were acquired using a Chirascan Spectrophotometer (Applied Photophysics, UK) in a 1 mm path length quartz cell with a scan range of 190–260 nm and 1 nm as step size. The spectra were corrected for the buffer signal.

The VCD spectra were measured in the 1800-800 cm^{-1} range using a Bruker FT-IR spectrometer equipped with the Bruker polarization modulation accessory PMA 50. In the PMA 50 module, the light beam is focused onto the sample passing through an optical low pass filter (blocking wavenumbers >1800 cm^{-1}), a KRS-5 wire grid polarizer, and a ZnSe Photoelastic Modulator (PEM) with an oscillation frequency of 42 kHz. The light is focused by a ZnSe lens to a MCT detector. The detector signal comprises two components: a low-frequency modulation which corresponds to the IR absorption bands, i.e., the A signal, and a high-frequency modulated signal (42 kHz) corresponding to the dichroic absorptions, i.e., the ΔA signal. Additionally, the reference signal direct from the PEM (42 kHz) is mixed to the high-frequency modulated detector signal. These two high-frequency modulated signals are demodulated by an internal synchronous demodulator integrated in the electronic units of the TENSOR and VERTEX series FTIR spectrometers. The VCD spectra were recorded with 1 h data collection time at 4 cm^{-1} resolution. The sample was held in demountable cell with CaF_2 windows and a 100 μm spacer. Spectra were measured in D_2O solvent at a concentration of 10 mg/mL. For each measurement, the intensity calibration factor was obtained using a multiple-wave retardation plate combined with the second wire grid polarizer, whereby the system tuning was exactly the same as for the sample measurement. The spectra were corrected by subtracting the absorption (or VCD) of the corresponding solvent and were plotted in Origin 8 software.

6.5.7 Polarization modulation infrared reflection absorption spectroscopy (PM-IRRAS)

The gold films with thicknesses of ~ 2000 Å were deposited onto micro-pillars (array of nickel (Ni) micro-pillars electroplated on glass substrate fabricated) mounted on rotating planetaries (no preferred direction or angle of incidence) by using thermal evaporator (Excel Instruments, India). These gold-coated micro-pillars were dipped into 0.1% (v/v) DMOAP solution in DI water for 5 min at room temperature and were then rinsed with DI water to remove unreacted DMOAP from the surface (see Appendix B). The DMOAP-coated micro-pillars were dried under a stream of nitrogen gas and kept in oven at 100 ºC. Then, 5CB was dispersed onto the micro-pillars.

Deposited PLL laden 5CB films onto DMOAP supported on micro-pillars coated with a uniformly deposited film of gold (~2000 Å) were examined by using PM-IRRAS. The deposited surface on a gold sample was mounted on an attachment for PM-IRRAS measurements within the PMA 50 compartment connected to the external beam port of a Bruker Tensor 27 FT-IR spectrometer. After reflection of the polarized light incident on the substrate at an angle of incidence of 82° from the surface normal, the IR beam was focused on a liquid nitrogen-cooled photovoltaic MCT detector in the PMA 50 cabinet. A photoelastic modulator (Hinds, PEM 90) was used to modulate the polarization of the light at a frequency of 84 kHz. Demodulation was performed with a lock-in-amplifier (Standford Research Systems, SR830 DSP). Before measurements, the spectrometer was allowed for a complete purge with nitrogen for at least 30 min. Each spectrum is the sum of 100 individual spectra collected at a resolution of 4 cm^{-1} with photoelastic modulator (ZnSe, 42 kHz, AR-coated) set to 1600 cm^{-1}. Data was collected as differential reflectance ($\Delta R/R$)/absorbance versus wavenumbers.

References

(1) Jena, B. K.; Raj, C. R. *Biosens. Bioelectron.* **2008**, *23*, 1285–1290.

(2) Rabenstein, D. L. *Nat. Prod. Rep.* **2002**, *19*, 312-331.

(3) Middeldorp, S. *Thromb. Res.* **2008**, *122*, 753-762.

(4) Gandhi, N. S.; Mancera, R. L. *Drug Discov. Today* **2010**, *15*, 1058-1069.

(5) Straus, A. H.; Nader, H. B.; Dietrich, C. P. *Biochim. Biophys. Acta* **1982**, *717*, 478-485.

(6) Danishefsky, I.; Rosenfeld, L.; Kuhn, L.; Lahiri, B.; Whyzmuzis, C. *Heparin and Related Polysaccharides, Structure and Activities* Ann. New York Acad. Sci. 556, Ofosu, F. A.; Danishefsky, I.; Harish, J. Ed.; The New York Academy of Sciences: New York, **1989**, p. 29-35.

(7) Capila, I.; Linhardt, R. J. *Angew. Chem. Int. Ed.* **2002**, *41*, 390–412.

(8) Rodrigo, A. C.; Barnard, A.; Cooper, J.; Smith, D. K. *Angew. Chem. Int. Ed.* **2011**, *50*, 4675–4679.

(9) Atha, D. H.; Lormeau, J.-C.; Petitou, M.; Rosenberg, R. D.; Choay, J. *Biochemistry* **1987**, *26*, 6454–6461.

(10) Lindahl, U.; Backstrom, G.; Thunberg, L.; Leder, I. G. *Proc. Natl Acad. Sci. USA* **1980**, *77*, 6551–6555.

(11) Mackman, N. *Nature* **2008**, *451*, 914–917.

(12) Castellot, J. J.; Favreau, L. V.; Karnovsky, M. J.; Rosenberg, R. D. *J. Biol. Chem.* **1982**, *257*, 11256-11260.

(13) Sy, M. S.; Schneeberger, E.; McClusky, R.; Greene, M. I.; Rosenberg, R. D.; Benacerraf, B. *Cell. Immunol.* **1983**, *82*, 23-32.

(14) Folkman, J. *Biochem. Pharmacol.* **1985**, *34*, 905-909.

(15) Jaques, L. B. *Pharmacol. Rev.* **1979**, *31*, 99-166.

(16) Corrigan, J. J. *J. Pediatrics* **1977**, *91*, 695-700.

(17) Vaheri, A. *Acta Pathol. Microbiol. Scand. Suppl.* **1964**, *171*, 7-98.

(18) Folkman, J. *Adv. Cancer Res.* **1985**, *43*, 191-196.

(19) Girolami, B.; Girolami, A. S. *Thromb. Hemostasis* **2006**, *32*, 803−809.

(20) Shvarev, A.; Bakker, E. *J. Am. Chem. Soc.* **2003**, *125*, 11192–11193.

(21) Ando, T.; Yamasaki, M.; Suzuki, K. *Protamine: molecular biology, biochemistry and biophysics;* Kleinzeller, A. Springer-Verlag, Ed; 1973, vol. *12*, pp. 1–109.

(22) Kim, Y.; Rose, C. A. *Pharm. Res.* **1995**, *12*, 1284–1288.

(23) Jaques, L. B. *Pharma Rev.* **1980**, *31*, 99–166.

(24) Brange, J.; *Galenics of insulin*, Springer-Verlag, Berlin, **1987**, p. 34

(25) Egawa, Y.; Hayashida, R.; Seki, T.; Anzai, J. *Talanta* **2008**, *76*, 736–741.

(26) Bromfield, S. M.; Barnard, A.; Posocco, P.; Fermeglia, M.; Pricl, S.; Smith, D. K. *J. Am. Chem. Soc.* **2013**, *135*, 2911-2914.

(27) Chen, X. T.; Xiang, Y.; Li, N.; Song, P. S.; Tong, J. *Analyst* **2010**, *135*, 1098–1105.

(28) Wright, A. T.; Zhong, Z. L.; Anslyn, E. V. *Angew. Chem. Int. Ed.* **2005**, *44*, 5679–5682.

(29) Zhong, Z. L.; Anslyn, E. V. *J. Am. Chem. Soc.* **2002**, *124*, 9014–9015.

(30) Sauceda, J. C.; Duke, R. M.; Nitz, M. *ChemBioChem* **2007**, *8*, 391–394.

(31) Sun, W.; Bandmann, H.; Schrader, T. *Chem. Eur. J.* **2007**, *13*, 7701–7707.

(32) Mecca, T.; Consoli, G. M. L.; Geraci, C.; Spina, R. L. Cunsolo, F. *Org. Biomol. Chem.* **2006**, *4*, 3763–3768.

(33) Wang, S. L.; Chang, Y. T. *Chem. Commun.* **2008**, 1173–1175.

(34) Brízá, T.; Kejík, Z.; Císárová, I.; Králová, J.; Mártásek, P.; Král, V. *Chem. Commun.* **2008**, 1901–1903.

(35) Wang, X. K.; Chen, L.; Fu, X. L.; Chen, L. X.; Ding, Y. J. *ACS Appl. Mater. Interfaces* **2013**, *5*, 11059–11065.

(36) Awotwe-Otoo, D.; Agarabi, C.; Faustino, P. J.; Habib, M. J.; Lee, S.; Khan, M. A.; Shah, R. B. *J. Pharm. Biomed. Anal.* **2012**, *62*, 61–67.

(37) Alino, V. J.; Pang, J.; Yang, K.-L. *Langmuir* **2011**, *27*, 11784–11789.

(38) Alino, V. J.; Tay, K. X.; Khan, S. A.; Yang, K.-L. *Langmuir* **2012**, *28*, 14540–14546.

(39) Bera, T.; Fang, J. *J. Mater. Chem.* **2012**, *22*, 6807–6812.

(40) Bera, T.; Fang, J. *Langmuir* **2013**, *29*, 387–392.

(41) Gupta, J. K.; Zimmerman, J. S.; de Pablo, J. J.; Caruso, F.; Abbott, N. L. *Langmuir* **2009**, *25*, 9016–9024.

(42) Khan, W.; Choi, J. H.; Kim, G. M.; Park, S.-Y. *Lab Chip* **2011**, *11*, 3493–3498.

(43) Kinsinger, M. I.; Buck, M. E.; Abbott, N. L.; Lynn, D. M. *Langmuir*, **2010**, *26*, 10234–10242.

(44) Lin, I.-H.; Miller, D. S.; Bertics, P. J.; Murphy, C. J.; de Pablo, J. J.; Abbott, N. L. *Science* **2011**, *332*, 1297–1300.

(45) Sivakumar, S.; Wark, K. L.; Gupta, J. K.; Abbott, N. L.; Caruso, F. *Adv. Funct. Mater*. **2009**, *19*, 2260–2265.

(46) Zou, J.; Bera, T.; Davis, A. A.; Liang, W.; Fang, J. *J. Phy. Chem. B* **2011**, *115*, 8970–8974.

(47) Gupta, J. K.; Sivakumar, S.; Caruso, F.; Abbott, N. L. *Angew. Chem. Int. Ed.* **2009**, *48*, 1652–1655.

(48) Yoon, S. H.; Gupta, K. C.; Borah, J. S.; Park, S.-Y.; Kim, Y. K.; Lee, J.-H.; Kang, I.-K. *Langmuir* **2014**, *30*, 10668−10677.

(49) Khan, M.; Park, S.-Y. *Colloids Surf. B: Biointerfaces* **2015**, *127*, 241–246.

(50) Choi, Y.; Lee, K.; Gupta, K. C.; Park, S.-Y.; Kang, I.-K. *J. Mater. Chem. B.* **2015**, *3*, 8659-8669.

(51) Lee, K.; Gupta, K. C.; Park, S.-Y.; Kang, I.-K. *J. Mater. Chem. B* **2016**, *4*, 704-715.

(52) Grant, D.; Long, W. F.; Williamson, F. B. *Biochem. J.* **1991**, *277*, 569-571.

(53) Kim, D.-H.; Park, Y. J.; Jung, K. H.; Lee, K.-H. *Anal. Chem.* **2014**, *86*, 6580−6586.

(54) Tjipto, E.; Cadwell, K. D.; Quinn, J. F.; Johnston, A. P. R.; Abbott, N. L.; Caruso, F. *Nano Lett.* **2006**, *6*, 2243-2248.

(55) Keiderling, T. A. *Nature* **1986**, *322*, 851-852.

Chapter 7

Conclusions and Future outlook

7.1. Conclusions

The work in this thesis explores a range of approaches that lead LC materials with properties that are potentially suitable for biological applications. The central motive of this thesis is mainly based on three objectives: First, we sought to explore new approaches for designing LC based sensors for biological applications in aqueous milieu; second, we sought to design LC materials that can achieve two-way communication with biological systems, both reporting on and understanding the interactions of the biological systems at molecular level. Finally, we sought to develop LC based principles go beyond aqueous milieu and hold promise to act as a marker for cells and cell based interactions. The approaches used and the results obtained in this thesis to achieve these goals are summarized below:

1. The very first approach involves the use of colloidal LC gels for biological amplification. Although, past studies demonstrate the promise of LC interfaces for reporting biomolecular interactions, the issue of how to integrate LCs within composite materials and microsystems to provide stable and robust free interfaces of LCs remains an open challenge. In this direction, we have demonstrated (Chapter 2 in this thesis) that CLC gels with LC-rich domains that span the thickness of the gel are stable under water and report adsorption of biological and synthetic amphiphiles at CLC interfaces. In particular, we have found that the sensitivity can be improved by forming a gel which is highly stable and can be tuned by manipulation of LC domain size and shape within CLC gels. Unlike LCs within TEM grids, these CLC gels have found to be self-supporting, mechanically strong and can be easily handled.

2. The second approach towards the design of LC materials for biological applications revolves around the new way of preparing LC droplets as described in Chapter 3. These systems possess attributes of large surface areas, rich phases, well-defined director

configurations and unique tunable optical properties that make them promising systems for the real time detection of biological analytes in aqueous milieu. But the issue of stability and high mobility limit their use as the basis of an analytical method. For this, we have demonstrated the use of lipid having higher surface activity for the preparation of LC droplets within confined boundary (i.e., grid). In this approach, we have prepared LC droplets which have higher stability (15 days) and can be easily characterized as compared to earlier reports (mobility of these droplets is restricted within the grid geometry). The additional attribute we have found is that the topological ordering of the LC within these droplets reports interfacial enzymatic reactions providing means for developing new responsive soft materials.

3. The second broad goal involves the use of LC systems for understanding the important polymorphic behavior of CL. In Chapter 4, we have demonstrated that LC not only provides simple, rapid and accessible method for the detection of CL in the micromolar range (0−10 μM) but also, understand the behaviors of the pH-dependent conformational forms of the CL at molecular level. We have provided evidence that the structural differences of CL conformers having different self-assembly can be differentiated using LC systems.

4. Finally, we have provided a new gateway for biological amplification using LC systems at the cellular level (Chapter 5). In this study, we have shown the interaction of model protein Poly-L-Lysine (PLL) with LC that trigger LC orientation. Then, LC droplets were fabricated with PLL and have shown that these PLL-coated droplets adhered strongly on the surface of cells likely through electrostatic interactions. The additional attribute is that the orientation of these PLL-coated LC droplets changes from radial to bipolar on adherence to cell surface and have also been found to detect the presence of toxic agents. Biocompatibility of these droplets made them to act as biomarker for cells and cell based interactions. We have also shown these PLL coated LC droplets can be used to mimic other important biomolecular interactions. For example, Annexin V–Phosphatidylserine interaction has investigated through modulation of these PLL-coated LC droplets. In addition, the important heparin and protamine interaction have also been described in Chapter 6 using these LC droplets. Heparin has been widely used as an anticoagulant during cardiovascular surgery or used to avoid thrombosis whereas protamine strongly binds with heparin; it

displaces anti-thrombin from heparin–anti-thrombin complex and thus reverses the anticoagulant effects of heparin.

7.2 Future outlook

Based on the experimental results and discussions from this thesis, we realized that the following investigations and studies can be done in future.

In Chapter 2, CLC gels offer the robust systems to report biological systems. However, these CLC gels can be used to report other biological and chemical sensing applications for future study. These systems should be studied for practical application.

The spontaneous organization of water droplets to well-defined LC droplets was observed in Chapter 3 and we have not fully understood the reason behind this transformation. We have studied the role of other surfactants and lipids ((sodium dodecyl sulfate (SDS), CTAB, lysophosphatidic acid (LPA), 1,2- dilauroyl-sn-glycero-3-phosphocholine (DLPC) and lipopolysaccharide (LPS)) for formation of stable droplets with radial LC configuration. But, the effect of surface charge of the glass slide with different functionalities can also be studied towards the droplet formation. The whole process of water to LC droplets change can also be monitored using fluorescence studies. In addition, contact angle measurements can also be done. However, in future investigation of this mechanism can provide several answers related to this study and also provide scope to improve several issues related to this technique for providing efficient LC droplet methodology.

The three conformational forms of CL have shown to be differentiated with LC systems in chapter 4. A possible direction of this research in future will be to study on real samples of CL. This study will provide the actual practical usage of this method and also provide insight about the CL behaviors at different conditions. CL is also known to bind with certain proteins (e.g., Alpha-synuclein). The qualitative, quantitative and also conformational behavior of CL in presence of these important and specific proteins can be studied and is potentially important.

PLL-coated LC droplets described in Chapter 5 can be studied for wide range of biological interaction on aqueous and cellular environments. In addition, Annexin V-PS interactions studied using PLL-coated LC droplets in Chapter 5 can be further extended to use in cell based apoptosis detection. PLL being a positively charged polyisopeptide, is known to interact with negatively charged proteins, lipids and even drug molecules. PLL surfaces are also used for drug delivery applications. However, this research is still at an early stage and many efforts are still needed for the use of these PLL-coated droplets for drug delivery purposes and discovering several interfacial phenomena related to cell biology.

APPENDICES

Appendix A

A.1 Calculation for speciation curves for the aqueous CL as a function of pH

The percentage of three different equilibrium species (H_2A, HA^- and A^{2-}) of CL present at given pH can be determined using general dibasic acid equations mentioned below

$$H_2A = \frac{[H^+]^2}{[H^+]^2 + K_{a1}[H^+] + K_{a1}K_{a2}} \quad (1)$$

$$HA^- = \frac{K_{a1}[H^+]}{[H^+]^2 + K_{a1}[H^+] + K_{a1}K_{a2}} \quad (2)$$

$$A^{2-} = \frac{K_{a1}K_{a2}}{[H^+]^2 + K_{a1}[H^+] + K_{a1}K_{a2}} \quad (3)$$

Where

$$K_{a1} = -\text{Antilog}\,(pk_{a1})$$

$$K_{a2} = -\text{Antilog}\,(pk_{a2})$$

$$[H^+] = \text{Antilog}\,(-pH)$$

For CL, pK_{a1} = 2.8 and pK_{a2}= 7.5. From these values K_{a1} and K_{a2} calculated are 1.6 x 10^{-3} and 3.2 x 10^{-8}, respectively.

A.2 Deconvolution of the PM-IRRAS spectra

The deconvolutions were carried out using the peak analyzer option (listed in the peak and baseline analysis) available in the Origin Pro version 8.5 software. Fitting was carried out using the Levenberg- Marquadt non-linear least squares method to obtain multiple fitted Gaussian curves and the fitting parameters were kept variable in order to prevent any bias during the fitting

procedure. The standard errors in the analyses for peak positions are ≤ 2 cm^{-1}. The percentage contents of various secondary structural elements (with respect to the cumulative peak fit with a total area of 100 %) were obtained during the fitting analysis.

Appendix B

B.1 Optical appearance of 5CB in response to PLL within micro-pillar assembly

For this, we hosted 5CB (4'-pentyl-4-cyanobiphenyl) in the micro-pillars supported on N,N-dimethyl-*n*-octadecyl-3-aminopropyltrimethoxysilyl chloride (DMOAP) treated glass slides. The DMOAP treatment of the glass anchors 5CB in an orientation that is perpendicular (homeotropic) to the LC-glass interface. When combined with the influence of DMOAP-coated glass slides (also causes homeotropic anchoring of the LCs), the 5CB film within micro-pillars presumes a uniform orientation that is perpendicular to both the surfaces (air as well as DMOAP). This leads to dark optical appearance of the E7 LC between cross polars as shown in Figure B.1a. Subsequently, in contact with aqueous solutions (Figure B.1b), the optical appearance of the LC became bright, consistent with an ordering transition of the LC induced by water. Interestingly, when we introduced PLL (M. wt. 225 kDa) into this an ordering transition was observed within a minute leading to dark optical appearance of the LC (Figure B.1c).

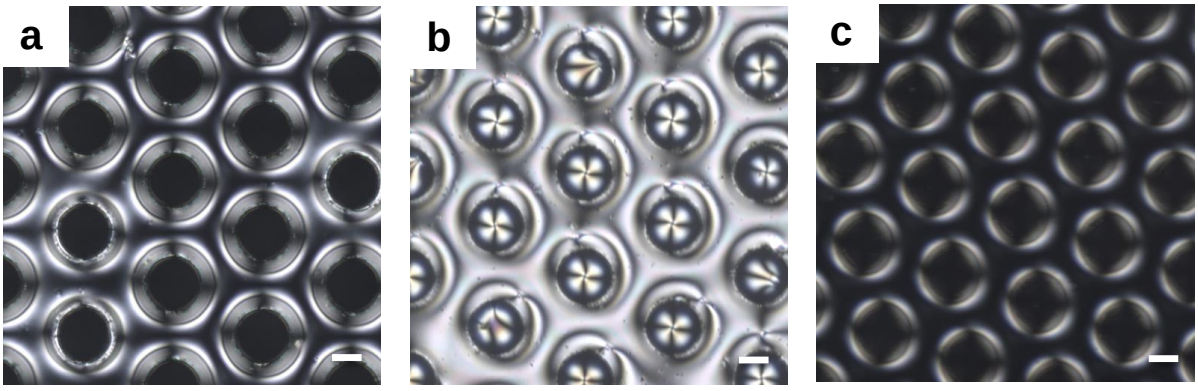

Figure B.1 Characterizing the micro-pillar array functionalized surfaces used for showing interaction of PLL with LC through POM a) Polarized optical microscopic images of LC film poured within micro pillars coated with DMOAP in contact with LC-air interface, LC

assumes homeotropic alignment throughout the film thickness corresponding to dark image b) LC-aqueous interface resulting in-plane birefringence of 5CB around the micro-pillars and c) PLL laden LC-aqueous interface which resumed the homeotropic alignment of LC and returned to a dark image.

B.2 PM-IRRAS spectra of DMOAP and 5CB film on gold deposited micro-pillar array assembly

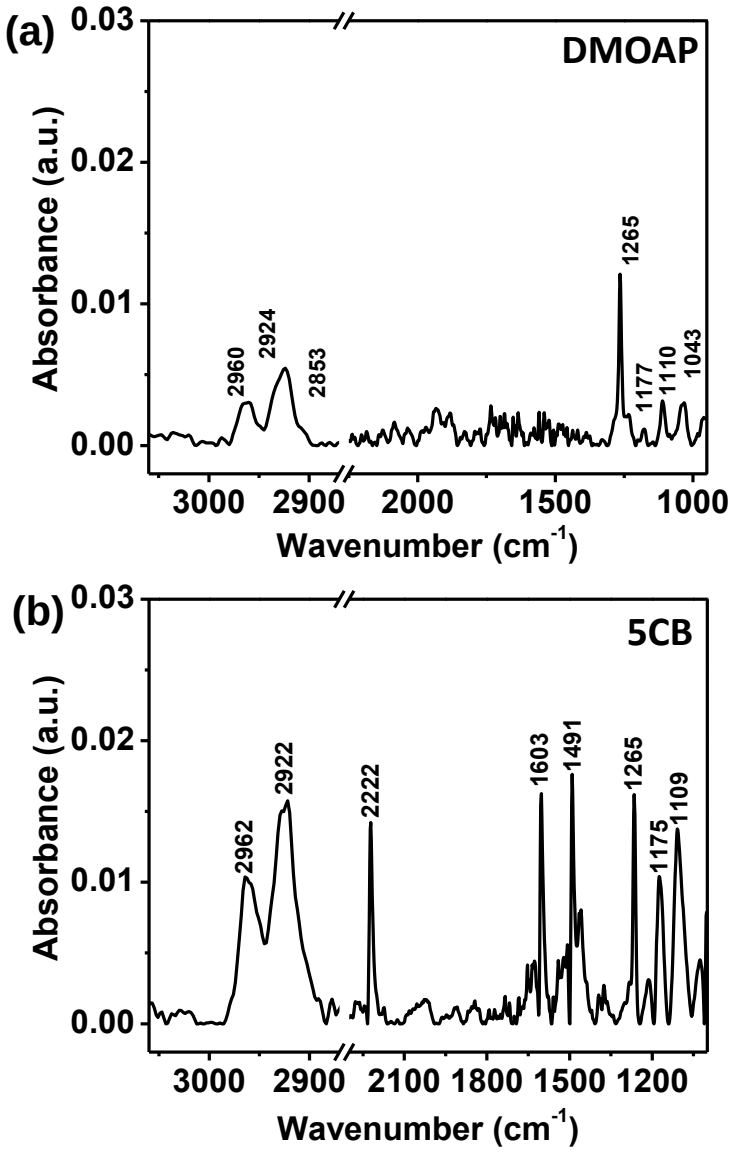

Figure B.2 PM-IRRAS spectra generated from gold deposited micro-pillar array coated a) with DMOAP and then b) 5CB film respectively.

For PM-IRRAS, first we functionalized gold coated micro-pillars (2–4 µm) with DMOAP. The IR spectra using polarization modulation of DMOAP-coated surface shows the characteristic peaks of Si–C (1265 cm^{-1}), Si–O (1177 cm^{-1}, 1110 cm^{-1}), C–O (1043 cm^{-1}) and CH_3 and CH_2 stretching (2960 cm^{-1}, 2924 cm^{-1}, 2853 cm^{-1}) as shown in Figure B.2a. Next, we poured the 5CB into the DMOAP-coated micro-pillars. Figure B.3b shows the strong absorption bands of C≡N (2222 cm^{-1}) along with aromatic C–C stretching (1603 cm^{1}) and aliphatic CH_2 and CH_3 stretching (2922 cm^{-1}, 2852 cm^{-1}, 2801 cm^{-1}) and C–H bending (1491 cm^{-1}).

B.3 Optimal concentration of Calcein-AM required for flow cytometry based experiment to assess the cytotoxicity of PLL-coated LC droplet

For this, cells (T84) were treated with different concentrations of Calcein-AM. The Calcein AM concentration is varied from 1 µM to 10 µM and analyzed by flow cytometry. Live cells showed green fluorescent calcein staining which was analyzed in FL1 channel. Histogram showing increase in Calcein positive cells with increasing concentration of Calcein-AM. From the histogram analysis it is evident that of 10 µM Calcein-AM treated cells show more calcein+ve cells (98.7%) compared to lower concentration of Calcein-AM treated cells (96%, 97.4% and 98.3%) (Figure B.3). These results conclude that 10 µM Calcein-AM concentration is optimum for flow cytometry based experiment to assess the cytotoxicity of PLL-coated LC droplet on these cells (T84).

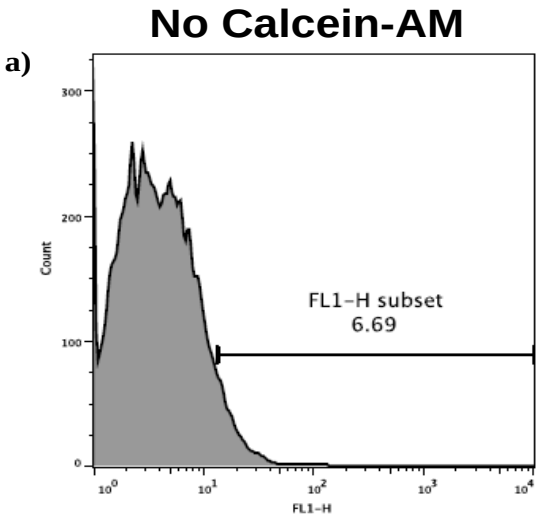

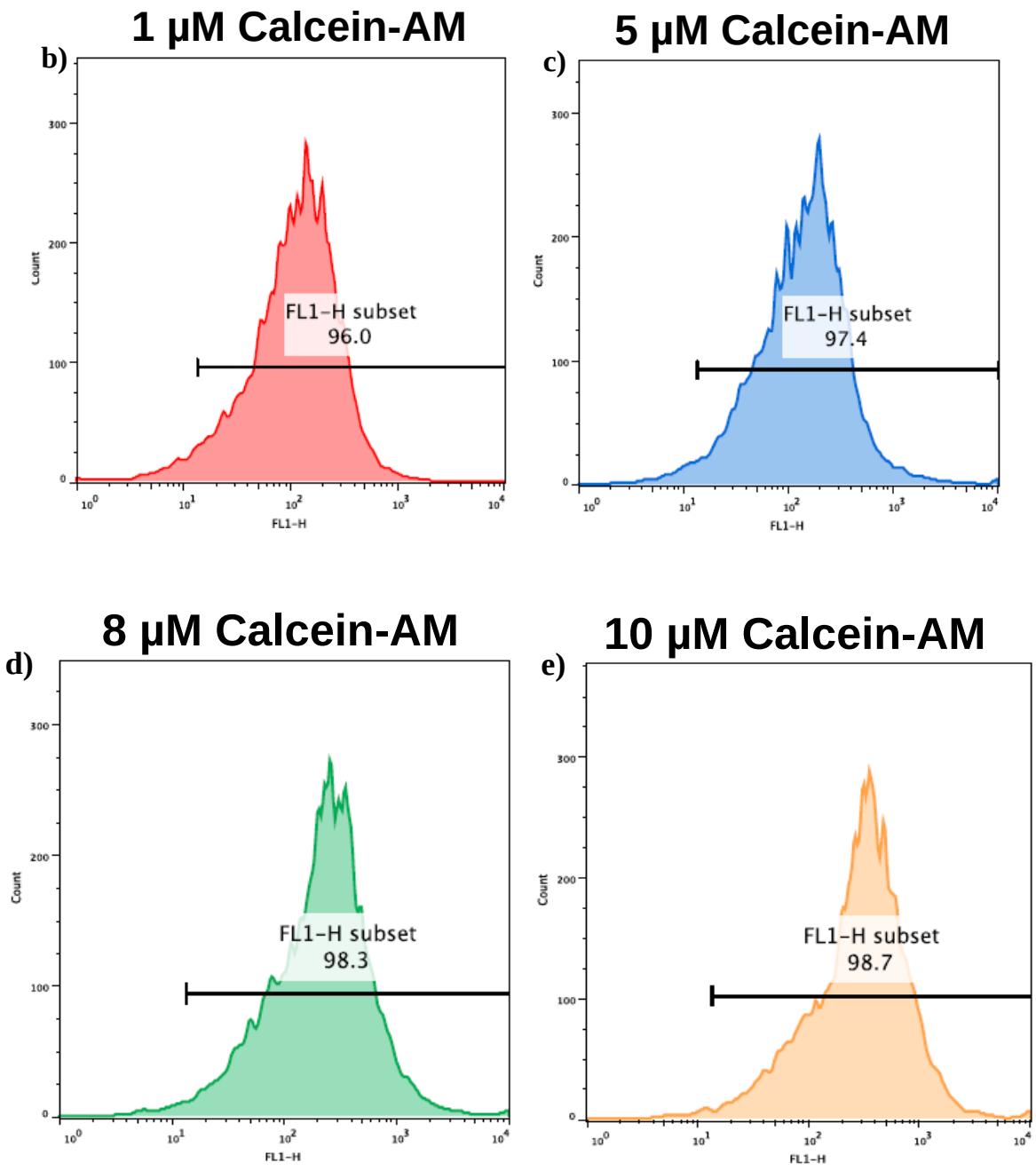

Figure B.3 Histogram showing increase in calcein positive cells with increasing concentration of Calcein-AM a) 0 µM, b) 1 µM, c) 5 µM, d) 8 µM and e) 10 µM for staining cells (T84).

List of Publications

(1) Agarwal, A.; **Sidiq, S.**; Setia, S.; Bukusoglu, E.; de Pablo, J. J.; Pal, S. K.; Abbott, N. L. Colloid-in-Liquid Crystal Gels that Respond to Biomolecular Interactions. *Small* **2013**, *9*, 2785-2792.

(2) **Sidiq, S**.; Das, D.; Pal, S. K. A new pathway for the formation of radial nematic droplets within a lipid-laden aqueous-liquid crystal interface. *RSC Adv.* **2014**, *4*, 18889-18893.

(3) **Sidiq, S**.; Pal, S. K. Lipid-Induced Structural Turnover of Water droplets to Liquid crystal Droplets. *AIP Conf. Proc.* **2014**, *1591*, 33-35.

(4) **Sidiq, S**.; Verma, I.; Pal, S. K. pH-Driven Ordering Transitions in Liquid Crystal Induced by Conformational Changes of Cardiolipin. *Langmuir* **2015**, *31*, 4741−4751.

(5) Das, D.;‡ **Sidiq, S**.;‡ Pal, S. K. A simple quantitative method to study protein lipopolysaccharide interactions by using liquid crystals. *ChemPhysChem* **2015**, *16*, 753-760 (‡ *Joint first authors*).

(6) **Sidiq, S**.; Prasad, G. V. R. K.; Mukhopadhaya, A.; Pal, S. K. Cell-surface sensors by probing Poly (L-lysine)-liquid crystal interactions that can monitor cellular environment. *Communicated.*

(7) **Sidiq, S**.; Pal, S. K. Poly (L-lysine)-liquid crystal droplets as a template for sensitive and selective detection of heparin and protamine. *Manuscript under preparation*.

(8) Ghosh, S.; Setia, S.; **Sidiq, S**.; Pal, S. K. A new visual test for p-quinone and its relevance to the biodiesel industry. *Anal. Methods* **2012**, *4*, 3542-3544.

(9) Setia, S.; **Sidiq, S**.; Pal, S. K. Microwave-assisted synthesis of novel oligomeric rod-disc hybrids. *Tetrahedron Lett.* **2012**, *53*, 6446-6450.

(10) Gupta, S. K.; Setia, S.; **Sidiq, S**.; Gupta, M.; Kumar, S.; Pal, S. K. New perylene-based non-conventional discotic liquid crystals. *RSC Adv.* **2013**, *3*, 12060-12065.

(11) Setia, S.; Soni, A.; Gupta, M.; **Sidiq, S**.; Pal, S. K. Microwave-assisted synthesis of novel mixed tail rufigallol derivatives. *Liq. Cryst.* **2013**, *40*, 1364-1372.

(12) Das, D.; **Sidiq, S**.; Pal, S. K. Design of bio-molecular interfaces using liquid crystals demonstrating endotoxin interactions with bacterial cell wall components. *RSC Adv.* **2015**, *5*, 66476-66486.

(13) Verma, I.; **Sidiq, S**.; Pal, S. K. Detection of creatinine using surface-driven ordering transitions of liquid crystals. *Liq. Cryst.* **2016**, doi:10.1080/02678292.2016.1161092.

Patent application filled

(1) Inventors: Pal, S. K; **Sidiq, S**.; IISER Mohali, Indian Patent Application No. 102/DEL/2014 dated 14.01.2014 entitled "*A novel technique for preparation of liquid crystal droplets."*

Review

(1) **Sidiq, S**.; Pal, S. K. Liquid Crystal Biosensors: New Approaches. *Proc. Indian. Natn. Sci. Acad.* **2016**, *82*, 75-98.

Honors, awards and recognitions

(1) The Dewan Jawahar Lal Nayar Memorial prize for best poster at 19th National Conference on Liquid Crystals (NCLC-19) in Nov, 2012 held at Thapar University, Patiala.

(2) "*Colloid-in-Liquid Crystal Gels that Respond to Biomolecular Interactions*" was featured as the Front Cover in Small.

(3) "*Colloid-in-Liquid Crystal Gels that Respond to Biomolecular Interactions*" This work was selected for Press Release; see the following link in The Indian Express.

http://indianexpress.com/article/cities/chandigarh/liquid-crystal-gel-could-replace-horse-shoe-crabs-in-tests/

(4) "*A simple quantitative method to study protein lipopolysaccharide interactions by using liquid crystals"* was featured as cover image in ChemPhysChem.

(5) *"A new pathway for the formation of radial nematic droplets within a lipid-laden aqueous-liquid crystal interface."* This work was selected for Press Release; see the following link in The Indian Express.

http://epaper.indianexpress.com/255025/Chandigarh/09-April-2014#page/21/1

(6) "*A new visual test for p-quinone and its relevance to the biodiesel industry*" was selected as Key Scientific Article in Renewable Energy Global Innovations. This article was also featured in the Front End of Biodiesel Magazine.

(7) Received DST-SERB International Travel Grant to attend the International Liquid Crystal Conference (ILCC-2014) held in Trinity College, Dublin, Ireland from 29th June to 4th July, 2014.

Conferences

(1) Oral presentation entitled "*Biocompatible liquid crystals droplets for monitoring cellular events*" **Sidiq**, **S**; Pal, S. K. at the 22nd National Conference on Liquid Crystals (NCLC-22) held at the DIT University, Dehradun, India (21st-23rd December, 2015).

(2) Poster presentation entiltled "*Lipid–induced structural reorganization of water droplets to liquid crystal droplets*" **Sidiq**, **S**.; Das, D.; Pal, S. K. at the 25th International Liquid Crystal Conference (ILCC-2014) held at the Trinity College, Dublin, Ireland (29th June to 4th July, 2014).

(3) Oral presentation entitled "*pH-driven Ordering Transitions in Liquid Crystal induced by Conformational Changes of Cardiolipin*" **Sidiq**, **S**; Verma, I; Pal, S. K. at the 21st National Conference on Liquid Crystals (NCLC-21) held at the Vikramajit Singh Sanatan Dharm (VSSD) College, Chhatrapati Shahu Ji Maharaj University, Kanpur, India (10th-12th November, 2014).

(4) Participated in *National Seminar on Crystallography 43A* held at the Indian Institute of Science Education and Research Mohali (IISERM), S.A.S. Nagar Mohali, India (13th -17th October, 2014).

(5) Poster presentation entiltled "*Spontaneous evolution of radial nematic droplets within a lipid laden aqueous liquid crystal interface*" **Sidiq**, **S**.; Das, D.; Pal, S. K. at the 20th National Conference on Liquid Crystals (NCLC-20) held at the Manipal Institute of Technology, Manipal University, Manipal, India (16th-18th December, 2013).

(6) Poster presentation entiltled "*Surface-Driven Ordering Transition in Thin Films of Colloid-in-LC gels for Optical Amplification of Biomolecular Interactions*" **Sidiq**, **S**.; Setia, S; Pal, S. K. at the 19th National Conference on Liquid Crystals (NCLC-19) held at the Thapar University, Patiala, India (21st-23rd November, 2012).

(7) Participated in *7th Junior Organic Symposium (JNOST)* held at the Indian Institute of Science Education and Research Mohali (IISERM), S.A.S. Nagar Mohali, India (14th-17th December, 2011).

NANO MICRO
small

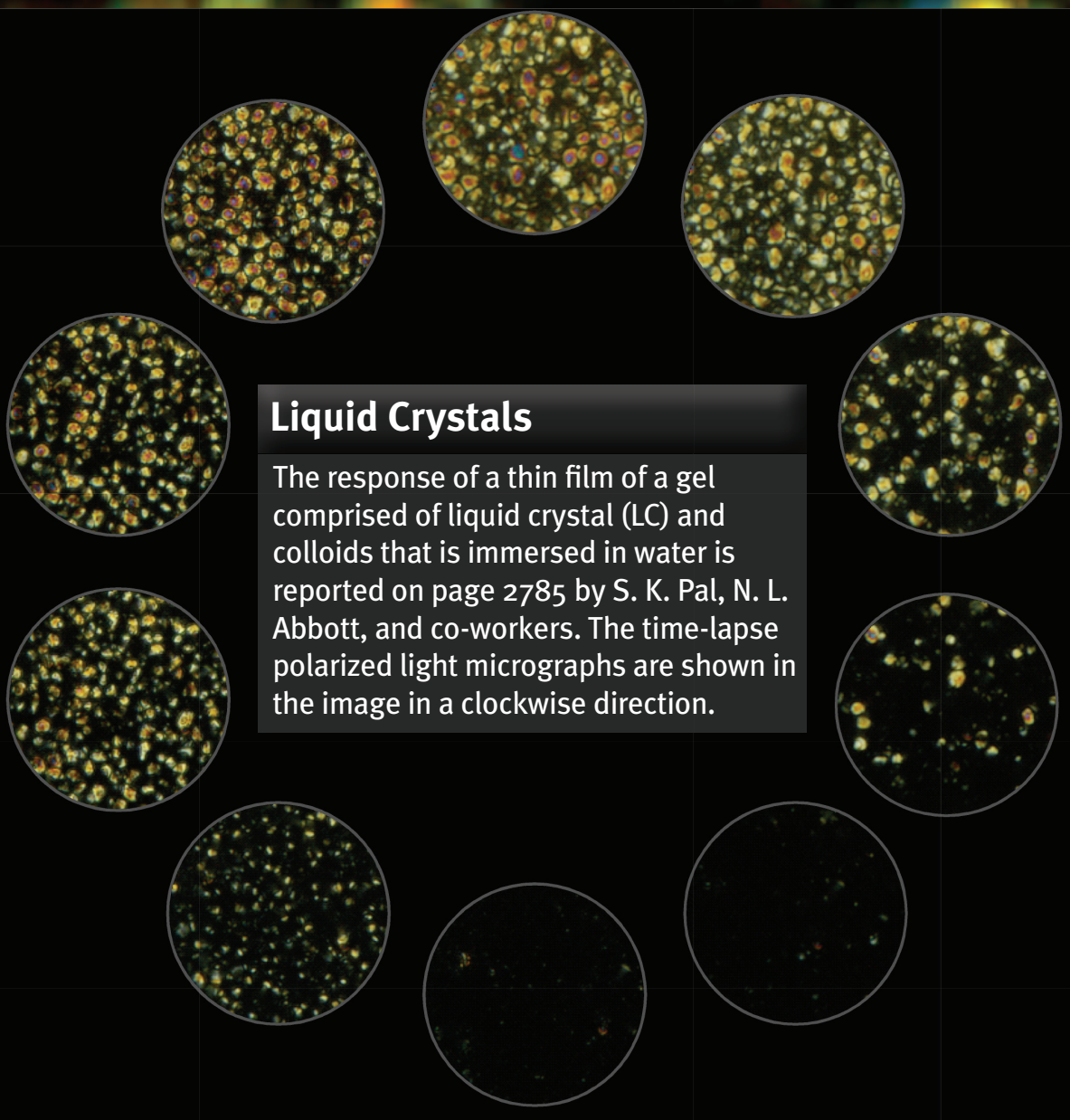

Liquid Crystals

The response of a thin film of a gel comprised of liquid crystal (LC) and colloids that is immersed in water is reported on page 2785 by S. K. Pal, N. L. Abbott, and co-workers. The time-lapse polarized light micrographs are shown in the image in a clockwise direction.

16/2013
WILEY-VCH

Colloid-in-Liquid Crystal Gels that Respond to Biomolecular Interactions
S. K. Pal, N. L. Abbott, and co-workers

A EUROPEAN JOURNAL

CHEMPHYSCHEM

OF CHEMICAL PHYSICS AND PHYSICAL CHEMISTRY

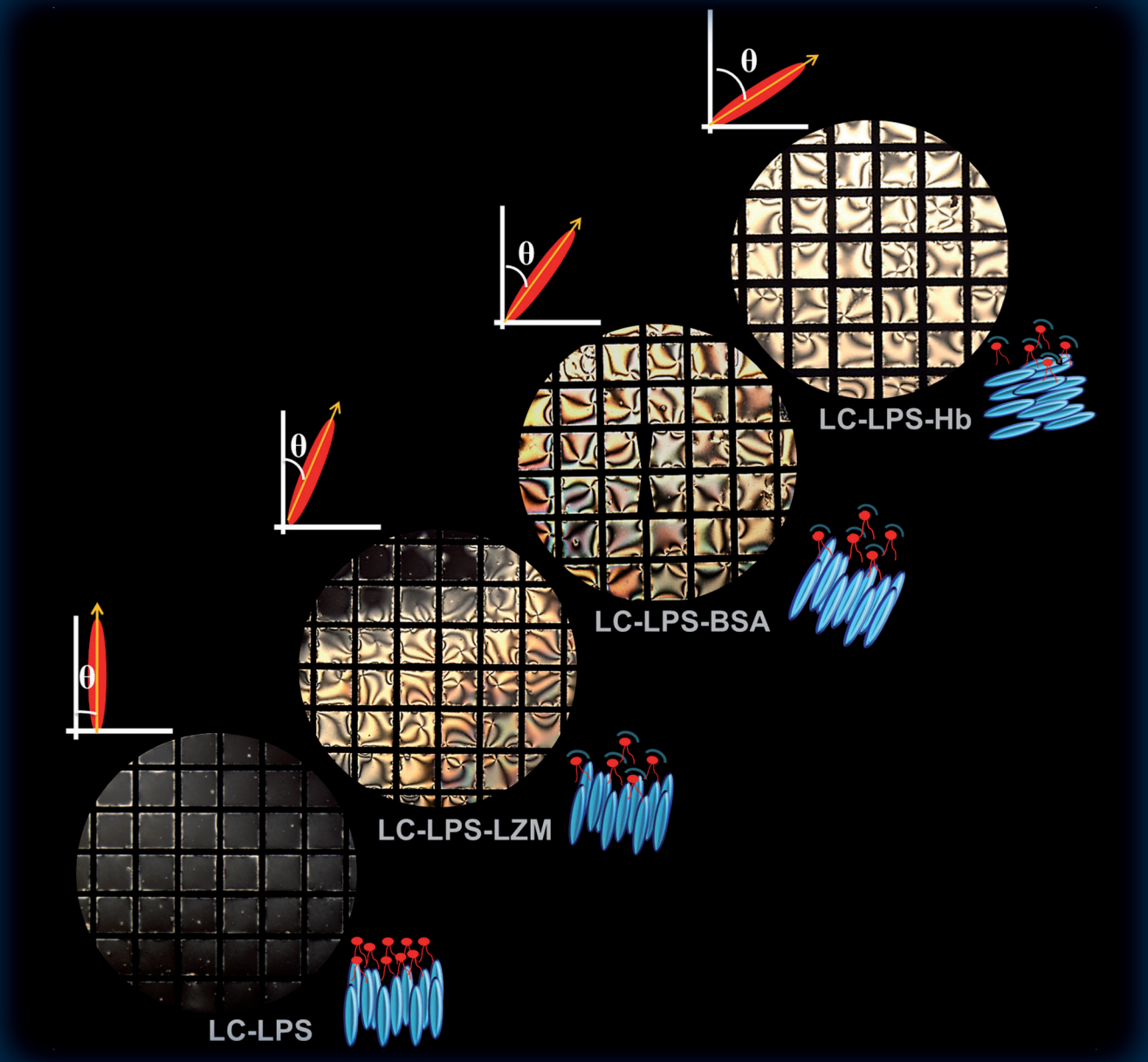

4/2015

A Journal of

ChemPubSoc Europe

The cover image illustrates the continuous change in the optical appearance of a thin film of liquid crystals (LC) at a lipopolysaccharides (LPS)-laden aqueous–LC interface following exposure to an aqueous solution of different proteins. The gradual increase in tilt angle (θ) values of the LC is in accordance with the greater binding affinity of the proteins to LPS, as described on p. 753 by S. K. Pal et al., IISER Mohali.

www.chemphyschem.org

WILEY-VCH